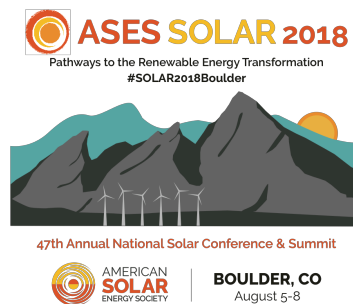




AMERICAN
SOLAR
ENERGY SOCIETY

Conference Proceedings



American Solar Energy Society
National Solar Conference 2018 Proceedings

Edited by

Jill Cliburn
Chair, SOLAR 2018

and

Paulette Middleton
SOLAR 2018 National Organizing Committee

Copyright © 2018 by the American Solar Energy Society

American Solar Energy Society

2525 Arapahoe Ave, Ste E4-253 Boulder, CO 80302

Email: info@ases.org

Web: <http://www.ases.org>

ISBN: 978-3-9814659-9-0

All rights reserved. No part of the publication may be reproduced, transmitted, in any form or by any means, electronic, mechanical, photocopying, recording or otherwise, without permission of the publisher, except in the case of brief quotations embodied in critical articles and review or where prior rights are preserved.

Produced by

International Solar Energy Society Wiesentalstr 50
79115 Freiburg
Germany

Tel: +4976145906-0 Fax: +4976145906-99 Email: hq@ises.org

Web: <http://www.ises.org>

Notice

Neither the International Solar Energy Society and the American Solar Energy Society, nor any one of the supporters or sponsors of the American Solar Energy Society National Solar Conference 2017 (SOLAR 2017) makes any warranty, express or implied, or accepts legal liability or responsibility for the accuracy, completeness or usefulness of any information, apparatus, product or process disclosed, or represents that its use would not infringe privately on rights of others. The contents of articles express the opinion of the authors and are not necessarily endorsed by the International Solar Energy Society, American Solar Energy Society or by any of the supporters or sponsors of SOLAR 2017. The International Solar Energy Society and the American Solar Energy Society do not necessarily condone the politics, political affiliation and opinions of the authors or their sponsors.

Table of Contents

Introduction

SOLAR 2018: Pathways to a Renewable Energy Transformation <i>Cliburn, J.</i>	1
--	----------

Scientific Program

Powering Third World Countries for the Same Cost as Building the Border Wall <i>Gaither, J., Anderson, K.R.</i>	4
Simulation and Lessons Learned from the Ivanpah Solar Plant Project <i>Tharp, J., Anderson, K.R.</i>	13
A Data-Driven Framework for Deploying Solar PV At Penn State University <i>Hoskins, M., Miller, S.W., Prinkey, M.</i>	23
Forecasting Carbon Emissions in States of Hawaii, California, Colorado, and Florida; The Effects of States' Renewable Portfolio Standards <i>Khoie, R., Calderon, A.</i>	32
Renewable Resources of the Northern Half of the United States; A Pathway to Total Renewability? <i>Khoie, R., Benefield, J., Ugale, K.</i>	39
Challenging Conventional Wisdom in the Age of Computing <i>Mansy, K.</i>	51
"Homebrew" Wind Turbines for Integration into Small-Scale Renewable Energy Systems <i>Martin, J., Amaral, D.</i>	62
Multi-Generation Modeling and Building Energy use optimization based on a Natural Gas driven Internal Combustion Engine <i>Okafor, G., Taherian, H.</i>	72
Preliminary Design and Analysis of Low-Cost Concentrating Offshore Solar Energy Innovations <i>Sankriti, M.</i>	85
Research Reveals the Hidden Methods to Democratize Solar <i>Schirtzinger, W.</i>	98
Comparative Analysis of Energy Storage for Photovoltaics: Electrical vs Virtual <i>Sikder, O., Jansson, P.M., Torres, C.</i>	105
A Low-Cost IoT Approach to Real-Time Cloud Motion Detection <i>Smithpeter, I.</i>	110
Providing Emergency Power and Surviving on Solar, Boulder, Colorado, Usa <i>Young, W.R., Schleith, S.</i>	119

Simulated Performance of a Photovoltaic Thermal Heat Pump System for Single-family Houses

Zare, A., Sarunac, N., Wang, W.133

Author Index

Index of Authors144

Introduction

SOLAR 2018: Pathways to a Renewable Energy Transformation

Jill Cliburn

ASES Conference Chair

SOLAR 2018, the 47th National Solar Conference of the American Solar Energy Society, was held at the University of Colorado, at Boulder, August 5–8, 2018. As the premier annual event for ASES, this conference has always reflected the times, beginning with a focus on pioneering technologies nearly 50 years ago, to creating a place for passive solar designers in the 70s and 80s, to sharing PV innovations in the 90s and increasingly promoting integrated solutions for the daunting problems of our age. Today, we are in caught in a maelstrom of environmental, technical and social change. These are nearly overwhelming times. And yet ASES membership nationwide has remarkable breadth, depth and power. Recognizing this, the Solar 2018 Conference committee decided to plan this Conference to bring cross-disciplinary interests and expertise to bear, especially on three of our most pressing energy challenges:

- Broadening access to solar, to give everyone a choice and a voice
- Innovating new energy systems, including clean electrification to maximize renewable resources and distributed energy solutions
- Resilience, preparedness and recovery from climate disruptions, using collaborative planning, solar technology and other sustainable solutions

ASES attracted more than 160 abstracts from academics, professionals, policy leaders and innovators in the solar industry. The Conference committee also invited more than a dozen outstanding presenters, who were well positioned to provide introductions to these cross-disciplinary discussions and to assure that diverse voices would be heard.

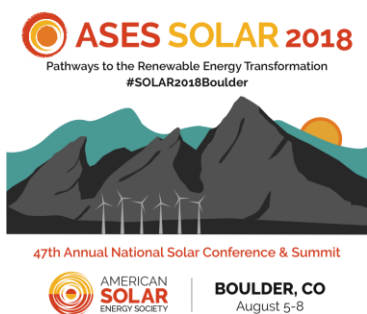
In addition, a *Solar in Your Community Challenge Workshop* was held concurrently with SOLAR 2018. It drew more than 40 participants from communities nationwide that have been participating in the SYC Challenge Program, sponsored by the U.S. Department of Energy, Solar Energy Technology Office to advance solar opportunities for low- and moderate income households and non-profits.

In introducing the opening plenary, program chair Jill Cliburn recognized the diversity in gender, age, race and background among SOLAR 2018 speakers and participants and extended a welcome, not only to participate in this Conference, but also to join ASES leadership. At this Conference, more than at any other, ASES recognized that the problems of the 21st Century, including climate change mitigation and adaptation, can only be solved with all hands working together, supported by an exceptionally broad and deep resolve.

At SOLAR 2018, that resolve was matched by a breadth and depth of technical excellence. This was reflected in papers, presentations and posters on a range of topics: clean electrification, distributed and micro-grid projects, large-scale renewables integration, the foundational scientific understanding of climate change and climate-related disasters, modeling of increasingly complex systems and business strategies, monitoring and control technologies and strategies, and a range of verification and evaluation reports, to name just a few. The Program from SOLAR 2018 documents the details of panels, presentations and speakers; it is a guide to finding many of the presentations that ASES has archived. In addition, ASES, working with the International Solar Energy Society, continues to publish Conference Proceedings, which will serve a global audience to support more work on these important topics, and to preserve the history of this important field. Note that in addition to the three topics selected for special attention at SOLAR 2018, this Conference continued to address many of the topics that have been a mainstay of our Society for many years—from the science of photovoltaics to the art and science of solar building design, to the careful observation of policy trends. Further, the Conference included many memorable moments of recognition for our Fellows, new inductees and award recipients, and for ASES members and newcomers who find our meetings to be the heart of a national solar community—a place for enduring friendship.

The Conference committee for SOLAR 2018 has hoped that *this year*, more than any other, would be a year for crossing the divides that sadly characterize this historic time. Now that the Conference is over, we are proud to say SOLAR 2018 participants rose to that challenge. ASES looks forward now to SOLAR 2019 and to meeting again on our pathway to a Renewable Energy Transformation.

Scientific Program



Conference Proceedings

ASES National Solar Conference 2018

Boulder, Colorado August 5-8, 2018

Powering Third World Countries for the Same Cost as Building the Border Wall

Jordan Gaither¹ and Kevin R. Anderson²

¹ California State Polytechnic University/STARE Lab, Pomona (USA)

² California State Polytechnic University/STARE Lab, Pomona (USA)

kranderson1@cpp.edu

Abstract

The border wall between Mexico and the United States has an estimated cost of \$30 billion. This same budget could be used as foreign aid to build solar farms in Third World countries. For example, three solar PV farms could be built in Kenya, three in Ethiopia, and one in Zimbabwe around the capital of Harare. The three solar PV farms in Kenya would have a combined power of 4 GW, the solar PV farms of Ethiopia would have a combined power of 4 GW as well, and the Zimbabwe plant would have a power 3.75 GW. Ethiopia would produce 9.49 billion kWh in the first year, Kenya would generate 9.1 billion kWh in the first year, and Zimbabwe would generate 8.05 billion kWh in the first year. This would give clean energy to 167 million people. The cost of building these farms would be about \$23.65 billion, leaving \$6.35 billion for additional infrastructure. These various solar PV systems were simulated and designed using the NREL SAM software suite. The presentation will summarize the results of this study including economic analysis via LCOE and hardware /system performance trade studies

Keywords: *PV farm, simulation, economics, modeling, third-world*

1. Introduction

Many immigrants leave their homes in search of a better future for themselves and their families. In 2016, 1.49 million people immigrated to the USA, and roughly 44 million immigrants currently live in this country per Zong et al. (2018). America is currently the wealthiest nation on Earth with an annual GDP of \$18.6 trillion (data.worldbank.org, 2018a). Even though this is the wealthiest nation on earth, it is not economically feasible for America to open its doors to the billions of people currently living in poverty. America cannot become home to everyone, but it can seek to improve the welfare of foreign nations, so their people will not feel the need to leave their homes to find a better one. For countries to compete and thrive in a global market, they need to have a constant and stable source of electricity. Building large solar PV farms in developing nations can help to build the economies of Third World nations and the standard of living for their citizens. To properly size the necessary solar PV farms, the simulated farms were compared to actual solar farms that exist in China and India. China constructed the Tengger Desert Solar Park in 2015, which has a power capacity of 1.55 GW, and India constructed the park spans across 43 km², while India's solar

park spans across an area of 24 km² (Weaver, 2018 , Kumar, 2018). A 1.55 GW solar farm was simulated in Ethiopia to see the energy yield that a farm of this size would produce in Ethiopia. The SunPower SPR-X22-475-COM modules were chosen because they have a power rating of 476.5W and a nominal efficiency of 22.04%. Each of the systems have 2-axis tracking because Ethiopia is located between the Tropic of Cancer and the Equator, Kenya lies on the Equator, and Zimbabwe lies between the Tropic of Capricorn and the Equator. If the systems were using single-axis tracking or a fixed orientation, they would not be able to capture as much of the Sun’s energy as the seasons change. Each system was simulated with a performance degradation of 0.5% per year to account for slow degradation of the panels over time. All solar panels will degrade over time, regardless of maintenance, but this can be minimized if proper maintenance is conducted on the system. Each solar farm was connected to 10,000 kWh battery bank, which is about 2,900 kWh less than what the average American uses in a year (data.worldbank.org, 2018b). This would provide enough electricity for the panels to rotate back to their original East-facing position after the sun sets. This will ensure that the panels will collect as much direct sunlight as possible when the sun begins to rise the next morning, and it will provide power to the main facility and monitoring stations after sunset. The simulations also accounted for potential losses that would likely occur in a real system: 5% annual soiling losses, 4.44% DC power losses, and 1% AC wiring losses. These small details are important for providing accurate results for the systems in the selected countries. Ethiopia, Kenya, and Zimbabwe were selected based on certain characteristics: geographical areas that can contain large scale solar farms, a low per capita GDP, population, energy consumption of the nation, regional stability, preexisting infrastructure, and necessary weather data for running the simulations. Geography of the area was important for several reasons: the PV farms need to be constructed in areas that are accessible, won’t flood during the monsoon season, and away from wildlife reserves. The per capita GDP was taken into consideration, because these solar farms are meant for countries that would not be able to afford purchasing these systems without foreign aid. Ethiopia was the first country to undergo the simulations. To offer some perspective on the comparison between electricity consumption of other nations versus the USA, Table 1 shows some important economic details.

Tab. 1: United States of America population and economic analysis

Population	325.7 million
GDP per capita	\$57,466.79 (USD)
Annual Electricity consumption	4.2 trillion kWh
Annual Electricity consumption per capita	12,986.74 kWh
Cost of electricity	\$0.13/kWh

The USA has a population of 325.7 million people, and it consumes over 4.2 trillion kWh of electricity every year. Ethiopia has a population of 102.4 million people, yet it only consumes 8.14 billion kWh per year, which is roughly 80 kWh per capita (www.worlddata.info, 2018). In comparison, the USA consumes 12,987 kWh per capita (data.worldbank.org 2018b). This means that in three days, the average American consumes more electricity than the average Ethiopian consumes in a year. Since the per capita GDP of Ethiopia is \$706.76 (USD), this means that the average person in Ethiopia lives on less than \$2 a day. The energy yield of the 1.55 GW solar farm was not large enough to completely power the nation, so it was resized and simulated until the proper size was found. Through-trial-and error, it was discovered that a 4.0 GW system is necessary to completely power the nation. The system has been oversized to account for degradation of the panels over time and potential energy loss of transporting the electricity throughout the nation. The first simulation was completed in Addis Ababa, the capital of Ethiopia, because this city lies in the center of the country (ww.nationsonline.org, 2018a). Simulations were also done in other areas of the country to find the best location for the solar PV farms. PV farms in Gondar and Dire Dawa produced the greatest annual energy yield, so the 4.0 GW system was split up into three systems: a 500 MW system in Dire Dawa, a 500 MW system in Gondar, and a 3.0 GW system in Addis Ababa. Even though the PV farm at the capital did not have the highest energy yield, the largest PV farm was placed here because electricity could easily be distributed from here. These PV farms will require thousands of people for construction, so having large cities next to these solar farms will be ideal for providing a necessary work force. Table 2 shows the populations of these cities, and Figure 1 shows the location of the solar farms on the map of Ethiopia.

Tab. 2: Ethiopia population and economic analysis

Population	102.4 million
GDP per capita	\$706.76 (USD)
Annual Electricity consumption	8.14 billion kWh
Annual Electricity consumption per capita	80 kWh
Cost of electricity	\$0.09/kWh
Addis Ababa Population	3,385,000
Gondar Population	207,044
Dire Dawa Population	607,231
Percent of Population with Access to Electricity	42%

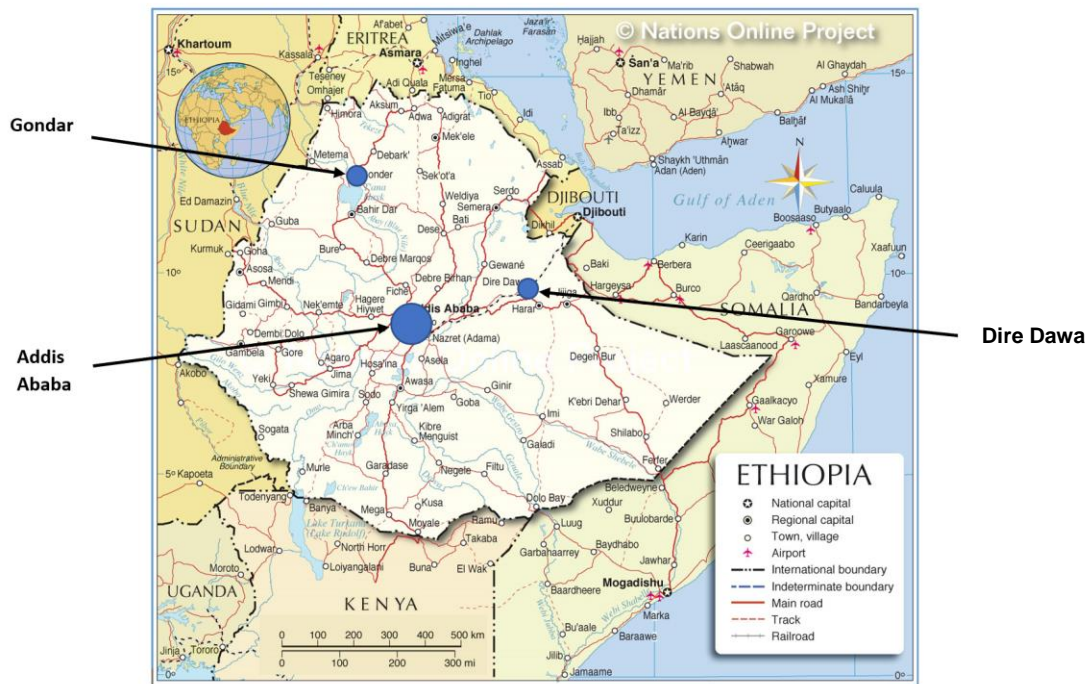


Fig. 1: Map of Ethiopia with location of proposed solar farms, map from www.nationsonline.org (2018a)

Table 3 shows the population of Kenya, its economics, and the electricity consumption and rates of the country. Figure 2 shows the proposed locations of the proposed PV farms in Kenya.

Tab. 3: Kenya population and economic analysis

Population	48.46 million
GDP per capita	\$1,455.36 (USD)
Annual Electricity consumption	7.67 billion kWh
Annual Electricity consumption per capita	158 kWh
Cost of Electricity	\$0.23/kWh
Lodwar Population	48,316
Marsabit Population	291,166
Eldoret Population	289,380
Percent of Population with Access to Electricity	56%

Kenya has the highest GDP per capita out of the three simulated nations, but it is still only 2.5% of the per capita GDP of the USA. It also has the highest electricity rate out of these three nations at \$0.23/kWh (stima.regulusweb.com/historic, 2018). The process for designing and simulating the PV farms in Kenya was similar to the process used for Ethiopia. Locations with the best solar insolation were selected for testing. Lodwar and Eldoret are not located on or near wildlife reservations, so they will not impose upon those restricted areas, but the PV plant in Marsabit needs to be constructed about 10 miles northeast of the

city to avoid interfering with the boundaries of the Marsabit National Reserve (www.nationsonline.org, 2018a). The population density is much greater in the southern part of Kenya than in the northern regions. Eldoret is located in the southwest region of Kenya and is much closer to the densely populated zones, so it was chosen as the location with the largest PV farm in Kenya to limit losses across the power lines. It is only 200 miles from the Kenya’s largest city and capital, Nairobi. Marsabit is 325 miles away north of the capital, while Lodwar is 370 miles north (www.nationsonline.org, 2018a). All three locations are less than 100 miles from the Kenyan border, so excess electricity could be sold to neighboring countries if connecting power lines were constructed, which would benefit the economy of Kenya. The systems at Lodwar and Marsabit each have a 500 MW power capacity, while the system at Eldoret has a 3.0 GW capacity.

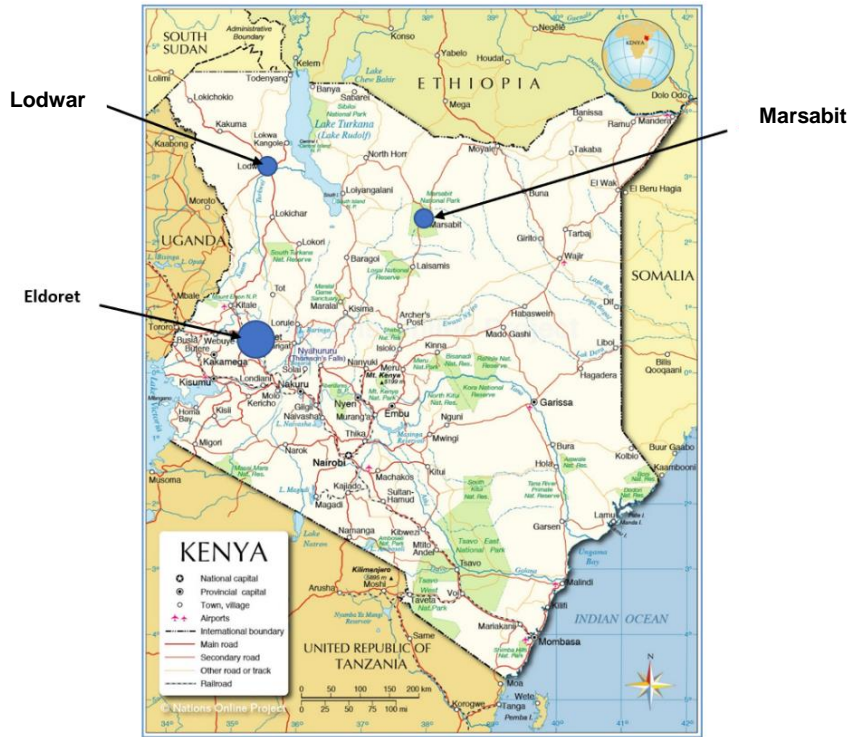


Fig. 2: Map of Kenya with location of capital of proposed solar farms, map from www.nationsonline.org (2018b)

Table 4 shows the population of Zimbabwe, its economics, and the electricity consumption and rates of the country while Figure 3 shows the location of the proposed PV farm in Zimbabwe.

Tab. 4: Zimbabwe population and economic analysis

Population	16.15 million
GDP per capita	\$1,008.60 (USD)
Annual Electricity consumption	7.63 billion kWh
Annual Electricity consumption per capita	472 kWh
Cost of Electricity	\$0.10/kWh
Harare Population	1,560,000
Percent of Population with Access to Electricity	38%

Zimbabwe has the smallest population of the three nations selected for this research, yet it consumes more electricity per capita than Kenya and Ethiopia combined. A 3.75 GW system was simulated near the capital of Harare to power the entire nation. Harare is close enough to the other large cities to avoid significant line losses that will come from transmitting power from the PV farm (www.nationsonline.org, 2018b). It is also close to the border of Mozambique and Zambia, countries that Zimbabwe could sell excess electricity. According to the World Bank, only 38% of the population of Zimbabwe has access to electricity (data.worldbank.org, 2018c). The excess electricity could also be used for disconnected villages once the infrastructure is built to connect them to the grid.



Fig. 3 Map of Zimbabwe with location of proposed solar farms, map from www.nationsonline.org (2018c)

Even though Zimbabwe uses almost the same amount of electricity as Kenya, the power capacity of the solar farm in Zimbabwe was designed to be a little smaller than the power capacity of the farms in Kenya because it has a smaller population. Since Kenya’s population is 3 times larger than Zimbabwe’s, it has the potential to grow larger and faster than Zimbabwe, which means that Kenya needs a larger power capacity for its solar farms as the growing population will require more electricity. Nevertheless, Zimbabwe needs a solar farm that is large enough to provide for the entire country’s power needs and provide enough electricity for potential growth of the nation. The system costs were simulated using wages and expenses that would be common in America. Using a more expensive cost analysis was necessary to avoid underestimating the total cost of the system. The system costs are listed below in Table 5. In the event that the cost of labor, system balancing, and installer margin and overhead can be reduced, the extra money can be used for building a larger system or for improving each nation’s infrastructure.

Tab. 5: System expenses

Component	\$/WDC
Module	0.64
Inverter	0.13
Balancing System Equipment	0.33
Installation labor	0.19
Installer Margin and Overhead	0.72

2. Simulation Results

The simulation tool NREL SAM was used to perform modeling of the proposed PV farms. The software tool NREL SAM has a proven track record as a turn-key tool for aid in designing and simulating renewable energy systems (Blair et al. 2012, Blair et al. 2014, Freeman et al. 2013, Freeman et al. 2014)). Each location chosen within Ethiopia, Kenya, and Zimbabwe was selected because solar farms in these areas yielded the greatest annual energy. Table 6 shows the results for the PV farms in Ethiopia.

Tab. 6: Cost and energy yield of proposed PV plants in Ethiopia

Plant Location in Ethiopia	Proposed PV Plant Number	Facility Power Capacity (GW)	Energy Yield (kWh/kW)	Annual Energy Yield (TWh) (1 st year)	Cost of Facility (Billion USD)	LCOE (real) (¢/kWh)
Addis Ababa	Plant 1	3.0	2,386	7.158	6.035	3.14
Dire Dawa	Plant 2	0.5	2,386	1.193	1.01	3.23
Gondar	Plant 3	0.5	2,283	1.141	1.01	3.10
Total	n/a	4.0	n/a	9.492	8.055	n/a

The plant in Addis Ababa is six times larger than the plants in Dire Dawa and Gondar, and it has the greatest annual energy yield at 7.158 TWh. Gondar has a slightly smaller annual energy yield than Dire Dawa even though they have the same power capacity. This difference is due to weather losses and does not have a significant impact on the overall yield of the system. In total, all three solar farms will produce 9.492 TWh for a country that only consumes 8.14 TWh annually. This means that the country's energy requirement will be completely fulfilled by the solar plants, and they will be able to sell the additional 1.35 TWh of energy to neighboring countries, or the people of Ethiopia will be able to enjoy using more electricity in their homes and businesses. The leveled cost of electricity ranges from 3.10 ¢/kWh to 3.23 ¢/kWh, while the current cost of electricity in Ethiopia is 9 ¢/kWh (ww.worlddata.info, 2018a). This means the cost of electricity will be decreased by around 60%. For a country whose people live on \$2 a day, this would provide significant savings on electricity. Table 7 shows the results for the PV plants in Kenya.

Tab. 7: Cost and energy yield of proposed PV plants in Kenya

Plant Location in Kenya	Proposed PV Plant Number	Facility Power Capacity (GW)	Energy Yield (kWh/kW)	Annual Energy Yield (TWh) (1 st year)	Cost of Facility (Billion USD)	LCOE (real) (¢/kWh)
Lodwar	Plant 1	0.5	2341	1.171	1.01	2.46
Marsabit	Plant 2	0.5	2,282	1.141	1.01	2.50
Eldoret	Plant 3	3.0	2,264	6.792	6.035	3.26
Total	n/a	4.0	n/a	9.194	8.055	n/a

Lodwar and Marsabit were selected as the locations for the 500 MW farms because they had the highest solar insolation and energy yield in Kenya, but they are farther away from Kenya's largest cities than Eldoret. Lodwar has the highest energy yield of the 3 sites at 2341 kWh/kW, and the LCOE at this location is only 2.46 ¢/kWh. The highest LCOE comes from Eldoret at 3.26 ¢/kWh, but this is only 14% of Kenya's current cost of electricity at 23 ¢/kWh (stima.regulusweb.com, 2018). This would also provide the people of Kenya with significant savings, and this may be necessary since most Kenyans live on \$4 per day. The Annual Energy yield of these PV farms is 9.104 TWh, compared to their current consumption of 7.67 TWh (recall, 1TWh = 1e9 kWh). This means Kenya would have an additional 1.434 TWh of electricity they could sell to neighboring countries or consume in their own homes and businesses at a significantly cheaper rate than their current electricity cost. Table 8 shows the results for the proposed PV plant in Zimbabwe.

Tab. 8: Cost and energy yield of proposed PV plant in Zimbabwe

Plant Location in Zimbabwe	Proposed PV Plant Number	Facility Power Capacity (GW)	Energy Yield (kWh/kW)	Annual Energy Yield (TWh) (1 st year)	Cost of Facility (Billion USD)	LCOE (real) (¢/kWh)
Harare	Plant 1	3.75	2146	8.047	7.542	3.44

The 3.75 GW power plant produces an annual yield of 8.047 TWh. Their current annual electricity consumption is 7.63TWh, so they will have an additional 4 GWh of electricity to use for whatever purposes they choose. Their LCOE is 3.44 ¢/kWh, which is 34.4% of their current electricity cost at 10 ¢/kWh. The cost of this system would be about \$7.542 billion (USD), and for a country whose annual GDP is \$16.62 billion, this would cost them 45.4% of their annual GDP. It would be necessary for America to purchase this system for Zimbabwe to improve their standard of living without putting crippling financial strain on the nation. Figures 4, 5, and 6 show the monthly energy production of the proposed PV plants in Ethiopia, Kenya, and Zimbabwe, respectively. Even though Zimbabwe is in the Southern Hemisphere and should have a higher energy yield during the fall and winter months, the energy production of the PV plants decreases between November to March because this is the Wet (Monsoon) Season (www.safaribookings.com, 2018). The Dry Season occurs between April to October, which is reflected in Figure 6 as the energy production is at its peak during these months.

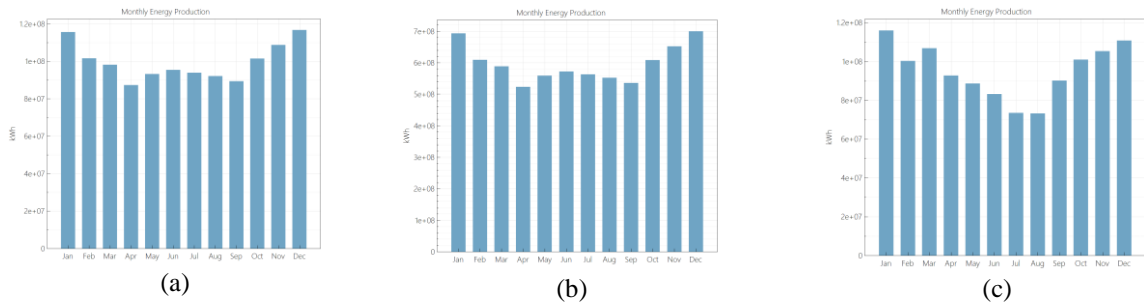


Fig. 4: NREL SAM simulation results of monthly energy production of proposed PV plant in Ethiopia (a) 500 MW proposed PV farm in Dire Dawa, (b) 3.0 GW proposed PV farm in Addis Ababa, (c) 500 MW proposed PV farm in Gondar

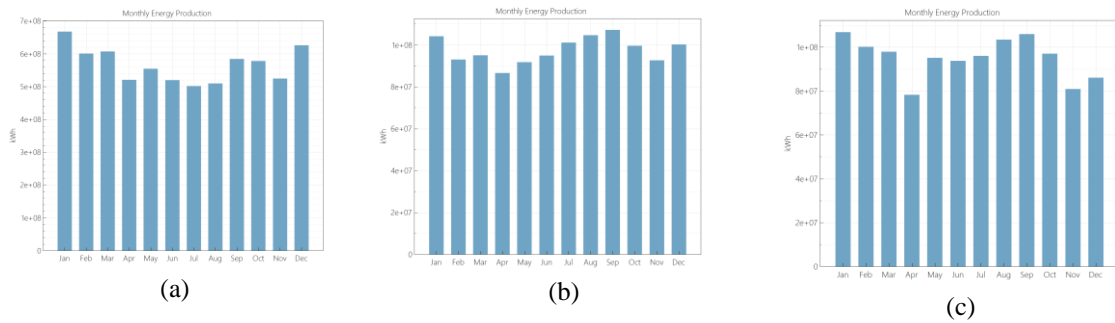


Fig. 5: NREL SAM simulation results of monthly energy production of proposed PV plant in Kenya

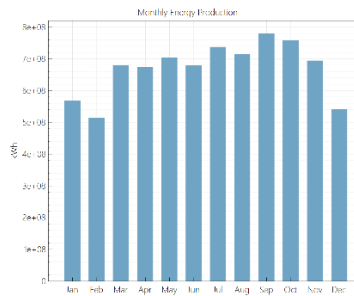


Fig. 6: NREL SAM simulation results of monthly energy production of proposed PV plant in Zimbabwe

Table 9 shows the amount of land required for building PV farms of this scale.

Tab. 9: Amount of land required for each proposed PV farm

Proposed PV farm location	Area (sq. miles)	Area (acres)
Addis Ababa, Ethiopia	17.518	11,212
Dire Dawa, Ethiopia	2.919	1,868
Gondar, Ethiopia	2.919	1,868
Lodwar, Kenya	2.919	1,868
Marsabit, Kenya	2.919	1,868
Eldoret, Kenya	17.518	11,211
Harare, Zimbabwe	21.898	14,014

The 500 MW PV farms would require almost 3 mi² of land for all the solar panels, while the 3.0 GW farms would require around 17.5 mi². This comes to a total of 23.356 mi² of land required for the solar farms in Kenya and Ethiopia. This area is almost as large as the city of Boulder, Colorado, which occupies roughly 25 mi² of land (United States Census Bureau, 2017). Zimbabwe requires 21.898 mi² of land for their 3.75 GW solar farm. The Topaz Solar Farm is a 550 MW solar farm that was constructed in San Luis Obispo, CA (www.power-technology.com, 2018). The PV farms in Kenya and Ethiopia have a capacity 7 times larger than the Topaz Solar Farm, meaning that these solar farms have the potential to create thousands of good-

paying jobs. Maintenance costs on the solar farms are also necessary for evaluation. The 500 MW solar farms will cost at least \$10 million for the first year of maintenance, while the 3 GW plants will cost roughly \$60 million (USD) a year to maintain. This means that Kenya and Ethiopia will have to spend \$80 million a year to maintain their facilities, with costs varying according to their inflation rates. The 3.75 GW plant in Zimbabwe will cost \$75 million to maintain for the first year. If Kenya sells its electricity at \$0.04/kWh, and it produces 9.104 billion kWh in the first year, they would make \$364.2 million in the first year. If Ethiopia and Zimbabwe sold their electricity for the same rate, the plants would make \$380 million and \$322 million, respectively. This would be more than enough money to continue operating the facilities, and the additional funds could go towards improving their infrastructure.

3. Discussion and Conclusions

The construction of these solar farms could have a tremendous impact on the lives of the 167 million people living in Ethiopia, Kenya, and Zimbabwe. The total cost of these seven systems was calculated using labor costs that would be similar to building PV systems in America. Labor costs in Africa are much cheaper than in America. Kenya has the highest per capita GDP of the three selected nations, and the highest minimum wage in Kenya is \$2.60 per hour, or \$288 per month (USD). To put this into perspective: if 10,000 Kenyans were paid \$600 a month to construct these sites for 2 years, the labor would only cost \$144 million, while the current labor cost of the 3 systems is estimated to be \$760 million. The remaining \$616 million could be used to improve the infrastructure of Kenya's electrical grid, providing power to millions of people without access to electricity. Additionally, the installer margin and overhead costs a total of \$2.88 billion for all three solar farms. This accounts for transportation of the modules and other potential expenses. Lodwar and Marsabit are not connected to railroads, so the transportation of all materials will have to be conducted via trucks on dirt roads. If this cost could be reduced as well, Kenya would have even more money to build up its infrastructure. These same cost reductions could be used for the solar farms in Ethiopia and Zimbabwe. Paying workers \$600 dollars a month means they would earn \$7,200 a year. This means the income of the solar farm workers in Zimbabwe would be 600% higher than the average per capita GDP, and the income for the Ethiopian workers would be 900% higher than the average per capita GDP. The saved expenses could be used to build up the infrastructure of these nations as well. Fifty-eight percent of the people in Ethiopia and 62% of the people in Zimbabwe do not have access to electricity (data.worldbank.org, 2018c) The additional money would be vital to providing electricity to the entire nation and connecting communities who do not have any access to electricity. The current power plants in each country should remain operational to provide electricity to the people at night. Massive battery banks could be installed to store some of the electricity that is gathered during the day, but this may not be a practical solution for an entire nation. Lithium-ion batteries are very expensive, recycling them is difficult, and if the batteries burst and spill into the environment, cleaning up the spilled contaminants would be very difficult (waste-management-world.com, 2018). Africa also experiences very intense rains during the Wet Season, would could damage large battery banks if they are not stored correctly. The most practical use for large battery banks would be storing electricity for the main cities to use at night. Limiting the batteries to large cities may help to avoid potential environmental hazards, and it would reduce the CO2 emissions that are created to power the most populated cities, but keeping the current power plants active may be the best solution for powering the nations at night. The current power plants may also become necessary once more communities gain access to the electrical grid. Additional transmission lines will be necessary for transporting the PV generated electricity throughout each nation. The cost of transmission lines varies depending on the voltage capacity of the lines. High-voltage 230kV power lines cost \$1 million per mile, while 139kV power lines cost \$390,000 per mile (www.xcelenergy.com, 2018, www.elp.com, 2018). Using the current left-over funds of \$6.35 billion, 16,282 miles of 139 kV power lines could be used throughout each of these countries, providing power to unreached areas or providing additional power to areas that have a higher electricity demand. If the 230kV power lines are used, the nations would be able to construct 6,350 miles of high-voltage lines. The billions of dollars saved during the construction of the PV farms could also be used to purchase thousands of miles of power lines. Millions of people would no longer have to live without electricity. Farms could power irrigation pumps for their fields, children could do their homework under luminescent bulbs instead of lanterns, communities could have consistent electricity, and economies could grow as nations are provided with constant, stable sources of power.

4. References

Blair, N., Dobos, A., Freeman, J., Neises, T., Wagner, M., Ferguson, T., Gilman, P., Janzou, S.

<http://www.nrel.gov/docs/fy14osti/61019.pdf>, accessed August 8, 2018.

Blair, N., Dobos, A., Sather, N. (2012). <https://www.nrel.gov/docs/fy12osti/54676.pdf>, accessed August 8, 2018.

www.elp.com/articles/powergrid_international/print/volume-18/issue-2/features/underground-vs-overhead-power-line-installation-cost-comparison-.html, accessed August 8, 2018.

Freeman, J., Whitmore, J., Kaffine, L., Blair, N., Dobos, A. (2014). <https://www.nrel.gov/docs/fy14osti/61497.pdf>, accessed August 8, 2018.

Freeman, J., Whitmore, J., Kaffine, L., Blair, N., Dobos, A.. (2013), <https://www.nrel.gov/docs/fy14osti/60204.pdf> , accessed August 8, 2018.

V. Rishi Kumar <https://www.thehindubusinessline.com/news/national/global-focus-on-kurnool-solar-park/article9945725.ece>, accessed August 8 2018.

“Electricity Cost in Kenya”, stima.regulusweb.com/historic, accessed August 8 2018.

“Political Map of Ethiopia.” www.nationsonline.org/oneworld/map/ethiopia-political-map.htm., accessed August 8 2018.

“Political Map of Kenya.” www.nationsonline.org/oneworld/map/kenya-political-map.htm, accessed August 8 2018.

“Political Map of Zimbabwe.” www.nationsonline.org/oneworld/map/zimbabwe-political-map.htm, accessed August 8 2018.

John F. Weaver <https://electrek.co/2018/01/29/10-really-cool-solar-power-installations/> accessed 30 January 2018.

“Electric Power Consumption” <https://data.worldbank.org/indicator/EG.USE.ELEC.KH.PC>, accessed August 8 2018.

“Access to Electricity” data.worldbank.org/indicator/EG.ELC.ACCS.ZS., accessed August 8, 2018.

“Energy Consumption in Ethiopia.” Worlddata.info, www.worlddata.info/africa/ethiopia/energy-consumption.php, accessed August 8 2018.

“Population, Total GDP Growth” worldbank.org/indicator/SP.POP.TOTL, accessed August 8 2018.

“GDP per Capita” data.worldbank.org/indicator/NY.GDP.PCAP.CD. accessed August 8 2018.

https://www.xcelenergy.com/staticfiles/xcel/Corporate/Corporate%20PDFs/OverheadVsUnderground_FactSheet.pdf , accessed August 8, 2018.

“Zimbabwe Weather & Climate.” www.safaribookings.com/zimbabwe/climate accessed August 8, 2018.

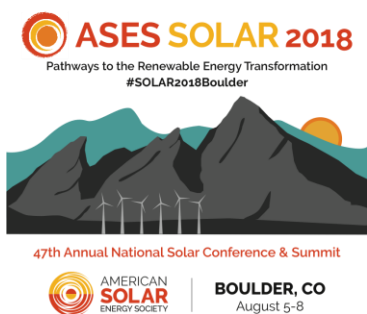
"2016 U.S. Gazetteer Files". United States Census Bureau., accessed Jul 25, 2017.

<https://www.power-technology.com/projects/topaz-solar-farm-california/>, accessed August 8,2018

“Energy Consumption in Kenya.” www.worlddata.info/africa/kenya/energy-consumption.php., accessed August 8, 2018.

“Energy Consumption in Zimbabwe.” www.worlddata.info/africa/zimbabwe/energy-consumption.php., accessed August 8, 2018.

Zong, Jie, et al. “Frequently Requested Statistics on Immigrants and Immigration in the United States.” Migrationpolicy.org, 27 Feb. 2018, www.migrationpolicy.org/article/frequently-requested-statistics-immigrants-and-immigration-united-states, accessed August 8, 2018.



Conference Proceedings

ASES National Solar Conference 2018

Boulder, Colorado August 5-8, 2018

Simulation and Lessons Learned from the Ivanpah Solar Plant Project

Jacob Tharp¹ and Kevin R. Anderson²

¹ California State Polytechnic University/STARE Lab, Pomona (USA)

² California State Polytechnic University/STARE Lab, Pomona (USA)

kranderson1@cpp.edu

Abstract

The Ivanpah CSP plant is studied herein. Ivanpah's Tower 1 central collector was simulated using the NREL SAM software toolkit. Input parameters for the Ivanpah CSP was found via public domain websites regarding Ivanpah. Outputs from NREL SAM were compared to hand calculated values and available data from the actual output of Ivanpah. Solar Irradiation data was used from the National Solar Radiation. The solar insolation data was taken for the year 2015 in which there is data available for the energy production from Ivanpah. The actual total output from Ivanpah 1 during 2015 was 209,975,000 kWh. It is published that Ivanpah underproduced significantly in 2015 meaning that calculated values are drastically greater than the data given. The simulations herein show that NREL SAM gave an annual output of 292,469,024 kWh and hand calculations gave an output of 318,414,566 kWh. The paper concludes with a section on lessons learned.

Keywords: *CSP, modeling, simulation*

1. Introduction

The Ivanpah CSP Plant was built utilizing three separate Power tower central collectors named Ivanpah 1, 2 and 3. The focus of this report will be Ivanpah 1, the first tower built. This is a 126 MW tower utilizing 53,500 heliostats of 14 m² focused at a 140 m tall tower and energy is harvested through a rankine cycle utilizing a Siemens SST-900 steam turbine (www.brightsourceenergy.com). This paper presents a case study of the Ivanpah solar plant including a comprehensive literature review regarding the motivation and construction of the facility. The case study provides insight into how the theory, modeling and actual performance data of a large scale concentrated solar energy project such as Ivanpah can be used to examine the overall efficiency and benefits of renewable energy technologies. The Ivanpah solar plant located in Southern Nevada was simulated using the National Renewable Energy Laboratory System Advisor Model (NREL SAM) simulation software with the power tower concentrating solar power utilizing direct steam option. The NREL SAM simulations includes information on performance of the system and data on the cost for the lifetime of the system including Levelized Cost of Energy (LCOE) and Internal Rate of Return (IRR). The outputs from NREL SAM are verified using measured data collected from the Ivanpah power-plant. The results are also compared to fundamental solar energy engineering theory. The paper concludes with a discussion on lessons learned from the Ivanpah solar project. The paper concludes with a narrative

illustrating how Ivanpah can be used as a learning tool and aid in rolling out renewable energy technologies to a wider population. This system was modelled in NREL SAM with parameters matching as close as possible to the actual design of Ivanpah 1. This includes heliostat size and layout, tower size, turbine design and location resource. Table 1 shows the various design parameters in which NREL SAM and the hand calculations were performed with to model the system. An aerial view of the Ivanpah CSP facility is shown in Figure 1.



Fig. 1: Ivanpah CSP Facility (www.ucsusa.org)

Ivanpah was built utilizing three separate Power tower central collectors named Ivanpah 1, 2 and 3. The total cost of the project was \$2.2B. The Ivanpah Solar Electric Generating System (ISEGS) is located in the Mojave Desert, near the California / Nevada border, in San Bernardino County, CA, USA. The project was certified by the Energy Commission on September 22, 2010, and began commercial operation in December 2013. The ISEGS is a 386 megawatt (MW) project consisting of three individually certified solar concentrating thermal power plants, based on distributed power tower and heliostat mirror technology, in which heliostat (mirror) fields focus solar energy on power tower receivers near the center of each heliostat array. Power Plant 1 is a nominal 120 MW plant located on approximately 914 acres and consists of 53,500 heliostats. Power Plant 2 is a nominal 133 MW plant located on approximately 1,097 acres and consists of 60,000 heliostats. Power Plant 3 is a nominal 133 MW plant located on approximately 1,227 acres and contains 60,000 heliostats. Each site has a single receiver and heliostat array. The focus of this paper will be Ivanpah 1, the first tower built. This is a 126 MW tower utilizing 53,500 heliostats of 14 m² (914 acres) focused at a tower 140 m tall, energy is harvested through a Rankine cycle utilizing a Siemens SST-900 steam turbine. This system was modelled herein using NREL SAM (<https://sam.nrel.gov/>). This includes heliostat size and layout, tower size, turbine design and location resource. The model results are presented and compared to reported performance. Main take-aways are the energy performance of the system and financial analysis, namely Levelized Cost of Energy (LCOE) and Internal Rate of Return (IRR). In each solar plant, one Rankine-cycle reheat steam turbine receives live steam from the solar collector located in the power block at the top of a tower. Each plant also includes two natural gas-fired steam boilers: an auxiliary boiler and a nighttime preservation boiler. The auxiliary boiler is used for thermal input to the steam turbine during the morning start-up cycle to assist the plant in coming up to operating temperature. The auxiliary boiler is also operated during transient cloudy conditions, in order to maintain the steam turbine. Each solar plant uses dry cooling to conserve water, and limited to a combined 100 acre-feet per year of water for plant operations. The use of water in the desert has always been a contentious issue, and the drought has made water an even bigger issue in the West. Dry-cooling allows the project to reduce water usage by more than 90% over solar thermal technologies that use "wet-cooling" systems. We use water in two ways: to clean the mirrors, and to produce steam for electricity generation. To conserve water, we use a dry cooling process to condense the steam back to liquid, which is then recycled back to the boiler in a closed loop cycle. All power plants use water; dry cooling uses less water than nuclear (helioscsp.com a). No thermal storage is used in the Ivanpah power plant. Ivanpah doesn't have storage, but most future projects, those that are being built in 2017 and beyond utilize thermal storage. The benchmark levelized cost of electricity (LCOE) for global CSP projects will fall below \$50/MWh in 2018, two of the industry's leading consultants predicted at CSP Seville 2017 (helioscsp.com b).

2. Modeling and Simulation

Herein the NREL SAM tool is used to model the Ivanpah 1 tower. The simulation tool NREL SAM was used to perform modeling of the proposed PV farms. The software tool NREL SAM has a proven track record as a turn-key tool for aid in designing and simulating renewable energy systems (Blair et al. 2012, Blair et al. 2014, Freeman et al. 2013, Freeman et al. 2014)). NREL SAM is a program from the National Renewable Energy Laboratory used to evaluate performance and financial viability of renewable energy systems. NREL SAM has models for various renewable energies including: Photovoltaics, concentrating collectors, central towers, biofuel, geothermal and wind. Power tower central collectors utilizing direct steam will be the focus of this report. Table 1 lists the pertinent input parameters for the NREL SAM model of Ivanpah Tower 1.

Tab. 1: NREL SAM model inputs

Number of Heliostats	53,500
Single Heliostat Area (m ²)	14.04
Total Heliostat Area (m ²)	751140
Tower Height (m)	140
Boiler Height (m)	23.8
Turbine	Siemens SST-900
Output Rating (MW)	126
Capacity Factor	27.4%
Location Resource	35.57°N 115.47°W

Utilizing the parameters from Table 1, the NREL SAM calculations were performed. Below the inputs for both the NREL SAM simulation and independent hand calculations using EXCEL are discussed. The outputs from each of these will be discussed in the results section against actual data collected from published performance data of Ivanpah. The two main focuses of this research are the energy performance of the system and financial analysis, namely LCOE (Levelized Cost of Energy) and IRR (Internal Rate of Return).

2.1 NREL SAM Modeling Methodology

NREL SAM takes into account many parameters when calculating the performance of the system, These include: heliostat, tower, central receiver and Rankine turbine designs. The inputs were made to closely resemble the values from Table 1. Figures 2 through 5 show the inputs used in NREL SAM Graphical User Interface (GUI) used to define, simulate and determine the performance of the system. This includes heliostat, Rankine cycle components and steam turbine generator.

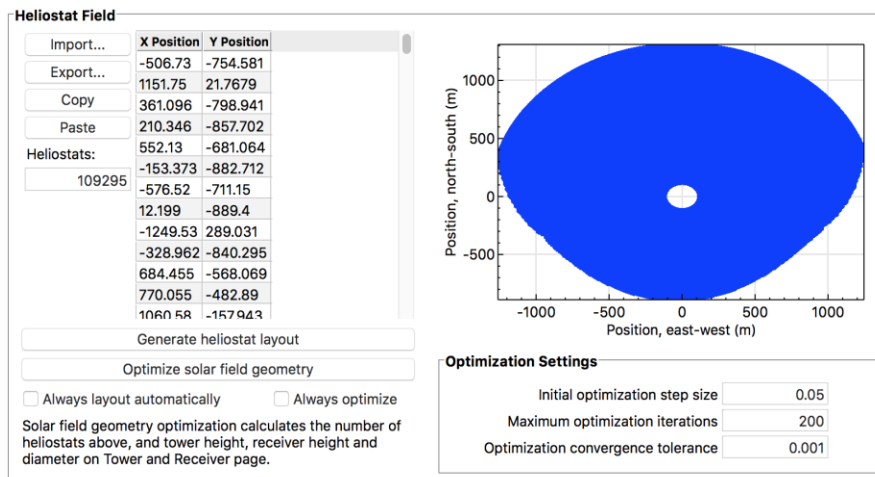


Fig. 2: Heliostat field NREL SAM GUI inputs

Heliostat Properties	
Heliostat width	3.2 m
Heliostat height	2.2 m
Ratio of reflective area to profile	1
Single heliostat area	7.04 m ²
Image error (slope, single-axis)	1.53 mrad
Reflected image conical error	4.32749 mrad
Number of heliostat facets - X	2
Number of heliostat facets - Y	8
Heliostat focusing method	Ideal
Heliostat canting method	On-axis

Heliostat Operation	
Heliostat stow/deploy angle	8 deg
Wind stow speed	15 m/s
Heliostat startup energy	0.025 kWe-hr
Heliostat tracking power	0.055 kWe
Design-point DNI	950 W/m ²

Atmospheric Attenuation	
Polynomial coefficient 0	0.006789
Polynomial coefficient 1	0.1046 1/km
Polynomial coefficient 2	-0.017 1/km ²
Polynomial coefficient 3	0.002845 1/km ³
Average attenuation loss	7.0 %

Fig. 3: Heliostat field NREL SAM GUI inputs

Direct Steam Receiver	
Receiver diameter	19.3891 m
Receiver height	23.8084 m
Number of groups of two panels	6
Number of panels	12
Coating Emittance	0.88
Coating Absorptance	0.94

Boiler	
Boiler height	10.4287 m
Maximum boiler flux	800 kWt/m ²
Outside diameter of boiler tubes	0.0254 m
Thickness of boiler tubes	0.002159 m
Boiler tube material	Stainless AISI...
Target boiler output steam quality	0.5
Boiler heat loss (estimated)	96 kW/m ²

Superheater	
Superheater height	8.47552 m
Maximum superheater flux	500 kWt/m ²
Outside diameter of superheater tubes	0.01905 m
Thickness of superheater tubes	0.001651 m
Superheater material	Stainless AISI...
Superheater outlet temperature set point	550 °C
Superheater heat loss (estimated)	80 kW/m ²

Reheater	
Reheater height	4.90415 m
Maximum reheater flux	350 kWt/m ²
Outside diameter of reheater tubes	0.0381 m
Thickness of reheater tubes	0.002159 m
Reheater material	Stainless AISI...
Reheater outlet temperature set point	500 °C
Reheater heat loss (estimated)	87.5 kW/m ²

Fig. 4: Rankine Cycle NREL SAM GUI inputs

Plant Design	
Design turbine gross output	137 MWe
Estimated gross to net conversion factor	0.9
Net nameplate capacity	123.3 MWe
Rated cycle efficiency	0.404
Design thermal input power	339.109 MWt
High pressure turbine inlet pressure	160 bar
High pressure turbine outlet pressure	40 bar
Design reheat mass flow rate fraction	0.85
Fossil backup boiler LHV efficiency	0.9
Steam cycle blowdown fraction	0.02

Fig. 5: Turbine design NREL SAM GUI inputs

The various parameters used to populate the GUIs of Figure 2 through 5 are taken from practical experience, web based research on the specifications of Ivanpah CSP, and taking defaults from NREL SAM. The financial analysis GUI of NREL SAM is shown in Figure 6. This interface allows the user to define the direct capital costs associated with the particular renewable energy project being analyzed. Here, the direct capital costs of the heliostat field, tower, receiver, and power cycle are input into NREL SAM.

Direct Capital Costs			
-Heliostat Field			
Reflective area	769,437 m ²	Site improvement cost	16.00 \$/m ² \$ 12,310,989.00
		Heliostat field cost	145.00 \$/m ²
		Heliostat field cost fixed	0.00 \$ \$ 111,568,336.00
-Tower			
Tower height	140 m		
Receiver height	23.8084 m	Tower cost fixed	3,000,000.00 \$
Heliostat height	2.2 m	Tower cost scaling exponent	0.0113 \$ 12,916,748.00
-Receiver			
Receiver area	1450.24 m ²	Receiver reference cost	48,800,000.00 \$
		Receiver reference area	1110 m ²
		Receiver cost scaling exponent	0.7 \$ 58,843,816.00
-Thermal Energy Storage			
Storage capacity	0 MWh	Thermal energy storage cost	0.00 \$/kWh \$ 0.00
-Power Cycle			
Cycle gross capacity	137 MWe	Fossil backup cost	0.00 \$/kWh \$ 0.00
		Balance of plant cost	0.00 \$/kWh \$ 0.00
		Power cycle cost	1,100.00 \$/kWh \$ 150,700,000.00
		Subtotal	\$ 346,339,904.00
-Contingency			
		Contingency cost	7 % of subtotal \$ 24,243,792.00
		Total direct cost	\$ 370,583,680.00

Fig. 6: Equipment capital cost NREL SAM GUI inputs

2.2 Excel Hand Calculations

In order to perform an indepent sanity check on the output produced by NREL SAM, an EXCEL spreadsheet was constructed based on hand-calculations. The performance of the system using EXCEL was modelled by taking the average annual solar irradiance for that location and multiplying it by the efficiency of the entire system including: collector losses, field losses and the steam turbine efficiency and finally by the total Heliostat area. Table 2 lists the efficiencies used in the EXCEL calculations.

Tab. 2: EXCEL hand-calculations component efficiencies

Component	Efficiency (%)
Convective / conduction parasitic losses	99.8
Radiative losses	93.7
Spillage losses	98.8
Reflective losses	90.0
Cosine / shadowing and blockage	82.9
Attenuation	94.6
Capacity factor	27.4

The various losses listed in Table 2 were based off of a design study done for solar thermal power plants done in 1979 by the Stearns Rogers Engineering company (www.powerfromthesun.net). The capacity factor was based off of the max efficiency of the Siemens SST-900 steam turbine (www.energy.siemens.com). The capacity factor is the efficiency of the steam turbine generator (ratio of its actual output over a period of time, to its potential output if it were possible for it to operate at full nameplate capacity continuously over the same period of time).

3. Results

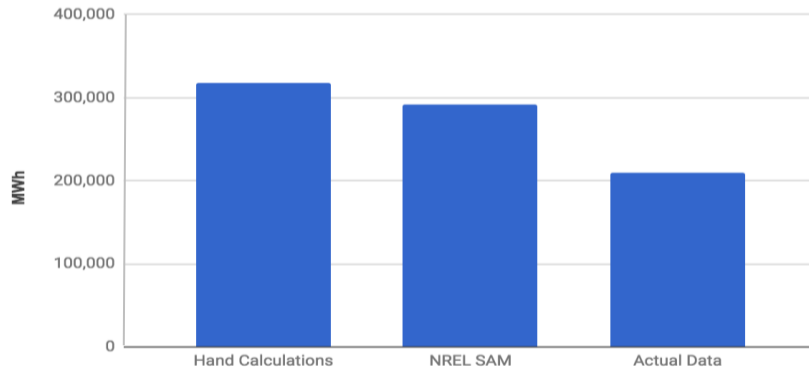
Results for the NREL SAM simulation and EXCEL hand-calculations are now compared to actual performace data for the Ivanpah CSP taken from (en.wikipedia.org). The performacne data used used for the year 2015 as shonw in Table 3.

Tab. 3: Ivanpah CSP Tower 1 performance data (<https://en.wikipedia.org>)

Year	Jan	Feb	Mar	Apr	May	Jun	Jul	Aug	Sept	Oct	Nov	Dec	Total
2014	5,632	4,460	4,946	9,130	15,879	23,722	12,277	16,807	19,743	17,455	15,993	5,922	151,966
2015	4,448	16,471	20,010	25,281	12,380	25,126	19,575	23,404	21,333	11,813	16,230	13,904	209,975
2016	7,599	23,686	18,427	13,284	26,006	32,875	31,796	24,403	26,860	20,616	19,663	10,440	255,655
2017	11,310	11,699	12,283	11,656	28,709	34,797	21,742	23,437	24,803				180,436
Total													798,032 MWh

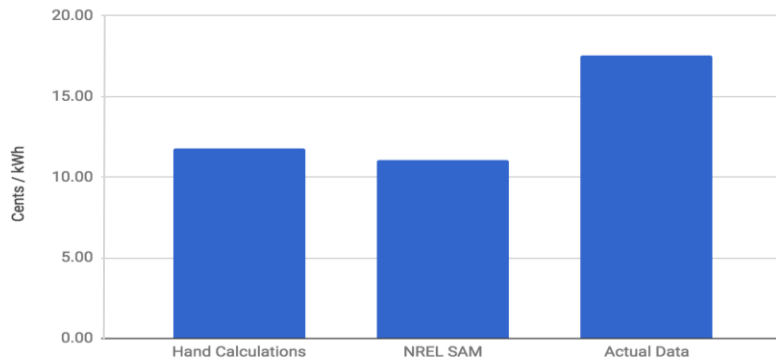
Table 4 shows the comparison of values of energy received (MWh) for EXCEL hand-calculations, NREL SAM simulation and data of Table 3 for Ivanpah Tower 1.

Tab. 4: Comparison of energy output



As shown in Table 4, the EXCEL hand-calculations were shown to have the largest output (being the most conservative), followed by the NREL SAM simulation, while the Ivanpah actual performance data was shown to be the worst. The actual output data of the Ivanpah CSP is lower than expected outcomes for the facility (<en.wikipedia.org>). The California Energy Commission (CEC) attributes this due to clouds, jet contrails and weather fluctuations (<en.wikipedia.org>). Table 5 shows the differences in LCOE of the different methods.

Tab. 5: Comparison of LCOE



The actual LCOE is the highest because the plant underproduced in the year 2015 causing the LCOE to jump when the cost of the plant is the same. Herein $LCOE = (\text{sum of costs over lifetime}) / (\text{sum of electrical energy produced over lifetime})$. There are two different types of LCOE that can be calculated: nominal and real. Which of these is calculated depends on whether the nominal or real discount factor is used in the energy production term of the LCOE equation. The nominal LCOE is higher than the real LCOE because the nominal LCOE is a current value calculation that is not adjusted for inflation, whereas the real LCOE is a constant-value, inflation-adjusted calculation. The real LCOE is generally preferred for long-term analysis (<http://solarprofessional.com>).

Table 6 gives a summary of the main outputs from the NREL SAM simulation financial-economic analysis. The key metrics to take from this study are the annual energy output of 292,469,024 kWh corresponding to a LCOE (real) of 11.09 cents / kWh and an IRR of 12.59%.

Tab. 6: NREL SAM financial-economic analysis output summary

Metric	Value
Annual energy (year 1)	292,469,024 kWh
Capacity factor (year 1)	27.1%
Annual Water Usage	57,353 m ³
PPA price (year 1)	14.62 ¢/kWh
PPA price escalation	1.00 %/year
Levelized PPA price (nominal)	15.17 ¢/kWh
Levelized PPA price (real)	11.93 ¢/kWh
Levelized COE (nominal)	14.10 ¢/kWh
Levelized COE (real)	11.09 ¢/kWh
Net present value	\$33,004,256
Internal rate of return (IRR)	11.00 %
Year IRR is achieved	20
IRR at end of project	12.59 %
Net capital cost	\$490,318,112
Equity	\$244,466,688
Size of debt	\$245,851,440

The salient take-aways from Table 6, are that the Ivanpah CSP Plant 1 affords an annual energy output of 292,469,024 kWh corresponding to an LCOE of 11.09 ¢/ kWh (110.9 \$/MWh) and IRR of 12.59%. This is in comparison US average LCOE of CSP in 2015 is 240 \$/MWh. Next, the transient behavior of the Ivanpah CSP Tower 1 is presented. NREL SAM produces time history trends of the energy production of the powerplant. Figure 7 shows the ratio of receiver power to state total (MWt) (blue trace) and cycle gross electrical power produced (orange trace) (MWe) for a 5 day period in June. Recall, MWe (Megawatts electric) refers to the electricity output capability of the plant, and MWt (Megawatts thermal) refers to the input energy required, i.e. a coal-fired power plant rated at 1000 MWe and 3000 MWt will require supply of 3000 MW of heat from burning coal for every 1000 MW of electricity it produces (www.energyeducation.ca).The decrease in the electricity production illustrated in Figure 7 is due to the inefficiencies of the Rankine cycle and and the turbine.

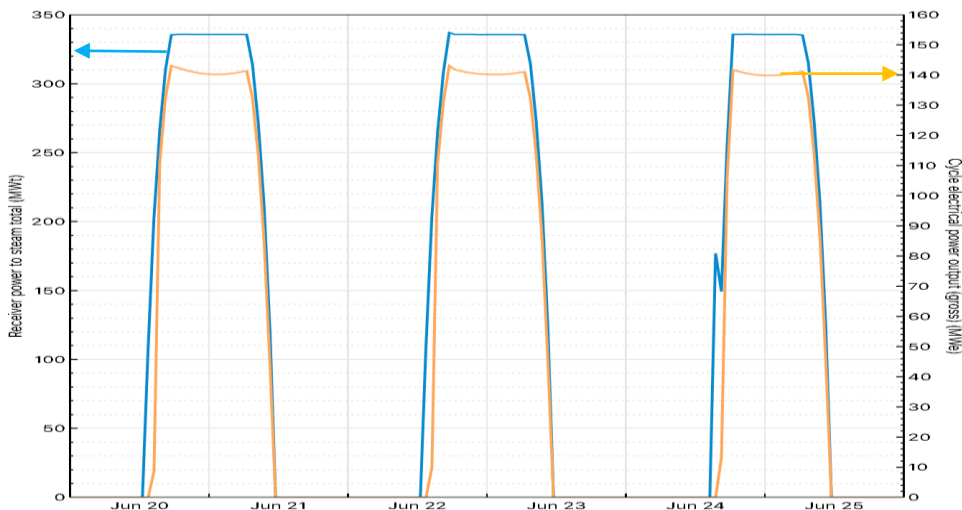


Fig. 7: NREL SAM receiver to steam power ratio and cycle electrical power output (blue trace = receiver power to steam total (MWt), orange trace = cycle gross electrical power output (MWe))

Figure 8 shows the total power generated from the system in the same period as above. Peaks and valleys correlate with bi-hourly irradiance data. Producing during the day and dropping below in dark hours.



Fig. 8: NREL SAM system power generated

Spreadsheets EXCEL calculations were performed using a yearly average Solar irradiance number in kWh/m²/day. This was then used along with the total area of the heliostat field and the efficiency given by Table 2 to find the kWh per year. This is shown in Table 7 below.

Tab. 7: EXCEL hand-calculation energy output

Component	Parametric value
Number of heliostats	53,500
Single heliostat area (m ²)	14.04
Efficiency	18%
Solar Irradiance per day (kWh/m ² /day)	6.5
Solar Irradiance flux (kWh/m ²)	2372.5
Total energy produced (kWh)	318,414,566

As shown in Table 7 this is the greatest calculation of energy output of all three methods (EXCEL, NREL SAM, actual performance data). The EXCEL calculations are over-conservative and place an upper bound on the analysis, since they were performed using a yearly average solar irradiance value. This data was then used along with the total area of the heliostat field and the efficiency to find the kWh per year. Calculation of LCOE and IRR using EXCEL were done by using cash flow values given by the NREL SAM simulation output. The IRR found from EXCEL was 12.43%. Table 8 shows a comparison of the calculated values of the energy production and the LCOE for each method (NREL SAM, EXCEL hand-calculations, actual data).

Tab. 8: EXCEL hand-calculation energy output

Method of analysis	Energy produced (kWh)	LCOE (¢/kWh)
NREL SAM simulation	292,469,024	11.76
EXCEL hand-calculation	318,414,566	11.09
Actual performance data	209,965,000	17.53

It is worth noting that an LCOE of \$50/MWh (5¢/kWh) is currently the baseline for CSP with TES (helioscp.com b). Thus, we see that the LCOE of Ivanpah 1, which does not utilize TES of 11.76 ¢/kWh is a factor of two greater than renewable energy technology of CSP with TES. The rationale for the energy production of the actual performance of the Ivanpah CSP Tower 1 is attributed to the use of natural gas fired auxiliary boilers as discussed below in the Lessons Learned section of this paper.

4. Lessons Learned

As noted above, the EXCEL hand calculations gave the greatest output of the system at 318,414,566 kWh. Next, was the simulations of NREL SAM predicted an output of 292,469,024 kWh. Finally, the actual output of Ivanpah was 209,975,000 kWh. This was much lower due to unexpected conditions experienced by the plant. The LCOE was calculated for each and they were 11.09 ¢/ kWh for NREL SAM, 11.76 ¢/ kWh for hand calculated data and 17.53 ¢/ kWh for actual performance data. If Ivanpah CSP Tower 1 was working at expected conditions then it would expect to closely resemble the results predicted by the NREL SAM model. Recently, several studies and reports have unveiled some of the reasons of sub-optimal performance of the Ivanpah CSP. In the study of (www.pe.com) it is noted that Ivanpah is using increasing amounts of natural gas. For 2015, the second year of Ivanpah’s operation carbon emission were 68,676 metric tons, more than twice the pollution threshold for power plants in California to be required to participate in the California state cap and trade program to reduce carbon emissions. The fundamental operating premise of Ivanpah is to use hundreds of thousands of mirrors oriented in an array to focus heat from the sun onto boiler towers, thus boiling the water and generating steam to drive turbines to produce electricity. However, the Ivanpah plant also employs natural gas fired auxiliary boilers at nighttime in order to keep the system primed and to heat water in the tower boilers, This allows electricity production to start up more quickly when the sun rises each morning. Natural gas is also burned during periods of intermittent cloud cover. The use of natural gas auxiliary boilers was not fully publically disclosed at the onset of the construction of the Ivanpah power plant (www.pe.com). Carbon emissions from Ivanpah per (www.pe.com) are shown below in Figure 8.

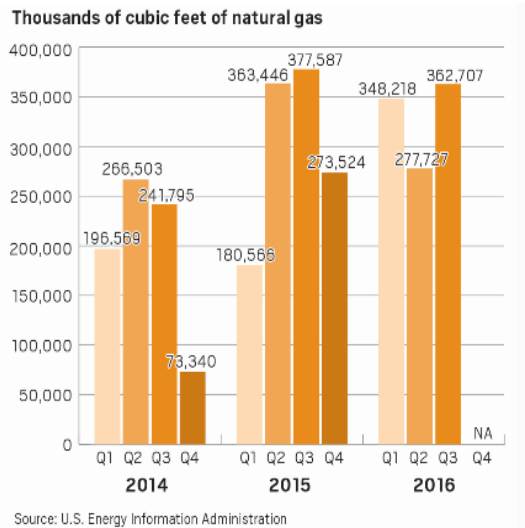


Fig. 8: Ivanpah carbon emissions (www.pe.com)

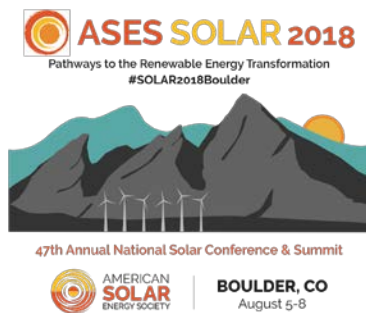
From the study (www.breitbart.com), it is reported that Ivanpah is using about 1.4 billion cubic feet of natural gas a year. Ivanpah has an exemption from state rules to qualify as an alternative energy source, because only 5% of its electrical generation is due to daylight burning of natural gas, according to the California Energy Commission. The report of (www.wsj.com) provides a commentary on the plant operational technical difficulties, which were not predicted upon installation of Ivanpah, such as the need for auxiliary gas boilers and unpredicted cloud, cover in the region of the 3500 acre (5.47 square miles) installation. According to the recent study of (www.renewableenergyworld) as of Feb. 2017 Ivanpah’s electricity generation improved dramatically with utput from one of the boilers improving to 80% since the plant opened in 2014.

5. Conclusion

This paper has presented the simulation and analysis of the Ivanpah CSP Tower 1 facility. The software NREL SAM has been used to simulated the performance of the system. Results from NREL SAM have been compared to EXCEL based hand-calculations as well as actual performance data for the Ivanpah CSP Tower 1 energy production. A comparison of LCOE and energy production is given. The paper concludes with a brief summary of lessons learned from research performed on the Ivanpah project.

6. References

- Blair, N., Dobos, A., Freeman, J., Neises, T., Wagner, M., Ferguson, T., Gilman, P., Janzou, S.
<http://www.nrel.gov/docs/fy14osti/61019.pdf>, accessed August 8, 2018.
- Blair, N., Dobos, A., Sather, N. (2012). <https://www.nrel.gov/docs/fy12osti/54676.pdf>, accessed August 8, 2018.
- <http://www.breitbart.com/california/2017/01/23/solar-inconvenient-truth-ivanpah-plant-top-fossil-fuel-burner>, accessed August 8, 2018.
- Freeman, J., Whitmore, J., Kaffine, L., Blair, N., Dobos, A. (2014).
<https://www.nrel.gov/docs/fy14osti/61497.pdf>, accessed August 11, 2018.
- Freeman, J., Whitmore, J., Kaffine, L., Blair, N., Dobos, A. (2013),
<https://www.nrel.gov/docs/fy14osti/60204.pdf>, accessed August 11, 2018.
<https://sam.nrel.gov/>, accessed August 11, 2018.
- http://www.brightsourceenergy.com/stuff/contentmgr/files/0/8a69e55a233e0b7edfe14b9f77f5eb8d/folder/ivanpah_fact_sheet_3_26_14.pdf, accessed August 11, 2018
- <https://www.ucsusa.org/clean-energy/renewable-energy/concentrating-solar-power-plants#.W2JeD3numQ> ,
accessed August 11, 2018
- https://en.wikipedia.org/wiki/Ivanpah_Solar_Power_Facility, accessed August 11, 2018
- https://energyeducation.ca/encyclopedia/Megawatts_electric, accessed August 11, 2018
- https://www.energy.siemens.com/ru/pool/hq/power-generation/steam-turbines/SST-900/downloads/SST-900_en.pdf, accessed August 11, 2018
- <http://helioscsp.com/brightsource-ivanpah-doesnt-have-storage-but-youre-going-to-see-storage-in-future-projects/>, accessed August 11, 2018
- <http://helioscsp.com/lcoe-of-50mwh-can-be-achieved-next-year-in-the-concentrated-solar-power>, accessed August 11, 2018
- <https://www.pe.com/2017/01/23/ivanpah-solar-plant-built-to-limit-greenhouse-gases-is-burning-more-natural-gas>, accessed August 11, 2018
- <http://www.powerfromthesun.net/Book/chapter10/chapter10.html>, accessed August 11, 2018
- <http://www.renewableenergyworld.com/articles/2017/02/generation-at-ivanpah-improved-dramatically-nrg-says.html>, accessed August 11, 2018
- <http://solarprofessional.com/articles/finance-economics/levelized-cost-ofenergy/page/0/3#.W2YO3numQ>,
accessed August 11, 2018
- <https://www.wsj.com/articles/high-tech-solar-projects-fail-to-deliver-1434138485>, accessed August 11, 2018



Conference Proceedings

ASES National Solar Conference 2018

Boulder, Colorado August 5-8, 2018

A DATA-DRIVEN FRAMEWORK FOR DEPLOYING SOLAR PV AT PENN STATE UNIVERSITY

Meghan Hoskins¹, Simon W Miller¹, and Michael Prinkey²

¹ The Pennsylvania State University Applied Research Laboratory, State College, PA 16803

² The Pennsylvania State University Office of Physical Plant, University Park, PA 16802

meh200@psu.edu

Abstract

The Pennsylvania State University has set greenhouse gas (GHG) emissions reduction goals that must be met with minimal impact on tuition rates. Investment in solar photovoltaic (PV) generation is a key part of this mission, and site selection is a critical component of the decision-making process. The decision framework Penn State developed to investigate the economic impacts of solar PV installation site selection on the University Park campus are detailed as a case study that other institutions, organizations, or corporations, could readily adopt. The case study shows the power of a data-driven, objective decision-making process to compare multiple (competing) criteria using a single framework to explore many possible solutions.

The framework relies on analyzing options through modeling the interaction of both decision-maker controlled and externally controlled factors, visualizing the impacts of potential decision tradeoffs on the outcomes over a range of possible futures, and developing preferences while exploring simulation resultant data. The methods and tools used during the process are described as are the results and insights gained by comparing options. Finally, the next steps in Penn State's transition to decreasing its GHG emissions are discussed.

Keywords: *solar investment, multi-objective decision-making, GHG emissions reduction, tradeoffs*

1. Introduction

The Pennsylvania State University (henceforth referred to as *The University*) has put a priority on decreasing its contribution to climate change, and thus has set specific goals to decrease its Greenhouse Gas (GHG) emissions. Energy usage is the largest contributor to the University's GHG emissions profile due to the electricity and heating/cooling needs of its 24 campuses and is the current focus of GHG reduction efforts. Reaching these reduction goals, while continuing and expanding the University's academic and research mission, involves focusing on energy conservation and energy efficiency wherever possible and investing in GHG reducing technologies (renewable energy generation) when fiscally responsible. The University is currently implementing a \$60 million 5 year investment towards energy efficiency *and* conservation initiatives while exploring potential technologies to remediate GHG emissions.

In particular, the University has already achieved some success in energy conservation (achieving

approximately an 18% reduction in GHG emissions from 2005 levels) albeit this was supplemented with the purchase of renewable energy credits (RECs). Reaching the reduction goal of 35% by 2020 will continue to be anchored with conservation efforts, but will be supplemented with an increased level of combined heat and power (CHP), low-carbon energy production, and hydropower. The strategy for 2020 and beyond will further integrate and increase the use of the suite of renewable technologies continually developing. A complete guide to the sustainability efforts at the University can be found at sustainability.psu.edu/energy-environment.

The research detailed in this paper explores the utilization of decision-making tools, simulation models, and human-in-the-loop processes to help define a robust decision-making strategy for deploying solar PV at the University Park campus. Solar PV is a mature technology with constantly improving finances, and it can be readily acquired, installed, and used to produce energy on all the campuses across the commonwealth, making it part of a strategic initiative. This study details the exploration of the feasibility and decision-making process to ascertain where solar PV would be a good investment for an organization similar to the University, decision-making criteria and strategy to make commitments, and processes and tools to aid in the decision-making process. The decisions made during the process and plans for future efforts are briefly described.

2. Background

The University currently owns facilities that could be generating energy using solar photovoltaics' (PV) on the buildings (e.g. roofs), land (e.g., agricultural), and parking structures. The University has reduced its campus greenhouse gas emissions by 18% since 2005 and has set its sights on the next reduction goal of 35% by 2020 (compared to 1990 levels). As the costs of solar PV installation and energy generation are consistently declining (see Barbose et al, 2016), it has become prudent to invest in the technology.

There are several options for financing the installation of PV panels. Direct Purchase (DP) is when an entity purchases the system and pays for it directly. Power Purchasing Agreements (PPA) is when a company installs their own system on an entity's property, for which the entity then pays the company for electricity at a contracted price. Finally, leases and loans, which are very similar to DP, however standard loan or lease agreements are made with a bank to finance the purchase. The DP and PPA financing options are compared in this study for both economic and sustainability decision criteria.

The future is stochastic in nature and uncertainty exists in the financial outlook. If the University were to invest strategically in solar PV now, what sort of futures may be realized? Is the current cost amenable such that tuition increases can be avoided (or minimized)? What effect would different grid electricity rates have on the overall project? Do any of the specific sites have conditions that would be more or less conducive to a solar installation? These questions led to quantifying those uncertainties wherever possible such that decision-makers can act upon criteria and assessments of robust investments by exploring their individual risk propensity to a multitude of potential outcomes.

A data-driven decision framework is a culmination of models, simulation, and visualizations. Here, we describe the incorporation of a financial model with a sustainability model into an adaptive decision assistance tool. Identification of potential sites was driven by a third-party, Lightbox Energy (www.lightboxenergy.com), who used screening criteria such as the size of the rooftop or solar area, the historic significance, the building function, and the proximity of the site to the power grid to evaluate well over 150 potential sites. These criteria, along with decision-maker solicited preferences, steered the conversation to a subset of top potential sites for detailed evaluation, including on-site assessments and analytics. The financial and environmental models constituted the tool that was used to assess more than 50 candidate sites on the University's main campus; sites were prioritized for solar PV development and a single site was selected for current development. The adaptive tool gives the University the ability to reassess the investment potential of various sites rapidly when market trends or infrastructure planning changes occur or the uncertainties in installation costs, grid energy prices, and site upgrade costs change. The tools can be leveraged to easily analyze trends, discover preferences, explore possibilities, and make and explain the resultant decisions.

The paper is organized by presenting the background on the decision making framework, then the tools used to accomplish the assessment (the models and visualizations) are described, and finally the resulting decisions and next steps are discussed.

3. Decision Framework

Analyzing the potential costs and benefits of installing solar photovoltaic (PV) electricity generation capacity at the University raises many important questions. Practical experience and research shows that much of decision making related to design is actually an iterative process of simultaneously looking for alternatives while refining an individual's value/preference function (Miller et al., 2013; Simpson et al., 2008); Balling (1999) referred to this process as *Design by Shopping*. This naturally imposes an iteration on the design decision making process. Building upon our experience and the current research, the proposed decision framework casts a decision problem in terms of external factors that the decision-maker must take into account in the decision process (X), levers the decision-maker may manipulate that constitute the actual decision (L), the system relationships (R), and the performance metrics on which the optimality of the decision is based (M). This XLRM framework (Lembert et al, 2003) aids decision-makers to ask questions under data-driven/data-supported thought experiments that address uncertainty in potential future actualization, such as

- How robust will the project be to energy rate changes?
- How would alternate installation costs affect the overall cost of the project?
- How robust will the project be to potential solar panel degradation?
- What are the drivers that affect the overall savings due to the project over the desired project lifecycle?
- What if the site conditions need improvement investments for the solar PV to be installed?

In order to answer the above questions, simulation models using uncertainty in process and financial parameters were sampled to identify and quantify the effect of what factors may impact the likelihood that the University would install a solar electricity generation capability on the University Park campus. Potential futures of these identified important factors were surveyed in the literature and from subject matter experts, from which relevant future scenarios were generated. The scenarios were then used to perform an analysis in OpenMORDM (Multi-Objective Robust Decision Making), an ARL/PSU developed tool (Hadka et al., 2015), to determine robust solar PV investments and inform the University of the impact of future uncertainty on their decision to invest. Both OpenMORDM and the ARL Trade Space Visualizer (ATSV, www.atsv.psu.edu) were used to analyze the costs and benefits of installing solar PV panels.

Through exploration of the aforementioned questions with the University decision-makers for a few representative solar PV installation sites, an understanding was reached of the specific preferences and trade-offs that needed to be better understood. Therefore, a higher fidelity and more accessible decision-making tool was developed with the University decisions-makers to answer the question of what sites out of 50 likely sites would make the best investment. This tool was used to assess the trade-offs between specific sites on the University Park campus.

3.1 Identification of Uncertain Model Parameters

Installation costs are the primary expense for solar projects that involve a direct purchase of the system due to the low cost of yearly maintenance on solar PV panels once they are installed. The installation costs of a PV system include both materials (panels, inverters, wiring, etc) and soft costs (labor, design, permitting, inspection, etc), and are generally reported as a cost per Watt. The major factors that affect the installation costs are size of the installation, hardware costs, labor rates, and condition and complexity of the installation site. This cost is directly correlated with the size of a solar PV system where small systems have a higher cost per watt compared to larger systems (Barbose et al, 2016). As system size increases, the labor and material requirements increase, but certain fixed costs may not change significantly and the economy of scale comes into play.

Other drivers of the installation costs are the variability and complexity of the installation site. This is due to the increasing labor necessary to complete complex installations (potentially including labor such as structural analysis), and the additional costs of renting and/or operating equipment for some installations, e.g., installation in a field versus a sloped building roof.

Another source of variability in solar panel installation costs is the cost of permits and inspections. The approval of the state or municipality will be required, and the cost to obtain these permits is typically a function

of the size of the system. This factored into the cost per Watt to install the system. Inspection and permit costs will vary depending on local laws, but they are generally more expensive per watt for smaller, residential systems. If the system is obtained via DP, these costs are not usually significant compared to other costs and will not have a large impact on the overall installation cost.

3.2 Model Definition

In the analysis performed here, installation costs were treated as a dollar per Watt value, with a different expected range for each installation site type considered. The range of values used in the analysis spans the range of average installation costs across the country, and is lower than the average Pennsylvania residential solar PV installation cost (\$4.50/W from SolarReviews (2018)). This is expected to be the case due to the University likely installing a larger commercial-type system, which should be cheaper to install than residential installations. The parking structures were assumed to cost the most, then buildings, and ground mounted land installations were the lowest with values in the range:

- Buildings (assuming a low-slope roof rack system): \$2-2.75
- Parking lot (assuming a carport w/structure): \$2.9 - 4.00
- Pasture land (assuming a ground mount w/footings): \$1.75 - 2.30

The cost drivers for a PPA are the contract base rate and the inflation rate, which are negotiated by the buyer and PPA provider at the time of purchase. As this cost is negotiated, it varies widely from location to location. In general, to be competitive in a specific region, the base PPA rate needs to be equal to or less than the current cost of electricity. PPAs are currently not common in Pennsylvania due to the low value of Solar Renewable Energy Credits (SRECs) in the state. The average contract rate of PPAs in Pennsylvania is \$0.10 – \$0.15/kWh (Heeter and O'Shaughnessy, 2016), making them financially feasible for locations such as Philadelphia, PA. For the University, the current utility rate is ~\$0.06/kWh. Thus, for a PPA to be financially desirable, the base rate would need to be competitive so a range of values were taken from \$0.06/kWh – \$0.10/kWh.

PPA agreements generally include an escalation rate, which is the annual rate at which the costs increase over the life of the contract. This rate is a negotiated contract term, thus there is variability associated with that value. The range of values used here was 2%/year – 3.5%/year (Sol Systems, 2016).

While installing solar PV panels is a large investment, the cost of the electricity generated by the panels is essentially free (plus some very small operation and maintenance costs). To calculate the financial impact of installing solar PV panels over the life of the investment, a comparison is needed against the cost of continuing to buy electricity from the grid, which also contains uncertainty. The cost of electricity varies over time and may increase or decrease significantly over the 20–30 year life of solar panels. The US Energy Information Administration (EIA, 2018) forecasts grid energy prices through 2040 for 21 different scenarios. The range of growth in prices among those cases is between 1.6 and 3.3%; the range of values used here as (exploratory) 1.5 – 5%. The larger utility escalation rate was included due to the possibility of increases in the net cost of buying electricity from the grid due to a carbon tax (Zalaznick, 2016) or other increase in the cost of energy due to environmental concerns.

Greenhouse gas emissions due to the electricity used on the University are directly related to the amount of grid energy purchased and the sources of that energy. For this study, carbon dioxide (CO₂) is examined. Currently the electricity generated in Pennsylvania is sourced from predominantly nuclear power, natural gas and coal (EPA, 2018a). The CO₂ emitted by this mix of fuels is approximately 1.38 metric tons per kWh (EPA, 2018b). Although the amount of CO₂ emitted by electricity generated for the utility grid will potentially change over the next 25 years, this uncertainty was outside the scope of this analysis. A constant value of 1.38 metric tons was used as the amount of CO₂ emissions *avoided* per kWh of electricity generated by the solar PV panels.

The amount of electricity generated by solar PV panels can be estimated using modeling tools such as Helioscope (www.helioscope.com) and Skelion (www.skelion.com). These tools use historic weather data to determine how much electricity will be likely to be generated at a specific location. Due to the uncertainty in future weather and any errors that could be inherent in the modeling of a PV system prior to installation, a range of values were used for the solar electricity production of a PV system for this analysis. The average value for Central Pennsylvania of solar electricity production is 1300 kWh/kW (communicated with subject

matter expert). For the OpenMORDM analysis, this was used as the baseline value, with a negative 20% to positive 20% sampling bound. When 50 high potential sites were defined, an output from Helioscope for each site was used without an uncertainty range.

Another potential uncertainty around the electricity generation from solar PV panels is degradation of the electricity generated by the PV panels over time. This is generally seen as the degradation of electricity generation due to normal wear and tear of the panels, and is estimated to be very low by panel manufacturers (0.4 – 0.7% per year). For the analysis here, a larger bound on panel degradation was used, considering 0.4 – 3% per year. The higher degradation rate per year could be due to circumstances such as new shading of a site (planting trees, or new buildings being constructed) or damage to panels (due to extreme weather events or other physical damage).

3.3 Modeling and Simulation

OpenMORDM (Hadka et al, 2015) was used to analyze the robustness of solar PV panel investments in the scenarios discussed in the previous section. A financial model generated by Lightbox Energy was integrated into OpenMORDM, with inputs and outputs as shown in Fig. 1. The inputs in bold were assigned feasible ranges as discussed in the previous section and the outputs in bold are those analyzed here.

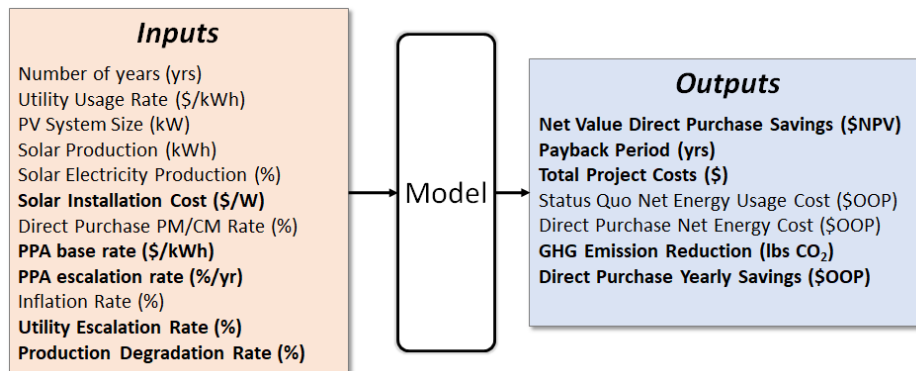


Fig. 1: Model input and output

This framework casts the decision problem using the XLRM framework of Lambert et al (2013) as:

- X = site data (size, type, potential solar generation), avoidable study rate, degradation rate, upgrades budgets, inflation rate, utility rate
- L = site, contract type (PPA, DP), \$/kWh price
- R = functional relationships
- M = levelized cost of energy (LCOE), first year budget impact, net savings, lbs of CO₂ avoided, payback period

States-of-the-world (SOW) are random samples from multi-dimensional distributions over the uncertainty across input parameters. For each site analyzed, sampling of the uncertainty distributions 5000 times (assuming independence) generated a rich dataset of SOWs from which trends were determined. Inputs that are not considered to be uncertain in this analysis include:

- the number of years over which to evaluate the investment – 25 years
- the size (in kW) of the system – value specific to each independent site
- the base utility grid rate – \$0.06362/kWh
- the reduction in greenhouse gas emissions – 1.38 mt CO₂/kWh

The other assumptions made in the analysis were:

- The University will always use all the electricity generated by solar PV panels on campus
- The CO₂ generated by the grid-produced electricity is constant over time
- Net Savings is equal to the Net Present Value of the yearly savings minus the initial system costs

- The payback period is the number of years required to recuperate the up-front costs of the system (for direct purchase)
- The PPA base cost and inflation rates are constant over the life of the contract

The major trade-offs analyzed in this first step were comparing the financial outcome of a DP to a PPA, the costs of different installation site types, and the cost of GHG emission reduction. After generation of the static dataset, tradeoffs were visualized and explored directly with the decision-makers. Through this process, specific preferences were determined and used to identify priority sites for solar PV installations. The following section shows the comparison between a DP and PPA as an example of trend identification using this type of analysis, and visualizations that led to the identification of the top priority solar PV installation sites.

4. Solar Feasibility Assessment

ARL/PSU analyzed sites across the University Park campus using on-site assessment information from Lightbox Energy. By including uncertainty in grid electricity costs, PPA rates, installation costs, and the University’s break even rate, the most robust investments over the lifetime of a solar PV installation’s useful life were determined. Visualizing and understanding the uncertainty inherent to SOWs and the tradeoffs between DP and PPA are highlighted in this section.

4.1 Analyse Trends

Figure 2 shows the relationships between each site and the LCOE and the first year budget impact for both DP and PPA. The violin plots show the *distribution* of LCOE per site for the realized SOWs (left side). Large sites have the best economics (lowest LCOE) and there is a wide range of LCOE for the building sites on campus. The lowest LCOE for the sites considered here is a direct purchase (DP) of a ground mounted solar PV installation. However, the first year budget impact (right side of Fig. 2) shows the drawback of a DP is its *much larger* financial impact up-front than a PPA (note the differences in the scale). The first year budget impacts for a DP are directly related to the size of the installation. Noted, by exploration of the SOWs in these visualizations, is that some building sites have the potential for lower first year budget impacts than other sites but other (often) non-quantifiable criteria reduces the prospect of selecting these sites.

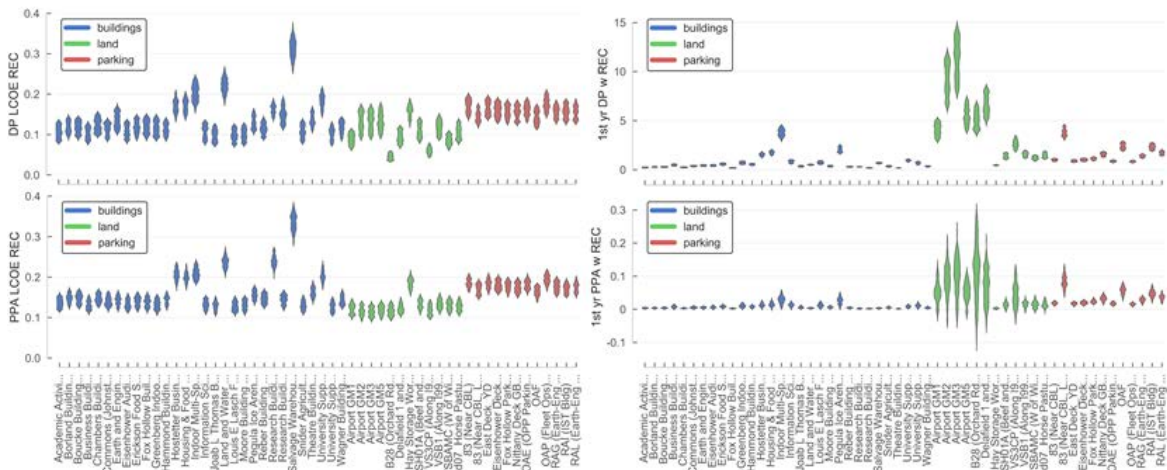


Fig. 2: LCOE and first year budget impact per site in normalized units (RECs will be bundled with the project, ensuring the University keeps its CO₂ emissions benefits)

4.2 Discover Preferences

Decision-makers explored the trends discovered in the data at the University in larger group meetings as well as individually. Decision-maker comments and questions during the meetings served to start the process of eliciting their preference and risk structures. Further specific information was gleaned when the higher fidelity model of the finances were created. For example, risk in the investment of solar PV was assessed by examining visualizations such as Fig. 3 whereby robustness of selecting a site and risk attitude could be entertained.

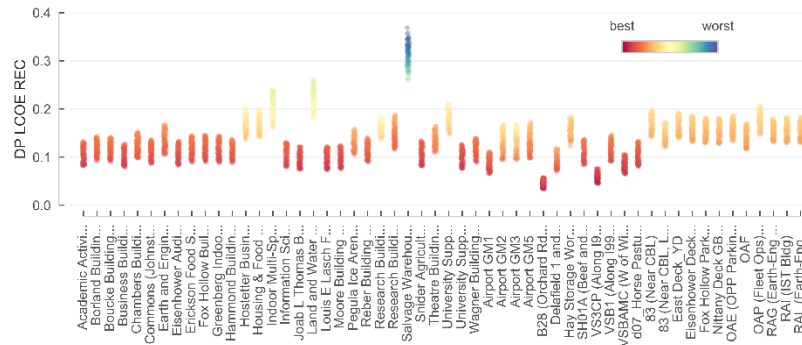


Fig 3. DP LCOE for individual sites, with color indicating preference for minimizing the LCOE and the DP first year budget impact.

In Fig. 3, the colored dots represent the SOWs that result when realizing the uncertainty through the assessment model. The color represents an assumed preference of minimizing LCOE (both DP and PPA) and the DP first year budget impact. Sites whose risk exposure is low have tight groupings of mostly reddish points, whereas higher risk sites contain a wider spread of points with more varied coloring.

Exploration of the data, highlighting trends and real-time impacts of decision criteria weightings/constraints with decision-makers made it clear that the top priority at the current time is to minimize the first year budget impact of a project. This priority resonated such that the GHG emissions avoided are maximized by developing solar on a larger site while still being financially feasible without tuition increases. Although this means that a PPA will be used for any projects currently pursued by the University, this will be reassessed as time passes so in future the financial benefits of a DP could be realized. Thus, the decision-maker preferences elicited were, for a PPA:

- Maximize the GHG emissions reduction
- Minimize the first year budget impact (thus focusing on a PPA)
- Minimize the operating budget impact (LCOE)

4.3 Explore Possibilities and Identify Priority Sites

Elicitation of the preference structure allows for focus on specific regions of the data. For example, here the main two preferences deal with GHG emissions and operating budget, therefore Fig. 4 shows the PPA LCOE against the amount of CO₂ emissions avoided. The left side plot shows all the SOWs for sites with a low LCOE such that the vertical “lines” are groupings of instances of SOWs for specific sites. Collapsing the uncertainty to the mean results in the right-hand plot. Individual sites are identified on the continuum of avoided GHG emissions and PPA LCOE. The circled site is simultaneously the lowest PPA LCOE (determined using external, non-quantifiable metric, e.g., not at the airport), and offsets the maximal CO₂ emissions of all the sites, making it the highest priority site for solar PV development at this time. As the plots also indicate, several additional sites might be of interest for development in the near future.

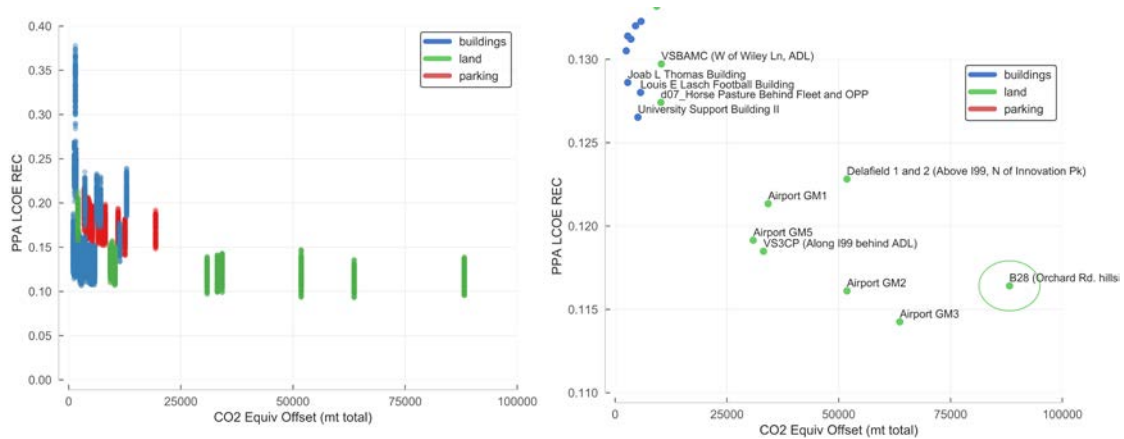


Fig 4. Relationship between PPA LCOE REC and CO₂ offsets for different sites evaluated for many SOWs. (left) SOWs (right) mean values zoomed in.

5. Conclusions

This feasibility analysis showed that if the most important decision-making factor is maximizing the amount of CO₂ avoided, then the direct purchase of solar PV systems for land sites would be the most robust investment at this time. However, when minimizing the first year budget impact of the investment is the highest priority, a power purchase agreement makes more financial sense. PPAs have the potential to be close to equivalent in cost to utility costs, and although historically Pennsylvania has not been a high PPA development area due to regulations and low market value of SRECs in state, that is changing.

By facilitating direct decision-maker interaction with data showing the potential financial outcomes of various investments, decision-maker preferences were determined. Once preferences were known, priority development sites were identified by maximizing the CO₂ emissions avoided and minimizing the first year budget impact. A single site is currently being developed at the University that was identified as the top priority site, and additional potential sites were identified through this process.

Although large scale solar PV investment on the Pennsylvania State University campus is not currently feasible due to financial constraints, the work completed here gives the University decision makers the tools and information they need to focus on the best campus sites, and to reassess the market quickly over the coming years. With continued technology improvements and market improvements for renewable energy generation, it is possible that the viability of all sites will improve in the short term (2-5 years).

6. Future Work/Discussion

Along with reassessing the main University campus, future work includes generating a more automated process for site feasibility analysis on other campuses around the State. There are varied economics and infrastructures at the other University campuses that could provide the University with additional opportunities for solar PV development. The University is engaging faculty and students to develop and deploy this methodology and identify potential sites for solar PV investments across Pennsylvania.

The framework and process presented here is expandable and adaptable to any organization, municipality, or institution interested in analyzing the tradeoffs and economic feasibility of renewable energy deployment. The majority of the tools used here are openly available. This could be reproduced at very low cost, giving anyone the power to analyze their own systems in a way that empowers them to make a data-driven decision.

7. References

- Balling, R. 1999. Design by Shopping: A New Paradigm? In *Proceedings of the Third World Congress of Structural and Multidisciplinary Optimization (WCSMO-3)*, vol. 1, pp. 295–297.
- Barbose, G., Darghouth, N., Millstein, D., Cates, S., DiSanti, N., & Widiss, R. 2016. Tracking the Sun IX: The

Installed Price of Residential and Non-Residential Photovoltaic Systems in the United States. *Lawrence Berkeley National Laboratory*. LBNL Report #: LBNL-1006036.

EIA, U.S. Energy Information Administration - EIA - Independent Statistics and Analysis. [online]. Retrieved August 13, 2018, from http://www.eia.gov/forecasts/aeo/data/browser/#/?id=8-AEO2016®ion=0-0&cases=ref2016~ref_rate&start=2013&end=2040&f=A&sourcekey=0

Environmental Protection Agency. [online] Power Profiler. Retrieved August 13, 2018 from <https://www.epa.gov/energy/power-profiler/>

Environmental Protection Agency. [online]. Emissions & Generation Resource Integrated Database (eGRID). Retrieved August 13, 2018, from <https://www.epa.gov/energy/emissions-generation-resource-integrated-database-egrid>

Hadka, D, Herman, J., Reed, P, & Keller, K. 2015. *An open source framework for many-objective robust decision making*, *Environmental Modelling & Software*, 74, 14-129.

Heeter, J., and O'Shaughnessy, E. 2016. *Using Power Purchase Agreements for Solar Deployment at Universities*. National Renewable Energy Laboratory, PR-6A20-66119. February 2016. <http://www.nrel.gov/docs/fy16osti/66119.pdf/>

Lempert, R. J., Popper, S. W., & Bankes, S. C. 2003. Shaping the next one hundred years: new methods for quantitative, long-term policy analysis. RAND, Santa Monica, CA.

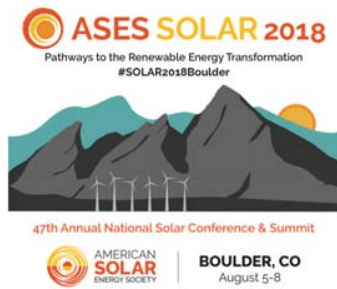
Miller, S. W., Simpson, T. W., Yukish, M. A., Bennett, L. A., Lego, S. E., & Stump, G. M. 2013. Preference Construction, Sequential Decision Making, and Trade Space Exploration. In *ASME International Design Engineering Technical Conference & Computers and Information in Engineering Conference*, 1-12, Portland, OR: DETC2013-13098.

Simpson, T., Spencer, D., Yukish, M., & Stump, G. 2008. Visual steering commands and test problems to support research in trade space exploration. In *12th AIAA/ISSMO Multidisciplinary Analysis and Optimization Conference*, 1-15, Reston, VA: AIAA-2008-2139.

SolarReviews. [online]. How much will it cost to install solar panels for your home. Retrieved August 13, 2018, from <https://www.solarreviews.com/solar-panels/solar-panel-cost/cost-of-solar-panels-in-pennsylvania/solar-panels-cost-in-centre-county/blanchard/>

Sol Systems. [online] The Sol Source. Retrieved August 13, 2018 from <http://www.solsystems.com/blog/wp-content/uploads/2016/11/PPA-RATE-Nov.png>.

Zalaznick, M. 2016. Yale tests carbon tax. *University Business*, 2016. <https://www.universitybusiness.com/article/yale-tests-campus-carbon-tax/>



Conference Proceedings

ASES National Solar Conference 2018

Boulder, Colorado August 5-8, 2018

Forecasting Carbon Emissions in States of Hawaii, California, Colorado, and Florida; The Effects of States' Renewable Portfolio Standards

Rahim Khoie, and Antonio Calderon

University of the Pacific, Stockton, California

Corresponding author: rkhoie@pacific.edu

Abstract

In this paper, we present four ARIMA (Autoregressive Integrated Moving Average) models for forecasting the future trends in carbon emissions of four states in the United States: the three states of Hawaii, California, and Colorado whose RPS (Renewable Portfolio Standard) laws set the most ambitious renewable targets, and the State of Florida, which presently has now RPS. The State of Florida is used as a baseline for comparing the effects of RPS laws on emissions. For each of the three states of Hawaii, California, and Colorado we run simulations under two scenarios. In scenario 1, we forecast the carbon emissions through 2050 of these states based on available emission data from 1980 through 2014, which include data for the years following the enactment of their RPS laws. In scenarios 2, we assume that no RPS laws were ever enacted in these states and use the emission data from 1980 to the year the RPS laws were enacted and forecast their carbon emissions through 2050. The results of the two scenarios are discussed in relation to the effectiveness of the RPS laws on emission reduction for these states.

Keywords: Carbon Emissions, Autoregressive Integrated Moving Average Model, Renewable Portfolio Standards

1. Introduction

In 2007, the U.S. total carbon emissions reached its peak of 5983 Million Metric Tons (MMT) which was 19% above its 1990-level, as shown in Fig. 1. Since then it has had a declining trend. Although the decline has not been monotonic, it did reach a trough of 5171 MMT in 2016 (U.S. EIA, 2017) (Statistica, 2016) which was only 2.84% above the 1990-level. This is a significant decline by any measure. Various researchers have cited different reasons for this decline, including:

- decline in the U.S. economy output in the years following the financial crisis of 2008-2009 (Peters, et. al. 2012) (Guardian, 2010),
- increase in use of natural gas (Feng, et. al., 2015),
- federal regulations imposed by Obama Administration (Adler, 2011) (McCarthy and Copeland, 2016),
- and state-mandated regulations, and in particular, the Renewable Portfolio Standards (LBL, 2016).

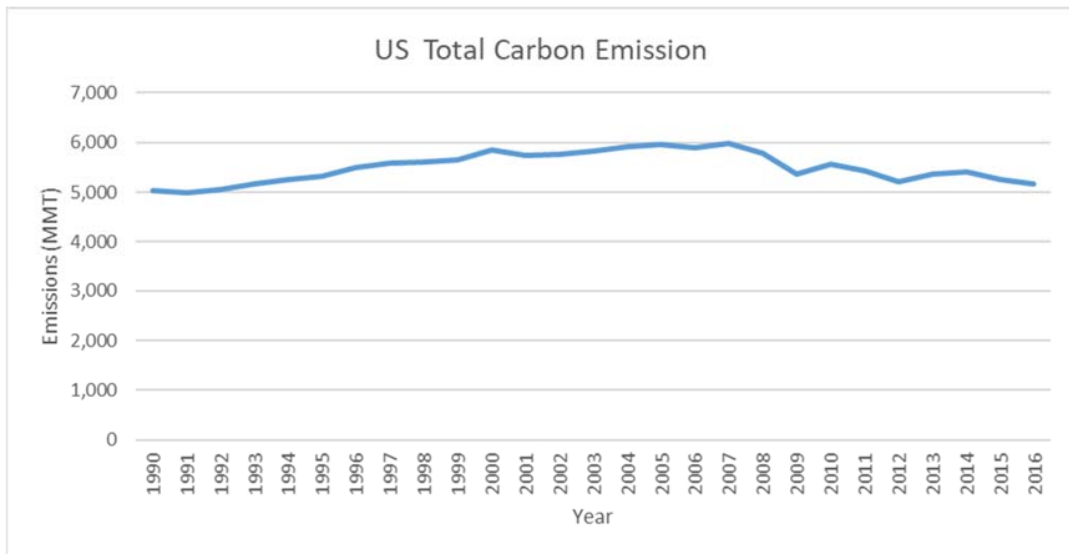


Fig. 1: The U.S. total carbon emissions from 1990 to 2016 (U.S. EIA, 2017)

In the absence of any federal mandate on reducing the U.S. carbon emissions, and in light of recent federal energy deregulations by present administration, and in particular, deregulation of coal industry, the role of states in mandating emission reduction is now more essential. A large number of states in the U.S. have enacted legislations mandating Renewable Portfolio Standard (RPS) requiring utility companies to produce a certain percentage of their electricity from renewable resources (U.S. EIA, 2012). While the state of Hawaii has the most ambitious target of 100% renewable electricity by 2045 (Hawaii State Energy Office, 2018), the state of California has set a goal of 50% renewable power production by the year 2030 (California Public Utility Commission, 2018). The state of Colorado requires production of 30% renewable electricity by 2020 (Colorado Energy Office, 2018). Overall, 29 states and the District of Columbia have adopted mandatory RPS along with 7 states that have voluntary goals (See Fig. 2) (LBL, 2016). The remaining states have no clear renewable energy policy including, ironically, the State of Florida, which has one of the most abundant supply of renewable resources, especially in solar energy (Khoie and Yee, 2015).

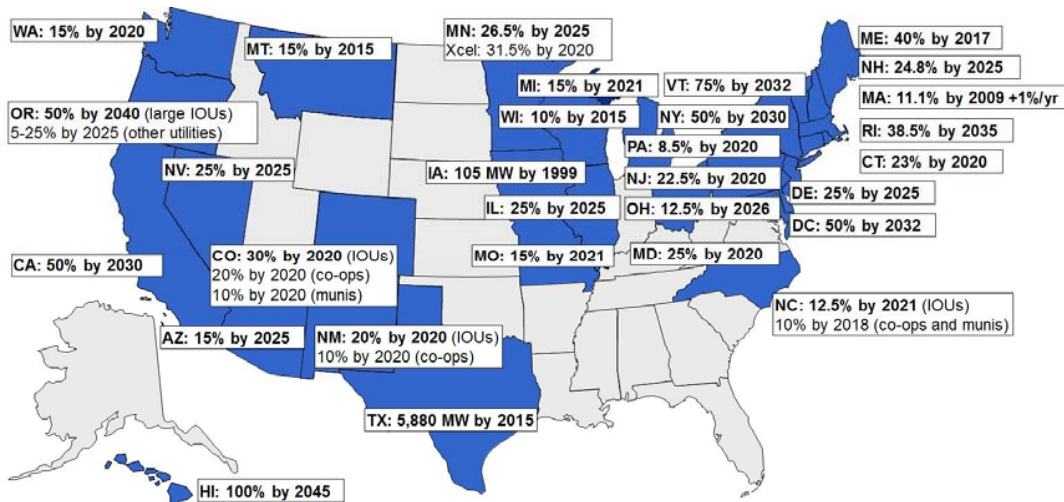


Fig. 2: Renewable Portfolio Standards of the United States (LBL, 2016).

In this paper, we present four ARIMA models for forecasting the future trends in carbon emissions of four states in the United States: the three states of Hawaii, California, and Colorado whose RPS laws set the most ambitious renewable targets, and the State of Florida, which presently has now RPS. The State of Florida is

Khoie and Calderon / ASES National Solar Conference 2018 Proceedings

used as a baseline for comparing the effects of RPS laws on emissions. For each of the three states of Hawaii, California, and Colorado we run simulations under two scenarios.

- In scenario 1, we forecast the carbon emissions through 2050 of these states based on available emission data from 1980 through 2014, which include data for the years following the enactment of their RPS laws.
- In scenarios 2, we assume that no RPS laws were ever enacted in these states and use the emission data from 1980 to the year the RPS laws were enacted and forecast their carbon emissions through 2050.

2. Autoregressive Integrated Moving Average (ARIMA) Model

The general form of the ARIMA model is given by (Chen, et. al, 2010):

$$y_t = \mu + \varphi_1 y_{t-1} + \varphi_2 y_{t-2} + \dots + \varphi_p y_{t-p} - \theta_1 \varepsilon_{t-1} - \theta_2 \varepsilon_{t-2} - \dots - \theta_q \varepsilon_{t-q} \quad eq. (1)$$

Where:

- y_t is the predicted value for year t ,
- y_{t-1} is the predicted value for year $t - 1$,
- μ is a constant term for a non-zero average trend,
- φ_p terms are autoregressive term (AR),
- p is the order of autoregressive process,
- θ_q terms are moving average parameters (MA),
- q is number of lagged forecast errors in prediction model,
- ε_q terms are forecast errors.

In order to stationarize the predicted trends and mask seasonal variations, the order of differencing parameter, d is determined for each state:

- California – ARIMA($p= 7, d= 1, q= 0$)
Average Max Error of $\pm 13.5\%$ @ 80% confidence
- Colorado – ARIMA($p= 12, d= 1, q= 0$)
Average Max Error of $\pm 24.4\%$ @ 80% confidence
- Hawaii – ARIMA($p= 13, d= 2, q= 1$)
Average Max Error of $\pm 18.3\%$ @ 80% confidence
- Florida – ARIMA($p= 17, d= 1, q= 0$)
Average Max Error of $\pm 28.7\%$ @ 80% confidence

When the order of differencing, $d = 1$ then $y_t = Y_t - Y_{t-1}$ and when
 $d = 2$ then $y_t = (Y_t - Y_{t-1}) - (Y_{t-1} - Y_{t-2})$.

In the above equations, y_t is the predicted value for the year t and Y_t is the value of original data at year t . The parameters p , and q are determined based on a Box-Jenkins (Chen, et. al., 2010) method using series of simulations resulting in least prediction error of known years. The adaptive nature of the model ensures that historical trends associated to policy changes are reflected in future trends.

The ARIMA model for each state is simulated using R- package and is validated with 2010-2014 emission data for each state from data reported by the U.S. Energy Information Administration (U.S. EIA 2017). The order of the fit is adjusted as appropriate to achieve a minimum absolute error between the predicted data and the know emission data in the years 2010 through 2014.

3. Results

The total annual carbon dioxide emissions from fossil fuel consumption for each of the four states is shown in Fig. 3. The years of enactment of RPS laws in states of California, Colorado, and Hawaii are marked in order to serve as an indicator in further analysis in comparing trends in carbon emissions before and since RPS laws were enacted. The states' emission data used in our simulations are for the years 1980 – 2014.

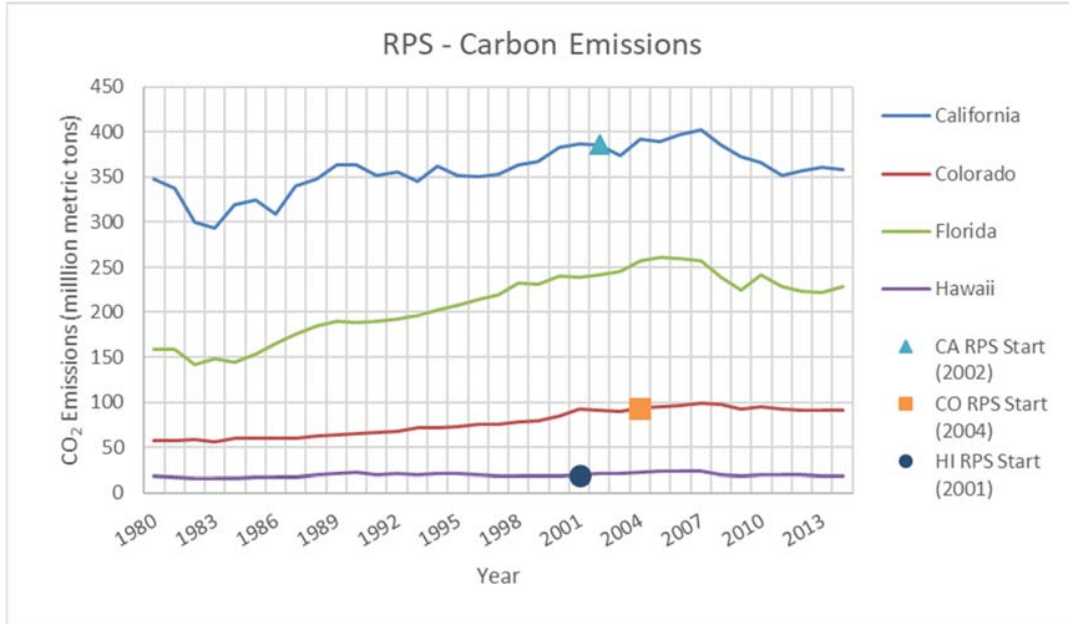


Fig. 3: The states' total carbon emissions from 1980 to 2015. The year of RPS enactment for each state is also marked. (U.S. EIA, 2016).

The State of California, as the largest economy in the United State has had the highest emissions of all states. In 1980, the state of California produced 348 MMT, which increased to 363 MMT in 1990 and reached its peak at 402 MMT in 2007. Since then it has declined to 358 MMT in 2014. Similar data for the other three states studied in this work are shown in Tab. 1.

Tab. 1: Highlights of emissions (in MMT) data for the four states studied in this work.

State	1980 Emissions	1990 Emissions	Peak Emission	Year of Peak Emissions	2014 Emissions
California	348	363	402	2007	358
Colorado	58	65	99	2007	92
Hawaii	18	21	24	2007	18
Florida	158	188	260	2005	228

Noteworthy in the above emission data are the following:

- The state of Florida has had the highest rate of increase in emissions in the 25 years between 1980 and 2005.
- The state of Colorado was on a sharp rise in emissions in the years prior to and leading to enactment of its RPS laws in 2004.
- The state of Hawaii's emissions while increasing from 18 MMT in 1980 to 24 MMT in 2007 (a relatively substantial rise), has had a relatively flat emission curve in the past 35 years.
- Most states reached their peak in 2007, except Florida, which reached its peak earlier in 2005.

Khoie and Calderon / ASES National Solar Conference 2018 Proceedings

The forecast results for the state of California are shown in Fig. 4. The green curve shows the emission forecast for the state with the enactment of RPS laws in California, which took place in 2002. The red curve shows the emission forecast if the state had not enacted any RPS laws. The forecast results for all four states are shown in Fig. 5.

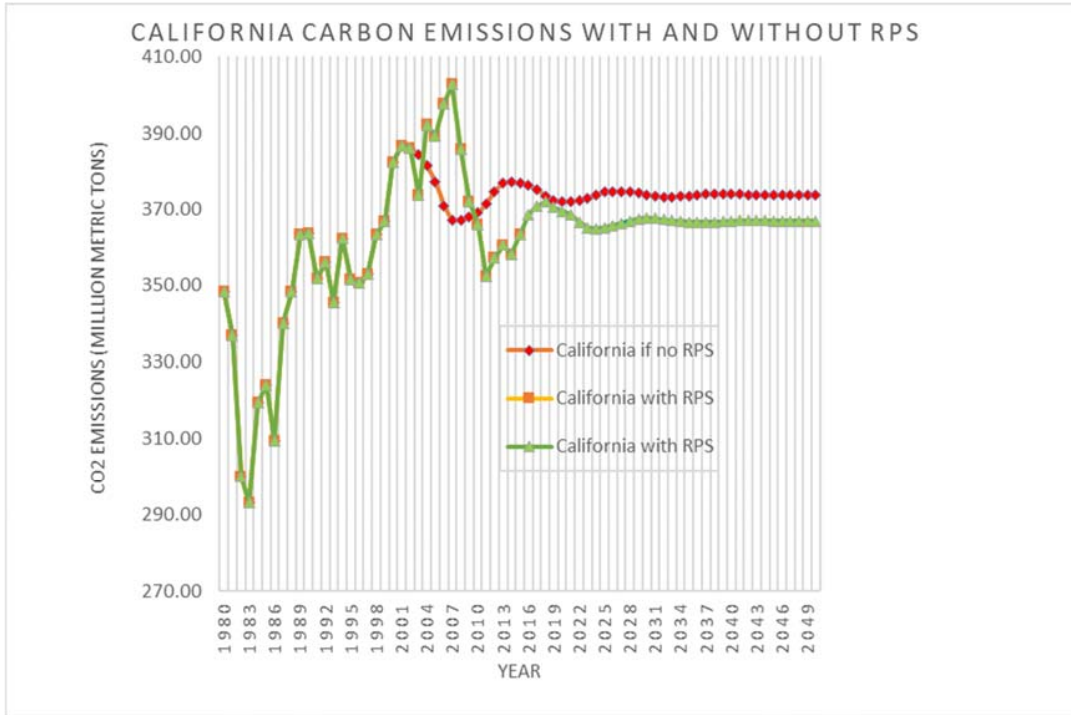


Fig. 4: ARIMA forecast results for the State of California with and without enactment of RPS.

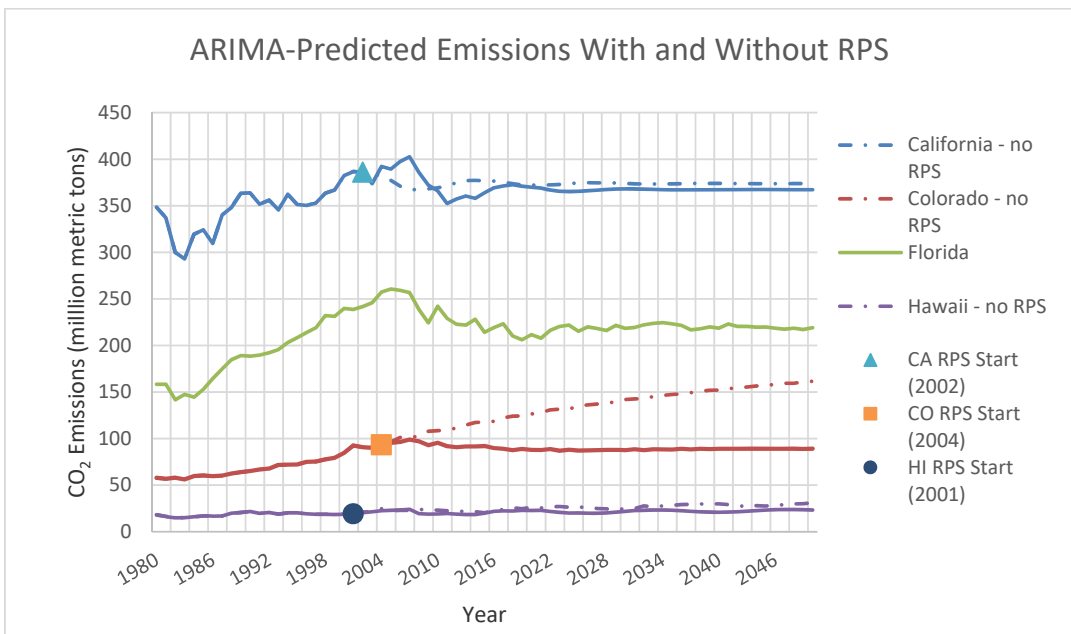


Fig. 5: ARIMA forecast results for all four states with and without enactment of RPS.

Khoie and Calderon / ASES National Solar Conference 2018 Proceedings

Our forecast results show that with the enactment of RPS laws in California, the state's 2050 emissions would reach 101% of its 1990-level, whereas without the enactment of its RPS laws, the state total emissions would have reached 103% of its 1990-level. The results shown in Figs. 4 and 5 for all four states are summarized in Tab. 2.

Tab. 2: The emissions of states as percentage of 1990-levels with and without RPS enactment

State	1990 Base Emissions	2014 Emissions	2014 Emissions as % of 1990-Base	2050 Emissions	2050 Emissions as % of 1990-Base
California	363	358	98%	367	101%
California if no RPS		377	104%	374	103%
Colorado	65	92	140%	89	137%
Colorado if no RPS		117	180%	162	248%
Hawaii	21	18	85%	23	107%
Hawaii If no RPS		22	100%	31	144%
Florida	188	228	121%	219	116%

As shown in Tab. 2, in all three states of California, Colorado, and Hawaii, the RPS laws have been effective in lowering their emissions both in 2014 and 2050 levels. In the state of Colorado, the RPS laws have been particularly effective. The state of Colorado's total emissions would have reach to 248% of its 1990-level, if the state had not adopted its RPS in 2004. With enactment of its RPS, the state of Colorado would produce 89 MMT of carbon emission which is 137% of its 1990-level. This is a significant reduction in emission by the state of Colorado, which was on a steep rise in emissions in the years prior to its enactment of RPS laws.

The state of Hawaii also would have seen a relatively significant rise in its emissions (144% of its 1990-level in 2050) had it not been for their ambitious renewable target of 100% by 2045. Our forecast model for the state of Hawaii predicts that the total emissions of Hawaii will be 107% of its 1990-levels in 2050. The state of Florida, without any RPS laws is expected to reach 219 MMT of total carbon emissions in 2050, which is 116% of its 1990-level. This increase in emissions by the state of Florida is in contrast to the three states of California, Colorado, and Hawaii in which the RPS laws were shown to be effective in keeping their emission levels from significantly rising in 2050.

4. Conclusions

The results of our ARIMA models (summarized in Tab. 2) show that in the three states with RPS, the total emissions in 2050 will likely be less than what they would been if the states had not adopted their RPS laws. For the state of Californai, the RPS laws would make a 2% difference (103% of its 1990-level without RPS versus 101% of its 1990-level with RPS) in total emissions in 2050. The state of Colorado the RPS laws would make a significant difference of 111% in total emissions (248% of its 1990-level without RPS compared to 137% of its 1990-level) in 2050. Similarly, the RPS laws in the state of Hawaii would account for a 37% difference in their projected emissions (144% of its 1990-level without RPS as opposed to 107% with RPS) in 2050. The state of Florida without any RPS laws will have total emissions that are 16% higher than its 1990 baseline.

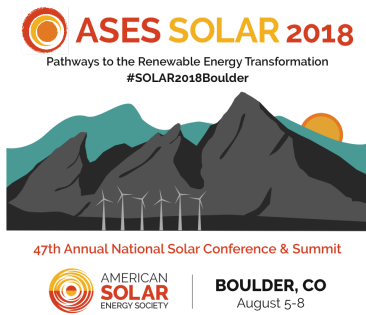
It is noteworthy that the RPS laws affect the emissions by the electricity sector and ARIMA modelling of emission by the electricity sector alone will result in different future trends, which may hide the effects that

Khoie and Calderon / ASES National Solar Conference 2018 Proceedings

production, transportation, installation, and operation of renewable electricity generation, have on other sources of emissions including residential, industrial, commercial and transportation sectors.

5. References

- Adler, J. 2011. Heat expands all things: The proliferation of greenhouse gas regulation under the Obama administration. *Harvard Journal of Law and Public Policy*, 421. <http://heinonline.org/>, Accessed March 2018.
- California Public Utility Commission, 2018. California Renewables Portfolio Standard, http://www.cpuc.ca.gov/RPS_Homepage/ Accessed: March 2018.
- Chen, P., Pedersen, T., Bak-Jensen, B. 2010. ARIMA-based time series model of stochastic wind power generation. *IEEE Transactions on Power Systems*. vol. 25, pp. 667-676.
- Colorado Energy Office, 2018. <https://www.colorado.gov/pacific/energyoffice/renewable-energy-standard>, Accessed March 2018.
- Feng, K., Davis, S., Sun, L., and Hubacek, K. 2015. Drivers of the U.S. CO₂ emissions 1997–2013. *Nature Communications*, 21 July 2015, Open Source. <https://www.nature.com/articles/ncomms8714.pdf>.
- Guardian, The, 2010. Global emissions of carbon dioxide drop 1.3%, say international Scientists. <https://www.theguardian.com/environment/2010/nov/21/carbon-emissions-fall-report>, Accessed March 2018.
- Hawaii State Energy Office. 2018. <http://energy.hawaii.gov/renewable-energy>, Accessed March 2018.
- Khoie, R. and Yee, V., 2015. A forecast model for deep penetration of renewables in the Southwest, South Central, and Southeast regions of the United States. *Clean Technologies and Environmental Policy*, Volume 17, pp 957–971.
- LBL, 2016. Electricity Markets and Policy Group. Renewable Portfolio Standards Resources. Lawrence Berkeley National Laboratory. 2016. Available: <https://emp.lbl.gov/projects/renewables-portfolio>. Accessed March 2018.
- McCarthy, J. and Copeland C. 2016. EPA Regulations: Too Much, Too Little, or On Track? Congressional Research Service, Library of Congress, December 30, 2016 <https://fas.org/sgp/crs/misc/R41561.pdf>, Accessed March 2018.
- Peters, G. Marland, G., Le Quéré, C., and Boden, T. 2012. Rapid growth in CO₂ emissions after the 2008–2009 global financial crisis. *Nature Climate Change*, 2012, <https://www.nature.com/articles/nclimate1332>, Accessed March 2018.
- Statista, 2016. The Statistics Portal: Energy and Environment Services, Electricity, US Carbon Emissions 1975-2016. Carbon dioxide emissions from energy consumption in the U.S. from 1975 and 2016. <https://www.statista.com/statistics/183943/us-carbon-dioxide-emissions-from-1999/> Accessed: March 2018.
- U.S. Energy Information Administration, 2012. Most States Have Renewable Portfolio Standards. February 2012. <https://www.eia.gov/todayinenergy/>. Accessed: March 2018.
- U.S. Energy Information Administration, 2016. Environment, U.S. Energy-Related Carbon Dioxide Emissions. <https://www.eia.gov/environment/emissions/carbon/>. Accessed: August 2018.
- U.S. Energy Information Administration, 2017. State Carbon Dioxide Emissions, Release Date: October 24, 2017, <https://www.eia.gov/environment/emissions/state/>. Accessed March 2018.



Conference Proceedings

ASES National Solar Conference 2018
Boulder, Colorado August 5-8, 2018

Renewable Resources of the Northern Half of the United States; A Pathway to Total Renewability ?

Rahim Khoie, Kyle Ugale, and James Benefield

University of the Pacific, Stockton, California

Corresponding author: rkhoie@pacific.edu

Abstract

We previously presented a model for deep penetration of renewables in the electricity sector of the southern half of the United States (Khoie and Yee, 2015). In this paper, we present a strategy for the northern half of the United States to utilize its available renewable resources to gradually decrease its reliance on fossil fuels in electricity generation and develop energy portfolios with increasing share of renewables. Using the electricity generation data from the U.S. EIA (U.S. Energy Information Administration, 2018a), and the renewable resource maps produced by NREL (National Renewable Energy Laboratory, Geospatial Data Science, 2018), we develop strategies for the states in the northern half of the U.S. We group these states into seven regions: West Coast, Mountain States, Middle West States, Lake States, Mid-Atlantic, South Atlantic, and New England states. For each region we determine when and if, the electricity generation from renewables will meet the region's electricity need while accounting for a 1% annual increase in electricity demand. The renewable resources included in our models are solar (photovoltaic), wind, hydro, biomass, and geothermal which vary greatly from region to region. We also include nuclear, coal, natural gas, and petroleum.

Keywords: *Pathway to total renewability, Renewable resources, Northern United States,*

1. Introduction

In 2017, the U.S. produced 4,015 billion KWh of electricity, of which 62.7% was generated from coal and natural gas and 20% from nuclear energy as shown in Fig. 1 (U.S. EIA, 2018b). In that same year, the renewables contributed 17.1% to the total generation of which 7.5% was from hydropower sources, 6.3% from wind, and a dismal 1.2% from photovoltaic solar cells. This level of utilization of renewables, especially wind and solar is extremely small compared to the level of natural abundance of these resources in the country. Although there has been a relatively significant increase in renewable electricity generation (roughly 5% increase from 2012 to 2017), the U.S. remains short of its true potential for a much deeper penetration of renewables in electricity generation over the next four decades. In fact, a study by the National Renewable Energy laboratory (NREL) has shown that even with the present state of the renewable

technologies, the United States has the potential to adequately supply 80% of its electricity demand in 2050 by using renewable resources (Mai, 2012).

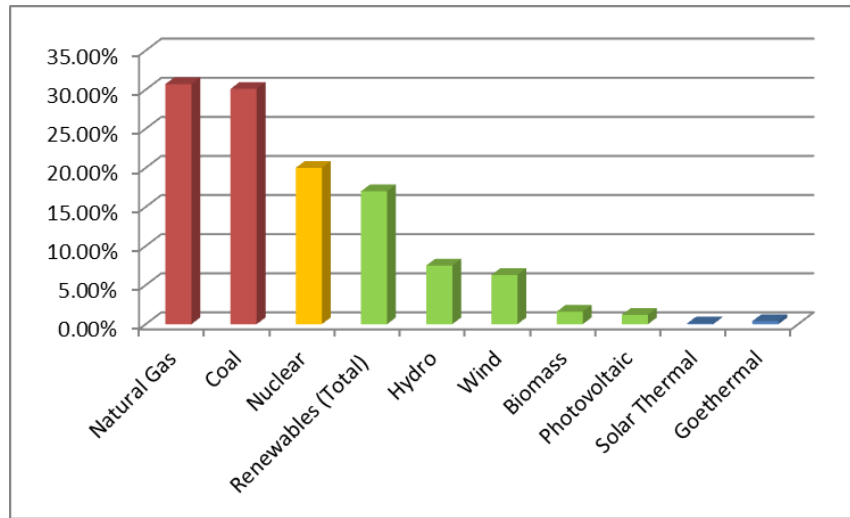


Fig. 1: The energy portfolio of the U.S. electricity sector in 2017 (U.S. EIA, 2018b).

The National Renewable Energy Laboratory has produced detailed maps of various renewable resources across the country. Referring to Figs 2 and 3, the United State has the following solar and wind resources (Hand, M. et. al., 2012):

- 80,000 GW of photovoltaic solar,
- 37,000 GW of concentrating solar thermal,
- 10,000 GW of wind,
- Furthermore, the distributed rooftop solar potential of the U.S. amounts to 700 GW.

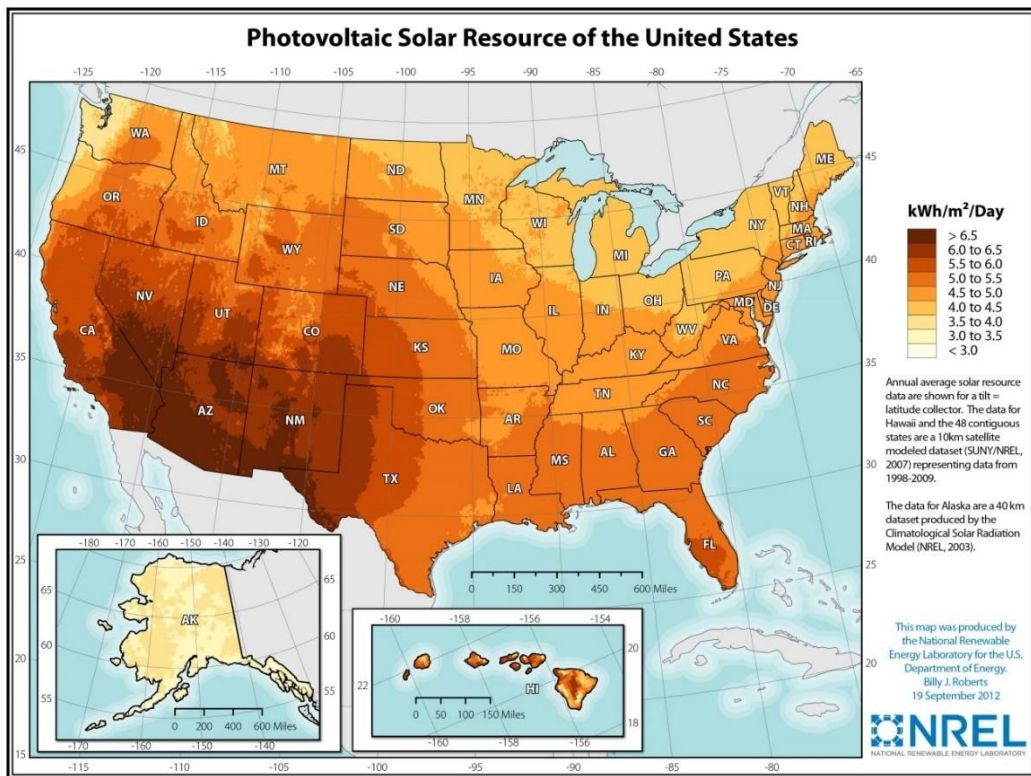


Fig. 2: Photovoltaic resources of the United States (NREL 2018a).

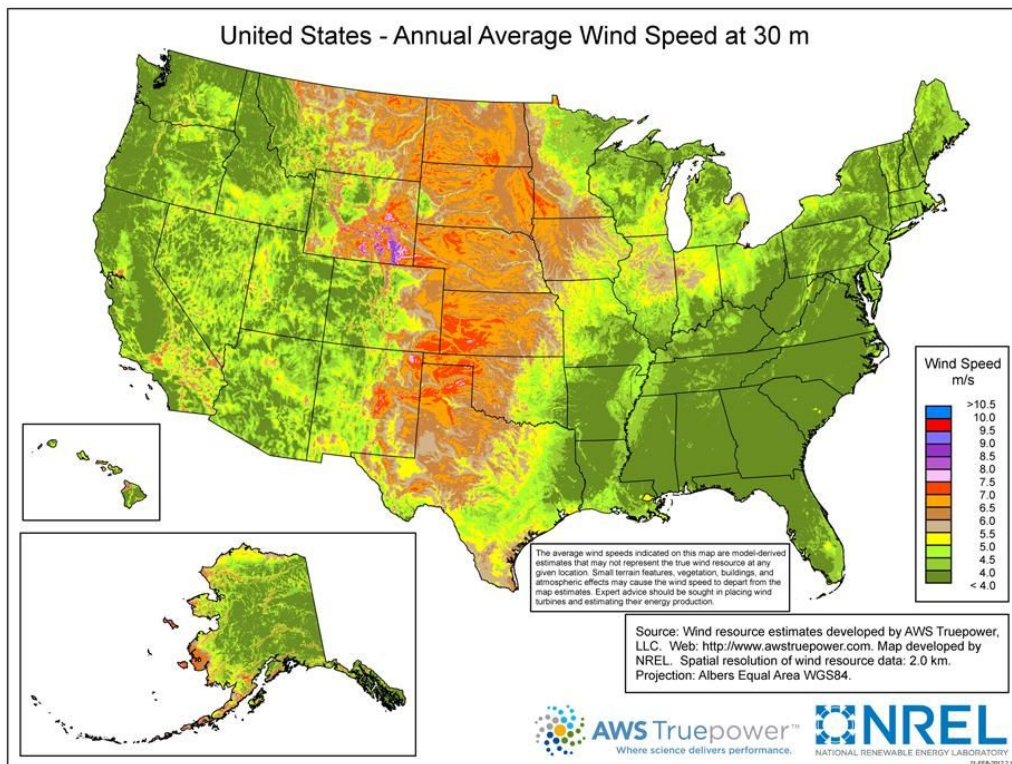


Fig. 3: Wind resources of the United States (NREL 2018b).

Additionally, the U.S. has roughly 500 GW of geothermal, 100 GW of biomass, and estimated 12 GW of non-powered dams (NDP) hydropower (Oak Ridge National Laboratory, 2018). The above represents a total potential capacity of more than 128,000 GW of renewable power. Comparing this colossal abundance of renewable resources to the roughly 1000 GW of electricity demand in the U.S., one wonders why we produce only roughly 170 GW of our electricity from renewables.

The southern half of the U.S. enjoys abundance of solar (especially southwest region) and wind (especially panhandle of Texas). (See Khoie and Yee, 2015). The northern half of the U.S. also has great potential in renewable generation. In this paper, we examine scenarios under which the northern states can gradually increase utilization of their renewable resources and reach energy portfolios in which the renewables are providing the fuel for either 100% of their electricity generation or a large portion of it.

2. 2. Regions in the Northern Half of the United States

We group the 28 northern states into seven regions as follows:

- The West Coast States: OR, and WA.
- The Mountain States: ID, MT, and WY.
- The Middle West States: ND, SD, and NE.
- The Lake States: MN, WI, MI, IA, IN, IL, and OH.
- The Middle Atlantic States: NJ, NY, and PA.
- The South Atlantic States: MD, VA, WV, and DE.
- The New England States: CT, ME, MA, NH, RI, and VT.

For each state in the regions, we determine the state’s total electricity demand and its energy portfolio in electricity generation in the year 2013 from the data published by the U.S. EIA. A sample of such data for the State of Oregon is shown in Fig. 4. We also determine the maximum renewable potential of each state from the data available from NREL. We then set out to determine the rate of growth in renewable penetration in the electricity sector of each state based on the model described below.

Oregon Energy Consumption Estimates, 2016

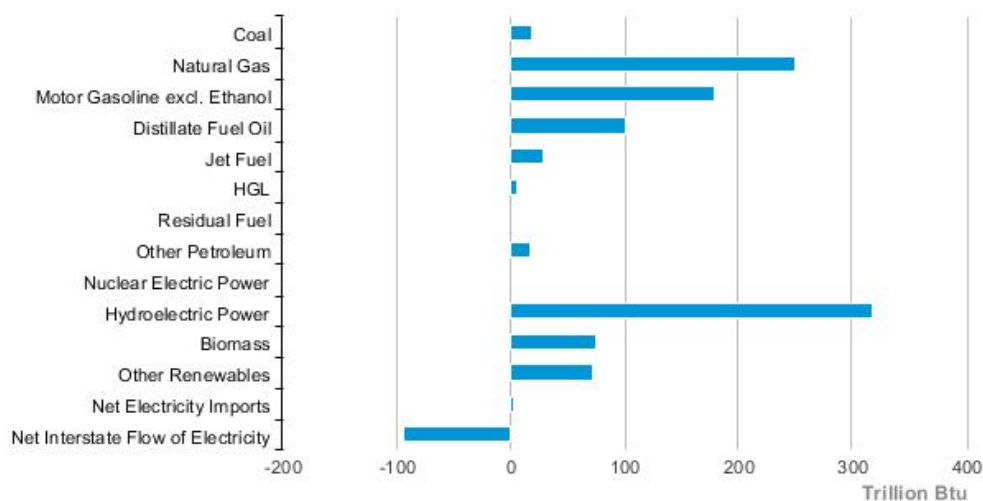


Fig. 4: Total energy consumption of Oregon in 2016 (U.S. EIA 2016a).

3. Model

We use a simple model in which the energy portfolio of each region is determined annually by increasing the renewable shares at appropriate annual rates (depending on the abundance of each of the renewable source in the region) while decreasing the non-renewable resources to meet the demand. The United States' electricity consumption is expected to increase from about 3,873 billion KWh (3873×10^9 KWh) in 2008 to about 5,021 billion KWh in 2035, roughly a 1% annual increase over the next 3 decades (U.S. EIA, 2010). As such, the regions' electricity demand of each year, $E_{demand}(t)$, is increased by 1% a year over the previous year:

$$E_{demand}(t) = E_{demand}(t-1) + 0.1 * E_{demand}(t-1) \quad eq. (1)$$

To meet the demand, the electricity produced in each year (t) is determined from the previous year ($t-1$) as given by:

$$E_{produced}(t) = E_{solar}(t) + E_{hydro}(t) + E_{wind}(t) + E_{biomass}(t) + E_{geothermal}(t) + E_{coal}(t-1) + E_{natural\ gas}(t-1) + E_{petroleum}(t-1) + \dots$$

Where the renewable production is increased annually as given by:

$$E_{renewable}(t) = E_{renewable}(t-1) + C_{renewable} * E_{renewable}(t-1) \quad eq. (3)$$

Where $C_{renewable}$ is a constant for each renewable resource, and is determined based on the available renewable resource of the region, the electricity demand of each region, and how long it will take the region to taper off of fossil fuels and produce its entire electricity from its renewable resources. The parameter $C_{renewable}$ has different values for each renewable resource in each region. Depending on the circumstance, $C_{renewable}$ takes values ranging from 0.01 to 0.05. Considering the cost associated with deep penetration of wind and solar (the most abundant resource relative to the demand in the region), the constant $C_{renewable}$ for wind and solar in all regions is never above 0.03. The target year for total renewability is set at 2050, and depending on the region's abundance of renewable, total renewable generation may occur prior to 2050, or in some cases, it may never occur.

If the electricity produced in a given year is less than the demand for that year, the difference will be made up by increasing the natural gas, as given by:

$$E_{natural\ gas}(t) = E_{natural\ gas}(t) + E_{consumed}(t) - E_{produced}(t) \quad eq. (4)$$

If the electricity produced in a given year is greater than the demand, the difference will be subtracted from the fossil fuels in the order of coal, petroleum, and then natural gas. Once the natural gas contribution reaches zero, the electricity produced will be allowed to surpass the demand. The simulations are performed in a matlab program, using EIA's Electric Power Monthly for April 2016 (EIA, 2016b).

4. Results

The results for all seven regions are shown in Figs. 5 through 11. In these figures, in the top graphs, the blue line is the total electricity generation in the region, the dashed red line is the electricity demand of the region, and the green line is the electricity produced from renewable resources in the region. In the bottom graphs, the contributions of nine resources to the total electricity generation of the region are shown and they include contributions from coal, petroleum, natural gas, (fossil fuels), nuclear, hydro (mostly run of river), wind, solar (photovoltaic), biomass, and geothermal. Note that in all these plots, the year (if any) that the renewable curve intersect the demand curve is the year the region will be able to produce its entire electricity demand from its renewable resources, beyond which the region is able to produce additional electricity to be used in other energy sectors, including transportation by electric vehicles.

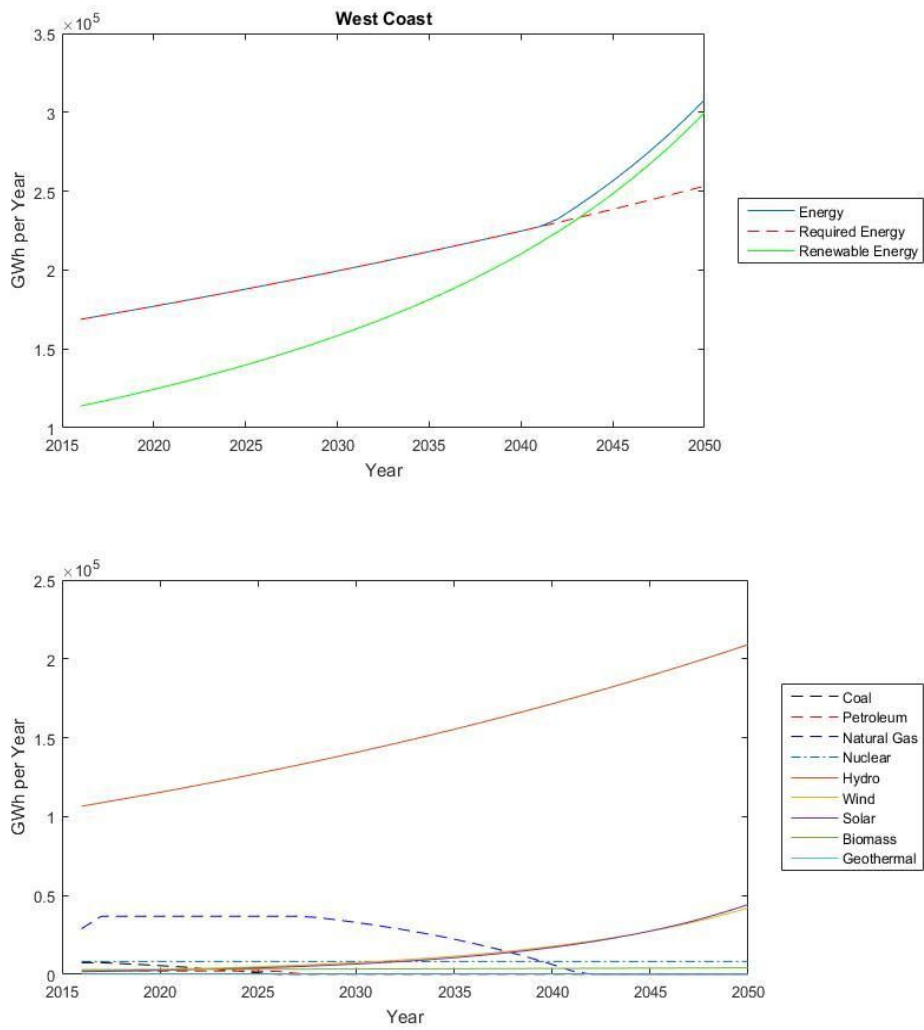


Fig. 5: Electricity generation from all resources in the West Coast States through 2050.

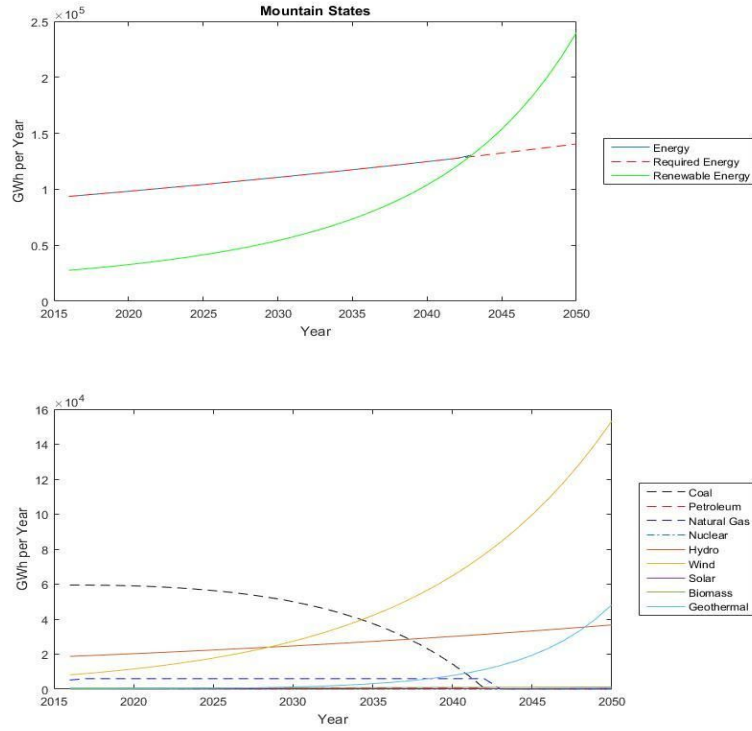


Fig. 6: Electricity generation from all resources in the Mountain States through 2050.

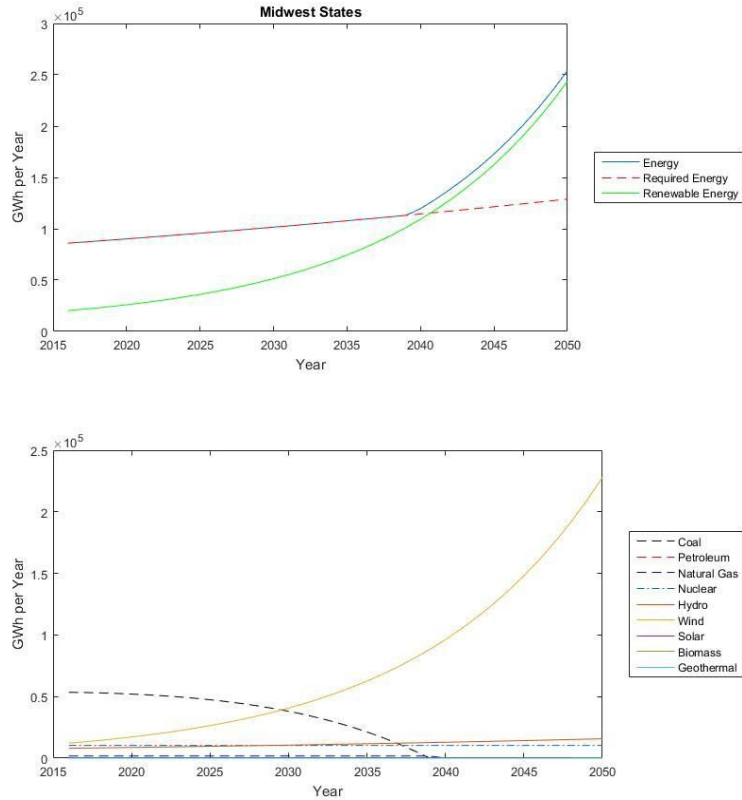


Fig. 7: Electricity generation from all resources in the Middle West States through 2050.

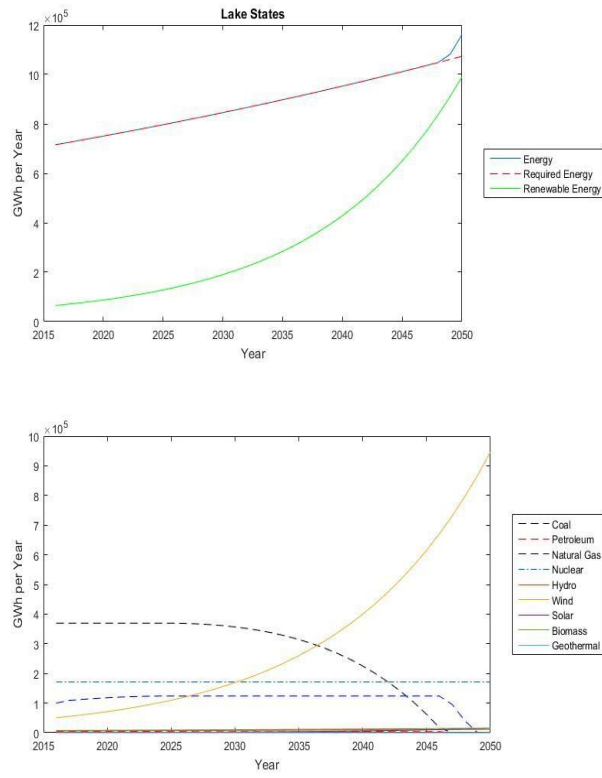


Fig. 8: Electricity generation from all resources in the Lake States through 2050.

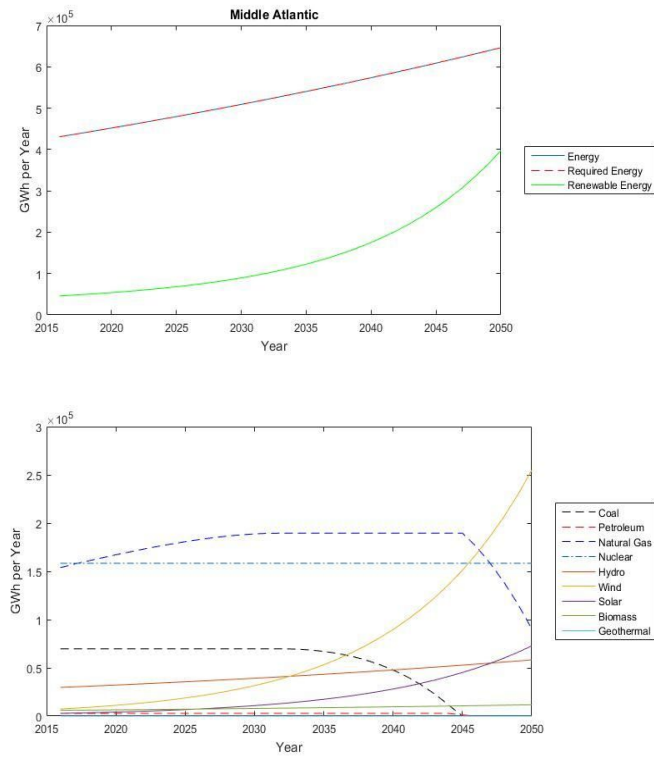


Fig. 9: Electricity generation from all resources in the Middle Atlantic States through 2050.

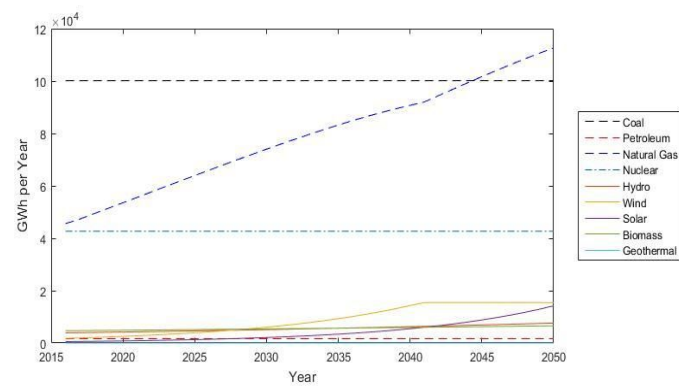
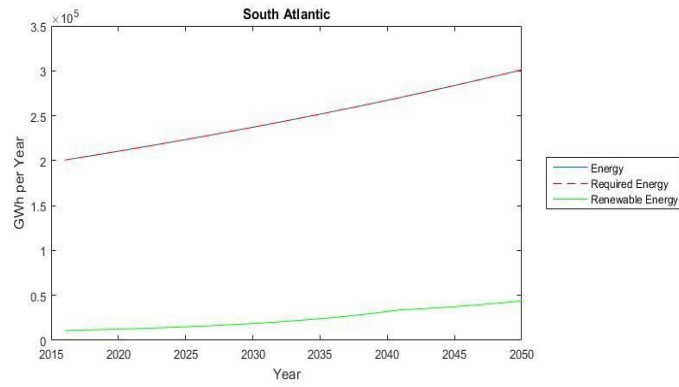


Fig. 10: Electricity generation from all resources in the South Atlantic States through 2050.

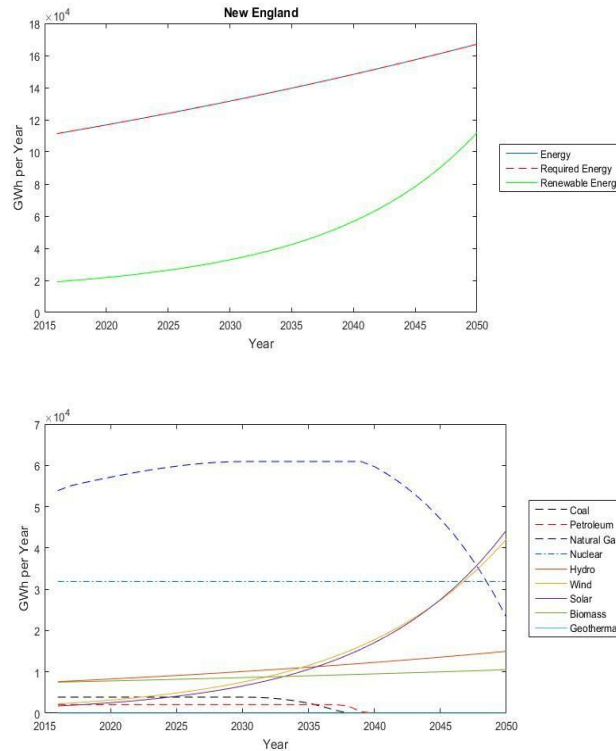


Fig. 11: Electricity generation from all resources in the New England States through 2050.

- The West Coast States: OR, and WA: This region with its vast hydro resources can become 100% fossil-fuel-free in as early as 2041, at which time the wind and solar will also be major contributors to its electricity production. Continued utilization of its renewables, the West Coast states would be able to produce roughly 45,000 GWh of surplus electricity.
- The Mountain States: ID, MT, and WY: This region, in large part due to its abundant wind resources can produce its entire electricity demand from renewables by 2039. At that time, solar resources would also be contributing relatively greatly to its portfolio. The Mountain States will be able to produce roughly 100,000 GWh of electricity, which is roughly 80% more than its total electricity demand.
- The Middle West States: ND, SD, and NE: The vast wind resources of this region, if utilized at 1% a year, will make this region 100% renewable by 2038. Continued utilization of wind (and other renewables) will provide a 120,000 GWh of surplus electricity in this region.
- The Lake States: MN, WI, MI, IA, IN, IL, and OH: This region could reach 100% renewable just beyond 2050, at which time; fossil fuels will produce roughly 80,000 GWh of electricity. The available wind and solar resources of this region, although contributing a major portion to electricity generation, would be just short of 100% renewable production.
- The Middle Atlantic States: NJ, NY, and PA: Although solar and wind can contribute greatly to its electricity generation, by 2050, this region would need roughly 250,000 GWh of its electricity to be generated from its non-renewable resources mostly natural gas and nuclear.
- The South Atlantic States: MD, VA, WV, and DE. This region will remain mostly dependent on its nor-renewable resources and will have the largest shortage of renewable generation (roughly 260,000 GWh) to meet its projected demand in 2050. At that time, wind and solar will contribute about 3,200 GWh to its electricity generation, which remains a small portion of its portfolio.

- The New England States: CT, ME, MA, NH, RI, and VT: In 2050, these states will have a total electricity need of 168,000 GWh with renewables producing 57,000 GWh, leaving the balance to be produced from non-renewables.

5. 5. Conclusions

The results shown in Figures 5 thru 11 are summarized in Tab. 1, which lists the years that the regions can produce their entire electricity demand from renewable resources. The West Coast, Mountain, and Middle West regions has the potential to become 100% renewable in the years 2041, 2039, and 2038, respectively. This is mostly due to the great abundance of wind energy, especially in the states of Montana, North Dakota, and South Dakota. Furthermore, these three regions can produce significant surplus of electricity.

The other four regions, namely Lake, Mid Atlantic, South Atlantic, and New England states will not be able to reach 100% electricity generation from their renewable resources. This is in part due to relatively less available renewable resources and relatively high electricity demand in these regions. This is particularly true in the South Atlantic region (Maryland, Virginia, West Virginia, and Delaware) where the shortage of renewable resources is the greatest. It is ironic that this region has abundance of coal resources. The utilization of off-shore wind (not included in this model) and distributed generation by renewables can to an extent mitigate this issue.

Tab. 1: The year the regions would be fossil fuel free in electricity generation (if ever).

Region	States	100% Renewable by	Shortage of Renewables (GWh)
West Coast	OR, WA	2041	0
Mountain	ID, MT, WY	2039	0
Middle West	ND, SD, NE	2038	0
Lake States	MN, WI, MI, IA, IN, IL, OH	Just beyond 2050	-80,000
Mid Atlantic	NJ, NY, PA	Never	-250,000
South Atlantic	MD, VA, WV, DE	Never	-260,000
New England	CT, ME, MA, NH, RI, VT	Never	-111,000

6. 6. References

7. Hand, M.M., Baldwin, S., DeMeo, E., Reilly, J.M., Mai, T., Arent, D., Porro, G., Meshek, M., Sandor, D., National Renewable Energy Laboratory, (2012). Renewable Electricity Futures Study. eds. 4. NREL/TP-6A20-52409. Golden, CO. http://www.nrel.gov/analysis/re_futures/. Accessed: August 2018.

8. Khoie, R and Yee, V, 2015. A forecast model for deep penetration of renewables in the Southwest, South Central, and Southeast regions of the United States. *Clean Technologies and Environmental Policy*. Vol. 17, No. 4, pp. 957-971.
9. Mai, T. 2012. National Renewable Energy Laboratory. Renewable Electricity Futures Study. Volume I, Exploration of High-Penetration Renewable Electricity Futures. http://www.nrel.gov/analysis/re_futures/ and in <http://www.nrel.gov/docs/fy12osti/52409-1.pdf>, Accessed March 2013.
10. NREL, 2018a. National Renewable Laboratory, Geospatial Data Science. <http://www.nrel.gov/gis/solar.html>. Accessed: August 2018.
11. NREL, 2018b. National Renewable Laboratory, Geospatial Data Science. <http://www.nrel.gov/gis/wind.html>. Accessed: August 2018.
12. Oak Ridge National Laboratory, 2018. <https://nhaap.ornl.gov/content/non-powered-dam-potential>. Accessed: August 2018.
13. U.S. Energy Information Administration, 2010. Annual Energy Outlook 2010: With Projections to 2035. Washington, D.C.: U.S. Department of Energy.
14. U.S. Energy Information Administration, 2016a. Oregon State Profile and Energy Estimates. <https://www.eia.gov/state/sid=OR/>. Accessed: August 2018.
15. U.S. Energy Information Administration, 2016b. Electricity, Electric Power Monthly. <https://www.eia.gov/electricity/monthly/>. Accessed: August 2018.
16. U.S. Energy Information Administration, 2018a. Electricity, Generation Data by State. <https://www.eia.gov/electricity/data/state/>. Accessed: August 2018.
17. U.S. Energy Information Administration, 2018b. Electricity in the United States. <https://www.eia.gov/energyexplained/>. Accessed: August 2018.



Conference Proceedings

ASES National Solar Conference 2018

Boulder, Colorado August 5-8, 2018

Challenging Conventional Wisdom in the Age of Computing

Khaled A. Mansy¹

¹ Oklahoma State University, Stillwater (USA)

Abstract

This paper examines what might be referred to as the “Designer’s Conventional Wisdom”. In both practice and academia, some designers still follow what they consider to be well-established design recommendations to make buildings more energy efficient by responding to site-specific sun angles and climate. Among the early schematic design recommendations are some that address building massing and orientation. In terms of building massing, it is advised to design rectangular buildings that spread from east to west; the longer the building is the more energy efficient it is. In terms of orientation, it is advised to orient the building to north and south rather than to east and west. In order to protect windows from the sun, overhangs should be used to protect south-facing glass, while vertical fins should be used for glass facing east and west. Nowadays, with the availability of powerful design-assisting tools, such as energy modeling computer programs, it is imperative that we examine the validity and/or accuracy of such conventional wisdom. This paper takes office buildings in the US as a case study in examining the aforementioned design recommendations grandfathered into design until our current time. The paper will examine the sensitivity of performance to such recommendations at different climatic zones within the United States.

Keywords: Energy performance, energy efficiency, energy simulation, eQuest, orientation, external shading devices, evidence-based design, design-assisting tools

1. The Problem

During the early stages of design, architects rely on their basic design knowledge to find simple answers to design problems. When it comes to considering building performance during the early schematic design stages, a certain set of generic design recommendations is often used (refer to the list below). Such recommendations belong to an inherited body of knowledge that was passed on from generation to generation and from master to apprentice. They gained the trust of today’s architects because of the long time they have been in use. This is what might be referred to as the “Designer’s Conventional Wisdom”. In academia, in most cases, the same inherited knowledge is currently being passed on from design faculty to students. Examples of such performance-related design recommendations are:

1. West is the worst orientation. Use smaller windows on west compared to east (Autodesk, 2018).
2. Orient rectangular buildings to north and south, not to east and west (Mazria, 1979).
3. The longer the building (east to west) is, the more energy efficient it is.

4. Differently oriented walls need different kinds of shading devices. Use external shading devices to shade windows. On the south side, use overhangs. On east and west, use vertical fins (Olgyay and Olgyay, 1957) and (Grondzik and Kwok, 2014).
5. For better performance, apply as many energy-saving measures as possible.

A real concern regarding the use of this Designer's Conventional Wisdom is the fact that it is still being passed on to architecture students unquestioned as inherited without being verified using readily-available advanced design-assisting tools. This paper aims to examine the validity and accuracy of such widely-used initial design recommendations taking advantage of government-validated energy simulation computer programs.

2. Methodology

The paper employs energy simulation of a simple office space to test the "performance sensitivity" to each single design recommendation under question. An energy model is built for a single perimeter thermal zone that represents a typical office space. Hourly simulation, using eQuest 3.64, is run for the model when facing eight different orientations (North, NE, East, SE, South, SW, West, and NW) once with no protection of windows, then with twelve design variations of external shading devices (Figure 1). For each simulation, performance sensitivity (to the two aforementioned design variables, i. e., orientation and external shading) is documented in terms of its Energy Use Index (EUI) in KBtu/sf.yr. The tabulated results (EUI values) are then used to assess the validity and accuracy of each of the design recommendations under question.

In each climate zone, besides the baseline for comparison (no external shading), the twelve tested design variations of external shading devices are (1) overhangs with protection factors of 0.20, 0.35, 0.50, and 1.00, (2) vertical fins with protection factor of 0.20, 0.35, 0.50, and 1.00, and (3) egg-crate with protection factors of 0.20, 0.35, 0.50, and 1.00 (Figure 1).

3. Energy Simulation

Energy performance of an office space, that is 15-ft (4.5 M) deep middle bay on a middle floor, is tested in three different climate zones. From the eight climate zones established by the International Code Council (ICC) (Figure 2), the energy model is tested in three representative cities that represent the warmest, the coldest, and a middle point in between within the continental United States. Miami, Florida, represents hot climate, Los Angeles, California, represents temperate climate, and Fairbanks, Alaska, represents cold climate. Future research may cover all eight climate zones. Refer to Table 1 for locations and climatic data of the eight cities representing climate zones within the USA.

The energy model is customized per climate zone according to the "Building Envelope Requirements" in Chapter 4 (CE) of the International Energy Conservation Code (IECC 2015). Refer to Table 2 for the IECC climate-specific building envelope requirements for commercial buildings. In each of the three tested climate zones, the exterior wall of the model is linked to a construction type of the maximum allowed U-factor in such climate zone. In terms of fenestration requirements, glass ratio is 40% of the gross above-grade wall area; assuming daylight responsive control. The window is linked to a glass type of the performance properties required by code for 0.2 Protection Factor (PF), while facing SEW (South, East, West). Although the code allows higher Solar Heat Gain Coefficient (SHGC) under greater PF and when facing north, in order to maintain consistency of the results by testing one variable at a time, only one SHGC value is used in each climate zone, regardless of the PF and orientation. Glass Visible Transmittance (VT) is kept to the code minimum at 1.1 x SHGC. All other input data into the energy model represent a typical office space in compliance with applicable codes (IECC), ASHRAE standards, and common practice. Occupancy is 200 SF/Person, heat gain from occupants is 250 Btu/sensible + 105 Btu/latent heat per person, required fresh air is 5.0 CFM/Person + 0.06 CFM/SF (ANSI/ASHRAE Standard 62.1-2016), illumination level is 25 fc, thermostat temperature is 72 °F (22.2 °C) in the summer and 70 °F (21.1 °C) in the winter, light load is 0.98 W/SF (IECC, 2015), equipment load is 1.3 W/SF, working hours are 9:00 am – 5:00 pm (Standard Time), equipment maintain thermostat temperature 8:00 am – 6:00 pm, mechanical equipment is an air-to-air heat pump with an economizer, and no heat recovery. Simulation is run for twelve months with US typical holidays using TMY3 weather files.

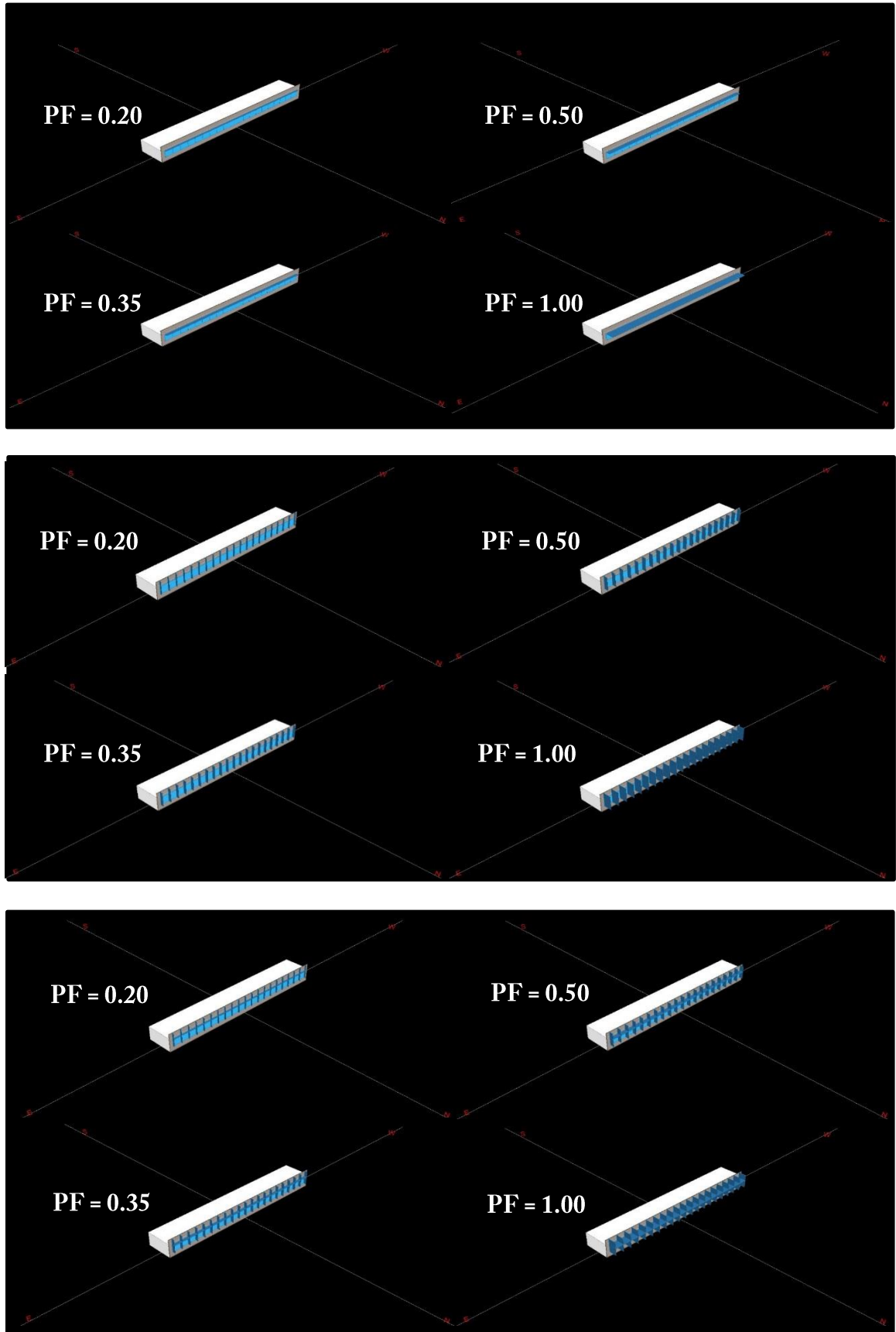


Fig 1: The twelve tested design variations of external shading devices. Three groups of (1) overhangs, (2) vertical fins, and (3) egg-crate

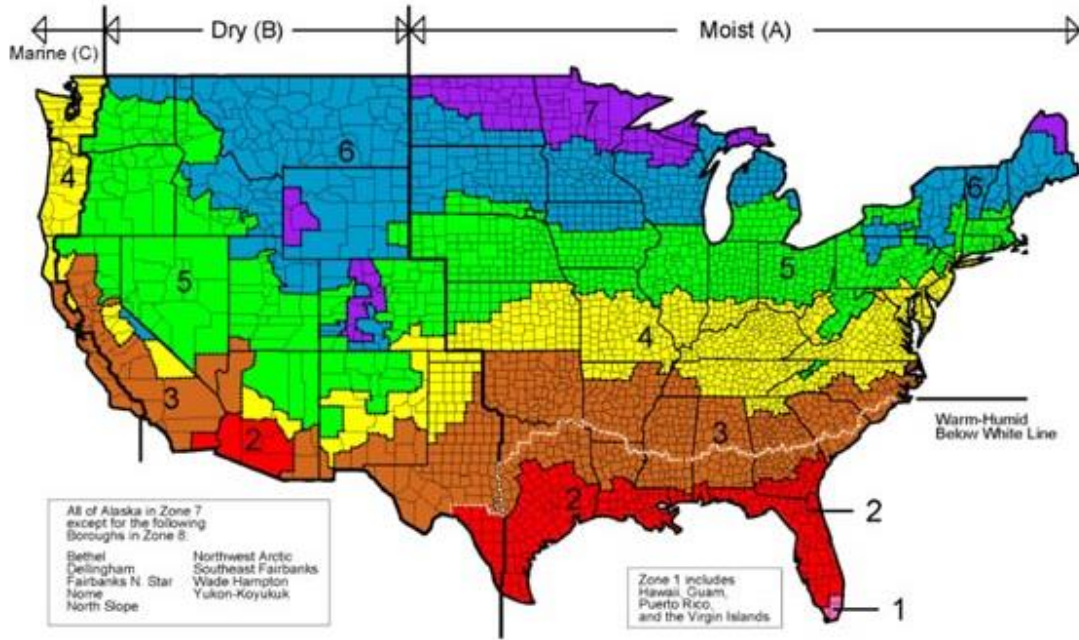


Fig 2: Climate zones, according to International Energy Conservation Code 2015

Table 1: Location and climatic data of the eight reference cities of climate zones within the USA

Climate Zone	City	State	Latitude (degrees)	Longitude (degrees)	Elevation (ft)	Time Zone (hr)	HDD65	CDD50
1A Hot, Humid	Miami	Florida	25.80	80.30	12	-5	200	9,474
2B Hot, Dry	Phoenix	Arizona	33.43	112.02	1,110	-7	1,350	8,425
3B Warm, Dry	Los Angeles	California	33.93	118.38	100	-8	1,458	4,777
4B Mild, Dry	Albuquerque	New Mexico	35.05	106.62	5,326	-7	4,425	3,908
5B Cold, Dry	Denver	Colorado	39.77	104.87	5,286	-7	6,020	2,732
6B Cold, Dry	Helena	Montana	46.60	112.00	3,893	-7	8,031	1,922
7 Very Cold	Duluth	Minnesota	46.83	92.18	1,428	-6	9,818	1,536
8 Extremely Cold	Fairbanks	Alaska	64.82	147.87	436	-9	13,940	1,010

Table 2: Building envelope requirements per climate zone (commercial buildings)

Climate Zone	City	State	Ext. Wall U-Factor (max)	Glass U-Factor (max)	Glass SHGC (max)			Glass VT (min)		
					PF<0.2	0.2<PF<0.5	0.5<PF	PF<0.2	0.2<PF<0.5	0.5<PF
1A Hot, Humid	Miami	Florida	0.077	0.500	0.250	0.300	0.400	0.275	0.330	0.440
2B Hot, Dry	Phoenix	Arizona	0.077	0.500	0.250	0.300	0.400	0.275	0.330	0.440
3B Warm, Dry	Los Angeles	California	0.064	0.460	0.250	0.300	0.400	0.275	0.330	0.440
4B Mild, Dry	Albuquerque	New Mexico	0.064	0.380	0.400	0.480	0.640	0.440	0.528	0.704
5B Cold, Dry	Denver	Colorado	0.064	0.380	0.400	0.480	0.640	0.440	0.528	0.704
6B Cold, Dry	Helena	Montana	0.064	0.360	0.400	0.480	0.640	0.440	0.528	0.704
7 Very Cold	Duluth	Minnesota	0.064	0.290	0.450	NR	NR	0.495	NR	NR
8 Extremely Cold	Fairbanks	Alaska	0.045	0.290	NR	NR	NR	NR	NR	NR

4. Performance Results

After performing energy simulation, all needed performance data are generated and tabulated in terms of the Energy Use Index (EUI). The performance of the case study office space is documented in Appendices 1, 2, and 3, which show the performance of the baseline (no protection) and the twelve variations of external shading. With the help of this dataset, it is possible to look carefully into the performance sensitivity to both of the orientation and the design of external shading devices in the three selected climate zones.

4.1. Performance in Hot Climate

In Miami, Florida, the sun is high in the sky almost all year long. Climate is hot with mild winters. Performance is dominated by the high need for cooling, with almost no need for heating, especially during working hours. In reference to simulation results for Miami (Appendix 1), the following conclusions can be drawn:

- Worst orientation is SW at EUI of 35.87 KBtu/sf.yr for windows without external shading (Table 3). SW remains to be the worst orientation even with external shading devices. However, SW is not significantly higher than SE and South. A deep overhang or egg-crate diminishes the effect of orientation on performance since EUI becomes almost flat regardless of orientation.
- Rectangular buildings facing north and south are more efficient than buildings facing east and west (Table 4). However, it is worth mentioning that the E&W orientation is only 5.8% higher than N&S without shading devices and can be up to 8.1% in case of deep vertical fins (PF = 0.5).
- Facing all orientations, overhangs are more effective than vertical fins; with potential energy savings of 16.85% in case of very deep overhangs (PF = 1.0). The only exception is with very deep vertical fins facing north and northeast.

Table 3: EUI of the perimeter office space in KBtu/sf.yr and relative to the index (north-facing)

Miami, FL									
	South	SW	West	NW	North	NE	East	SE	South
Baseline (no protection)	35.60	35.87	34.33	32.20	30.00	32.60	35.07	35.60	35.60
Relative to index	1.187	1.196	1.144	1.073	1.000	1.087	1.169	1.187	1.187
% Higher than index	18.67%	19.56%	14.44%	7.33%	0.00%	8.67%	16.89%	18.67%	18.67%
	highest				index				
Los Angeles, CA									
	South	SW	West	NW	North	NE	East	SE	South
Baseline (no protection)	28.27	28.20	27.20	24.53	22.27	24.44	26.60	27.73	28.27
Relative to index	1.269	1.266	1.222	1.102	1.000	1.098	1.195	1.246	1.269
% Higher than index	26.95%	26.65%	22.16%	10.18%	0.00%	9.76%	19.46%	24.55%	26.95%
	highest				index				
Fairbanks, AK									
	South	SW	West	NW	North	NE	East	SE	South
Baseline (no protection)	34.67	35.93	36.60	36.20	36.20	38.13	37.80	35.80	34.67
Relative to index	0.958	0.993	1.011	1.000	1.000	1.053	1.044	0.989	0.958
% Higher than index	-4.24%	-0.74%	1.10%	0.00%	0.00%	5.34%	4.42%	-1.10%	-4.24%
	highest				index				

Table 4: Combined EUI of two perimeter spaces facing two opposite orientations (north & south, and east & west) in KBtu/sf.yr and relative to the index (index is north-facing with no protection)

	Miami, FL			Los Angeles, CA			Fairbanks, AK		
	N&S	E&W	E&W/N&S	N&S	E&W	E&W/N&S	N&S	E&W	E&W/N&S
No Protection	32.80	34.70	105.8%	25.27	26.90	106.5%	35.43	37.20	105.0%
Overhang, PF = 0.20	31.83	33.30	104.6%	24.47	25.87	105.7%	34.90	36.63	105.0%
Overhang, PF = 0.35	31.20	32.43	104.0%	24.03	25.23	105.0%	34.53	36.30	105.1%
Overhang, PF = 0.50	30.63	31.63	103.3%	23.57	24.60	104.4%	34.23	36.00	105.2%
Overhang, PF = 1.00	29.30	30.10	102.7%	22.77	23.17	101.8%	33.83	35.27	104.2%
Vertical Fins, PF = 0.20	32.37	34.70	107.2%	24.53	26.10	106.4%	35.07	37.03	105.6%
Vertical Fins, PF = 0.35	31.77	34.27	107.9%	24.07	25.67	106.6%	34.77	36.87	106.0%
Vertical Fins, PF = 0.50	31.43	33.97	108.1% Max.	23.87	25.43	106.6%	34.73	36.87	106.1% Max.
Vertical Fins, PF = 1.00	30.37	32.50	107.0%	23.07	24.77	107.4% Max.	34.67	36.60	105.6%
Eggcrate, PF = 0.20	31.53	33.47	106.1%	23.93	25.20	105.3%	34.63	36.57	105.6%
Eggcrate, PF = 0.35	30.60	32.23	105.3%	23.23	24.33	104.7%	34.33	36.30	105.7%
Eggcrate, PF = 0.50	29.87	31.23	104.6%	22.73	23.63	104.0%	34.13	36.03	105.6%
Eggcrate, PF = 1.00	28.87	29.47	102.1%	22.00	22.47	102.1%	34.40	35.73	103.9%

4.2. Performance in Temperate Climate

In Los Angeles, California, the sun is still relatively high in the sky. Climate is relatively temperate due to proximity to the Pacific Ocean. However, building performance is dominated by cooling with the need of some heating in the winter. In reference to simulation results for Los Angeles (Appendix 2), the following conclusions can be drawn:

- The worst orientation is south at EUI of 28.27 KBtu/sf.yr for windows without external shading (Table 3). South remains to be the worst orientation only in case of not-so-deep overhangs, otherwise SW is the worst for all other variations of external shading.
- Rectangular buildings facing north and south are more efficient than buildings facing east and west (Table 4). However, it is worth mentioning that the E&W orientation is only 6.5% higher than N&S without shading devices and can be up to 7.4% in case of deep vertical fins (PF = 1.0).
- Facing all orientations, overhangs are more effective than vertical fins; with potential energy savings of 16.27% in case of very deep overhangs (PF = 1.0). The only exception is when the building is facing North, NE, and NW where vertical fins become more effective than overhangs.

4.3. Performance in Cold Climate

In Fairbanks, Alaska, the sun is low in the sky almost all year long. The climate is extremely cold and building performance is dominated by heating with much less need for cooling. In reference to simulation results for Fairbanks (Appendix 3), the following conclusions can be drawn:

- The worst orientation is NE at EUI of 38.13 KBtu/sf.yr for windows without external shading (Table 3). NE remains to be the worst orientation except in case of deep fins and egg-crates.
- Rectangular buildings facing north and south are more efficient than buildings facing east and west (Table 4). However, it is worth mentioning that the E&W orientation is only 5.0% higher than N&S without shading devices and can be up to 6.1% in case of deep vertical fins (PF = 0.5).
- Facing all orientations, overhangs are more effective than vertical fins; with potential energy savings of up to 7.69% in case of very deep overhangs (PF = 1.0). The only exception is when the building is facing North, NE, and NW where vertical fins become more effective than overhangs.

5. Conclusions

With the help of the calculated EUI values (Appendices 1, 2, and 3), it was possible to examine the performance sensitivity to both orientation and design variations of external shading and draw climate-specific conclusions, as listed in the following:

1. In terms of worst orientation: In climates dominated by cooling, the worst orientation is the south or SW. In climates dominated by heating, NE is the worst orientation. Here, it is worth mentioning that this result contradicts previous research results in which SE was found to be the worst orientation in climates dominated by cooling (Mansy et al., 1999). Cooling load of a space facing SE may be higher than when facing all other orientations only when the HVAC system is set to respond to the occupied thermostat temperature starting the same time when employees first enter the space (no pre-cooling). In such case, the HVAC system must respond to very high cooling load in the early morning due to sudden change in occupancy coupled with extracting stored heat in space.
2. Assuming no external shading devices, rectangular buildings facing north and south outperform buildings facing east and west in all climates, including climates dominated by heating. However, compared to buildings facing N&S, buildings facing E&W only consume an additional 5.0% to 6.5% in annual energy consumption, which is not as significant as designers may initially assume.
3. Here, it is worth mentioning that when rectangular buildings do not have windows on the short sides, the length of the building has no effect on building performance. In such case, the EUI of the building remains equal to the average EUI of the two opposite sides of the rectangle, regardless of how long the building is. A possible exception would be when the HVAC system is capable of transferring heat between thermal zones facing the two opposite directions (such as closed-loop heat pump systems).

4. The interesting observation is that overhangs outperform vertical fins in all three climate zones when facing all orientations, except the north. EUI values obtained from the simulation clearly show that: (1) overhangs are significantly more effective than vertical fins in hot climates, (2) overhangs are slightly more effective than vertical fins in temperate climates, and (3) both overhangs and vertical fins are somehow effective in cold climate, in which overhangs still outperform vertical fins.
5. Tabulated EUI values clearly make the case for the fact that implementing multiple energy saving measures (to the same building) does not mathematically add up, which is often an interesting subject of discussion with design students. For example, when an overhang results in 2.00% energy saving and a vertical fin saves 1.78%, the egg-crate integrating both together does not save 3.78%, it actually saves 2.67%. Shading the same area of the glass twice does not yield energy savings twice. The same principle is true in case of applying multiple measures that simultaneously affect the same load component, i.e., solar load component, transmitted load component, internal heat gain component, and outside air load component.

It should be noted that designers should be cautious if they refer to the EUI values generated in this paper. These EUI values apply to a perimeter thermal zone on which envelope load has the greatest influence. EUI of a complete building that includes a mix of perimeter and internal thermal zones is typically lower. Another precaution is due to using the same HVAC system, an air-to-air heat pump, in all three climates. Air-to-air heat pumps lose efficiency when heating in a very cold climate like Fairbanks, Alaska. Therefore, lower EUI values may be achieved in cold climate when using gas-fired heating equipment.

6. References

- ASHRAE 2016. ANSI/ASHRAE Standard 62.1 Ventilation for Acceptable Indoor Air Quality, 2016.
- Autodesk, 2018. Autodesk Knowledge Network, <https://knowledge.autodesk.com>, 2018
- Grondzik and Kwok, 2014. Mechanical and Electrical Equipment for Buildings, 12th ed., John Wiley & Sons Inc., New Jersey, USA, 2014
- IECC 2015. International Code Council, International Energy Conservation Code, 2015.
- Mansy, Dolan, and Krawczyk, 1999. Climate Responsive Forms, energy conservation through building form and orientation, Sustain 1999, UAE.
- Mazria, 1979. The Passive Solar Energy Book, Expanded Professional Edition, Rodale Press, Emmaus, Pennsylvania, 1979.
- Olgyay and Olgyay, 1957. Solar Control and Shading Devices, Princeton University Press, Princeton, New Jersey, 1957.

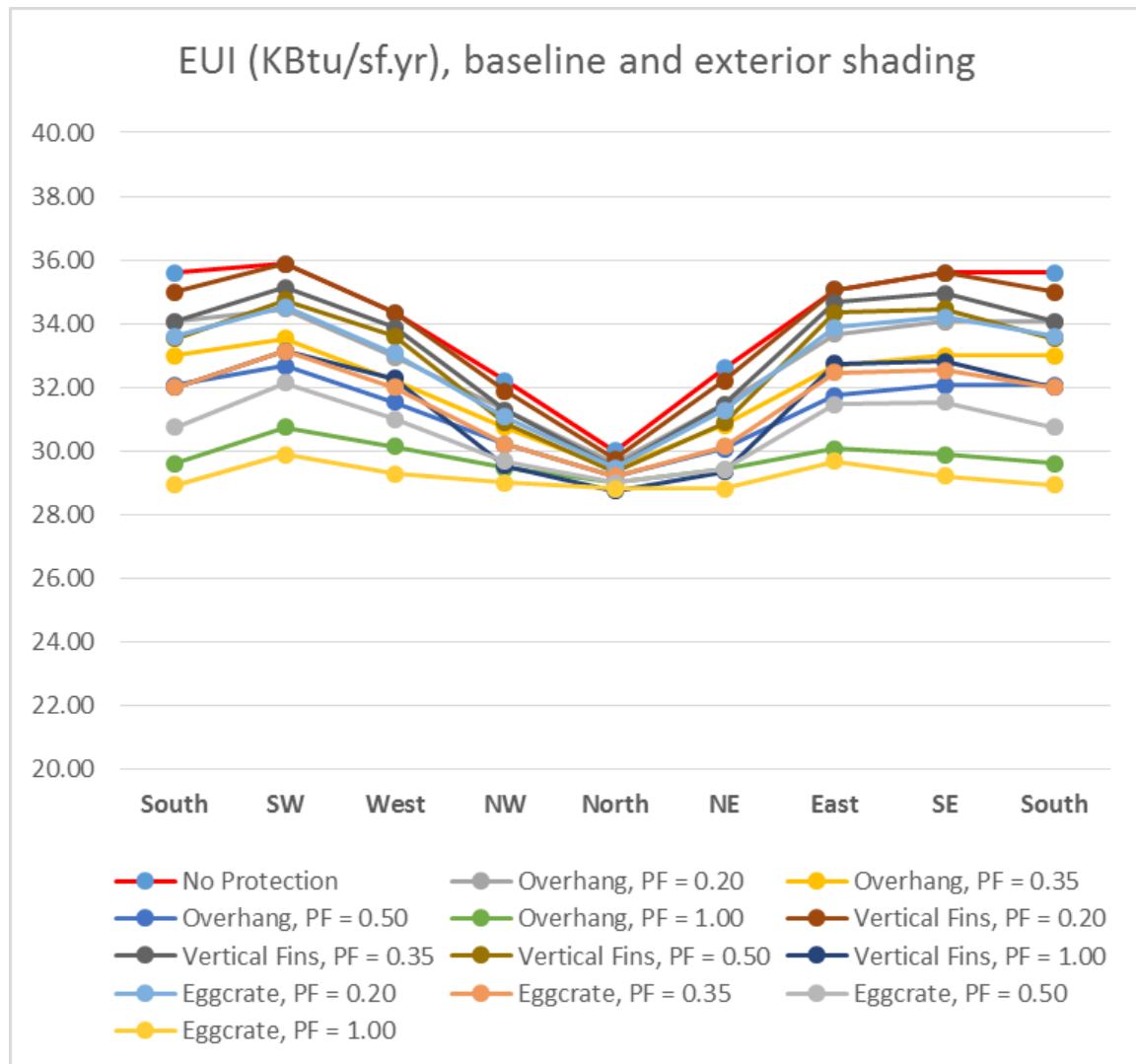
Appendix 1: Dataset for Miami, Florida

Energy simulation results in EUI (KBtu/sf.yr) of the baseline model (no protection) and 12 design variations of external shading devices in Miami, Florida (Climate Zone # 1).

Miami, FL

EUI Per Orientation in KBtu/sf.yr

	South	SW	West	NW	North	NE	East	SE	South
No Protection	35.60	35.87	34.33	32.20	30.00	32.60	35.07	35.60	35.60
Overhang, PF = 0.20	34.07	34.47	32.93	31.27	29.60	31.47	33.67	34.07	34.07
Overhang, PF = 0.35	33.00	33.53	32.20	30.73	29.40	30.80	32.67	33.00	33.00
Overhang, PF = 0.50	32.07	32.67	31.53	30.20	29.20	30.07	31.73	32.07	32.07
Overhang, PF = 1.00	29.60	30.73	30.13	29.47	29.00	29.40	30.07	29.87	29.60
Vertical Fins, PF = 0.20	35.00	35.87	34.33	31.87	29.73	32.20	35.07	35.60	35.00
Vertical Fins, PF = 0.35	34.07	35.13	33.87	31.27	29.47	31.47	34.67	34.93	34.07
Vertical Fins, PF = 0.50	33.53	34.73	33.60	30.87	29.33	30.87	34.33	34.47	33.53
Vertical Fins, PF = 1.00	32.00	33.13	32.27	29.53	28.73	29.33	32.73	32.80	32.00
Eggcrate, PF = 0.20	33.60	34.53	33.07	31.07	29.47	31.27	33.87	34.20	33.60
Eggcrate, PF = 0.35	32.00	33.13	32.00	30.20	29.20	30.13	32.47	32.53	32.00
Eggcrate, PF = 0.50	30.73	32.13	31.00	29.67	29.00	29.40	31.47	31.53	30.73
Eggcrate, PF = 1.00	28.93	29.87	29.27	29.00	28.80	28.80	29.67	29.20	28.93



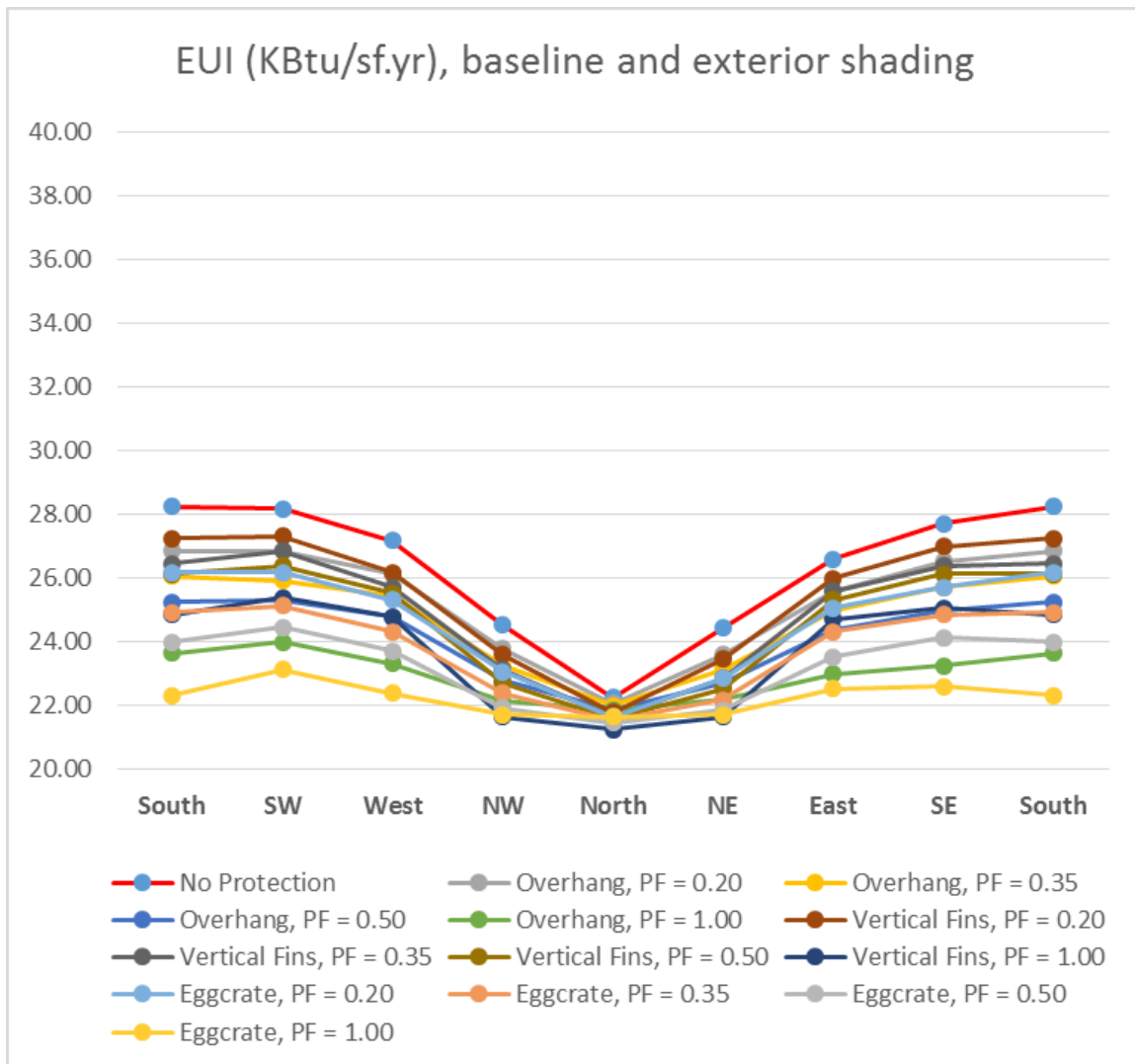
Appendix 2: Dataset for Los Angeles, California

Energy simulation results in EUI (KBtu/sf.yr) of the baseline model (no protection) and 12 design variations of external shading devices in Los Angeles, California (Climate Zone # 3).

Los Angeles, CA

EUI Per Orientation in KBtu/sf.yr

	South	SW	West	NW	North	NE	East	SE	South
No Protection	28.27	28.20	27.20	24.53	22.27	24.44	26.60	27.73	28.27
Overhang, PF = 0.20	26.87	26.87	26.13	23.80	22.07	23.60	25.60	26.53	26.87
Overhang, PF = 0.35	26.07	25.93	25.47	23.27	22.00	23.13	25.00	25.73	26.07
Overhang, PF = 0.50	25.27	25.33	24.80	22.80	21.87	22.73	24.40	25.00	25.27
Overhang, PF = 1.00	23.67	24.00	23.33	22.13	21.87	22.20	23.00	23.27	23.67
Vertical Fins, PF = 0.20	27.27	27.33	26.20	23.60	21.80	23.47	26.00	27.00	27.27
Vertical Fins, PF = 0.35	26.47	26.87	25.73	23.13	21.67	22.87	25.60	26.40	26.47
Vertical Fins, PF = 0.50	26.13	26.40	25.53	22.73	21.60	22.53	25.33	26.13	26.13
Vertical Fins, PF = 1.00	24.87	25.40	24.80	21.67	21.27	21.67	24.73	25.07	24.87
Eggcrate, PF = 0.20	26.20	26.20	25.33	23.07	21.67	22.87	25.07	25.73	26.20
Eggcrate, PF = 0.35	24.93	25.13	24.33	22.40	21.53	22.20	24.33	24.87	24.93
Eggcrate, PF = 0.50	24.00	24.47	23.73	21.93	21.47	21.87	23.53	24.13	24.00
Eggcrate, PF = 1.00	22.33	23.13	22.40	21.73	21.67	21.73	22.53	22.60	22.33

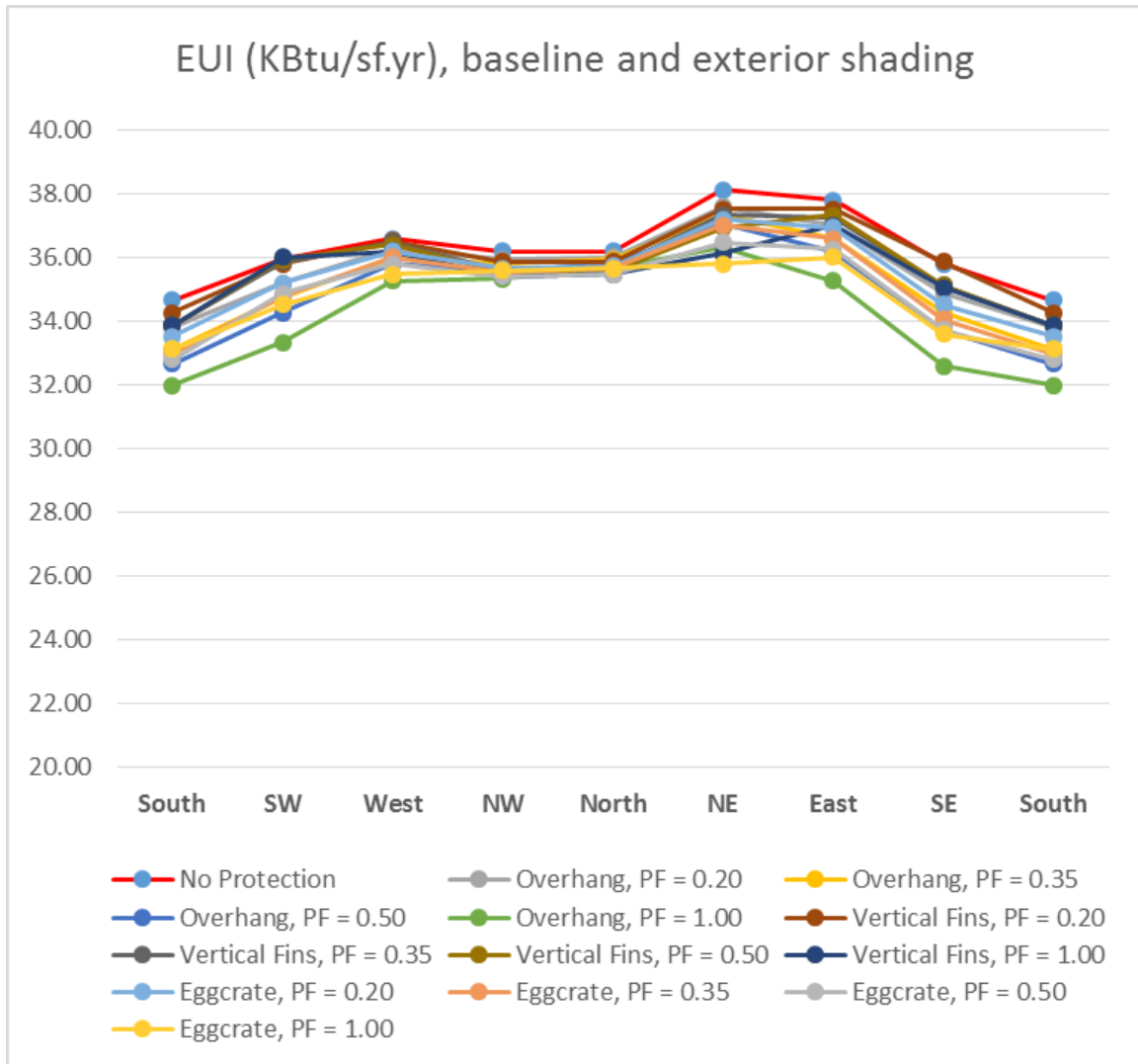


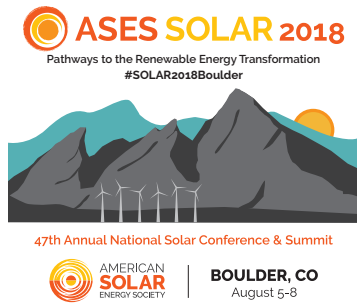
Appendix 3: Dataset for Fairbanks, Alaska

Energy simulation results in EUI (KBtu/sf.yr) of the baseline model (no protection) and 12 design variations of external shading devices in Fairbanks, Alaska (Climate Zone # 8).

Fairbanks, AK

EUI Per Orientation in KBtu/sf.yr	
	South SW West NW North NE East SE South
No Protection	34.67 35.93 36.60 36.20 36.20 38.13 37.80 35.80 34.67
Overhang, PF = 0.20	33.80 35.20 36.27 35.93 36.00 37.60 37.00 34.87 33.80
Overhang, PF = 0.35	33.13 34.73 36.00 35.80 35.93 37.33 36.60 34.27 33.13
Overhang, PF = 0.50	32.67 34.27 35.80 35.60 35.80 37.07 36.20 33.73 32.67
Overhang, PF = 1.00	32.00 33.33 35.27 35.33 35.67 36.33 35.27 32.60 32.00
Vertical Fins, PF = 0.20	34.27 35.80 36.53 35.87 35.87 37.53 37.53 35.87 34.27
Vertical Fins, PF = 0.35	33.87 35.87 36.47 35.60 35.67 37.33 37.27 35.13 33.87
Vertical Fins, PF = 0.50	33.87 35.93 36.40 35.53 35.60 36.93 37.33 35.13 33.87
Vertical Fins, PF = 1.00	33.87 36.00 36.20 35.40 35.47 36.13 37.00 35.07 33.87
Eggcrate, PF = 0.20	33.53 35.20 36.20 35.67 35.73 37.20 36.93 34.53 33.53
Eggcrate, PF = 0.35	33.00 34.80 36.00 35.53 35.67 37.00 36.60 34.07 33.00
Eggcrate, PF = 0.50	32.80 34.87 35.80 35.40 35.47 36.47 36.27 33.73 32.80
Eggcrate, PF = 1.00	33.13 34.53 35.47 35.60 35.67 35.80 36.00 33.60 33.13





Conference Proceedings

ASES National Solar Conference 2018
Boulder, Colorado August 5-8, 2018

“Homebrew” Wind Turbines for Integration into Small-Scale Renewable Energy Systems

Jack Martin¹ and Deborah Amaral¹

¹Handy Village Institute, Saxapahaw, North Carolina (United States)

deborah@handyvillage.com

Abstract

Inspired by their experiences installing integrated renewable energy systems and trainings at the Midwest Renewable Energy Association and the Centre for Alternative Technology, a small team in North Carolina developed the Handy Village Institute. Using the plans crafted and tested by Otherpower, the Institute has offered workshops in building small wind turbines to participants from other countries and regions of the United States. In 2018, participants included six members from three southern Louisiana Native American tribes, who will install the turbine they built to provide renewable energy at their tribal center.

Keywords: *integrated renewable energy, cooperative, small wind, homebrew wind turbine, tribal renewable energy, land loss, climate change, Midwest Renewable Energy Association, Otherpower, Handy Village Institute, Centre for Alternative Technology, Native American tribes, motivate, enlighten, empower, Lowlander Institute, trade skills, electrical, woodworking, fiberglass, steel, metal, fabrication, power generation, design, theory*

1. Introduction

The former Solar Village Institute offered renewable energy installations (solar, wind, hydro, biodiesel). However small wind was a problem, which required a team to install and maintain. But, the more significant problem was warranties that were not honored and the exit of manufacturers. Jack Martin and Chris Carter thought a coop arrangement might alleviate the team problem. Deborah Amaral and Chris attended trainings at the Center for Alternative Technology in Wales and wanted to offer similar trainings here in the US and the **Handy Village Institute** was born. Jack, Deborah and Chris took the Midwest Renewable Energy Association’s Homebrew Wind Turbine Workshop with Dan Bartmann of Otherpower, and attended the MREA Energy Fair and Small Wind Conference. We erected our turbine made in that workshop.

We then planned and executed our first Homebrew workshop. We build from scratch using 100% locally-generated Renewable Energy. Attendees learn theory and the skills (steel

fabrication-cutting, welding, grinding, electrical- coil winding and magnets, fibreglassing and woodworking for blades and tails). Our second turbine has been erected on a tower on an grass-fed beef farm which is partnering with the local energy coop (Randolph Electric Coop). While on display before being raised on the tower, a cow rubbed against, and damaged, one of the hand-carved blades. We repaired that within a few days.

At present, our wind coop owns six homemade machines which our team services. Our workshops have had attendees from Central America, the Caribbean, Africa and the United States. We have built up our team of instructors, craftspeople/makers, and maintainers. This year with the help of the Lowlander Institute we had six people representing three tribes from Louisiana build a machine. It will power their tribal center. We hope to be offering workshops for all six tribes of the region in the near future. One tribe is in the process of relocating due to rising waters, which has covered 98% of their homeland in the past 2 decades. We all desire local Renewable Energy.

2. Links

Other Power

<https://www.otherpower.com>

Lowlander Center

<https://www.lowlandercenter.org>

<https://www.lowlandercenter.org/news-and-updates/2018/5/15/alternative-energy-through-homemade-wind-turbines>

First Nations

Press

National Geographic

<https://news.nationalgeographic.com/2016/05/160525-isle-de-jean-charles-louisiana-sinking-climate-change-refugees/>

New York Times

<https://www.nytimes.com/interactive/2018/02/24/us/jean-lafitte-floodwaters.html>

Tribal Websites

<http://pactribe.tripod.com>

<http://www.isledejeancharles.com>

Video

https://www.youtube.com/watch?v=Ai9nxn_Ykck

Handy Village Institute on YouTube

<youtu.be/F8JddQimaLQ>

<youtu.be/aBlpvo-1Zdk>

Home Power Hour Radio (Podcasts)

<https://wcomfm.org/programs/home-power-hour/>



The **Handy Village Institute** trains adults using trade skills to build small wind turbines. These scratch-built turbines can be used to generate electricity on a small farm or business scale.

We recently hosted six members from three Native American tribes from Southern Louisiana. Some have lost 98% of their land due to subsidence, storms, and sea level rise. They will be installing a renewable energy system at their new tribal center using the wind power generator participants made in our workshop.

The **Handy Village Institute** primarily offers workshops for adults seeking to gain knowledge about and experience in:

- practicing small-scale energy generation and storage,
- managing and using water, soil, and vegetation resources on their landscapes,
- engaging in working relationships with like-minded individuals.

With the intention of ensuring transmission of essential aspects of local human culture related to food, shelter, and furnishings.

Our experiences living off-grid, installing renewable energy systems, studying, practicing, teaching, traveling worldwide, and engaging with our community at home through times of abundance and disaster have inspired us to create a folk school in the Piedmont region of North Carolina.

June 2015 found the **Handy Village Institute** team at the Midwest Renewable Energy Association, building our own wind turbines in the “Homebrew” Wind Turbine workshop they offer each year before the Midwest Renewable Energy Fair. Dan Bartmann, of Otherpower, was our instructor, and we purchased the turbines that we built in this workshop, installing the larger one at our site in North Carolina. It has powered our off-grid system on those cloudy days and any nights when the wind blows.

We realized that the experience we had of using simple, often salvaged, parts and hand tools to fabricate a sturdy and reliable power generating machine teaches many different types of lessons that we were eager to share. During our first three years of offering Dan Bartmann’s workshop at the **Handy Village Institute**, we have hosted guests from as far away as Africa and the Caribbean, as well as our own southeastern US.

Programs

Wind Turbines

- Wind turbine fabrication
- Wind turbine assembly
- Blade manufacturing
- Axile flow generator
- Frame making

Wind Towers

- Wind tower fabrication
- Wind tower assembly
- Cable and harness
- Wind tower erection

Shop Skills

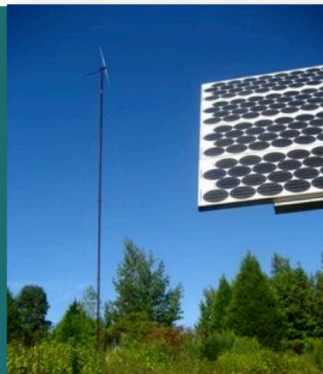
- Cutting workshop
- Welding workshop
- Woodworking workshop

Small-Scale Energy Generation Systems

- Small solar-carriage
- Solar kit
- Light electric vehicle (LEV) charging
- Balance of systems (BOS) controller
- Storage
- Inverter
- Wiring

Homestead- Scale Resources

- Biogas
- Compost
- Vermiculture
- Blacksmithing
- Gardening/harvesting
- Greenhouses
- Foraging
- Fiber

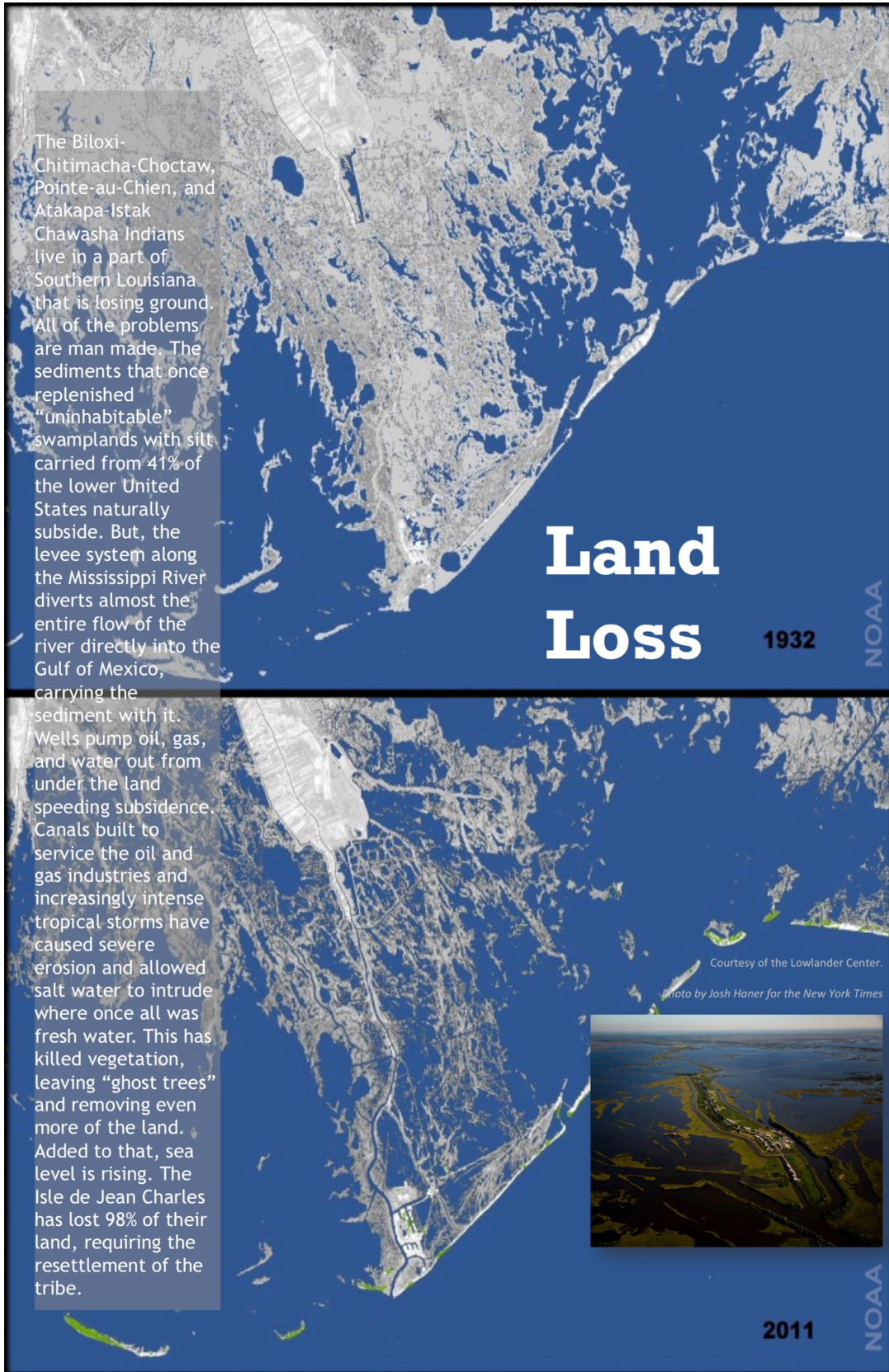


Community Speaker Series

- Efficient appliances
- Small wind conference
- Renewable Energy Future
- Solar Pioneers
- Electric bike- Light Electric Vehicle
- Small Solar
- Integrated Utility Unit
- TINY Houses
- Water Management
- Biofuels
- Compost
- Garden Planning
- Greenhouses
- Poultry
- Aquaponics
- Foraging
- Blacksmithing

Our program provides hands-on experience in skills needed for woodworking, metalsmithing, fiberglass and electrical fabrication. Participants build confidence, self-reliance, and community among diverse future renewable energy leaders.





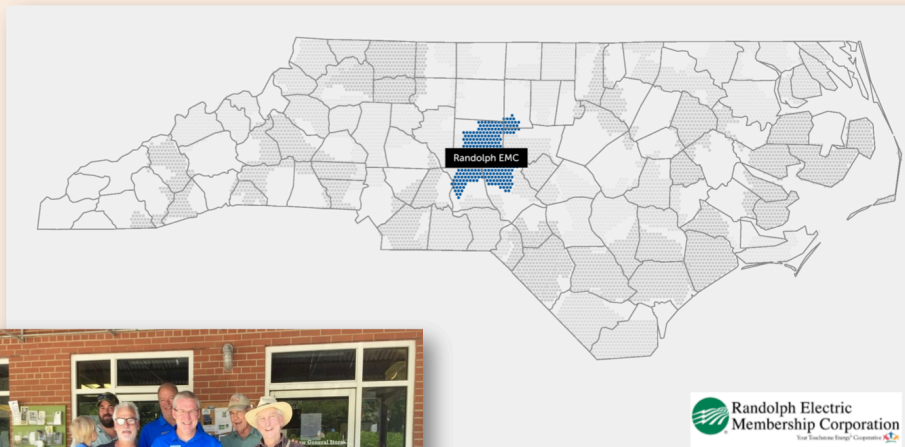
“I recently had the privilege to attend a Wind Turbine making workshop for our Tribe. WOW! The technology is amazing and exactly what our community needs. The ability to be self-reliant again is amazing. Our community has been devastated by repeat hurricanes and other environmental issues. These issues often cause interruptions in utility service. The wind turbine technology could give our Tribal homes a way to function without relying on the power companies. It is extremely important for this technology to be explored and put into practice for our tribe.”

— *Workshop participant*

“Alternative energy sources are one key element that offers hope of stability for the communities. For many years several of the coastal Tribes have talked about energy independence and sought ways to achieve such status. It is important that the alternatives to energy are affordable, easy to operate and are location appropriate. The most recent exploration on energy independence has been wind energy through the development of wind turbines. The wind turbine project provides an affordable source and is reproducible by community members.

“Recently a group of 6 people from 3 Coastal Tribes traveled to North Carolina to be part of a wind turbine workshop. The goal was to build a wind turbine that will be placed at the Pointe au Chien Tribal center greenhouse. Learning the process was as important as the outcome. Each member of the team learned skills needed to produce the turbine, thus having working knowledge to replicate their creation. Handy Village Institute was the host for the workshop. The goal of our coastal communities is to host the next workshop in Louisiana so that more people from the Tribes can learn how to build a turbine, thus creating more turbines, resulting in more energy sustainability for the coastal communities.”

— *Lowlander Center*



Electric Cooperatives

Local Power and Local Food

Randolph Electric Membership Corporation is a rural electric cooperative working hard to prepare its member-owned system for the future. Polling membership about its interest in using more renewable power demonstrated huge support. About 30% of the respondents said they would be willing to pay slightly higher rates for renewable power. A handful of large solar farms are already part of the Co-op. It is experimenting with time-of-use prices for electric car charging. This will create incentives for members to spread out their electrical loads over time.

The Co-op is analyzing distributed generation technologies to enhance its system, providing greater cost savings to members and increasing reliability.

Charles "Doc" Sydnor is a member who raises grass-fed Red Devon cattle. Doc's small wind turbine was built in the first Handy Village Institute workshop. The Co-op is both studying and partially supporting his planned small wind and solar PV hybrid system.



Picture Source: <http://www.braeburnfarms.com/products/cows/>

Process of Building a "Home Brew" Wind Turbine

Stator

Wind and
Cast Coils



Rotor

Place and Cast
Magnets



Nacelle

Grind Hub, Set Axle, Insert and Grease Bearings, then Test



Blades

Carve and Layout Blades



Tail

Fabricate



Power Generator

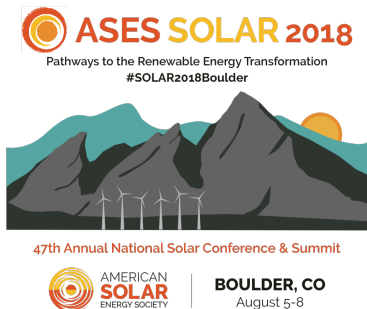
Assemble



Success

Celebrate!





Conference Proceedings

ASES National Solar Conference 2018

Boulder, Colorado August 5-8, 2018

Multi-generation Modeling and Building Energy use optimization based on a Natural Gas driven Internal Combustion Engine

Gabriel Okafor¹ and Hessam Taherian²

¹ University of Alabama at Birmingham, Birmingham (USA)

² University of Alabama at Birmingham, Birmingham (USA)

¹ gabrielo@uab.edu

² taherian@uab.edu

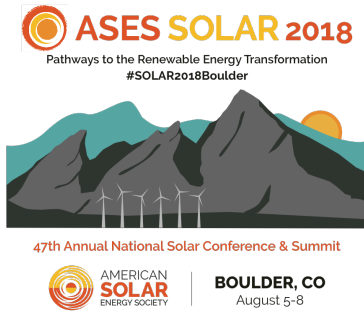
Abstract

Science and technological advancement, environmental pollution, government policies and rising energy costs have long since begun redefining the way power is generated, distributed and utilized. Considering the much higher standards relative to common practices, distributed energy power generation has proven to be a viable alternative to centralized power generation due to the many advantages such as energy generation and control independence, lower greenhouse emissions and significant reduction in transmission losses. This research considers a natural gas-powered internal combustion engine (ICE) with heat recovery and trigeneration capabilities or combined cooling heating and power (CCHP) as well as renewable energy incorporation including solar panels and possibly solar thermal. Research objective is to create an accurate working numerical model that in future can be compared with an experimental model for verification and optimization. TRNSYS software is used to create a numerical model by assembling the components as it would be in real life and running a simulation. In modeling the building, Sketchup and OpenStudio will be used to create thermal zones as in a single-family two story detached house with conventional floor plans. The model will then be imported into the TRNSYS environment for further analysis. Optimization of the system would be primary, and with a targeted energy utilization factor of 95%, this research will seek to provide substantial and convincing data for future installations.

Keywords: *Solar, Power generation, CCHP, TRNSYS, ICE, Natural gas, Heat recovery*

1. Introduction

In this modern age, several factors continually raise the bar on acceptable system operations and performance levels. In the power and energy industry this dynamic shift has been significant. The cost of energy, pollution levels, sustainability, resource conservation and policy restrictions are a microcosm of such factors that encourage substantial optimization. As a result, contrary to the mainstay centralized power generation and distribution, regionalized multi-generation of energy resources for residential and industrial building needs is beginning to expand and attract attention in the United States. It promotes greener energy generation with a negligible carbon footprint by employing the use of hybrid renewable systems, implementing end user energy independence and power control, enhancing fuel efficiency and improving the energy utilization factor (EUF). In this research, the proposed power generation system is a hybrid combination of heating, cooling and power generation (CHCP), where the primary energy source is a natural gas internal combustion engine (ICE) employing extensive heat recovery processes. According to previous studies, by exploiting the huge amount of waste heat rejected by the operating power cycles of the generator the EUF of the system can be improved significantly, with natural gas-powered ICE reaching as high as 81% as against an average of about 38% for thermal power generation systems. (Santo, 2012). Similar research has been done by (Abu-Hamdeh, 2015) and (Taherian, 2017) seeking to optimize the generator size to match residential load demand.

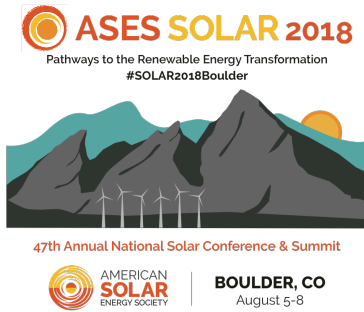


Conference Proceedings

ASES National Solar Conference 2018

Boulder, Colorado August 5-8, 2018

Several subtle information gaps exist that makes this research imperative. Firstly, research on ICE generators needs to be done and categorized by location and climate type, while including other renewable sources and varying operating conditions. To accomplish this, specifications and performance data from a specific generating unit can be used to simulate power generation and building energy use in the Birmingham area and in addition, extensive heat recovery for space heating and hot water storage has been integrated into the system to achieve assured and greater savings. Renewable energy sources and storage (thermal and electrical) is also incorporated. An emphasis on cleaner and efficient energy was recently brought to light when a small island village in Alaska saved considerable amounts of energy consumed and associated costs by transiting from a majorly fuel oil-based electricity generation to carbon-neutral biomass generation.



Conference Proceedings

ASES National Solar Conference 2018

Boulder, Colorado August 5-8, 2018

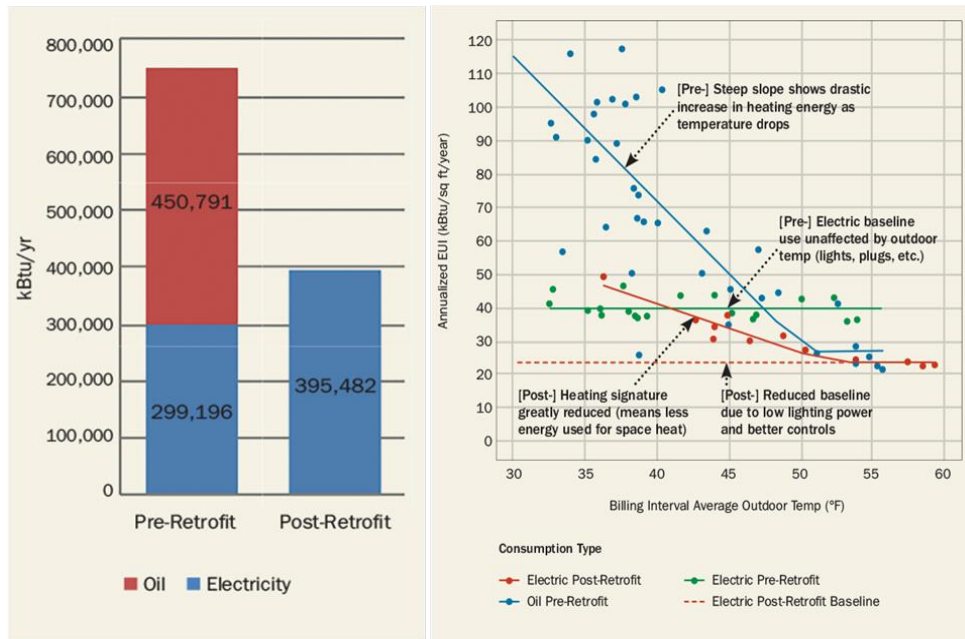


Fig 1: Pre and post retrofit data from Sitka. (Heller, 2018)

Primary design features included reduced load, proper equipment sizing, optimization, and the use of high efficiency pumps and heat recovery ventilators. The energy-efficiency designs in Sitka, Alaska not only eliminated the use of fuel oil but showed how modern buildings can move toward a carbon-neutral, energy-efficient future (Heller, 2018).

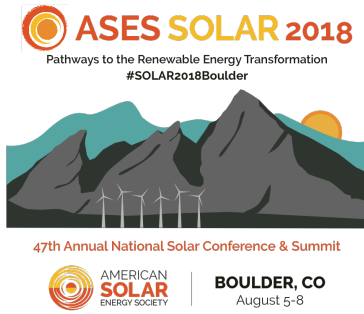
Preceding studies have compared hybrid natural gas-powered micro-turbines and central power generation systems, the EUI of the former was reported to exceed 90% as against an average of about 30% for the latter counterpart. This is achieved by exploiting the huge amount of waste heat rejected by operating power cycles. Like the central power systems, conventional steam plants run on the Rankine cycle, which is a significant culprit of waste heat rejection. To compensate for the losses, central combined cycle steam generators only slightly improve the efficiency. It must be noted however that without employing multi-generation functionalities, the natural gas-based electricity generating systems appear to be somewhat costlier than grid electricity use.

Generators, electrochemistry and photovoltaics represents the broad spectrum of power generation methods that have been applied in several systems. Power generation equipment like solar panels are used to capture solar energy while turbines can be run by several different movers such as steam from fossil fuel, nuclear boilers, wind and water current from dams and spillways for hydroelectricity. In recent times environmental concerns amongst other determinants have shaped and somewhat defined the global approach to power generation and its predominant methods. The demand for cleaner energy has led to the development of multi generation power generation that comprise of different energy systems employing optimum renewable energy (RE) utilization. Due to the rising cost of energy for socio-economic development and ever stringent environmentally safe codes and standards, the importance of RE development in these times cannot be overstated.

2. Literature Survey

2.1. Distributed Energy Power Generation (DEPG)

Distributed Energy Power Generation goes by several different terms like Distributed energy resources (DER),

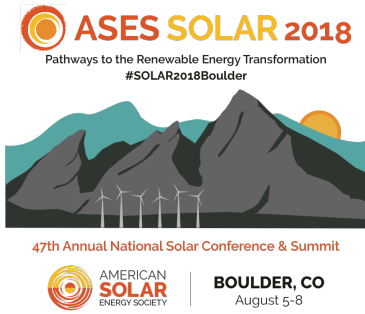


Conference Proceedings

ASES National Solar Conference 2018

Boulder, Colorado August 5-8, 2018

On site generation (OSG) or District/decentralized energy. They are small to medium scale systems that serve as an alternative to the customary centralized power generation and distribution system. They are regarded as an advancement to the customary central base station power technologies and are deployed in compact systems able to generate and supply power on a district or regional basis. Although it has been notoriously associated with high initial capital costs per kilowatt, accelerated research and development in this area has brought about better designs and highly optimized solutions that can generate and distribute energy in the most efficient way possible. Hybrid renewable energy sources are frequently employed and several multi generation systems are integrated into single units that can serve the power needs of residential, commercial and regional buildings alike. There are



several technologies associated with DEPG with each having its merits, demerits and applications.

2.2 Combined Heating and Power (CHP)

Many definitions of Combined Heat and Power (called cogeneration) have appeared in scholarly literature. As defined by Clarke Energy Cogeneration is the simultaneous generation of work and useful heat from the same primary energy source. Work shall mean either mechanical or electric energy.

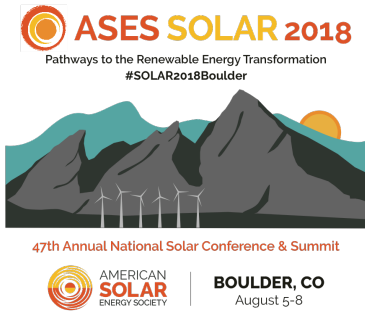


Fig 2: Schematic of a CHP system (Gu et al., 2014)

Substantial measures are required to reduce the emission of greenhouse gases and the avoidance of a fast depletion of fossil fuels. Many sources mention that the amount of heat wasted during electricity production and industrial activities is enough to cover a substantial part of the demand for heat. According to a 2008 IEA model of cogeneration in G8 countries, expansion of cogeneration technology in France, Germany, Italy and the UK would increase primary fuel savings by almost 200% in 2030. In the United States, The Department of Energy is attempting to stimulate cogeneration and have instituted a target of 20% CHP generation capacity by 2030. (Enc.Field, 2017)

3. Methodology

A numerical model was run using TRNSYS Simulation studio to obtain time step performance data of the design as suggested by (Fumo & Chamra, 2010) and emphasized by (Chahal, 2016) in papers advocating for the use of numerical analysis for realistic residential building energy modelling. TRNSYS can analyze transient systems as well as thermal and electrical energy system modeling. Dynamic Numerical Modeling and associated calculations can be done using this package.



ASES National Solar Conference 2018
Boulder, Colorado August 5-8, 2018

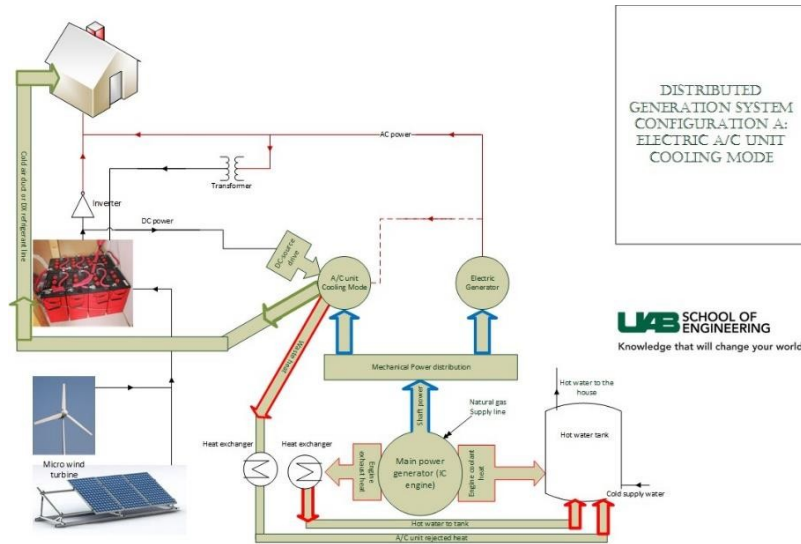


Fig 3: Initial DPEG System Configuration

To initiate, a simple power generation system based on an ICE was modeled to serve as a control or base-case for assessment purposes. Other features were thereafter added to the system sequentially. The primary energy source is a natural gas-powered ICE. Initial calculations were based on a core power output of 9KW, with a 1.5 ton mini-split heat pump (HP) system which will be used for cooling and heating purposes and finally a 7.2 kWh battery bank however during the course of this research some changes were made between the initial and final configuration as shown in figures 3 and 5. Currently the generator unit has a maximum power output of 8KW AC with coefficient of performance (COP) target at 2.5 and a Power Factor of 0.98. In the numerical modeling, the building was modeled as a single-family two stories detached house with conventional floor plans. Several modifications and iterations were carried out to determine optimum configuration set ups. The project was also developed further with Open Studio (OS) to improve the accuracy of the results.

3.1 Building Model Description

A key component to the computer model of the power generation system is the residential conditioned and occupied space. To accurately represent the real-life system a small two-story single-family house was modelled with SketchUp (Trimble Inc. 2018) and TRNBUILD.

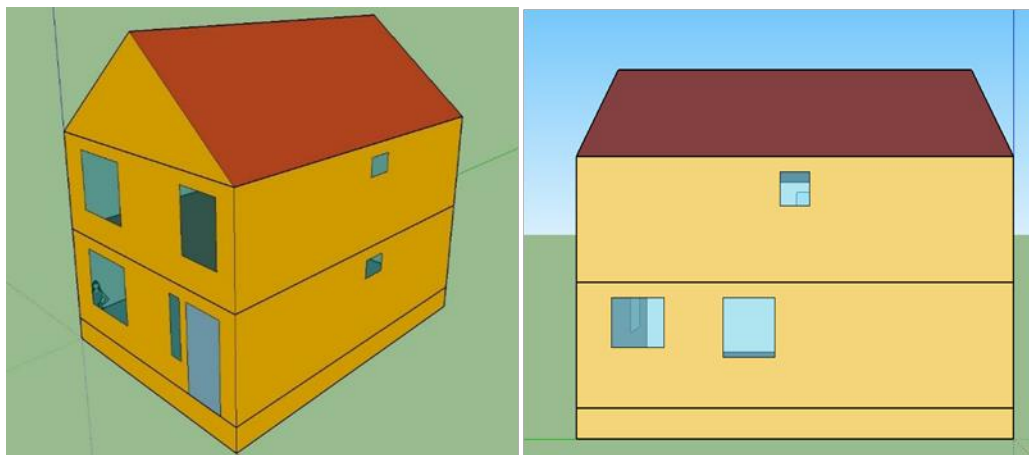
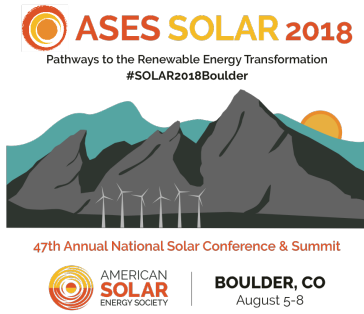


Fig 4: Building Model in SketchUp



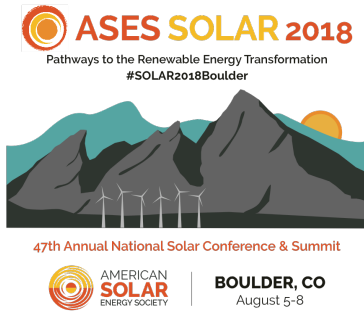
Conference Proceedings

ASES National Solar Conference 2018

Boulder, Colorado August 5-8, 2018

SketchUp is used for building design and construction. It's use also includes programming, diagramming, design development, detailing and documentation of building features. In other to use the Sketchup file on the TRNSYS model a plugin was utilized to make the file compatible.

Figure 4 shows the isometric and side views of the house 3D model. It is a two-story house with a footprint of about 600 square feet. The building is split into two thermal zones corresponding to the first and second floors,



Conference Proceedings

ASES National Solar Conference 2018

Boulder, Colorado August 5-8, 2018

enabling independent temperature control for each floor. In addition, distinct features such as the attic and crawlspace were incorporated to adequately represent the building style in the local community. The wall, floor and roof sections along with the material properties for the ceiling, doors and windows were also defined to match the conventional trends in construction materials used for single-family homes.

3.2 TRNSYS Model Description

A TRNSYS project is typically setup by connecting components referred to as “types” graphically in the Simulation Studio. Every component is defined by a mathematical model in the TRNSYS simulation engine which dictates its operation and energy balance within the model. It also has a set of matching proformas which is a black-box description of any component as it contains information about inputs, outputs, parameters, etc. The Simulation Studio generates a text input file for the TRNSYS simulation engine. That input file is referred to as the deck file. (Specialists, 2017)

At the core of the model is a natural gas ICE set to run at about 60 percent power output. The exhaust gas, oil cooler and cooling jacket water both flow into individual sensible heat exchangers that facilitate heat transfer for hot water storage. The storage capacity is neglected in the heat exchanger models. Exhaust gases from the ICE is split using a flow diverter to serve the hot water tank (HWT) and space heating. A bypass heat exchanger facilitates heat transfer between cold unconditioned air coming from the building and hot gases, while thermostats are used to initiate or cut of the heat flow within a temperature band of 21°C to 23°C. The exhaust gases are also set to bypass the hot water tank in a situation where additional water heating is not required. Similarly exhaust gases are bypassed and dumped into the surroundings when additional space heating is not required and a dry fluid cooler (radiator) is used as a backup cooling system for the jacket water. An 8 by 3 Solar Photovoltaic (PV) array with 330W modules serve as the renewable energy source. A generic inverter and charge regulator considers load demand from the building model while controlling the charging and discharging of a standby 8 by 3 720Wh battery bank. The size of the battery bank was determined by running the model with the control criterion that excess generated energy can be sufficiently stored for later use.

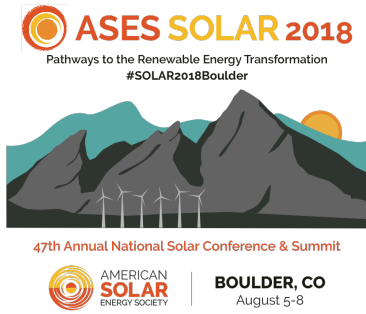
Table 1 and 2 below show the input and output parameters for the major components. The input parameters are fed to receiving components from the output of other components, external data files or equation data solvers.

Tab. 1: Major Components' Input Parameters

ICE	HWT	HP
Intake air temperature	Inlet Recycle temperature	Return air temperature
Intake air temperature	Inlet Recycle temperature	Return air temperature
Desired output power	Inlet Recycle flow rate	Return air humidity ratio
Jacket fluid temperature	Inlet Recycle temperature	Return air %RH
Jacket Fluid flow rate	Inlet Supply temperature	Return air flow rate
Oil Cooler temperature	Inlet Supply flow rate	Inlet Pressure
Oil Cooler flow rate	Top Loss temperature	Fan pressure rise
Aftercooler temperature	Bottom Loss temperature	Outside air temperature

Tab. 2: Major Components' Output Parameters

ICE	HWT	HP
Exhaust Temperature	Outlet Recycle Temperature	Outlet air temperature
Exhaust Flow Rate	Outlet Recycle Flow Rate	Outlet air humidity ratio
Jacket Water Outlet Temp.	Outlet Usage Flow Rate	Outlet air %RH

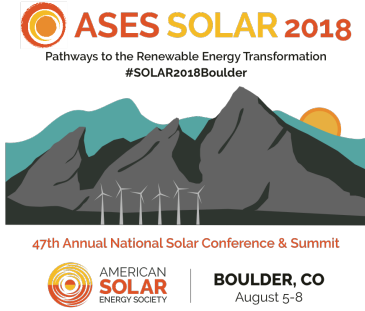


Conference Proceedings

ASES National Solar Conference 2018

Boulder, Colorado August 5-8, 2018

Jacket Water Flow Rate	Outlet Usage Temperature	Outlet air flow rate
Oil Cooler Outlet Temp.	Table text	Outlet air pressure
Oil Cooler Flow Rate	Table text	Total cooling rate
Electrical Power	Table text	Sensible cooling rate



Conference Proceedings

ASES National Solar Conference 2018

Boulder, Colorado August 5-8, 2018

4. Results and Discussion

It is important to note that the primary tool for this research, TRNSYS simulation studio is highly flexible in terms of what type of system can be modelled, nevertheless with this advantage in adaptivity comes the higher risk of researchers easily mixing up parameters and that can lead to runtime errors, loss of result repeatability and data reliability. Therefore, one of the primary goals of this research was to obtain a working model with accurate, reliable and repeatable data based on specified conditions. Some of the trends are explained accordingly.

The building that was modeled was split into two thermal zones, one for each floor. The setpoint for the two zones is set to 22°C with a dead band of 2°C. To achieve this the supply fan from the cross-flow heat exchanger used for exhaust heat recovery is set to supply heated air when the temperature drops below 21°C, while the air source heat pump supplies cool air when temperature goes above 23°C and supplementary heating when temperature goes as low as 17°C. The system was able to maintain an average annual temperature of 21°C for both zones. Figure 6 shows the current temperature distribution of the model.

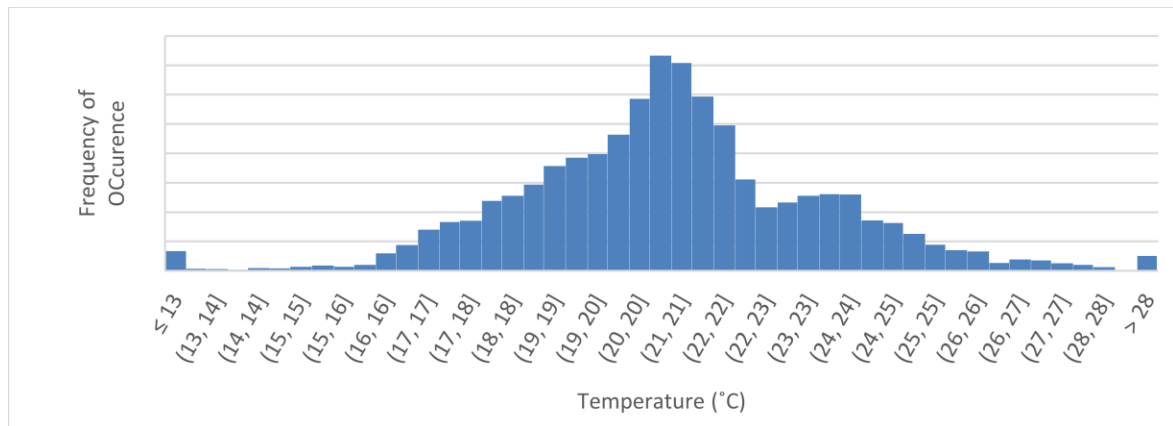
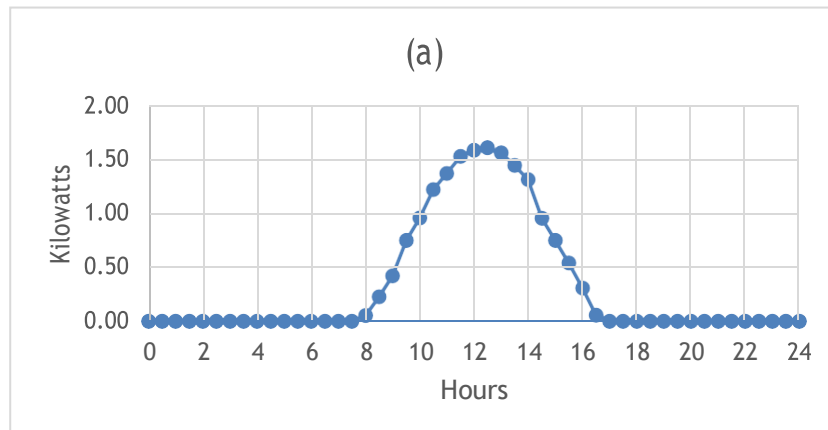
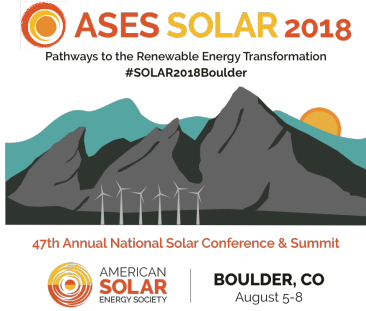


Fig 6: Temperature distribution for first floor

The data in figure 6 shows that in 8760 hours of the year, the set temperature bracket of 20°C to 24°C was met 65% of the time. The unmet hours for low temperatures $\le 16^\circ\text{C}$ and high temperatures $\ge 26^\circ\text{C}$ are insignificant as can be observed above. It must be noted that many of the unmet hours are unoccupied unmet hours.





Conference Proceedings

ASES National Solar Conference 2018
 Boulder, Colorado August 5-8, 2018

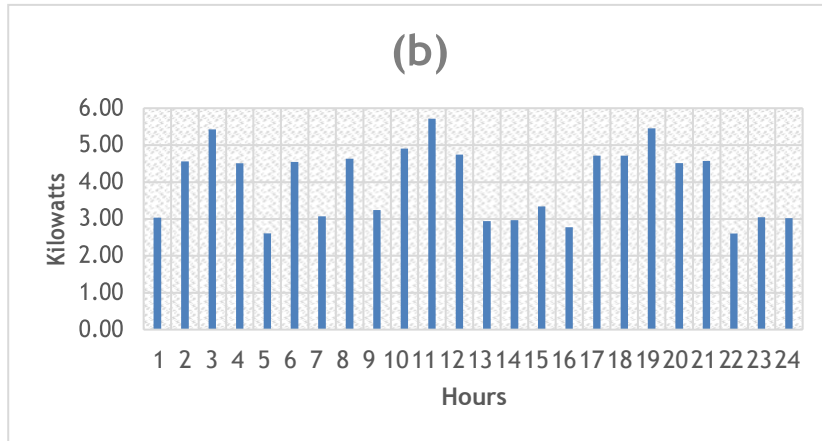


Fig 1: (a) Solar PV generation and (b) Building Energy Use

Figure 7 shows data harvested from the power systems. A familiar trend for the solar PV generation can be observed in (a) while the building energy use over 24 hours is shown in (b). An 8 by 3 solar array with 330 W rated modules was modelled and its annual generation stood at 11900kwh, a value considerably close and only 6% greater than that generated by the National Renewable Energy laboratory PV performance tool that estimated an annual generation of 11200kwh (Laboratory, 2018). The heat transfer between thermal fluids and heat exchangers which represents heat recovery throughout the year currently stands an 36000kwh. This is achieved by strategically placing heat exchangers to recover and utilize heat that would otherwise have been lost to the process or environment.

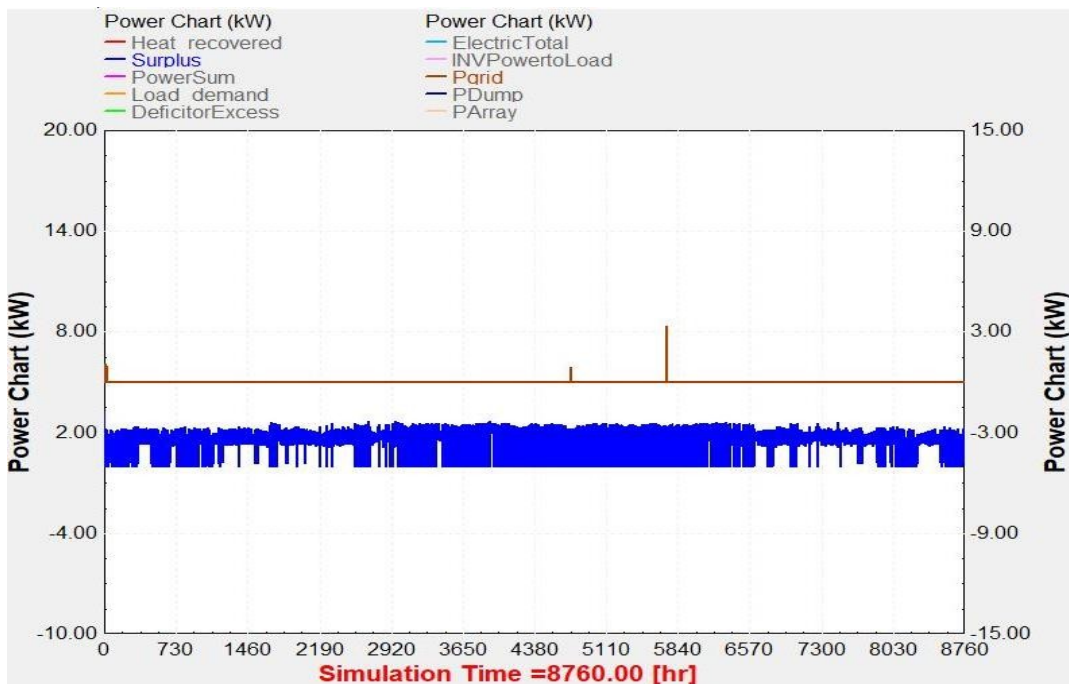
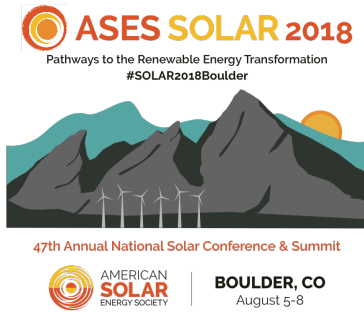


Fig 8: Energy Use and Production Monitor



Conference Proceedings

ASES National Solar Conference 2018

Boulder, Colorado August 5-8, 2018

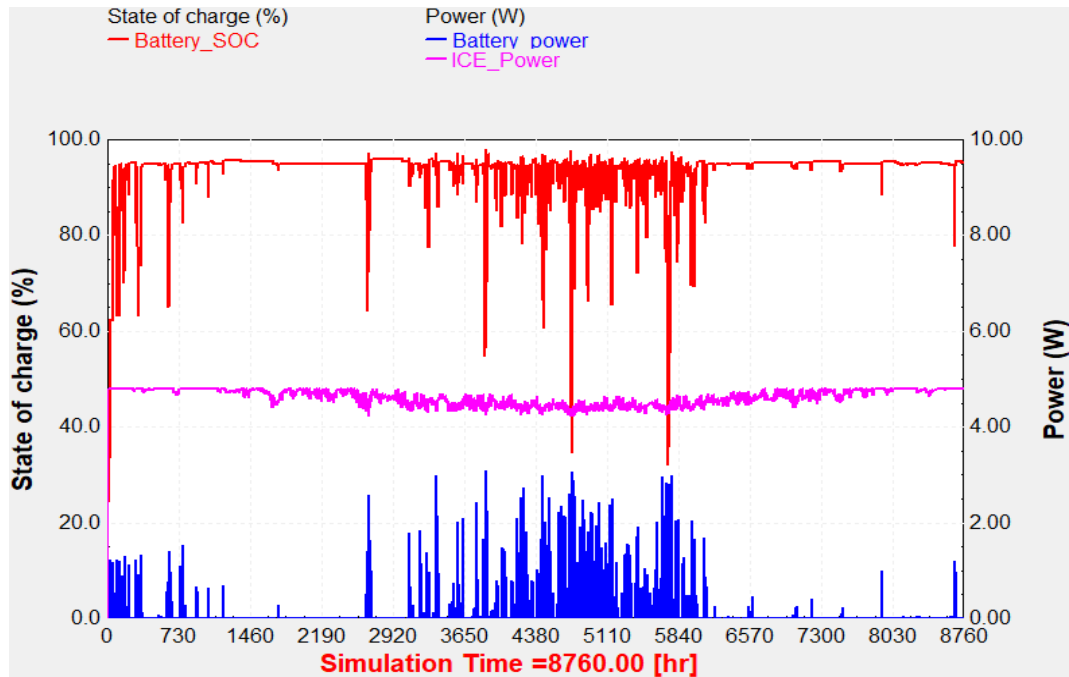


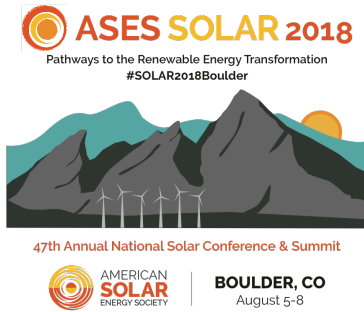
Fig 9: Battery Bank and ICE Energy Monitor

Figure 8 is a TRNSYS chart showing the energy balance of the multi generation model. The charts are plotted on the left and right axis and have been separated accordingly in the legend. Surplus represents the excess energy produced by the current model. This is important especially considering the generator is only running at about 60%. Excess energy can therefore be employed in charging a larger battery bank or sold back to the grid in locations where policies allow such actions.

The energy model is almost totally off-grid as the energy taken from power utility “Pgrid” is nil almost throughout the year. Figure 9 on the other hand shows a plot of the battery bank state of charge (SOC) on the left axis. The fluctuations arise as the battery is charged and discharged according to load demand signals sent to the inverter/regulator. It also shows the right axis plots of battery power and ICE generation. The battery SOC is plotted as a percentage, battery power represents the energy sent to charge the battery to maintain SOC above a set low limit of 35%, to prolong the life of batteries. Finally, the ICE power shows the energy generated from the ICE, shown for relative comparison purposes. The ICE has a power rating of 8KW, however for this research it was set to run hovering around 5KW. This translates to lower fuel burn rates and therefore lower fuel cost.

5. Conclusion

Distributed hybrid power generation is leading a new era in the energy sector and opens avenues to the use and integration of heat recovery and cleaner energy in the mainstream power sector. This research has successfully modeled such a system using several software packages. Birmingham, Alabama was the design location and the model was run for 8760 hours (an entire year). Heat recovery and solar energy was expansively used, the building conditions and main equipment operations were analyzed, and the results are compliant and reasonable with what is required for a typical family house. The current model’s energy use is relatively low, and all building needs have been adequately accounted for. Consequently, energy cost is expected to be low, as there is near zero energy pulled from the grid as well as a considerable energy surplus from the ICE, heat recovery and solar PV multi generation systems. Furthermore, the base model is very flexible and can easily be applied to different locations and building types. The adaptable feature of the model avails researchers the opportunity to carry out further optimization and development in the future.



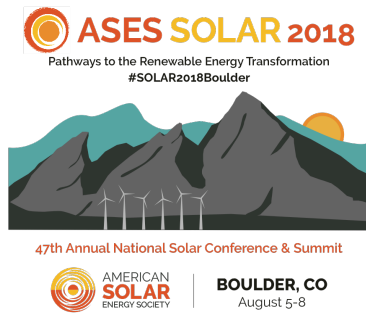
Conference Proceedings

ASES National Solar Conference 2018

Boulder, Colorado August 5-8, 2018

6. References

- Abu-Hamdeh, O. (2015). Optimization of Distributed Power Generation System Components for a Residential Building. ASHRAE Transactions, 121, 1AA.
- Chahal, S. S. (2016). Energy Analysis of a Solar House Using Simulink and TRNSYS: University of Alabama at Birmingham, Graduate School.
- Ene.Field. (2017). Retrieved from <http://enefield.eu/>
- Fumo, N., & Chamra, L. M. (2010). Analysis of combined cooling, heating, and power systems based on source primary energy consumption. Applied Energy, 87(6), 2023-2030.
- Gu, W., Wu, Z., Bo, R., Liu, W., Zhou, G., Chen, W., & Wu, Z. (2014). Modeling, planning and optimal energy management of combined cooling, heating and power microgrid: A review. International Journal of Electrical Power & Energy Systems, 54, 26-37.
- Heller, J. (2018). Powering An Alaska Village. High Performance Building Magazine(Summer 2018). Laboratory, N. R. E. (2018). PVWatts®
- Santo, D. E. (2012). Energy and exergy efficiency of a building internal combustion engine trigeneration system under two different operational strategies. Energy and Buildings, 53, 28-38.
- Specialists, T. E. S. (2017). TRYNSYS 17 Documentation Retrieved from <http://www.trnsys.com/tess-libraries/>
- Taherian, G. (2017). Analysis of Distributed Generation with Renewable Energy Sources in ASHRAE Climate Zone 3a. TFEC (2379-1748), 1165-1172. Doi:10.1615/Tfec2017.Ewp.018125



Conference Proceedings

ASES National Solar Conference 2018

Boulder, Colorado August 5-8, 2018

Preliminary Design & Analysis of Low-Cost Concentrating Offshore Solar Energy Innovations

Mithra Sankrithi¹

¹ RIC Enterprises, Edmonds, WA (U.S.A.)

Abstract

Innovations in offshore floating solar energy systems are presented, which cost-effectively leverage simple, low risk & elegant configurations for synergistically harvesting electricity & usable heat. Preliminary designs along with technical & cost analyses are presented for several systems suitable for private owners, public or commercial waterfront entities, utility-scale applications & enabling applications for cities with 100% renewable goals. Examples of cost-reduction enablers that reduce levelized cost of energy (LCOE) include use of lightweight low-cost inflatable subsystems for low-concentration reflectors, low-cost dual-axis tracking for a floating array, elimination of land use, and CPV liquid cooling that can also transfer usable heat for hot water, building, swimming pool or process heat as well as solar district heating/cooling and desalination. Synergistic integration of multiple offshore renewables including offshore solar, wind, tidal or ocean current, and ocean thermal energy systems (OTEC) is also presented as an enabling means to achieve minimized LCOE in some geographic locations.

Keywords: solar, offshore, land use, low-cost, LCOE, innovation, concentrating, cogeneration, heating, CPV, heliostatic, tracking, electricity, heat, district heating, district cooling, efficiently, solar thermal, synergistic, wind, tidal, ocean, OTEC, desalination, 100% renewable

1. Introduction

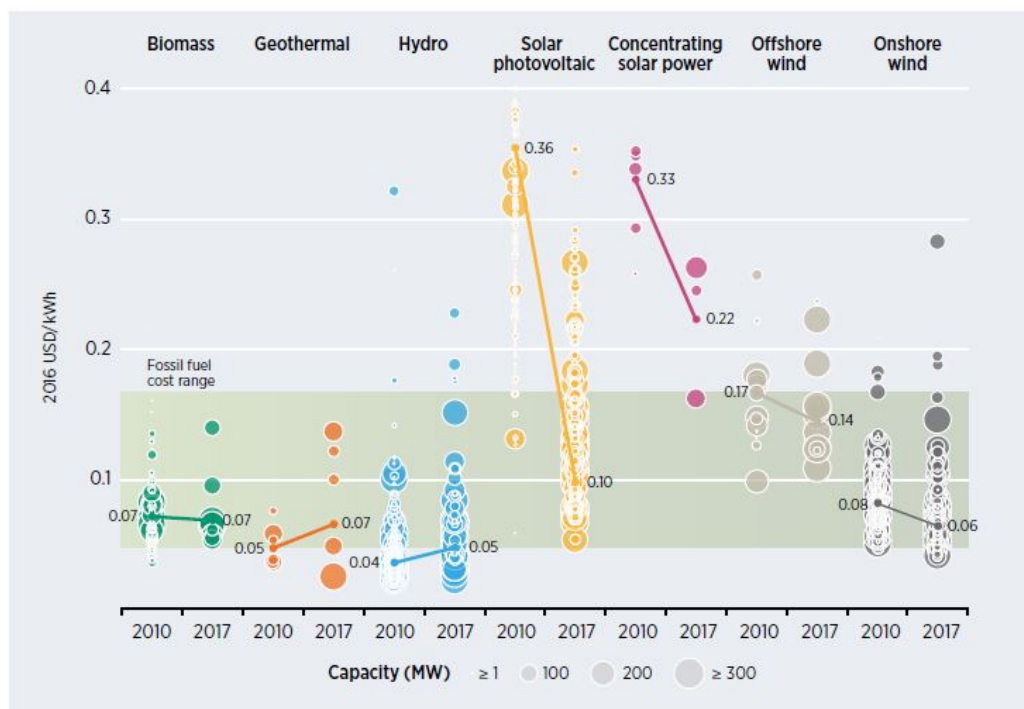
Current photovoltaic solar modules harvest 15- 20% of incoming solar energy, using solar cells such as high-efficiency monocrystalline silicon solar cells. The balance 80 - 85% of incoming solar energy is wasted as waste heat dumped into the environment. Despite this poor harvest efficiency, current solar modules offer simplicity, reliability and low levelized cost of energy (LCOE) and hence are experiencing strong market growth worldwide. The solar energy industry could grow even more rapidly if means were available to double or triple solar energy harvest as a percentage of incoming solar energy, while also avoiding land costs by moving to cost-effective offshore solar power systems. This paper presents a portfolio of low-cost solar innovations ranging from (i) 'SuperSurya' low-cost rooftop cogeneration modules that provide both electricity and usable heat (for hot water, space heating & swimming pool heating); to (ii) Efficient Concentrating Cogeneration Offshore Solar (ECCOS) Systems that can vary in scale from small private systems to very large systems that provide electricity and district heating / district cooling to coastal cities with zero land use and unprecedented low LCOE for offshore systems; to (iii) ECCOS systems synergistically combined with collocated offshore wind, offshore tidal/ocean current or OTEC systems.

2. Background: Challenge & Opportunity

The challenges of global climate change are well-known in the scientific community, and to some extent across the realm of government leaders and the public at large. One particularly worrisome, but possible worst-case scenario, is that if the global temperature rises by 10° C or more, the entire icecaps of Antarctica and Kalaallit Nunaat would likely melt, submerging one third of humankind living in coastal areas (Zolfagharifard, 2014). As a counterpoint to the existential threat posed by this challenge, the opportunities for solar power are extraordinarily promising, with more than enough potential for solar energy to meet 100% of humankind’s energy needs. The forecast 2040 mean rate of global energy consumption is estimated at 27,300 gigawatts (GW), and forecast electricity production at 4,170GW (Energy Information Administration, 2016). By contrast, the total solar radiation that falls on the Earth’s surface is ~ 90,000,000 GW. Recoverable solar power is greater than 1,000,000 GW and thus far exceeds humankind’s current needs or needs into the foreseeable future.

While recoverable solar power is greater than 1,000,000 GW and thus far exceeds humankind’s current needs, accelerated implementation of solar energy systems to replace fossil fuel energy systems will require that renewable systems levelized cost of energy (LCOE) must be competitive or lower than fossil fuel systems (Fig. 1). A key reason for the rapid growth of simple, reliable photovoltaic systems such as basic solar panels, is that their LCOE has been rapidly reduced, dropping from 36 cents/kW-hr in 2010 to 10 cents/kW-hr in 2017.

Figure ES.1 Global levelised cost of electricity from utility-scale renewable power generation technologies, 2010-2017



Source: IRENA Renewable Cost Database.

Note: The diameter of the circle represents the size of the project, with its centre the value for the cost of each project on the Y axis. The thick lines are the global weighted average LCOE value for plants commissioned in each year. Real weighted average cost of capital is 7.5% for OECD countries and China and 10% for the rest of the world. The band represents the fossil fuel-fired power generation cost range.

Fig. 1: Levelized Cost of Energy (LCOE) Comparisons (IRENA, 2017)

Some limitations of simple solar panels include their relatively poor efficiency, with typical silicon solar panels only converting 15 to 20% of solar energy into useful electric energy, as well as fundamental difficulty in meeting base load needs due to relatively low capacity factors, with solar power generation stopping at night and reducing during periods of cloud cover. Innovations to improve solar harvest and enable further reductions of LCOE will be vital to enable further acceleration of cost-effective solar energy systems to serve both electric power and heating/cooling needs around the World.

3. Cost Reduction Leveraging Innovations in Low-Cost CPV with Cogeneration

In addition to continued evolutionary improvements in efficiency and cost of photovoltaic solar modules, achievement of further significant reductions in levelized cost of energy (LCOE) will require additional cost-reduction enabling innovations across several areas. Some key high-leverage cost-reduction enablers are:

- 1) Use of a low-concentration concentrating photovoltaic (CPV) subsystem, with 5 to 10 suns concentration to enable more electricity from each photovoltaic cell:
Enables kWh / Sq.m. of PV receiver to increase by ~ 400% to 800%
Enables PV receiver cost / kWh to decrease ~ 70% to 80%
Enables continued use of nonexotic silicon photovoltaics
Feasible with simple & robust tracking and cooling subsystems
- 2) Use of a low-cost inflatable concentration subsystem with a framed membrane linear concentrating reflector with an inflatable upper volume and ETFE transparent membrane protective cover
Relative to a typical steel & toughened glass concentration mirror:
Enables concentration subsystem weight & capital cost reduction of ~ 50% to 80%
Enables concentration subsystem cleaning & repair cost reduction of ~ 60% to 90%
- 3) CPV liquid cooling that also transfers usable heat for hot water, home or building space heating, swimming pool heating, or solar cooling using absorption chillers
Harvested energy increases from ~ 12% - 22% to ~ 60% - 80% of insolation
Usable heat in kWh can be ~ 300% to 500% added harvest over electricity
Cogeneration system cost may increase ~ 15% - 30% over pure electric CPV

RIC Enterprises has captured key innovation elements of these high-leverage cost-reduction enablers in two foundational patents (Fig. 2).

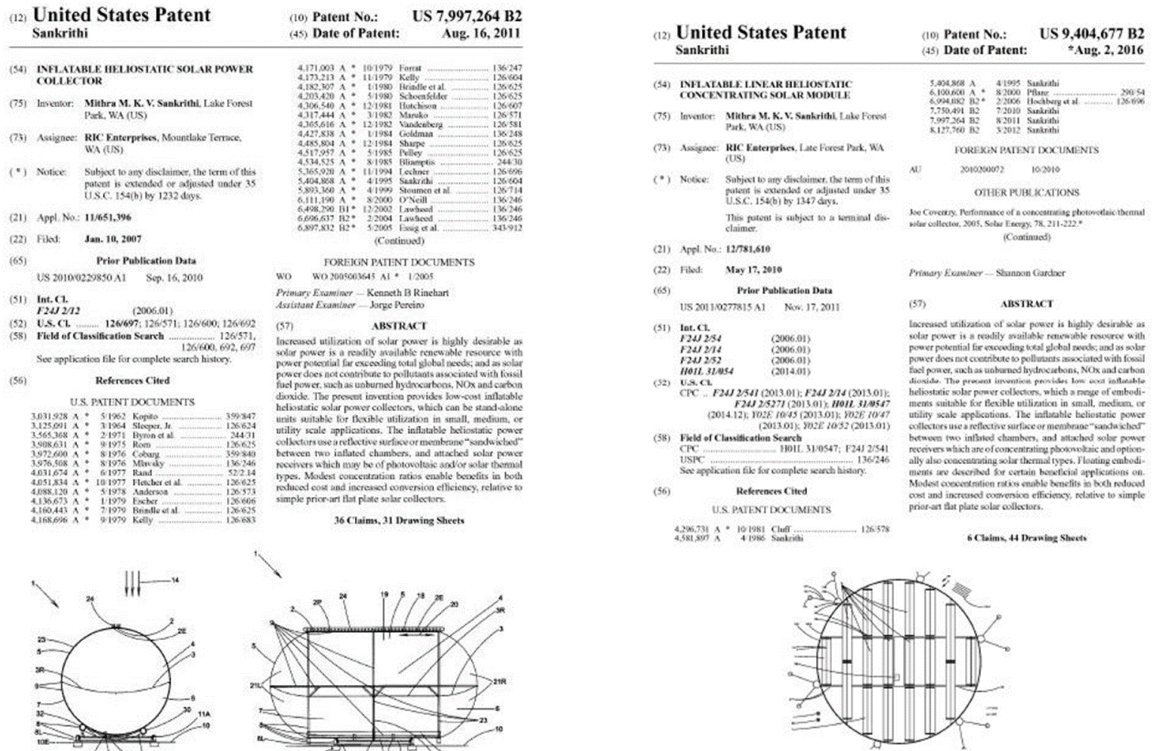


Fig. 2: Foundational Intellectual Property for Some Key Solar Cost-Reduction Innovations

It should be noted that the innovations for cost-reduction are primarily of an applied design and architectural nature, and do not rely on nascent high-technology subsystems that can substantially increase cost and risk.

Subsystems are intended to be simple, reliable, and robust. Some of the subsystems that have been tested by RIC Enterprises include:

- Use of a reflective concentrating framed membrane reflector
- Use of a low-cost inflatable structure with a transparent protective weather cover
- Use of an Ethylene Tetrafluoroethylene (ETFE) transparent weather cover that self-cleans in rain
- Use of heliostatic tracking subsystems
- Use of a CPV cooling system
- Demonstration of an inverted-stow protection concept for storm and hail conditions

A representative set of design criteria to integrate the above-described high-leverage cost-reduction enablers into a rooftop low-cost cogeneration system include:

- Size to 1.75 kW electricity plus 5.25 kW usable heating @ 65 – 75° C
- Meet typical home electricity, hot water & space heating needs with 1-2 modules & net-metering
- Length < 19'4" to enable transport in standard 20' containers
- Low-concentration ratio leverages cost-effective liquid-cooled Si solar cells
- Framed inflatable concentrating reflector modules with ETFE self-cleaning covers
- Modular design for low-cost transportation, installation, maintenance & repair
- Sun-sensor and two-axis actuators for elevation and azimuth control
- Aluminum welded structure for low cost, strength and aesthetics
- Base structure adapts easily for roof or optional ground mounting

An integrated configuration designated ‘SuperSurya’ has been designed responsive to these design criteria, and is illustrated in Fig. 3.

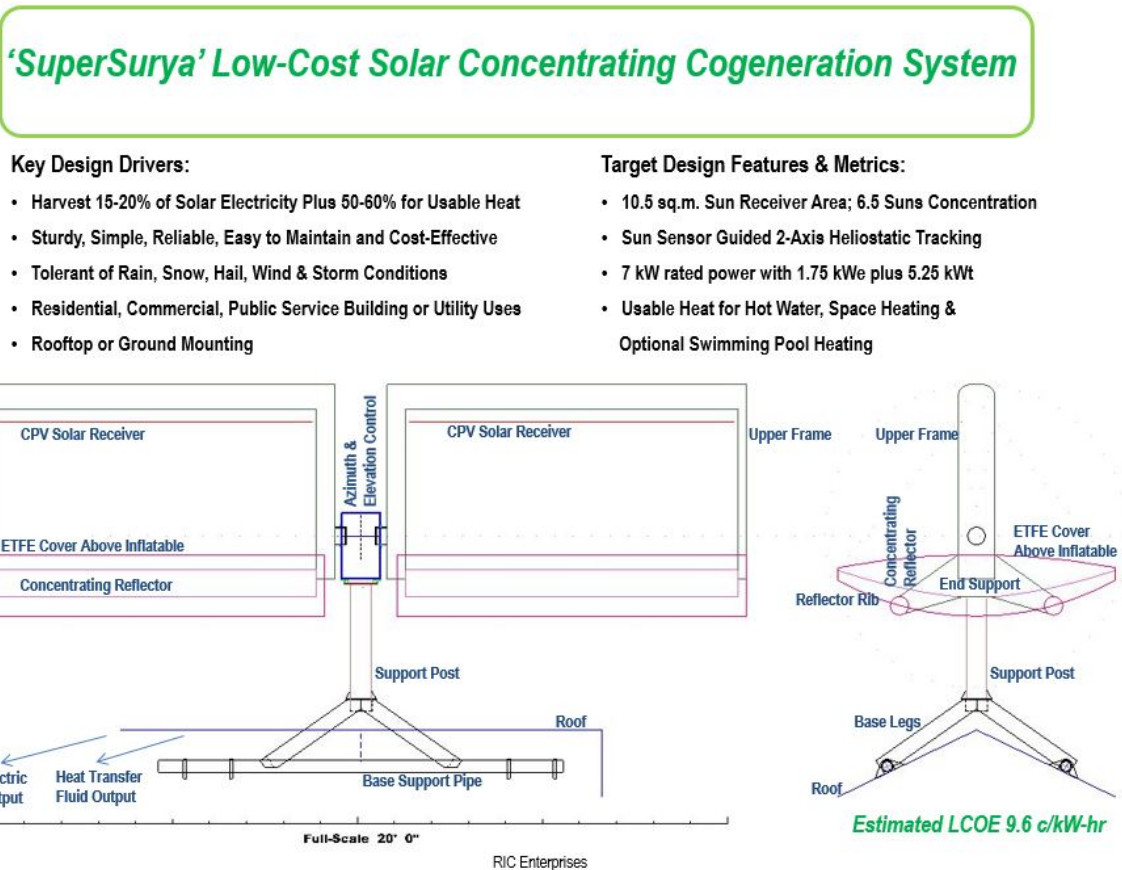


Fig. 3: ‘SuperSurya’ Configuration Integrating LCOE Reduction Enablers

It is conservatively estimated that ‘SuperSurya’ can achieve an LCOE of approximately 9.6 cents per kW-hr, or at least 10% lower than conventional simple solar panels, with the following assumptions:

- 75% of harvested energy is usable heat
- capital cost up from \$2100/kW to \$3000/kW
- capacity factor up from 18% to 35%
- O&M costs triple
- Using the NREL Simplified Life Cycle Cost of Energy (LCOE) calculator

Even more dramatic cost metrics will be possible as these new rooftop cogeneration systems mature, and holistically serve home electricity and heating energy needs, with space heating and hot water heating using 40% and 20% of total home energy, in some typical cases. For homes with swimming pools, the percentage of total energy used for heat increases even more, making cogeneration systems like SuperSurya even more attractive.

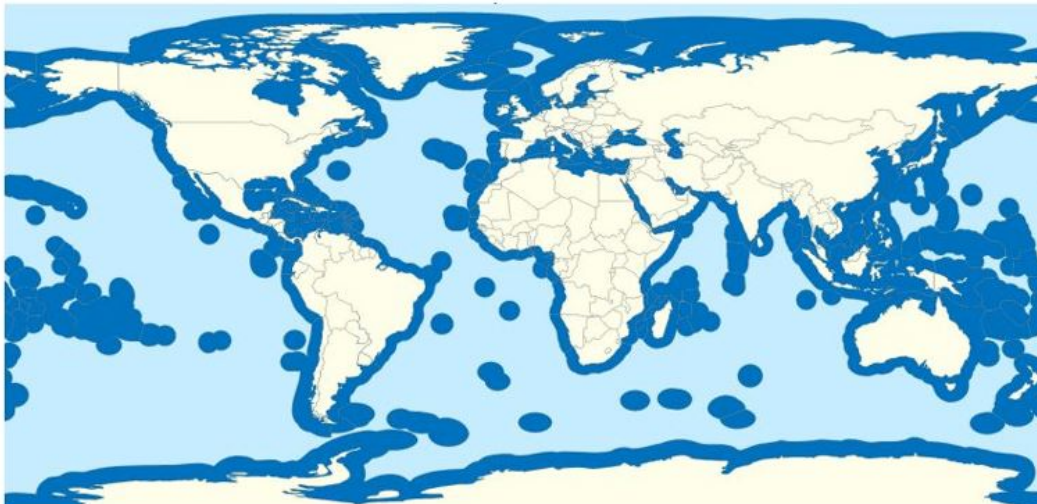
4. Efficient Concentrating Cogeneration Offshore Solar (ECCOS) Systems

Utility-scale solar energy systems, whether using PV, CPV, or solar thermal technologies, all have the downside of using large spaces of land that could otherwise potentially be used for a variety of land uses ranging from residential to commercial to industrial to agricultural to natural spaces for plants and animals.

This provides strong motivation for a strategic vision for future cost-effective offshore solar systems, which could potentially meet the entire world's energy needs using waters within the 200 nm Exclusive Economic Zones (EEZs) of the nations of the world (Fig. 4).

100% RENEWABLE WITH ZERO LAND USE ?

Over 25 million square kilometers of ocean are in "sufficient" insolation areas for Concentrating Offshore Solar (COS) Systems, within the 200 nmi "Exclusive Economic Zones" of the nations of the World. *Use of just 3% of this area is more than sufficient to meet 100% of forecast human energy needs of around 240,000 terawatt-hr per year for 2040.*



<https://www.nationstates.net/page=dispatch?id=545595>

RIC Enterprises

" International Energy Outlook 2016 "

<https://www.eia.gov/outlooks/ieo/world.cfm>

Fig. 4: Offshore Solar Potential in Exclusive Economic Zones (EEZs) (Barry, 2016)

Two key cost-reduction enablers associated with offshore solar are:

- 1) Offshore installation yields elimination or near-elimination of land cost
Avoided land cost can exceed \$2 million per acre, in coastal urban areas

such as the San Francisco Bay area

- 2) Use of heliostatic azimuth control by rotating an entire floating array rather than rotating individual solar modules

Number of azimuth control actuators decreases by ~ 50% to 99.9%

Azimuth control subsystem cost decreases by ~ 40% to 99%

The cost savings associated with offshore solar are, of course, offset in part by needing floatation systems as well as underwater transmission systems.

Some offshore solar systems have already been implemented in a few areas such as Japan with a 13.7 MW floating solar photovoltaic plant on a reservoir (Brown, 2018) and China with a 150 MW floating PV plant in a \$151 million project (Kenning, 2017), that avoid land cost but do not include the other cost reduction enablers noted above. These Japan and China offshore systems harvest sunlight to produce electricity, but their LCOE is expected to be higher than terrestrial installations in low land cost areas such as desert areas, because of the floatation and transmission systems needed.

To accelerate implementation and enable more cost-effective widespread deployments of offshore solar, it would be highly beneficial to apply the *low-cost* and *cogeneration* features of the SuperSurya system, to offshore solar power systems as well. One particular vector of this opportunity would be to replace land-based solar district heating systems, such as the strongly growing district heating systems in Denmark (Dansk Fjernvarme, 2018), with offshore solar cogeneration systems that can provide both *electricity* and *district heating* or *district cooling* while avoiding land costs.

Key economic drivers for Efficient Concentrating Cogeneration Offshore Solar (ECCOS) System include the fact that the majority of global insolation falls offshore; offshore design avoids land use, and many opportunities for synergies exist for cogeneration of electricity, usable heat, desalination, etc. The scalability of ECCOS systems is particularly important as a large-scale growth enabler, with customers including:

- waterfront homeowners
- public service or commercial buildings
- agricultural or industrial customers
- waterfront airports like New York JFK, San Francisco SFO & many more
- waterfront cities or counties, with electric as well as district heating & district cooling opportunities

At the smallest end of the ECCOS opportunities lie “Mini-Scale ECCOS Systems,” which leverage many of the SuperSurya low-cost enabling features in a simple, robust design of an innovative floating system as shown in Fig. 5. Mini-Scale ECCOS Systems can be used beneficially for a wide variety of urban and rural customer classes. Key attributes of the Mini-Scale Efficient Concentrating Cogeneration Offshore Solar Systems include:

- 5 kWe + cogenerated 10 kWt
- Suitable for grid-connected or off-grid applications
- CPV electricity plus usable heat for a solar hot water tank, solar building space heating & swimming pool heating
- ***Efficient, cost-effective, no land use***
- Rain or Spray wash to clean
- Solar Modules inverted stow for storm survival
- Modular design for easy replacement of modules

LCOE is estimated at 10.6 cents per kW-hr, using the NREL LCOE calculator.

Mini-Scale ECCOS Systems can also be combined in an array surrounded by a security and wave blocking perimeter floating fence. An array of 20 Mini-Scale ECCOS Systems could generate 100kWe plus 200 kWt of usable heat, and could be ideal for a variety of community, commercial and small industrial users. LCOE is estimated at 9.6 cents per kW-hr.

Scaling up from Mini-Scale ECCOS Systems, the next scale is called Small-Scale, and the next Medium-Scale. A Medium-Scale Efficient Concentrating Cogeneration Offshore Solar System including desalination is illustrated in Fig. 6. Desalination systems can provide a very valuable synergistic benefit with cost-effective desalinated water for desert or dry climate coastal cities or communities. Advantages of low temperature

desalination include low cost through use of modest temperature heat sources, low environmental heat losses, low corrosion and scaling rate, and flexibility and reliability (Gude, 2007).

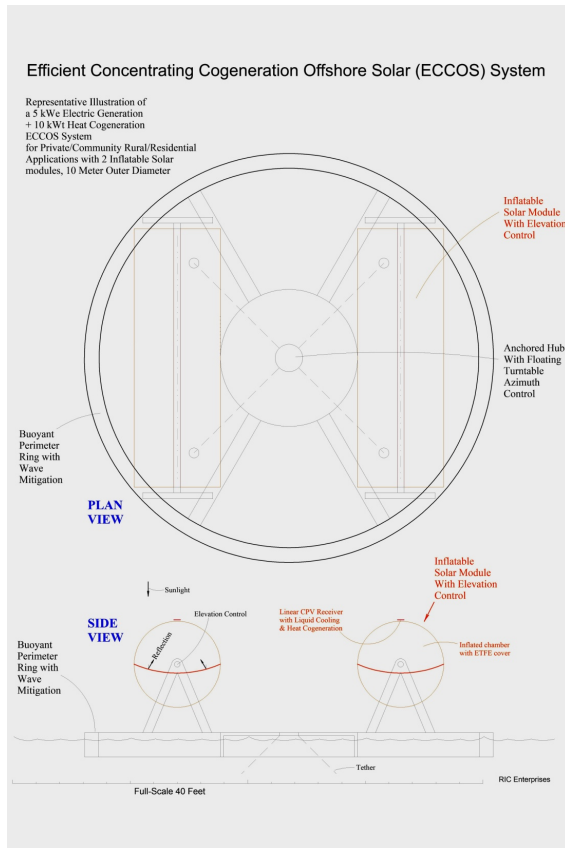


Fig. 5: Mini-Scale ECCOS System

MEDIUM-SCALE ECCOS SYSTEM WITH DESALINATION

Medium-Scale Concentrating Offshore Solar (COS) System with Desalination System

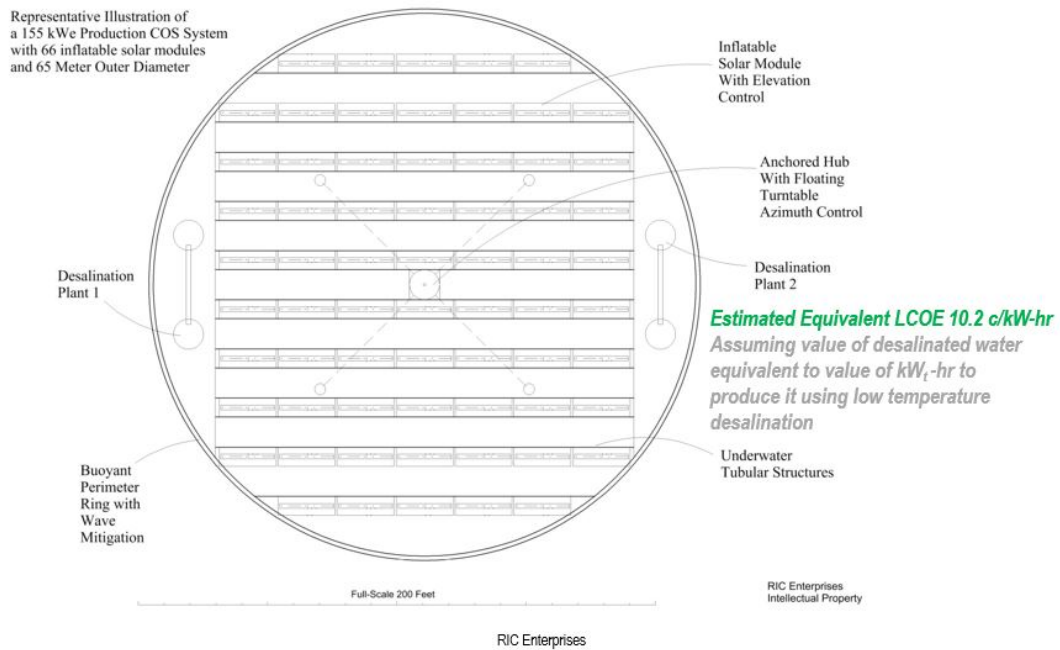


Fig. 6: Medium-Scale ECCOS System with Low-Temperature Desalination

The next major scale for ECCOS systems comprises Mega-Scale ECCOS Systems, as illustrated in Fig. 7. Mega-Scale Efficient Concentrating Cogeneration Offshore Solar Systems present a unique innovative configuration that is ideally suited to deliver a combination of electric power along with district heating and cooling for waterfront cities and communities, with unprecedented offshore renewable system economics and LCOE. Mega-Scale ECCOS Systems can also include a Rankine or Steam Cycle Subsystem to provide solar thermal based supplementary electric power. The Rankine Cycle subsystem could leverage geothermal energy turbines with a 130° C heat source, or conversely more high-technology higher thermodynamic efficiency subsystems leveraging direct steam generation (DSG) at up to 600° C.

The ideal suitability of Mega-Scale ECCOS Systems can be understood with much greater clarity by considering a specific example application, shown in Fig. 8 for the San Francisco Bay area with its very large energy needs, very large population, and very high land values. ECCOS Systems could meet 100% of Bay Area energy needs with just 2% of the Bay water area!

A few other examples of well-suited applications for Mega-Scale ECCOS Systems include the urban areas associated with Salt Lake City, Chicago, Orlando and New York to name just a few specific examples. The Great Salt Lake in Utah is an ideal location with a freeze-resistant salt water lake in a location with a cold winter, where district heating would be highly beneficial. Chicago would also greatly benefit from winter district heating, but because Lake Michigan freezes in the winter, the ECCOS Systems will need a perimeter ring of unfrozen water that can be achieved using adaptations of current freeze-prevention technologies using water bubblers or water circulators. Orlando has many lakes suitable for ECCOS Systems that can enable the city to achieve its ambitious 100% renewable goals, and the ECCOS Systems can provide both electricity and synergistic district cooling to meet Orlando needs, leveraging ammonia-water absorption chiller technologies that are well-known and well-proven. For New York, a great many suitable salt water locations exist for Mega-Scale ECCOS Systems that can provide electricity plus hot water as well as district heating and cooling as needed in different seasons. Skyscrapers, apartment blocks, commercial and industrial buildings, and all three major New York area airports could benefit from 100% renewable electricity, heat and cooling, with Mega-Scale ECCOS Systems and some measure of storage for both electricity and heat.

Many international locations would also greatly benefit from the combination of low LCOE, zero land use, and synergistic provision of district heating and cooling as required, and a few examples include Rio de Janeiro, Istanbul, Mumbai, Hong Kong, Tokyo and Singapore. Note that the authorities in Singapore are already considering offshore solar in the seas off this leading city-state of Southeast Asia. The ECCOS System provides a more cost effective innovation with multiple synergistic benefits, and should prove to be a very attractive option for Singapore's future success and economic growth.

An even larger scale version of the Efficient Concentrating Cogeneration Offshore Solar System comprises Ultra-Large Open Ocean Utility-Scale ECCOS System, as illustrated in Fig. 9 below. Ultra-large systems are likely to be located in Exclusive Economic Zone (EEZ) waters within 200 nautical miles of the shore, but too far from shore for economic direct transport of heat for district heating. On the other hand, at different geographic locations it would be beneficial for these to synergistically produce combinations of: (i) electricity from CPV, (ii) additional electricity from a Rankine Cycle solar thermal subsystem, (iii) desalinated water, and (iv) solar powered hydrogen generation from the ocean water, where the hydrogen can be used locally for night generation as well as shipped to shore either as compressed gas, liquid hydrogen, or metal hydrides, and subsequently used in a hydrogen economy subsystem of a green economy. Open ocean installations will require larger and more robust wave barriers for ocean waves, and damage prevention modes for hurricanes, typhoons, cyclones and tsunamis.

Many global applications of Ultra-Large Utility-Scale Efficient Concentrating Cogeneration Offshore Solar Systems can be in bays or in the open ocean, including the Pacific off California, the Gulf of Mexico, the Mediterranean and Black and Red Seas, and the Arabian Sea offshore from India and South China Sea offshore from China and the nations of Southeast Asia. These can be instrumental in a global paradigm-shift to leverage offshore solar to meet worldwide needs with near-zero carbon footprint and near-zero land use !

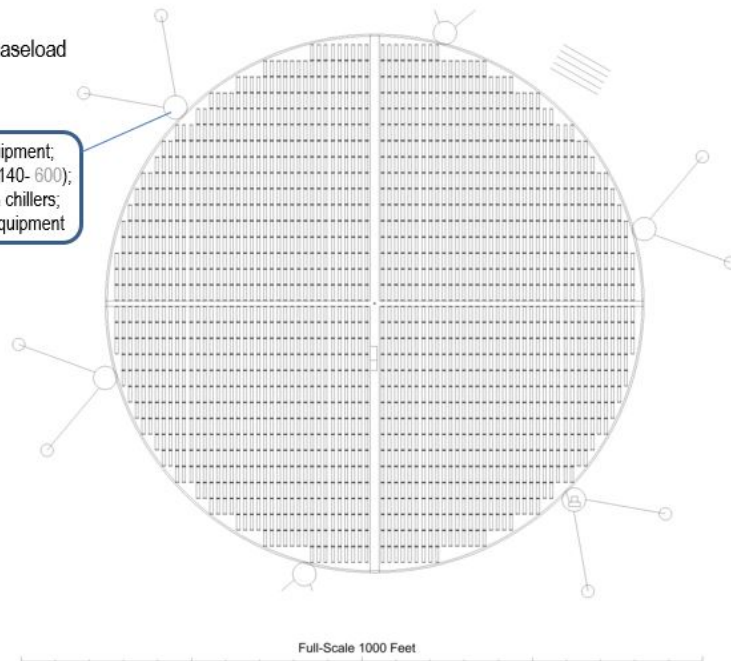
In view of the fact that in many offshore locations, there are other renewable energy sources besides solar energy, it can also be highly cost-effective in these particular locations, to share common subsystems such as anchoring subsystems and shore connection subsystems (e.g., electrical power and insulated heat transfer piping) across multiple different but synergistic renewable energy offshore systems.

MEGA-SCALE ECCOS SYSTEM

25 MW_e from CPV plus
65 MW_t for district heating / cooling
with optional steam cycle 5-10 MW_e for baseload

Tethered barge with power conditioning equipment;
Thermal storage tanks (0, ambient, 70, 95, 140- 600);
Steam powerplant; Solar cooling absorption chillers;
Monitoring, control, maintenance & repair equipment

Underwater cables and insulated piping
connecting to landside electrical customers,
district heating and cooling customers,
commercial customers, industrial customers,
agricultural customers, public sector customers



Estimated LCOE 5.6 c/kW-hr

Best Economics for
Waterfront Cities

RIC Enterprises

Fig. 7: Mega-Scale ECCOS System Enables Cost-Effective Electricity + District Heating / Cooling

MEGA-SCALE ECCOS SYSTEMS – EXAMPLE LOCATIONS

San Francisco Bay Area

Use of just 2% of bay water areas (8 sq.mi.) can accommodate
200 Mega-Scale ECCOS Systems:

- 5 GW_e from CPV plus
- 13 GW_t for district heating / cooling
- plus optional steam cycle 1-2 GW_e for baseload
- avoided land cost ~ \$10 billion @ \$2 million / acre

Mean electricity consumption by County (GW_e)

San Francisco	0.66
San Mateo	0.50
Santa Clara	1.92
Alameda	1.23
Contra Costa	1.10
Solano	0.37
Sonoma	0.34
Marin	0.15
Total Bay Area	6.27

ECCOS Systems plus some thermal and electrical
storage could plausibly meet 100% Bay Area energy
needs with low risk, lowest-cost-renewable generation
whilst avoiding land use.

Sources: Google Maps,
Rand McNally Road Atlas
<http://ecdm.energy.ca.gov/electriccounty.aspx>



RIC Enterprises

Fig. 8: San Francisco Bay Area Application for Mega-Scale ECCOS Systems

ULTRA-LARGE OPEN OCEAN UTILITY-SCALE ECCOS SYSTEM

400 MWe Efficient Concentrating Cogeneration Offshore Solar (ECCOS) System

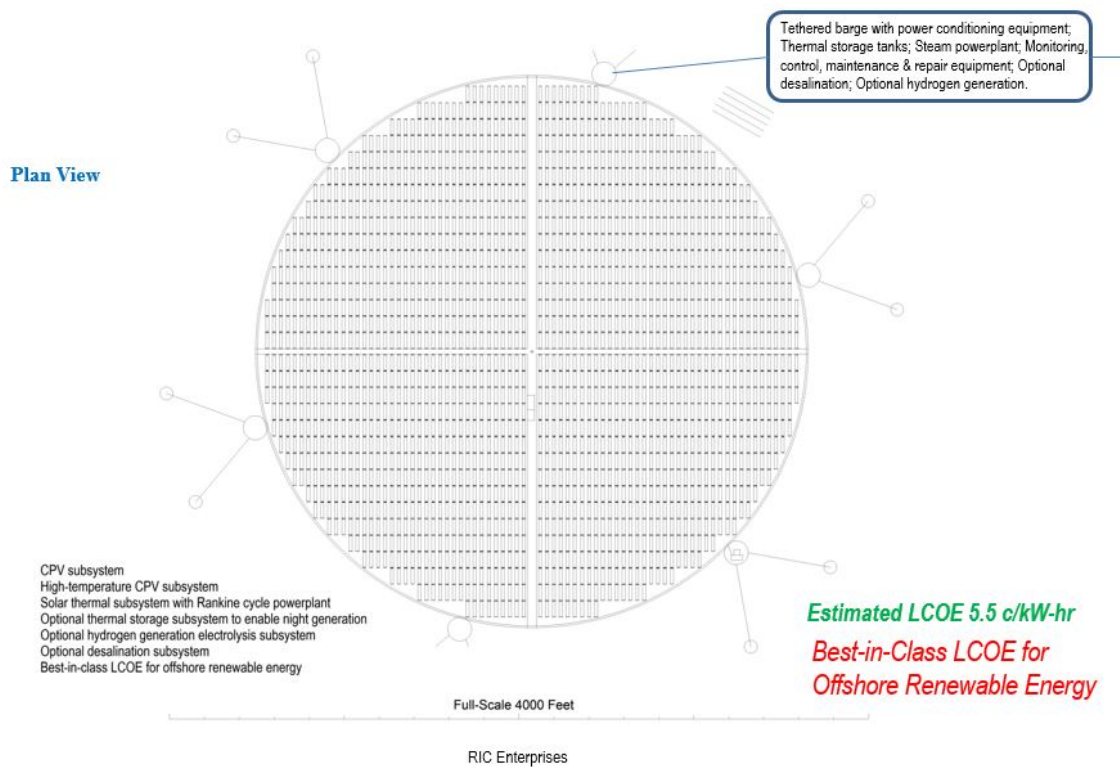


Fig. 9: Ultra-Large Utility-Scale ECCOS System

To be more specific, in order to achieve both increased capacity factor and even more LCOE reduction relative to best-in-class utility-scale ECCOS Systems, these ECCOS Systems can, in selected geographic locations, be synergistically integrated with:

- Offshore wind energy technologies
- Ocean and tidal current technologies
- Ocean thermal energy conversion (OTEC)
- Transmission technologies including high voltage / superconducting power lines and insulated piping for district heating and cooling
- Storage technologies including thermal storage, phase change storage, seasonal storage, batteries, hydrogen, pumped hydro, etc.

A few foundational innovations in very large diameter, vertical axis offshore wind and hydrokinetic renewable energy harvesting devices, are captured in RIC Enterprises patents noted in Fig. 10 below, and these can be easily combined with an ECCOS System to harvest solar power in an inner circle within the very large diameter ring of the wind and hydrokinetic harvesting system. The multiple systems can share underwater tethering systems as well as energy transmission systems to the shore.

As a highly promising example of where Efficient Concentrating Cogeneration Offshore Solar (ECCOS) Systems could be synergistically combined and integrated with tidal current and offshore wind harvesting systems, the Bay of Fundy separating Nova Scotia from New Brunswick and Maine, offers tremendous potential with its world-class tidal range combined with healthy wind and solar potential as well.

In a corresponding vein, the extraordinary power of the Gulf Stream ocean current flowing north along the coast of Florida, Georgia and the Carolinas offers a unique opportunity to synergistically combine the power of the Sun, the wind, and the ocean current with ECCOS systems integrated with very large diameter vertical axis wind and water current harvesting systems.

Another synergistic opportunity is to combine ECCOS Systems with Ocean Thermal Energy Conversion (OTEC) systems in regions where deep cold water is available, such as offshore from Hawaii. The temperature differential between the heated CPV cooling fluid and the pumped up deep water “cold sink” will enable greater

thermodynamic cycle efficiency than for either the solar thermal subsystem of the ECCOS system by itself, or a stand alone OTEC by itself. Offshore from Hawaii, integration with an offshore wind system is also an attractive and very likely beneficial synergistic opportunity. These synergistic opportunities can be instrumental in helping Hawaii achieve its ambitious 100% renewable goals while minimizing land use.

SYNERGY OPPORTUNITIES FOR ECCOS SYSTEMS WITH VERTICAL AXIS OFFSHORE WIND & OCEAN / TIDAL CURRENT SYSTEMS

U.S. Patent Jul. 6, 2010 Sheet 43 of 56 US 7,750,491 B2

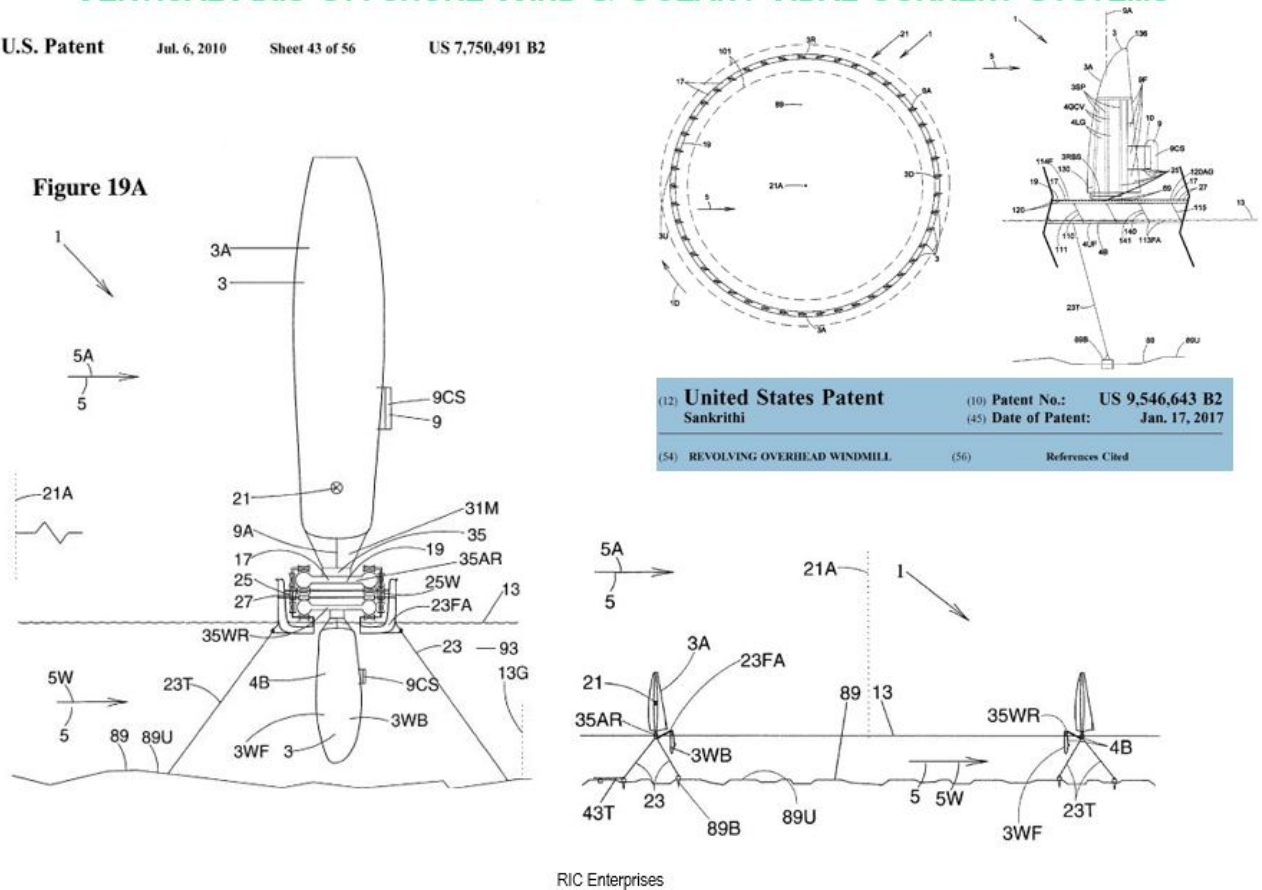


Fig. 10: Offshore Wind & Hydrokinetic Very Large Diameter Vertical-Axis Systems

Based on the several examples outlined above, it can be concluded that Efficient Concentrating Cogeneration Offshore Solar (ECCOS) Systems have extraordinary potential to play a highly beneficial, cost-effective and pivotal role in enabling many cities and other jurisdictions with 100% renewable energy goals, to achieve those ambitious and challenging goals. RIC Enterprises looks forward to collaborating with other members of ASES, ISES and the renewable energy community in enabling a cost-effective green future for our kids, grandkids and generations to come.

5. References

Barry, Max, Nation States. 2016.

<https://www.nationstates.net/page=dispatch/id=545595>

Brown, Frederic, Kyocera JV inaugurates 13.7 MW floating PV plant in Japan. March 27, 2018. PV Magazine.

<https://www.pv-magazine.com/2018/03/27/kyocera-jv-inaugurates-13-7-mw-floating-pv-plant-in-japan/>

Dansk Fjernvarme, Solar District Heating – Inspiration and Experiences from Denmark, Jan. 2018. English Version for IEA SHC Task 55.

<http://task55.iea-shc.org/Data/Sites/1/publications/SDH%20Inspiration%20Experience%20DK%20v5.pdf>

Energy Information Administration, Total Energy Statistics & Analysis. 2016.

<https://www.eia.gov/totalenergy/>

Gude, VG, Low Temperature Desalination: An Option for Sustainability and Energy Savings. 2007. New Mexico State University.

http://www.gwpc.org/sites/default/files/event-sessions/Gude_Veera.pdf

IRENA, International Renewable Energy Agency, Renewable Power Generation Costs in 2017. 2017.

<http://www.irena.org/publications/2018/Jan/Renewable-power-generation-costs-in-2017>

Kenning, Tom, World's largest floating solar plant comes partially online in China. Dec 11, 2017.

<https://www.pv-tech.org/news/worlds-largest-floating-solar-plant-comes-partially-online-in-china>

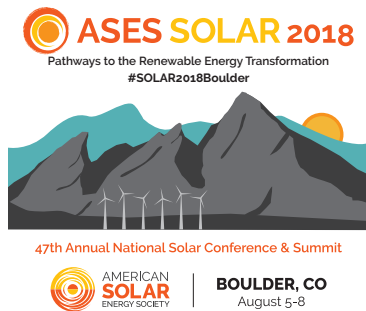
Sankrithi, M, Sankrithi, U, 2010. Prototype Development and Testing of Inflatable Concentrating Solar Power Systems. SOLAR2010, Paper 0251.

Sankrithi, M, Sankrithi, U, 2012. Beneficial Applications of Inflatable Heliostatic Mirrors. World Renewable Energy Forum, Paper 0273.

Sankrithi, M, Watkins, S, 2016. Collaborative Prototype Development & Test Project for a Novel Hybrid Solar Concentrating Cogeneration System, SOLAR2016, Conference Proceedings.

Zolfagharifard, E, Would You be Underwater if the Polar Caps Melted? Daily Mail, 21 April 2014.

<http://www.dailymail.co.uk/sciencetech/article-2609338/Would-YOU-underwater-polar-caps-melted-Map-reveals-planet-look-like-sea-levels-rose-260ft.html>



Conference Proceedings

ASES National Solar Conference 2018
Boulder, Colorado August 5-8, 2018

Research Reveals the Hidden Methods to Democratize Solar

Warren Schirtzinger¹

¹ High Tech Strategies, Inc., Seattle (United States)

info@hightechstrategies.com

Abstract

Several US cities stand out as being relatively effective in broadening the access to and use of solar power. The locations where adoption of solar has been the most prolific are located across the nation, from California to New Jersey. They represent various geographies, climate zones, and population demographics. But they all have in common a noticeable increase in solar panel installations thanks to the same mainstream-solar-adoption formula.

The conventional beliefs surrounding solar adoption focus on a few key factors: reducing the cost of solar panels, the importance of solar in combating climate change, and pro-solar policies or incentives. Yet an examination of the real reasons people adopt solar reveals factors and motivations that are very different than what is commonly believed. The formula for encouraging people to make a lasting transition to a clean energy future is based on reducing perceived risk.

Strategic initiatives designed to reduce the perceived risk of adoption are required to achieve a sustainable transformation. These initiatives create permanent change so the market does not regress to lower levels of utilization at some later time.

Drawing on the transformational success of specific locations across the US, the author guides stakeholders who are promoting the acceptance and adoption of solar power, how to increase adoption, boost policy effectiveness and reduce costs.

Keywords: solar adoption, market transformation, grid-connected photovoltaics, electric power, renewable energy, distributed generation, clean energy

1. Introduction

The solar industry has long been characterized by ups and downs that are often triggered by external forces or policies beyond its control. Continued reliance on policy makers to adopt favorable political frameworks and instruments to promote fast and steady growth of solar and other renewables is, at best, a strategy that will lead to unpredictability.

Whenever government support for solar declines, we are reminded of how important it is for renewable energy markets -- especially solar power -- to operate independently of government support. The solar industry needs regulatory certainty, but it also needs to become sustainable on its own; a process that is

referred to as *market transformation*.

Market transformation is the strategic process of intervening in a market to create lasting change in market behavior by removing identified barriers or exploiting opportunities to accelerate the adoption of all cost-effective solar power as a matter of standard practice. The key words here are *lasting change*. Because government subsidies do not create lasting change, we need to identify ways to intervene in the solar market in a way that accelerates the adoption of solar, but also leads to a sustainable market.

Several useful models of market transformation describe industry transitions in terms of the changing nature of the user. The model called Diffusion of Innovation for example describes a market's acceptance of a new technology in terms of the types of consumers it attracts throughout its useful life. The underlying thesis of the Diffusion of Innovation model is that the adoption of new products or technologies occurs in a specific order through a social system comprised of five distinct segments. It is probably the most well established model in many high-tech industries because it provides useful insight at all stages of market development.

Subsequent adaptations of the diffusion model -- including *The Tipping Point* and the *Technology Adoption Lifecycle* -- maintain a reliance on the psychological and social attributes of various end users, rather than the product. However, studies of successful and lasting market transformation in the solar industry reveal that it is the product that determines the degree of solar acceptance and adoption.

2. Innovation Frameworks and Models

Originally published in 1957 by Joe M. Bohlen, George M. Beal and Everett M. Rogers at Iowa State University, the underlying thesis of the Diffusion Process is that innovations are absorbed into any given user base in stages corresponding to psychological and social profiles of segments within that user community¹. The process can be represented by a bell curve with definable stages; each associated with a definable group, and each group making up a predictable portion of the whole community. Everett Rogers extended this popular theory about how, why, and at what rate new ideas and technology spread in his book *Diffusion of Innovations*².



Fig. 1: Diffusion of Innovation model

The prescription for success in introducing a new product or technology into any community is to work the curve from left to right, focusing first on the innovators, growing that market, then moving on to the early adopters, growing that market, and so on. To do this effectively, it is necessary to know and understand the psychological characteristics of each group of buyers.

The psychographics of each group in the adoption process influences the development and dynamics of the market. For example, each group places a different value on product intangibles, and on endorsements or references from other groups. As products move through the adoption process, intangibles and user references assume more importance. Often, pioneering new products lose their initial prominence because a new entrant is more successful in product positioning based on a more effective mix of intangibles. This can be the case even if the second product is not technically superior.

The concept of dynamic change in the perceptions of products is reinforced by the concept of the adoption process. In 1957, researchers at Iowa State College were able to track the diffusion of information and purchase patterns of a new product: hybrid seed corn. They found that purchase and use (or adoption) behavior fell into understandable patterns. They found that five distinct “segments” of an adoption population could be described. They noted the different characteristics of persons in these five groups, and hypothesized about the way word-of-mouth influences purchase behavior.

Five groups were identified as follows:

Innovators—2.5% of the population

They pursue new technology products aggressively. Because technology is a central interest in their life, Innovators embrace the nuts and bolts of how a new technology actually works. And they play perhaps the most straightforward and unambiguous role: to understand and assess new technologies or methodologies and endorse those with true technical superiority over currently available alternatives.

Early Adopters—13.5%

They buy into new product concepts very early in their life cycle, but unlike innovators, they are not technologists. Often referred to as visionaries, early adopters match emerging technologies or new ideas with industry-specific opportunities to drastically reshape existing markets. In other words, they identify business opportunities for a strategic leap forward. Early adopters have the imagination to see the world as it could be (rather than as it is) and the ambition to try to make those possibilities the new reality.

Early Majority—34%

They are driven by a strong sense of practicality and seek demonstrable gain backed by a defensible cost-benefit analysis. Referred to as Pragmatists, the Early Majority wants to see well-established references before investing substantially. As a group they are comfortable with their ability to handle a technology product. Members of the Early Majority insist on following industry standards and best practices.

Late Majority—34%, and

They share all the concerns of the early majority, but are not comfortable with their ability to handle a technology product. Members of the late majority always wait until something has become an established standard. The Late Majority is risk averse, price sensitive, and has the tendency to follow rather than lead.

Laggards—16%

They simply don't want anything to do with new technology, for any variety of reasons, some personal and some economic. Laggards avoid adoption to the bitter end.

The core insights embedded in Rogers' Diffusion of Innovation is that the adoption of new ideas occurs in a specific order through a social system. Rogers' research was updated specifically for high-tech products by Lee James while working at Regis McKenna, Inc. in Portland, OR⁴. Lee James was also the person who created the Right Turn on Red Law while working at the Federal Energy Administration during the 1970s oil crisis, using his marketing skills to encourage conservation.

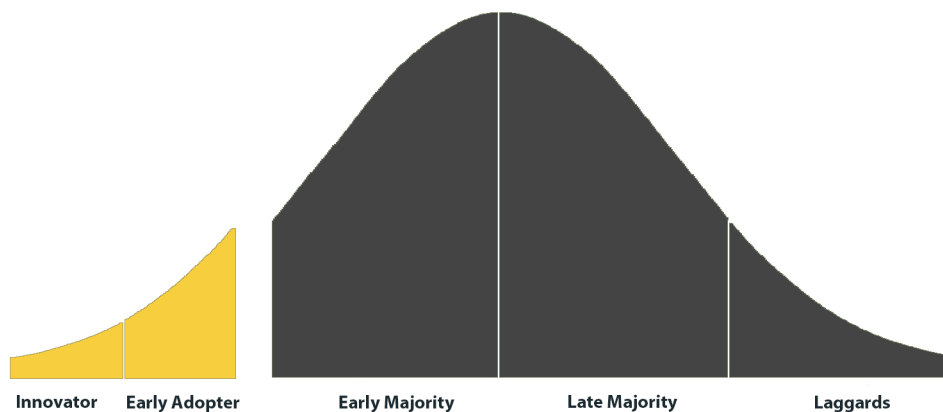


Fig. 2: High-Tech Marketing Chasm model

As a technology marketer and consultant Lee James recognized the need for a key modification: a significant gap, or *chasm*, between early adopters and the early majority⁴. James noticed that high-tech products don't follow the same pattern of adoption as other non-technical products. He observed that high tech products often struggle to gain mainstream acceptance, and even fail, even though they are initially well received. If a company can “cross the chasm,” commercial success becomes inevitable, as sales then occur largely through a social process of one peer imitating another.

The research demonstrated a number of elements of purchase behavior, including the dynamic nature of how products are purchased. Innovators, for example, are motivated by being first, while late adopters are primarily interested in a proven, fully-tested solution. The primary value of the research was the development of the idea of an *adoption process*. New product acceptance could finally be understood and even diagramed.

3. Public Policies Blur Market Effects

The principles behind Diffusion of Innovations have repeatedly guided high-tech products and companies to the achievement of mainstream market acceptance, public support and commercial success. And some of the history and experience behind diffusion theory can be translated into helpful guidance for the solar industry.

However there is a fundamental difference between subsidized markets for solar power, and unsubsidized markets for technology-based products. The strategies historically employed to spur expansion of the solar (PV) market include some type of policy-based incentive or subsidy. Lowering *cost per watt* through public policy has been the key to unlocking a vast potential market for photovoltaics.

Solar products are typically subsidized or supported with the primary goal of achieving economies of mass production and eliminating barriers to use. Examples include:

- federal and state buy-down programs
- coordinated government procurement of PV
- elimination of barriers to capital formation
- legislative packages supporting distributed energy
- legislative and regulatory assistance to states
- prohibition of restrictive covenants and ordinances

End-user research shows these policy-based incentives act to blur the adoption effects of the market for solar products. The psychographic sequence that is the foundation of diffusion theory (innovator - early adopter - early majority - late majority) is actually skewed by government or utility programs designed to encourage or accelerate the adoption of solar. Public policy blurs market dynamics.

In addition to understanding the inherent difficulties in measuring localized, psychographic behavior, you must factor in the effect of public policy and incentives. In most cases, government policy will reduce risk in the eyes of a mainstream customer so that adoption occurs before it normally would in a purely commercial [unsubsidized] setting or market.

This skewing effect on solar adoption was first discovered by Steven Strong, Don Osborn, and Dr. Donald Aitken when conducting a review of the Sacramento Municipal Utility District (SMUD) PV Pioneer Program in 1999⁵. People who fit the psychographic description of the early and late majority were among the first to sign up for residential solar because the combined effect of SMUD's multi-faceted solar program lowered risk so dramatically, it caused pragmatic buyers to adopt solar early, rather than late.

The bottom line is solar adoption is influenced by a unique set of artificial variables, making buyer-transition points in diffusion models even harder to recognize.

4. The Hidden Formula

The psychographics of each group in the adoption process influences the development and dynamics of an unsubsidized market. Each group places a different value on product intangibles, and on endorsements or

references from other groups. As products move through the adoption process, intangibles and user references assume more importance. Also critical to understanding the adoption process is the underlying motivation of each group. Innovators for example love to be first to try something new. Whereas early adopters are motivated by their desire to transform their company or life into something much better.

With solar, buyer behavior patterns are no longer reliable indicators of market dynamics, therefore stakeholders and promoters of solar power are left with one proven tactic to attract the mainstream population -- using proven, risk-lowering techniques that are known to attract pragmatic buyers.

Decades of research show that the characteristics and motivations of mainstream buyers are consistent regardless of the technology that is being adopted. Before a pragmatic, mainstream buyer adopts a new technology it must meet the following requirements:

- a. the product must be evolutionary, not revolutionary
- b. the product must enhance the system the buyer has now, not overthrow it
- c. the product must improve an existing operation, not change it
- d. the product offering must be a complete solution (also known as the low-risk recipe)
- e. the buyer must not be required to fine tune or troubleshoot the product
- f. the product must work properly and integrate easily with the exiting infrastructure
- g. the vendor cannot disappear after installation
- h. the product or system must be purchased from a market leader
- i. the vendor must provide references and/or referrals from an identical type of customer

Given that 84% of the population looks for ways to avoid risk, a framework for the delivery of low-risk solutions can be applied to accelerate the acceptance and adoption of renewable energy. "The Low Risk Recipe" is a concept that describes the socially acceptable methods of accelerating change when a market has been subsidized. Discontinuous innovations like solar require a very specific set of risk-lowering attributes in order for the mainstream population to accept and then adopt. These proven methods of market transformation have the ability to help scale innovative programs both broadly and rapidly.

For example, utilities and/or one of their partners can deliver the *low risk* requirements of mainstream buyers. Rather than social interaction as the primary driver of solar adoption as highlighted in diffusion theory, a low-risk program (consisting of both tangible and intangible attributes) can be assembled through various agencies, vendors and programs, and offered together in a way that reduces risk and meets the pragmatic needs of the mainstream population.

The impact of a utility or familiar vendor offering a low-risk product makes all the difference. All of the requirements of a pragmatic, mainstream buyer are satisfied:

- a. solar helps the system of electric supply get better or *evolve*
- b. the solar system compliments the electric grid by providing distributed generation. It does not replace the grid
- c. solar provides renewable generation which is an improvement over non-renewable methods
- d. the system delivered is a complete solution, delivered through a combination of providers and programs
- e. the customer receives a turnkey system that does not need to be fine tuned
- f. the solar panels work properly and integrate easily with the exiting [grid] infrastructure
- g. the utility evaluates solar installers and works only with contractors who are reliable
- h. the utility offers a choice of reliable vendors, allowing the customer to buy from a perceived market leader
- i. references and referrals are provided by neighbors or industry-specific users

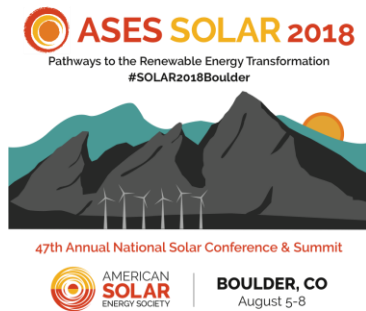
5. Conclusion

Despite diffusion theory's long history of successful guidance for high-tech companies and other innovators, the idea that you can accelerate the adoption of solar through social dynamics alone is incorrect. Because of the blurring effect caused by public policy and regulation, solar must be offered as a complete solution by a known supplier who makes the buying experience familiar and low risk. For solar to achieve mainstream

market acceptance, it must be standardized, minimize disruption and integrate with existing systems. And the system's intangible attributes must be as strong or stronger than the tangible attributes of the technology itself. This formula for democratizing solar has been partially assembled and is starting to be implemented in several locations across the US, and the conclusions of this study have been verified.

6. References

- [1] Bohlen, J. M.; Beal, G. M. (1957), The Diffusion Process, Special Report No. 18 Agriculture Extension Service, Iowa State College 1: 56–77.
- [2] Rogers, E. M., (1962). Diffusion of Innovations, Glencoe: Free Press.
- [3] Levitt, T., (1980) Marketing Success Through the Differentiation of Anything. Harvard Business Review, January – February, p.83-91
- [4] James, L., (1992) The High-Tech Product Lifecycle. Software Association of Oregon Publications, volume 3, number 2
- [5] Aitken, D.W. ; Schirtzinger, W. ; Strong, S. (2000), SMUD’S PV PROGRAM: Past, Present, and Future. A Report to the Sacramento Municipal Utility District
- [6] Osborn, D.E., (2000) “Sustained Orderly Development and Commercialization of Grid-Connected Photovoltaics: SMUD as a Case Example”, Advances in Solar Energy XIV, American Solar Energy Society in the reference list, but may be mentioned in the text.



Conference Proceedings

ASES National Solar Conference 2018

Boulder, Colorado August 5-8, 2018

ASES National Solar Conference 2018

Comparative Analysis of Energy Storage for Photovoltaics: Electrical vs Virtual

Orthi Sikder¹, Camille Torres² and Peter Mark Jansson³

¹ Bucknell University, PA (United States)

² Polytech Tours, Tours (France)

³ Assoc. Professor ECE, Faculty Director BCSE, Bucknell University, PA (United States)

Abstract

The recent successful deployment of 100+ MWhr battery in South Australia by Tesla to solve grid problems with the intermittent generation of renewables places an economic stake in the ground for energy storage. Virtual energy storage at the Bucknell University Residential Microgrid testbed has demonstrated that multiple kWhrs of electricity can be successfully shifted during utility heating and cooling peaks at a fraction of the cost of batteries. While load management and pre-cooling and pre-heating of residential dwellings have been discussed historically as potential solutions to intermittent generation from photovoltaics (PV), our work in a live test bed definitively demonstrates that load shifting can be the electrical equivalent of battery energy storage while maintaining occupant comfort and satisfaction. It is our hope to reinvigorate the discussion about these options because they are not only more economic than physical electrochemical batteries but they represent a much more sustainable pathway to meet utility near term electricity storage needs.

Keywords: energy storage, microgrid, residential photovoltaic system, battery, virtual storage

1. Introduction

Photovoltaic (PV) systems are recognized as promising renewable energy resources to meet the world's growing electricity demand. After evolving over the last two decades, PV has proven to be a mainstream source of electricity. Today the world is experiencing rapid growth of solar electric technologies. As a matter of fact, some power grids across the world are struggling to keep up with the technological advances, increased penetrations and growing cost-competitiveness of renewable energy sources like PV.

The United States, China, Germany, Japan, United Kingdom and India are currently leading installers of PV [1]. Annual new additions of photovoltaics to world electric grid are shown in Figure 1.

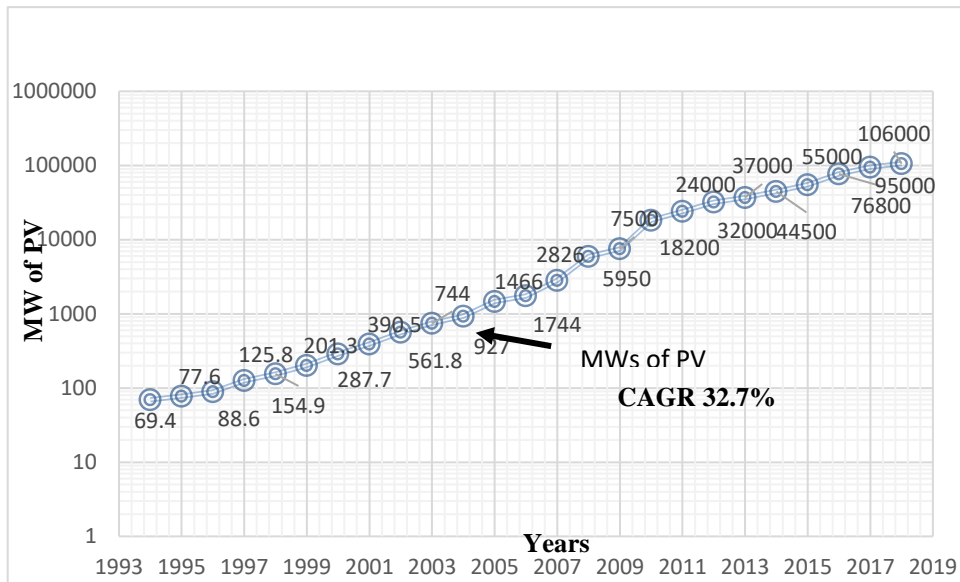


Fig 1: Annual new addition of photovoltaics to global total installed PV

Figure 1 shows the annual addition of new PV to the world’s grids (in MW) over the last 25 years. Here, the plot is in logarithmic scale and it is linearly increasing at the same time. From the plot, we can see that every 5 to 6 years the new PV capacity has increased an order of magnitude. The compound annual growth rate (CAGR) represented by grid-tied photovoltaics averaged nearly 33% per year over the last 25 years as costs of this technology plummeted. PV in 2018 is projected to be as high as 106 GW [2-3].

Since PV is clearly an intermittent source of electrical energy due to its diurnal cycle and susceptibility to poor weather (cloud cover), electrical energy storage has now become a fast growing sector in the solar marketplace. According to market research; the electrical energy storage market exploded to annual installation size of 6 gigawatts (GW) in 2017 and it may grow to over 40 GW by 2022 (\$6.8B) – from an initial base of only 340 MW installed in 2013 (\$400-\$600/kWh in 2015) [4-5].

2. Problem Statement

To help elucidate the temporal problem associated with PV generation, we will begin by discussing some typical load profiles and usage trends. Let us pick a typical summer day with an average outdoor temperature profile [shown in Fig 2 (a)]. For a typical residential home with a PV system as its renewable energy resource, the net load profile and PV generation profile will look as graphed below [in Fig 2 (b,c)].

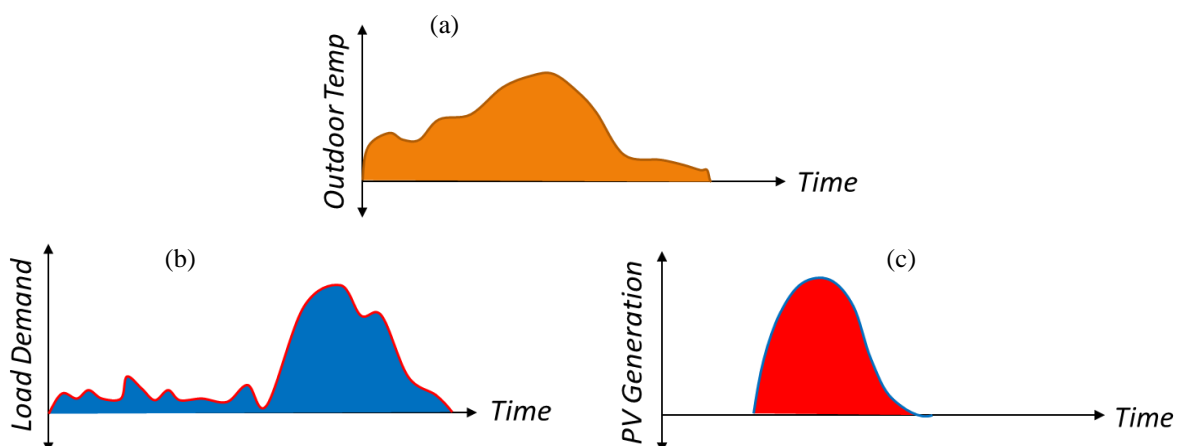


Fig 2: A typical day’s (a) temperature profile; (b) load profile; (c) PV generation profile.

Fig 2(b) and 2(c) clearly illustrates that the peak load demand and peak PV generation are not occurring simultaneously. More clearly, if we superimpose the demand over generation, we will get the result as in Fig.

3(a). This implies that, the peak generation from PV system is not being used to meet the peak load in a typical day. There exists a time gap between these two. In order to meet the peak demand by PV generation we can either store the generated PV energy with electrical storage systems and dispatch the energy later when usage is high. Otherwise, we can simply sell the energy to the main grid at a low price and draw energy from the main grid when the peak demand hits again at the cost of higher energy prices.

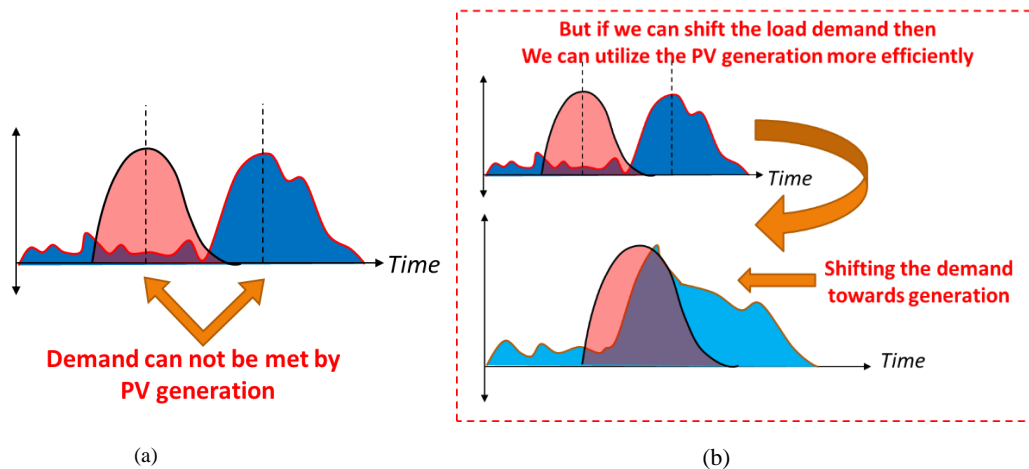


Fig 3: (a) Superimposition of a typical day's load profile over PV generation profile (b) Demand shifting can help optimize PV energy utilization

For decades, the most popular form of energy storage has been batteries. In a battery, we store energy in the form of chemical energy. Later, that energy is turned back into electricity for usage. There are some other forms of energy storage available such as: flywheels, hydrogen systems, pumped hydro, compressed air energy storage etc. However, almost all kinds of conventional energy storages come with several limitations. They are often very expensive, have limited capacity, require timely maintenance, use natural resources and have adverse environmental impacts. Hence, with all these inadequacies, scientists continue to think about an alternate form of energy storage over the troublesome and expensive conventional ones.

3. Research Motivation

A load management system can create more load if more power is available from a PV system than is being used currently to make sure no energy is wasted [Fig 3(b)]. For example: a load management can adjust a smart thermostat (if available) to store more energy in the dwelling thermally. Various techniques enable a load-management environment and can be classified into six categories: peak clipping, valley filling, load shifting, strategic conservation, strategic load growth and flexible load shape [6]. Therefore, it is possible to shift load from peak periods to off peak periods in a way that can potentially provide cost savings both to the consumer and utility grid operators. However, to carry out the load shifting and peak clipping without changing consumer preferences, some form of energy storage is necessary. Such storage acts as a conduit between peak and off-peak loads. To perform load shifting, peak clipping, valley filling and flexible load shape techniques in cost-effective ways, a possible and potential candidate is virtual energy storage (VES) systems.

The ability to shift load and store energy thermally internal to a house as well as activate diversion loads as necessary to store excess energy gives the Microgrid a form of virtual energy storage [7-8]. It is considered virtual, because the energy stored cannot be recovered as electricity to be used in grid. The energy is instead consumed at the time of generation as is done in the utility power grid. The difference is that the energy consumption is controlled by the microgrid to be done at the most beneficial time. If selling solar energy back to the main grid is not desired due to unfavorable conditions, the energy can rather be stored in the thermal mass of the house through use of the heating, ventilation and air-conditioning (HVAC) system. This energy is recovered later by not using the HVAC system as much and allowing the internal temperature to float back to a normal set point range or desired set point according to the load management protocol [9-11]. There are two main reasons for choosing HVAC as the variable load. First, heating and cooling is still considered to be one of the largest loads which accounts for about 48% of the energy use in a typical U.S. home, making it the largest energy expense for most of the residential homes [12]. Second and most importantly, HVAC systems offer us the simple yet great opportunity to use the thermal mass of the building by pre-heating or pre-cooling this mass and using its thermal storage potential for shifting electrical loads away from the utility peak period.

4. Research Methodology and Results

In this work, we have explored an extensive empirical analysis of thermal storage based virtual energy storage systems. To do so, we have been using the Bucknell Residential Microgrid System as our testbed. It is a residential home. The system has PV array and a natural gas generator as distributed resources and a main-grid connection. The grid is also equipped with smart thermostats and a smart electricity metering system that allows real-time load monitoring. At the same time, the grid has a raspberry-pi based central control unit that can be utilized to provide a web-based smart load management scheme in the residential home. It is important to note that the residential home considered in this work is well insulated.

We consider the microgrid system with two operating conditions depending on the load management: normal and experiment. We randomly picked 2 summer days to compare the results and find theoretical validation of our claim: July 2 and July 3, 2018. These two days are considered experiment day and normal operation day respectively. They are very similar in terms weather as shown in Figure 4(a). The energy price profile for these two days are shown in Figure 4(b). On July 2, 2018, the experiment day, the load management was done according to the day ahead local marginal price from PJM. According to that, the house was precooled for 3 hours at 68° F from 1 pm to 4 pm and then the variable load HVAC system was forced off for next 3 hours from 4 pm to 7 pm with only fan running, the indoor temperature was allowed to rise by 6° F overall.

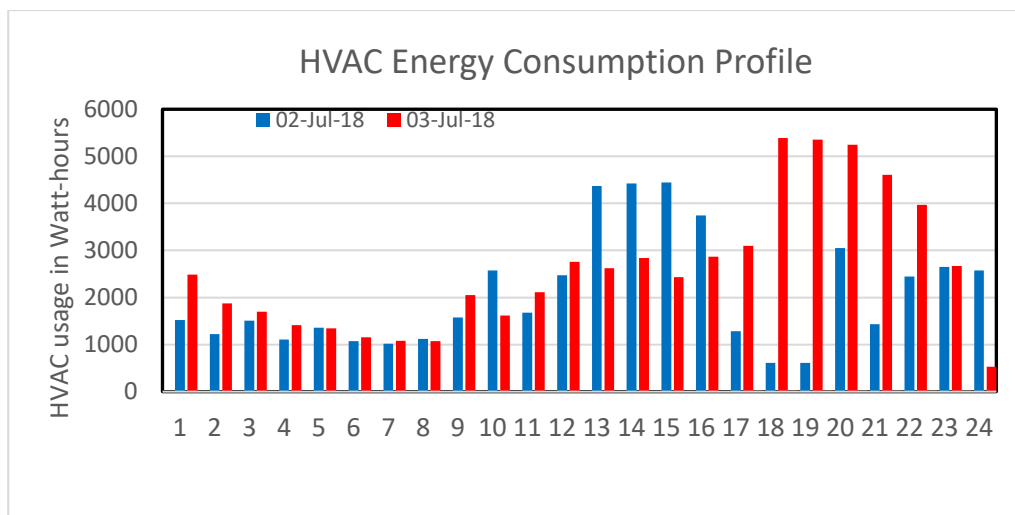
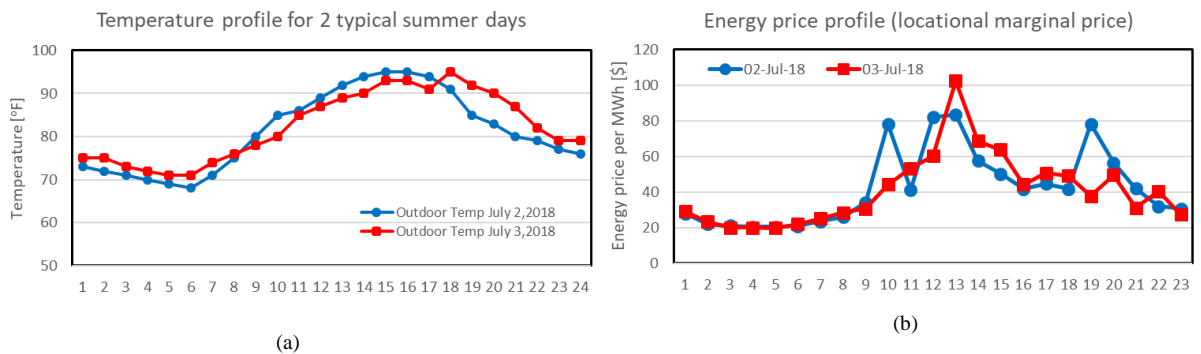


Fig 4: Two typical summer day's (a) temperature profile; (b) energy price profile (c) energy consumption by HVAC.

On July 3, 2018 the HVAC system ran at its own pace without any external interruption and control with the normal setting temperature 72 °F. Figure 4(c) shows the comparison in HVAC system energy consumption between these two days. It also shows, how clearly the peak load can be shifted to the period of the day when PV generation is available. Not only that, by quantifying the energy usage, we find that the experiment day HVAC usage is 12.43 kWatt-hours less than the normal operation day.

On closer inspection: The Experiment day HVAC usage was 49.883 kWh
 The Normal operation day HVAC usage was 62.314 kWh
 Average energy price on normal day \$39.25 / MWhr
 Utility Cost saving = 48.79 cents daily = \$14.64/ month

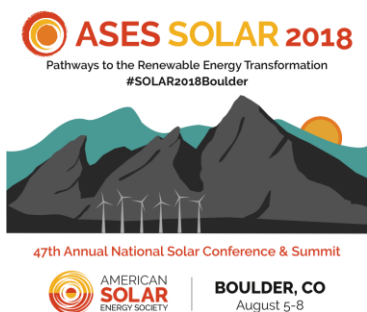
Also on average, electricity sources emit 1.222lbs CO₂ per kWh. [13] So clearly it reduces the carbon footprint on the environment.

5. Conclusion

Virtual energy storage has proved itself both financially and environmentally beneficial to a grid with renewable resources like solar system. While we are utilizing the solar generation for meeting peak demand, we are saving the same amount of energy not being drawn from the main electrical grid reducing our cost for usage and carbon footprint on environment. It is also helping by reducing energy consumption during high price period creating scope for extra savings. The future prospect of this research work will be to create the optimal range of thermal mass and find out the critical design criteria required for a microgrid system than can provide such benefits and explore the long term benefits of virtual energy system over conventional energy storage systems.

6. References

- [1] "Solar PV - Statistics & Facts", <https://www.statista.com/topics/993/solar-pv/>
- [2] Jäger-Waldau, Arnulf. (2017). PV Status Report 2017. 10.2760/452611.
- [3] IRENA (2018), Renewable Power Generation Costs in 2017, International Renewable Energy Agency, Abu Dhabi.
- [4] "US Energy Storage Market Tops the 1 GWh Milestone in 2017", <https://www.greentechmedia.com/articles/read/us-energy-storage-market-tops-the-gwh-milestone-in-2017/>
- [5] "Facts and Figures", <http://energystorage.org/energy-storage/facts-figures>
- [6] C. W. Gellings, "The Concept of Demand-Side Management for Electric Utilities," Proceedings of the IEEE, vol. 73, no. 10, pp. 1468-1470, 1985.
- [7] P. Diefenderfer and P. M. Jansson, "Rationalization of a residential microgrid on PJM," 2014 IEEE PES T&D Conference and Exposition, Chicago, IL, USA, 2014, pp. 1-5.
- [8] P. Asare, C. Ononuju and P. M. Jansson, "Preliminary quantitative evaluation of residential virtual energy storage using power sensing," 2017 IEEE Sensors Applications Symposium (SAS), Glassboro, NJ, 2017, pp. 1-6.
- [9] M. Avci, M. Erkoç and S. S. Asfour, "Residential HVAC load control strategy in real-time electricity pricing environment," 2012 IEEE Energytech, Cleveland, OH, 2012.
- [10] D. T. Nguyen and L. B. Le, "Joint Optimization of Electric Vehicle and Home Energy Scheduling Considering User Comfort Preference," in IEEE Transactions on Smart Grid, vol. 5, no. 1, pp. 188-199, Jan. 2014.
- [11] H. Karami, M. J. Sanjari, S. H. Hosseinian and G. B. Gharehpetian, "An Optimal Dispatch Algorithm for Managing Residential Distributed Energy Resources," in IEEE Transactions on Smart Grid, vol. 5, no. 5, pp. 2360-2367, Sept. 2014
- [12] "Heating & Cooling", Department of Energy, ENERGY.GOV, <https://www.energy.gov/public-services/homes/heating-cooling>
- [13] <https://thelukewarmersway.wordpress.com/2016/03/27/concentrations-are-calculated-emissions-are-estimated/> ; accessed on 22 Aug



Conference Proceedings

ASES National Solar Conference 2018

Boulder, Colorado August 5-8, 2018

ASES National Solar Conference 2018

A Low-Cost IoT Approach to Real-Time Cloud Motion Detection

Ian Smithpeter

Colorado State University, Fort Collins, CO (USA)

iansmithpeter@yahoo.com

Abstract

As solar energy accounts for a larger portion of power grids around the world, it becomes necessary to mitigate the power output variability caused by intermittent cloud cover. When applied to a photovoltaic (PV) array, this variability limits the percentage of energy in a power grid generated by solar power. This limitation applies to both grid tied and islanded power systems. Many strategies exist to mitigate these effects, including the use of backup generators but efficient hybrid solar power systems require accurate short-term forecasting of sharp changes to ground horizontal irradiance (GHI) to minimize fuel usage. This work describes an Internet of Things (IoT) network of inexpensive nodes equipped with pyranometers and explores a simplex optimization method of calculating cloud motion vectors (CMVs). The IoT network was successful in reliably measuring GHI but limited by the chosen communication modules. The simplex optimization method was found to be comparably accurate and marginally more stable in calculating CMVs when compared to the more commonly utilized Most Correlated Pair method.

Keywords: *Internet of Things, solar power, irradiance forecasting, distributed sensor network*

1. Introduction

Solar power output is directly related to either the observed ground horizontal irradiance (GHI) or direct normal irradiance (DNI). Solar power is often implemented in a hybrid system with a diesel generator to smooth power output across variable irradiance. Solar power output on days with full sun is easily modeled using a tool such as the PVLIB toolbox from Sandia National Laboratories (Stein et al., 2016) to predict maximum irradiance and subsequent solar power output from a system at any given time. Overcast days yield a fraction of the solar power output of clear days, but changes to instantaneous power output occur gradually and are easily mitigated. Days with intermittent cloud cover pose a challenge as the average power output can vary by 40% across a 15 minute window (Suri et al., 2014) and instantaneous power output can change by 80% within a 60 second window. To efficiently implement a solar-diesel power system without large, expensive energy storage it is necessary to accurately forecast short-term observed irradiance fluctuations caused by passing cloud shadows.

One form of forecasting observed irradiance involves calculating cloud motion vectors (CMVs) to predict when a cloud shadow will cross an observation point. The first methods for calculating CMVs were derived in the 1960s using satellite imagery for weather forecasting purposes (Menzel, 2001). Since then, work has been done to calculate CMVs with the application to irradiance forecasting using sky-facing cameras (Chow et al., 2011, 2015; Urquhart et al., 2015) and arrays of pyranometers (Aryaputera et al., 2015; Bosch et al., 2013; Yang et al., 2014). This project explores a low-cost Internet of Things (IoT) solution for solar irradiance forecasting using a wireless network of pyranometers. It also provides a method for detecting intermittent cloud cover that causes sharp power variability and presents an alternate numerical method for calculating CMVs.

2. Network Setup

2.1 Overview of Test Location

The sensor network utilized for this study was installed at the Methane Emission Technology Evaluation Center (METEC) located at the Foothills Campus of Colorado State University. Adjacent to the Rocky Mountains in northern Colorado, this area is prone to rapid changes in cloud cover and is therefore a great location to observe irradiance variability. Twelve nodes with uncalibrated pyranometers were placed along the METEC perimeter, one reference node with a calibrated pyranometer was placed near the center of the site, and a gateway node that connected perimeter nodes to the internet was placed in a building on the east side. All node locations can be seen in Figure 1. The nodes span 250 meters East-West and 150 meters North-South giving a maximum inter-node spacing of 270 meters.

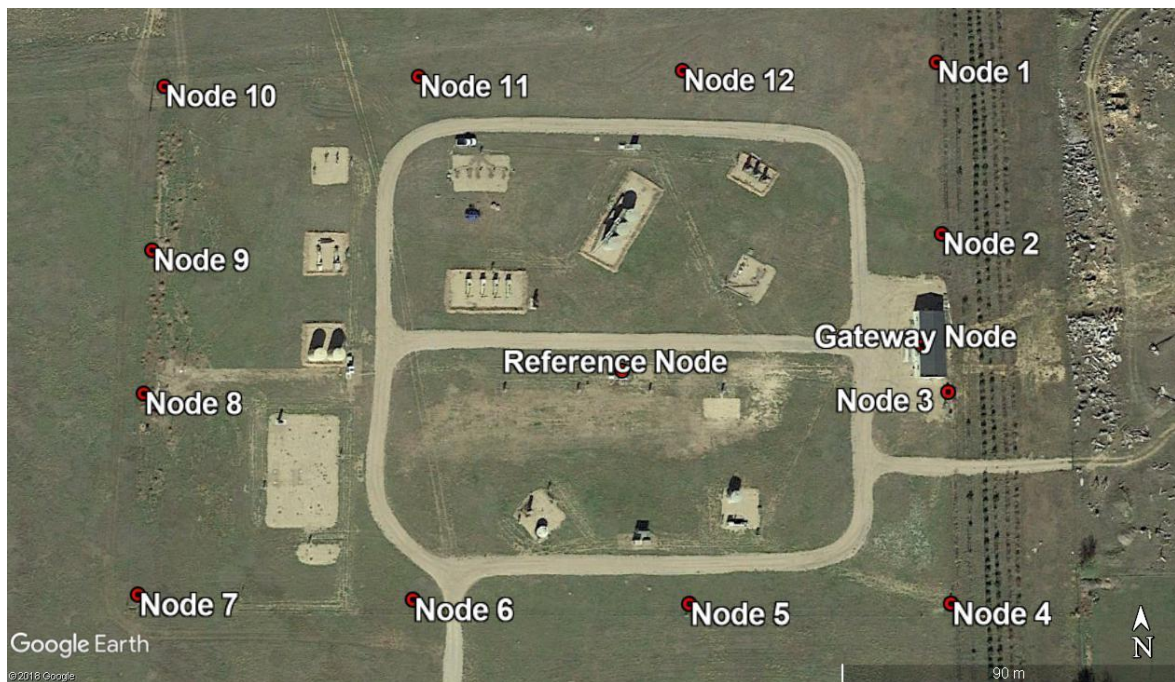


Figure 1: Sensor Node Locations

2.2 Hardware

Each of the perimeter nodes utilizes a STM Nucleo as the central processor. Voltage output from an uncalibrated photodetector pyranometer is measured using a 16-bit Analog-to-Digital Converter (ADC) while time and location information is provided by a GPS receiver. Readings are transmitted to the gateway node using an XBee 2.4 GHz radio module. Power is supplied by a 70Watt solar panel and 35 Amp-Hour battery that allows nodes to run for at least one week of full overcast and completely recharge in one day of full sun. The complete hardware of a perimeter node installed at METEC is shown in Figure 2.



Figure 2: Perimeter Node Hardware

The gateway node utilizes a Beaglebone Black as the central processor and an XBee 2.4 GHz radio module for communication with perimeter nodes. The gateway node was wired hard-wired to power and internet at METEC, but it could easily be connected to solar power and a cellular modem for deployment in remote locations. The reference node uses a similar setup to the gateway node, only replacing the XBee radio with a 16-bit ADC connected to a factory calibrated pyranometer.

The photodetector pyranometers fitted to all perimeter and reference nodes were built from kits purchased from the Institute for Earth Science Research and Education (David Brooks, 2007). Each photodetector pyranometer measures irradiance using a 470Ω resistor soldered across the terminals of a PDB-C139 photodetector. The photodetector is fitted inside a PVC tube covered with a Teflon disk to evenly diffuse light from a wide range of solar zenith angles. The reference node is fitted with a factory calibrated Kipp & Zonen SP Lite 2 pyranometer that was taken as GHI truth. Comparing the photodetector to the reference pyranometer demonstrated a very strong linear correlation. Irradiance readings from the photodetector and reference pyranometers were measured simultaneously at 10 Hz for 72 consecutive hours. Comparing the two sets of readings yielded a correlation coefficient, $\rho=0.9993$, and a coefficient of determination, $R^2=0.9985$, as seen in Figure 3.

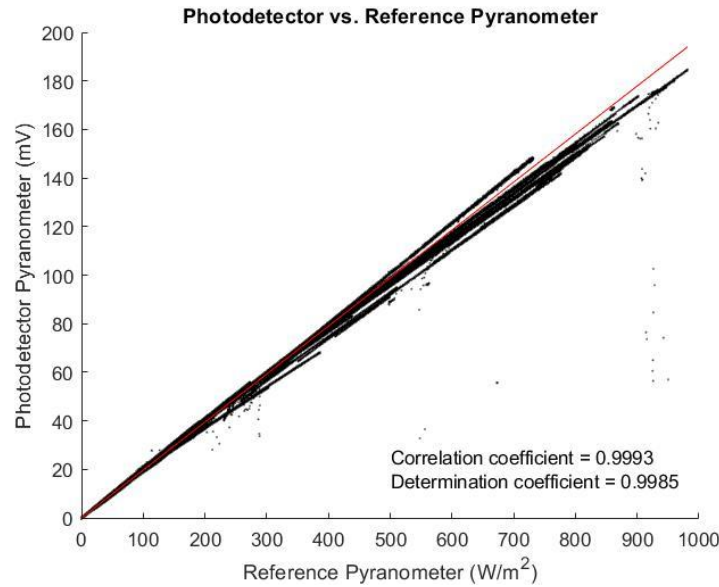


Figure 3: Photodetector Accuracy

3. Methods

This project compares two different CMV calculation methods. The first method used is the Most Correlated Pair (MCP) method as derived by Bosch et al. (Bosch et al., 2013). This method assumes that readings from two sensors are well correlated but yield the highest correlation coefficient when lagged by some non-zero amount in time. After calculating the time lag of maximum correlation for each pair of nodes, the pair of nodes with the highest correlation coefficient is assumed to be the most aligned with CMV direction. The azimuth between this most correlated pair of nodes is taken as the cloud direction azimuth and the speed is calculated by dividing the distance between the two nodes by the calculated time lag. Because this method has been well established, it is used as a benchmark comparison for the Simplex Cross-correlation Method (SCM).

SCM builds on the MCP method by making three assumptions about cloud shape and applying a simplex algorithm to further refine the CMV approximation. SCM uses the same three assumptions as the LCE method derived by Bosch et al. (Bosch et al., 2013), but applied to the entire array of pyranometers. It is assumed:

- (i) Linear cloud edge across the sensor array
- (ii) Constant CMV while passing over the sensor array
- (iii) Cloud shadow passes over all sensors

For time periods less than 1 hour, (ii) generally holds true. For slow GHI transitions caused by passing stratus clouds (i) and (iii) almost always hold true with sensor spacing $O(1 \text{ mile})$. For sharp GHI transitions caused by passing cumulus clouds (i) and (iii) usually hold true for all sensors if maximum inter-sensor spacing $O(100\text{m})$, and a subset of sensors located along the cloud's path for larger spacings.

3.1 Irradiance as a Function of Cloud Motion Vector

The CMV is modeled as a traveling planar edge with a direction azimuth α , edge azimuth β , and speed v . Taking any arbitrary pair of nodes N_i and N_j , line d_{ij} is drawn from N_i to N_j . Angle Θ is the azimuth angle of line d_{ij} . Given that a cloud edge crosses node N_i at time t_i and node N_j at time t_j , the time delta between the cloud edge crossing the two nodes Δt_{ij} is:

$$\Delta t_{ij} = t_j - t_i \tag{eq. 1}$$

This time delta can be calculated by tracing the point on the cloud edge C_i that passes directly over node N_i to its position when the cloud edge crosses node N_j . This creates line d'_{ij} that represents the true distance the cloud travels in time Δt_{ij} as shown in Figure 4 so that:

$$d'_{ij} = \Delta t_{ij} * v \tag{eq. 2}$$

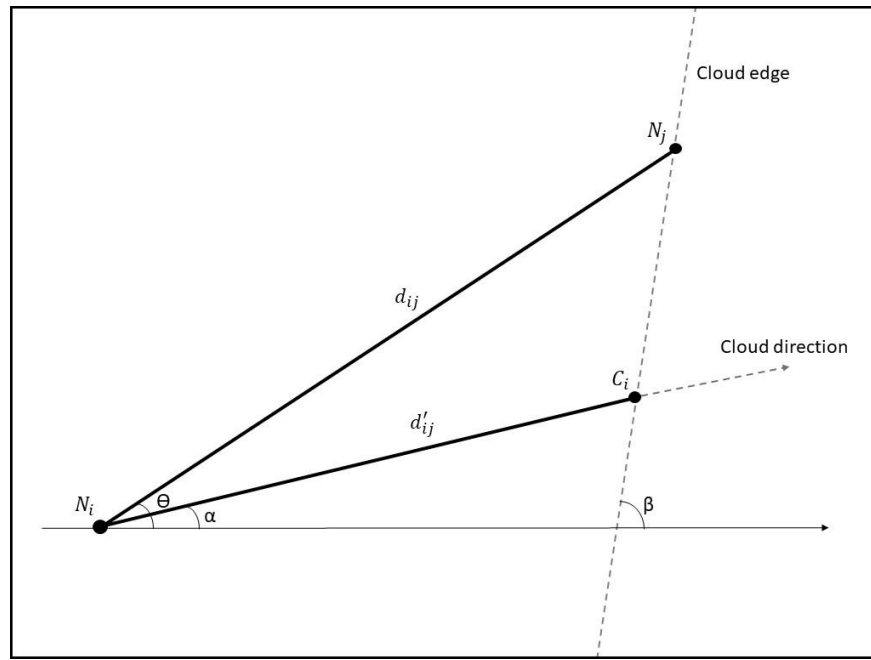


Figure 4: Cloud Crossing Geometry

The length of d'_{ij} can then be solved geometrically using a pair of right triangles such that:

$$d'_{ij} = d_{ij} [\cos(\theta_{ij} - \alpha) - \sin(\theta_{ij} - \alpha) \cot(\beta - \alpha)] \quad (\text{eq. 3})$$

In the case that CMV direction is parallel to the cloud edge (eq. 3) is undefined but assuming (iii) this case is impossible as the cloud edge doesn't cross any nodes. In case that CMV direction is perpendicular to the cloud edge, equation (3) can be simplified to:

$$d'_{ij} = d_{ij} \cos(\theta - \alpha) \quad (\text{eq. 4})$$

Combining (eq. 2) and (eq. 3) gives the analytical solution for the time delta Δt_{ij} between the cloud edge crossing nodes N_i and N_j :

$$\Delta t_{ij} = \frac{d_{ij} [\cos(\theta_{ij} - \alpha) - \sin(\theta_{ij} - \alpha) \cot(\beta - \alpha)]}{v} \quad (\text{eq. 5})$$

3.2 Cloud Motion Vector as a Function of Irradiance

A CMV is calculated from irradiance by comparing the matrix of measured time deltas $\Delta \mathbf{t}$ and the matrix of time deltas from an approximated CMV $\Delta \mathbf{t}'$ between every arbitrary pair of nodes. For each pair of nodes N_i and N_j an error measure of the CMV approximation e_{ij} is calculated as the squared difference between the measured and approximated time delta such that:

$$e_{ij} = \|\Delta t_{ij} - \Delta t'_{ij}\|^2 \quad (\text{eq. 6})$$

Taking the sum of the matrix of individual error measures yields a total error measure for the CMV approximation:

$$E = \sum_{i,j} \|\Delta t_{ij} - \Delta t'_{ij}\|^2 \quad (\text{eq. 7})$$

This total error measure can be expanded with (5) to create a CMV error function of variables α , β , and v :

$$E(\alpha, \beta, v) = \sum_{i,j} \left\| \Delta t_{ij} - \frac{d_{ij} [\cos(\theta_{ij} - \alpha) - \sin(\theta_{ij} - \alpha) \cot(\beta - \alpha)]}{v} \right\|^2 \quad (\text{eq. 8})$$

Backing out the CMV from this error function is now a tri-variate minimization problem. An initial CMV guess is found using the pair of nodes most aligned with the cloud direction. The pair of nodes with the largest time delta containing the first and last nodes the cloud shadow crossed is assumed to be most aligned with CMV direction. Taking the first node crossed as N_i and the last node crossed as N_j , the initial guess cloud

motion azimuth α_0 becomes the azimuth angle between the pair of nodes θ_{ij} . Cloud edge azimuth is predominantly orthogonal to the motion azimuth (Bosch et al., 2013), so β_0 is assumed to be perpendicular to α_0 . The initial guess speed v_0 is then found by dividing the distance between nodes d_{ij} by the measured time lag Δt_{ij} . With this initial guess CMV, the error function (8) is minimized using the Nelder-Mead downhill simplex algorithm (Nelder and Mead, 1965). Other algorithms were considered, but the unstable Jacobian and Hessian of the error function rules out any gradient or quadratic algorithms.

3.3 Quality Control

Each individual sensor is not synchronized to measure GHI simultaneously, so the data from all sensors is first resampled to exactly 10 Hz. The resampled time series values are found using linear interpolation. To remove daily trend information caused by the solar position, measured irradiance is divided by the local clear-sky index generated using the PVLIB toolbox from Sandia National Laboratories (Stein et al., 2016).

Before attempting to calculate CMVs across a given window, it must first be determined if any detectable cloud edges occurred in that time window. The measured irradiance is first down-sampled to a 10 second interval to ignore small changes between readings. The Manhattan distance for this window is found by summing the discrete derivative of this down-sampled irradiance sequence. If the Manhattan distance is greater than the average clear sky index across the window it can be assumed that at least one sharp transition has taken place. To ensure (iii) holds true, CMVs are only calculated when all nodes see at least one sharp transition. This can be seen in Figure 5 where CMVs are not calculated during overcast periods, periods with full sun, and when a shadow passes over only one node.

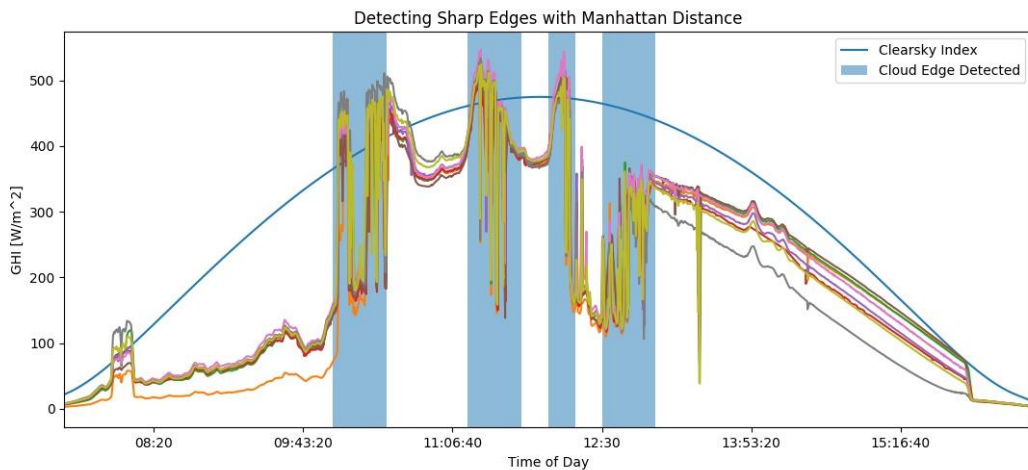


Figure 5: Manhattan Distance Example

Time deltas between nodes are calculated by maximizing the cross-correlation function between two sensors as defined by Bosch et al. (Bosch et al., 2013). The cross-correlation coefficient ρ_{ij} between the time series for two sensors is calculated at a range of time lags to create a function $\rho_{ij}(\Delta t)$. The time lag with the highest cross-correlation coefficient is taken as the time delta between the two nodes. To ensure (i) and (iii) hold true, poorly correlated sensor pairs must be removed. If the maximum cross-correlation coefficient for a pair of sensors $\rho_{ij} < 0.79$ the time delta between this pair is ignored when calculating CMVs.

3.4 Validation

Both methods were compared against validation data obtained by combining 449 MHz wind profiler observations from the NWS station located 51 kilometers Southeast in Platteville, CO (US Department of Commerce, n.d.) with ceilometer observations from the NOAA Automated Weather Observation Station (AWOS) located 20 kilometers Southeast at the Fort Collins-Loveland Regional Airport (National Centers for Environmental Information, n.d.). Combining observed cloud ceiling height with the wind profile speed and direction gives a reasonable estimate of CMVs passing over the test site. Because often multiple ceilings are reported with different heights and velocities, only times with one reported cloud ceiling are used for validation. The location of the AWOS ceilometer and Platteville wind profiler in comparison to METEC can be seen in Figure 6.

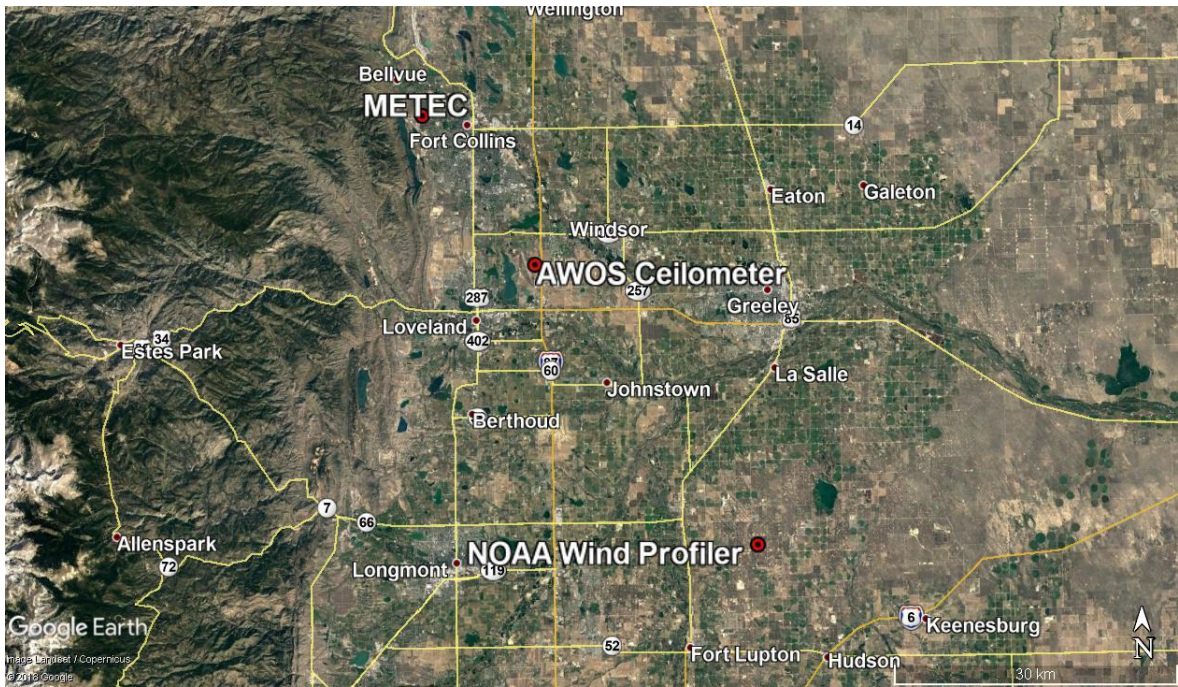


Figure 6: Validation Data Source Location

4. Results

CMVs were calculated across a rolling 15-minute window with a 5-minute step and any CMVs with velocity greater than 50 m/s are thrown out. The averaged CMVs were compared to validation data based on three metrics: Root-Mean Square Error (RMSE) (eq. 9), Mean Bias Error (MBE) (eq. 10), and the Pearson correlation coefficient of cloud speed and azimuth. Because cloud azimuth has no stable expected value over an extended period of time, MBE was only calculated for cloud speed.

$$RMSE = \sqrt{\frac{\sum_N (x_n - \bar{x}_n)^2}{N}} \tag{eq. 9}$$

$$MBE = \frac{\sum_N (x_n - \bar{x}_n)}{N} \tag{eq. 10}$$

Validation data was acquired for 10 months between September 2017 and June 2018. From this period, intermittent clouds were detected concurrently with reported validation data on 41 days yielding over 1200 CMV comparisons. Both CMV calculation methods performed comparatively well to validation data as shown in Figure 7. The calculated CMVs show a strong correlation with validation data in speed and azimuth.

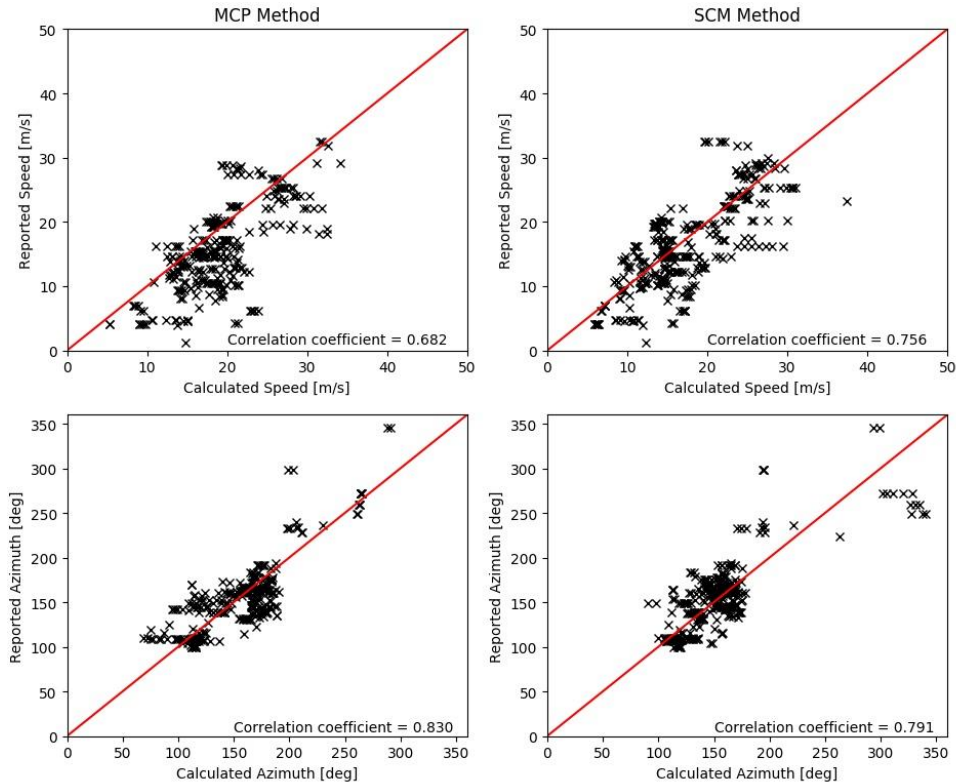


Figure 7: Calculated CMVs vs. Validation Data

The performance metrics of calculated CMVs against validation data is shown in Table 1. Both methods performed comparably in speed and azimuth RMSE, but the MCP method showed greater bias towards high speed measurements.

Table 1: Calculated CMV Performance vs. Validation Data

	MCP	SCM
Speed RMSE	4.54 m/s	3.54 m/s
Speed MBE	1.86 m/s	1.17 m/s
Speed Correlation Coefficient	0.682	0.756
Azimuth RMSE	17.7°	18.5°
Azimuth Correlation Coefficient	0.830	0.791

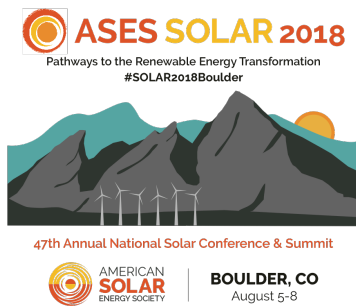
5. Conclusions

An IoT network of low-cost pyranometers was implemented at CSU’s METEC facility consisting of 12 uncalibrated photodiode pyranometers and one factory calibrated pyranometer. After comparing CMVs calculated using the SCM and MCP method it was found that the network could approximate CMVs with a RMSE of around 5 m/s and 24° compared to validation data acquired from a fusion of ceilometer and profiler data. This type of network shows great promise in predicting irradiance for use in hybrid solar-diesel power systems.

While 12 nodes with photodetector pyranometers were installed at METEC, reliability issues in the XBee radio modules used resulted in data from a maximum of seven nodes to be used in calculating any CMV. In future iterations of this project, a more reliable radio module will be used to increase network efficiency and ensure that all nodes provide a reliable data stream for calculating CMVs. The newly developed SCM shows promise in improving calculated CMV accuracy over existing methods but requires some adjustment to provide consistent, measurable improvement. Techniques of approximating CMVs for non-linear cloud edges and multiple cloud layers with different velocities may also be explored.

6. References

- Aryaputera, A.W., Yang, D., Zhao, L., Walsh, W.M., 2015. Very short-term irradiance forecasting at unobserved locations using spatio-temporal kriging. *Sol. Energy* 122, 1266–1278. <https://doi.org/10.1016/j.solener.2015.10.023>
- Bosch, J.L., Zheng, Y., Kleissl, J., 2013. Deriving cloud velocity from an array of solar radiation measurements. *Sol. Energy* 87, 196–203. <https://doi.org/10.1016/j.solener.2012.10.020>
- Brooks, D., 2007. Measuring Sunlight at Earth's Surface: Build Your Own Pyranometer [WWW Document]. *Inst. Earth Sci. Res. Educ.* URL <http://www.instesre.org/construction/pyranometer/pyranometer.htm> (accessed 6.12.18).
- Chow, C.W., Urquhart, B., Lave, M., Dominguez, A., Kleissl, J., Shields, J., Washom, B., 2011. Intra-hour forecasting with a total sky imager at the UC San Diego solar energy testbed. *Sol. Energy* 85, 2881–2893. <https://doi.org/10.1016/j.solener.2011.08.025>
- Chow, C.W., Belongie, S., Kleissl, J., 2015. Cloud motion and stability estimation for intra-hour solar forecasting. *Sol. Energy* 115, 645–655. <https://doi.org/10.1016/j.solener.2015.03.030>
- Menzel, W.P., 2001. Cloud tracking with satellite imagery: From the pioneering work of Ted Fujita to the present. *Bull. Am. Meteorol. Soc.* 82, 33–47.
- National Centers for Environmental Information, n.d. Automated Weather Observing System (AWOS) [WWW Document]. URL <https://www.ncdc.noaa.gov/data-access/land-based-station-data/land-based-datasets/automated-weather-observing-system-awos> (accessed 6.12.18).
- Nelder, J.A., Mead, R., 1965. A Simplex Method for Function Minimization. *Comput. J.* 7, 308–313. <https://doi.org/10.1093/comjnl/7.4.308>
- Stein, J.S., Holmgren, W.F., Forbess, J., Hansen, C.W., 2016. PVLIB: Open source photovoltaic performance modeling functions for Matlab and Python. *IEEE*, pp. 3425–3430. <https://doi.org/10.1109/PVSC.2016.7750303>
- Suri, M., Cebecauer, T., Skoczek, A., Marais, R., Mushwana, C., Reinecke, J., Meyer, R., 2014. Cloud cover impact on photovoltaic power production in South Africa. *Proc. SASEC*.
- Urquhart, B., Kurtz, B., Dahlin, E., Ghonima, M., Shields, J.E., Kleissl, J., 2015. Development of a sky imaging system for short-term solar power forecasting. *Atmospheric Meas. Tech.* 8, 875–890. <https://doi.org/10.5194/amt-8-875-2015>
- US Department of Commerce, N., n.d. PSD Wind Profiler Data [WWW Document]. URL https://www.esrl.noaa.gov/psd/data/obs/sites/view_site_details.php?siteID=pvl (accessed 6.12.18).
- Yang, D., Dong, Z., Reindl, T., Jirutitjaroen, P., Walsh, W.M., 2014. Solar irradiance forecasting using spatio-temporal empirical kriging and vector autoregressive models with parameter shrinkage. *Sol. Energy* 103, 550–562. <https://doi.org/10.1016/j.solener.2014.01.024>



Conference Proceedings

ASES National Solar Conference 2018

Boulder, Colorado August 5-8, 2018

SOLAR 2018: PROVIDING EMERGENCY POWER AND SURVIVING ON SOLAR Boulder, Colorado, USA

William R. Young, Jr. SunTree Consulting, Inc. Florida Renewable Energy Assn 612 Indian River Avenue Titusville, Florida, USA, 32796 Fl_byoung@hotmail.com

Susan Schleith Florida Solar Energy Center University of Central Florida 1679 Clearlake Road Cocoa, Florida, USA, 32799 susan@fsec.ucf.edu

ABSTRACT

Since Hurricane Hugo in 1989, solar has been used to provide electricity in disaster emergencies. Portable and consumer solar items powered lights, chargers, water pumps, radios and refrigerators.[1] What is notable is that historically, homes and businesses had utility interactive photovoltaic (PV) systems connected to the utility grid with battery storage. When buildings lost utility power, the PV/battery system provided power.

In 2000 that changed. Net metering practices were introduced and batteries were eliminated from many photovoltaic systems. In the aftermath of Hurricane Charlie in 2004, despite sunny skies many grid-tied PV homes were 'dead in the water', or shall we say, 'dead in the sunshine' without the ability to access their own PV systems' power. Advance mitigation is the key to energy resilience. Some PV designs are once again including battery storage, protecting the systems from disaster power outages. Auxiliary distribution panels are often added to the design to assure emergency power to essential or critical items.

From 2010 through 2014, the Florida Solar Energy Center, a research institute of the University of Central Florida, through the SunSmart Schools Emergency Shelter program, installed 118 utility-interactive (solar+storage) PV systems with batteries on schools throughout Florida.[2] These schools benefited from the onsite production of clean, silent solar electricity during daylight hours. If there happened to be a utility power disruption, these schools that doubled as emergency shelters were able to tap into battery power to keep essential items powered.

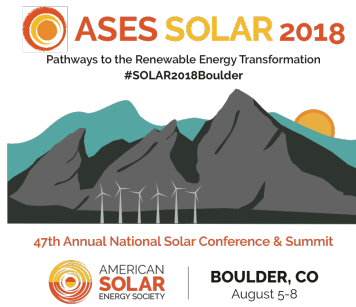
The schools were real time tested during the 2016- 2017 hurricane seasons. After hurricanes Matthew and Irma, requests were made of the schools for information about the performance of their PV systems. Information was gathered from staff and administration from the SunSmart Schools. Only 3 school systems sustained damage and were still functional.

This data provided noteworthy support for the importance of solar + storage and valuable 'lessons learned' on school staff awareness and education. Some of the schools were used as shelters by local emergency management. However, a major problem was full utilization, as school staff and emergency management personnel overlooked the full potential of this resource. In designating shelters, some schools with solar were forgotten and in those that were used, staff turnover and time elapsed since system installation created a gap in understanding of how to use what was available. Just providing a PV-powered shelter is not enough; training and periodic hands on exercises are needed to fully utilize this resource.

1. INTRODUCTION

Since the early 1800s, hurricanes have impacted the modern development of the eastern Atlantic coast. The U.S. has been affected by an increasing frequency of disasters, manmade and natural, as the number of declared disasters in this country has grown by over 400 percent since the 1950s. In 2015, the Federal Emergency Management Agency (FEMA) declared over 100 disasters, including fires, tornados, hurricanes and floods [4]. Disasters damage or destroy nature, resources, utilities, property, homes and businesses and

1



Conference Proceedings

ASES National Solar Conference 2018

Boulder, Colorado August 5-8, 2018

impact the local and regional economy. Many disasters damage thousands of residences and businesses, leaving them without functional water, sewage, communications, utilities, shelter and other life support services.

In 1960, Hurricane Donna damaged thousands of residences and businesses in Florida. This storm prompted a few home builders to offer hurricane-resistant houses as a marketing advantage over other builders. Houses were built with a lower rise angle on the roof, a secondary power panel for critical load items and an electrical outlet for safely connecting a gasoline generator. In 1989, a small group of solar companies provided portable solar electric (photovoltaic/PV) devices to survivors of Hurricane Hugo who were without power. At the time, the solar industry was producing consumer items and stand-alone photovoltaic (PV) systems with energy storage that met some of the basic needs for electricity.

Following Hurricane Andrew in 1992, building codes were strengthened to include hurricane tie-down straps and other structural practices [1]. Due to Andrew, the first organized effort was established to respond to hurricanes with solar equipment. The Florida Solar Energy Center, Florida Department of Transportation, U.S. Department of Energy, Sandia Laboratory, National Renewable Energy Laboratory and the solar industry provided various types of solar equipment for emergency power where the utility was out.

In 2004, Hurricanes Charley, Jeanne, Frances and Ivan, striking in succession, changed the way the United States prepares for disaster response and the way the Federal Emergency Management Agency (FEMA) responds to disasters. The solar industry and disaster organizations were learning how to coordinate with each other. Net metering had been established in 2000, prompting the elimination of storage/batteries from many PV systems as a cost saving measure. This proved to be a poor idea as many PV owners were left without power, thinking mistakenly their PV system would continue to operate after the utility went out.

Hurricane Sandy in 2012 was the deadliest and most destructive hurricane of the Atlantic hurricane season, and the second costliest hurricane in United States history with 285 fatalities and over 65 billion dollars in damages. Sandy was a category 3 hurricane with

winds over 115 mph, causing massive flooding and damage in 24 states and the Caribbean [4]. Over 9 million people lost electricity, generating massive consumer and business losses. Vastly increased electrical consumption and dependence in our high-tech world has changed the marketplace and put pressure on utilities to keep electricity flowing. Utilities are working to upgrade and modernize the grid through natural gas-fueled power plant conversions, deployment of distributed generation operations, using other energy sources, applying smart grid design and other efforts. Individual homeowners and businesses can apply new distributed energy concepts using renewables for resilient, sustainable power, limiting the effects of disasters and other power failure issues.

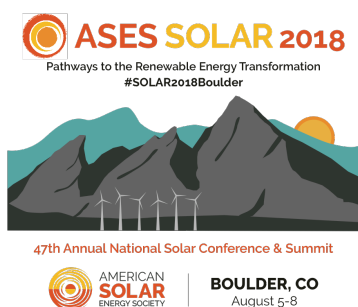
By 2014, 10 kWp PV arrays with storage had been installed on 118 schools in Florida designated as disaster shelters.[3] Identical designs were used to lower costs through volume purchase and to ensure ease of maintenance as shown in Fig. 1.

Figure 1. PV at Apollo Elementary.

Fortunately, solar is becoming more mainstream as an energy source and an effective emergency power option. In 2017, another fury of hurricanes (Harvey, Irma and Maria), classified as Category 4 storms, bore down on the Caribbean and the Atlantic coast. By this time, some home owners, businesses and utilities were equipped with solar installations. The solar industry and disaster organizations quickly responded with solar electric systems, replacing damaged utility equipment.

2. RESPONSE VERSUS MIGATATION

When a major disaster strikes, tens of thousands of disaster workers with thousands of tons of disaster



Conference Proceedings

ASES National Solar Conference 2018

Boulder, Colorado August 5-8, 2018

relief supplies will respond, costing millions of dollars. The Federal Emergency Management Agency (FEMA) has determined that mitigating the effects of a disaster in advance is more cost effective and humane than staging thousands of disaster response workers and deploying thousands of pieces of equipment. FEMA's cost-effective recommendation is to mitigate the effects of a disaster through disaster-resistant building design, adding the component of sustainable renewable energy for power. Utility power is becoming more resilient and reliable as renewable energy sources are being implemented into distributive generation applications. The solar industry is learning about use of solar for disaster recovery and disaster recovery organizations have learned about the value of solar applications.

The first known response to a disaster with solar powered equipment was with a small group of solar companies providing portable solar powered devices to survivors of Hurricane Hugo in 1989. Both in the Caribbean Islands and North Carolina, thousands of people were without electrical power for lights, medical equipment, communications, water and sanitation. These companies provided several hundred lanterns, battery chargers, radios, portable power units and trailer-mounted generators that were powered by solar energy. The items were portable PV consumer devices carried to tent camps, damaged homes, businesses and shelters. None of the items were designed for disaster relief, but the camping equipment and stand-alone systems sent were amenable to disaster relief applications.

Hurricane Andrew provided a proving ground for the limited number of consumer and stand-alone solar products available at that time. The Florida Department of Transportation (FDOT), the Florida Solar Energy Center (FSEC) and Sandia National Laboratory (SNL) teamed to assemble and provide PV power systems for the first organized disaster response effort using solar equipment. In the years that followed, SNL and the National Renewable Energy Laboratory (NREL), working with FSEC, funded the development of solar-powered equipment designed specifically for disaster recovery applications. Formal research was begun to define needs, collect data, develop and test equipment for use in disasters. Workshops were organized to transfer information to the solar industry and disaster response organizations.

More companies entered the market, providing consumer items and portable photovoltaic devices designed specifically for disaster relief efforts. Solar systems designed to power building and micro-grids are being created for use during power outages and as emergency power backup systems during disasters.

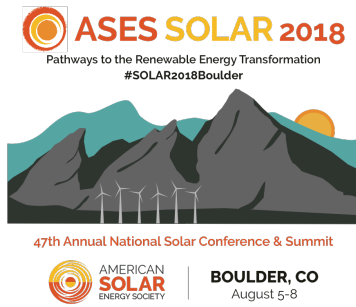
Designing and building fortified disaster resistant, zero energy renewable powered buildings is resilience, sustainable and cost effective in mitigating the effects of a disaster.

Fundamental to mitigating the effects of a disaster in the most cost effective manner requires preparation and planning well in advance of the event. With resilience and sustainability as the goal, a key requirement is the design and construction of fortified disaster-resistant, zero energy, renewable-powered buildings.

3. MAIN POWER GENERATION

The 21st century brought the development of renewable energy sources, including solar, wind, bio- mass and water. A modern grid with interconnected power plants over vast areas forms a Distributed Generation (DG) network as shown in Fig 2. As utilities grew from city power to regional to nationwide coverage, the distributed generation concept evolved through the integration of multiple energy sources into one complete package.[5] Inter-connecting diverse sources keeps the grid up even if one or more energy sources fails. Modern monitoring and control of the grid forms a smart grid that provides greater resilience and reliability than ever before.

Modern technology has not solved all energy security problems, as the utility grid experiences power outages and brownouts. Many people are familiar with the causes of down time of conventional utility power and the distribution grid from time to time. The electrical failure is seldom the central plant electrical generator. Sometimes the failure is caused by a system overload that



Conference Proceedings

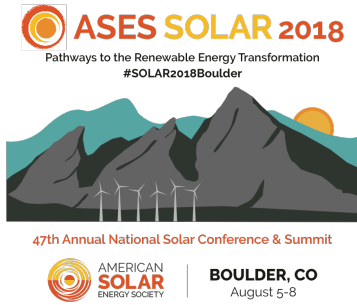
ASES National Solar Conference 2018
Boulder, Colorado August 5-8, 2018

requires parts of the system to be shut down selectively to prevent generator overload. Many times, a tree falls and breaks a power line, pole or other utility electrical equipment. However, the main cause is extreme weather events, like ice storms, tornados, lightning, wind storms, hurricanes and floods [9].

3

Commented [SS1]: I think I understand what you are trying to say but not sure it sounds exactly right.

I don't know that my attempt sounds right either.



Conference Proceedings

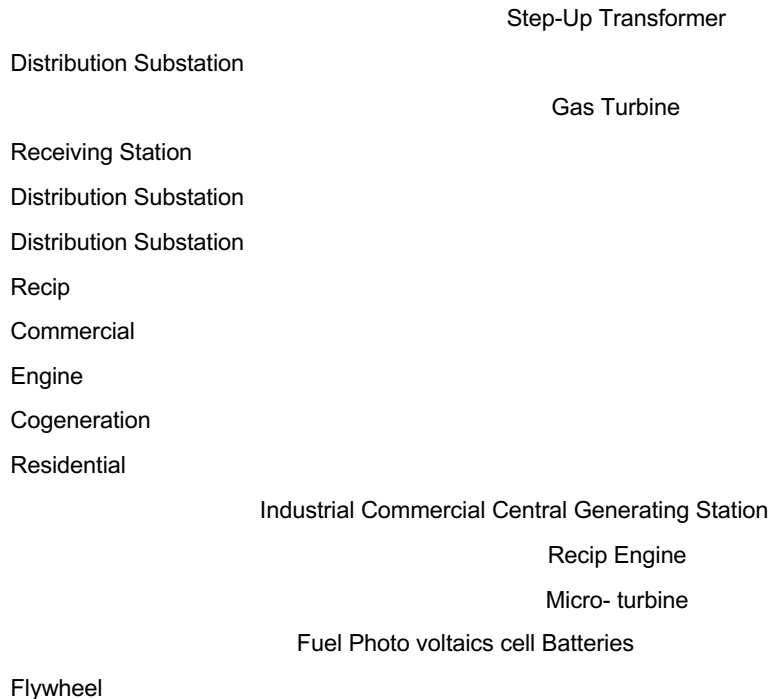
ASES National Solar Conference 2018
Boulder, Colorado August 5-8, 2018

Figure 2. Modern U.S. Utility Grid, (FSEC)

PV power systems for buildings are much larger than portable and consumer items. Alternating Current (AC) electricity generated by an inverter at 60 cycles sine utility waveform is commonly known as ‘home power’. A system on a building consists of a PV array, PV controller and inverter, as well as conventional electrical power equipment items such as fuses, circuit breakers, batteries, combiner boxes and power panels as shown in Fig 3.

Figure 3. Photovoltaic power system (FSEC).

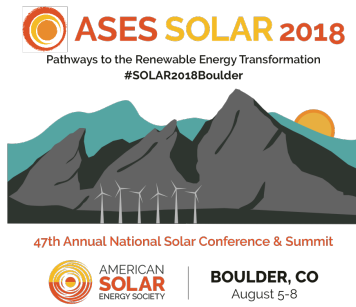
Stand-alone designs with storage (not connected to the utility grid) for remote locations were the precursors to modern PV systems [7]. Utility interactive inverter systems with storage were later developed, allowing PV to be a source of building power. Also, utility scale PV systems were deployed with arrays in the several megawatt range. For buildings, grid-tied inverter PV systems without storage came along after 2000 to save on the cost of batteries and problems related to batteries using the utility as the battery benefiting from net metering savings. In 2004, hurricane season came with four hurricanes crossing Florida, and thousands of people with grid-tied PV systems learned their system did not work without the grid interconnection, showing



the importance of site storage systems during utility power outages.

Photovoltaic and balance of system component technologies have advanced in efficiency, performance and reliability to rival anything that utilities can do, and in a more environmentally sound and cost- effective manner. Just last year (2017), an inverter manufacturer developed a grid-tied inverter that has a portion of its power provided without the grid.

Photovoltaic systems are subject to similar failure issues as utility power plants, such as extreme weather, fallen trees and loose



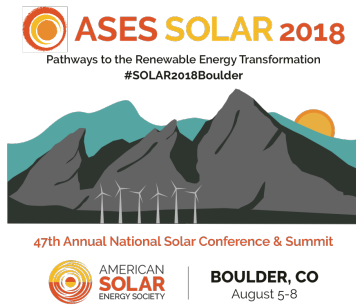
Conference Proceedings

ASES National Solar Conference 2018
Boulder, Colorado August 5-8, 2018

or corroded connections. PV systems are subject to battery failure, controller failure and module failure. Like any other equipment, a preventive maintenance program can keep these failures at a minimum. The benefits are that properly installed and maintained solar is reliable. Its fuel (sunlight) is free, renewable and produces no noise or pollution. Unlike a gasoline or diesel generator, a solar system poses no threat of carbon monoxide poisoning.

4. MITIGATING A DISASTER

Local, state and federal emergency management entities have a plan for response and recovery and work to restore the community to a point where it can rebuild itself. The most critical time is the first 72 hours after a disaster, when survivors are fending for themselves until help arrives. This is why people should already have a disaster plan and own a disaster kit, as help cannot get to survivors until first responders evaluate needs and can move into place. Emergency management encourages people



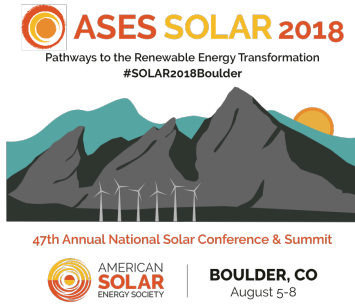
Conference Proceedings

ASES National Solar Conference 2018
Boulder, Colorado August 5-8, 2018

to assemble a disaster kit that includes water, food and first aid items. Typically, it takes about 3 days to 3 weeks to respond to a disaster and at least 3 years for people to recover, rebuild and resume their lives. [5]

Another way to reduce disaster-related damage and financial loss is by creating buildings that are truly disaster-resistant, energy efficient as possible and powered with renewable energy; then, truly sustainable homes and businesses can be realized. The Institute for Business and Home Safety (IBHS) has a Fortified Building Program with standards beyond normal building safety codes with 3 levels of design for creating stronger, safer buildings. DOE has a Zero

4



Conference Proceedings

ASES National Solar Conference 2018

Boulder, Colorado August 5-8, 2018

Energy Home Program, where the building produces as much energy as it consumes for a very energy-efficient building design. The ultimate goal is to combine the two programs for structurally sound buildings that provide sustainable operational use before and after a disaster. Renewable energy sources, such as solar thermal, photovoltaic, wind and biomass are sustainable, where fossil fuels are not and will one day be exhausted.

Homeowners and business leaders should evaluate their energy needs and operational activities. This involves identifying critical energy needs and incorporating the concept of critical operations power supply design into a home or commercial building. During a power outage, a homeowner may want to have electricity for a lamp, a refrigerator and a radio. A business may need a few lights for customer safety and a cash register to complete sales transactions. Most people would consider these items critical to maintaining home or business operations and personal lifestyle until utility power is restored. [7]

Essential needs can be powered through a backup power source and can be connected through a subpanel to the renewable energy source and the main utility power panel. When the utility power is operational, essential items are powered as usual; during a power outage, the backup energy source powers items through an essential/critical subpanel. This configuration can be designed and operated like an uninterruptable power supply (UPS) to ensure essential/critical items are always powered. This scenario works for bi-modal inverter designs, but not grid-tied only configurations. During normal times, utility interactive PV power can provide excess energy to decrease electricity bills.[7] Of course, stand-alone PV systems not connected to the utility grid are already properly configured for effective disaster operation, as the load and supply are matched. Therefore, multiple PV system configurations can be used in a distributed generation configuration. One system powers the critical load, one is grid-tied for HVAC and one with storage for other important load uses in a demand-side management operation based on the importance of maintaining operational functionality of the energy need. Some inverter systems are smart enough to do load shedding and perform priority loading to maximize energy use. Many of these applications have dual use, adding to their financial benefit.

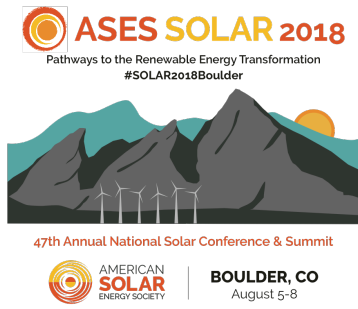
5. SOLAR FOR SCHOOLS

The DOE had an established Solar for Schools Program and the Florida Solar Energy Center joined in 2003. The Florida program began with funding from the Florida Energy Office (FEO) to install photovoltaic systems on selected schools. The program was initially designed as a way to raise awareness and to provide experience and understanding of photovoltaic technology to students, teachers and the general public. Some of the math and science requirements of the Florida Sunshine State Standards were also met by this educational effort.

The educational component of the program included professional development (PD) for teachers, free solar curriculum and a kit of materials not typically found in the classroom. The curriculum activities and kit provided opportunities for hands-on, minds on learning through the theme of solar technology, which also tied together science, technology, engineering and mathematics (STEM). The PD workshops immersed the teachers into the activities using the kit of materials, which they would then use at their school with their students.

Initially, 47 schools received grid-tied PV systems designed with a 1 to 6 kW array operating as an educational demonstration application.[2] By 2005, the program was renamed SunSmart Schools and the hurricane season of 2004 led to the expansion of the program to include larger PV systems with storage to be installed on schools designated as emergency shelters. In 2008, Middleton High School in Tampa was the first school to receive a bi-modal 10 kW system with battery storage. The system was installed on the shelter part of the school as a viable application for use during power outages and disasters. This was an example of a real-life application that generated power during normal times as well as during and following emergencies when utility power was unavailable.

In 2010, FSEC received a federal grant with matching state and utility funds which provided bi-modal PV systems to 118 schools

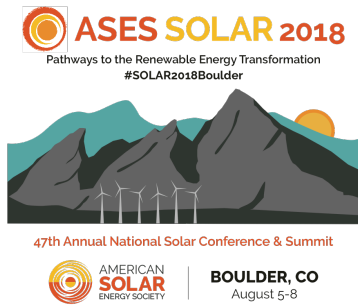


Conference Proceedings

ASES National Solar Conference 2018
Boulder, Colorado August 5-8, 2018

designated as emergency shelters and was renamed SunSmart Schools Emergency Shelter (SSES) program. Of the 67 counties in Florida, 47 counties participated in the

5



Conference Proceedings

ASES National Solar Conference 2018
Boulder, Colorado August 5-8, 2018

program, covering most of the state area and coast line, as shown in Fig. 4.

Figure 4. Florida Map school locations.

Each school participated in a selection process involving several steps: application, external review, site inspection, identification of critical loads and signing of a School Agreement. Schools that applied had to meet minimum criteria that included their status as a shelter, local demographics, the school's energy education plan and level of commitment to the project. Because the PV systems became the property of the schools once the installations were completed, each school was required to sign a "School Agreement" specifying ongoing expectations. The final location of the PV system was determined based on physical site issues. The first consideration was whether there was an area large enough for a ground-mounted array of this size. The school had to agree to install an IT port for the data monitoring system, send two teachers to attend a professional development workshop where they would become familiar with their PV system, participate in solar lessons, and receive a kit and solar curriculum to use in their classroom, and allow at least one facilities manager to participate in system maintenance training. It was also expected that each school would incorporate solar energy education into their school curriculum.

6. PV EMERGENCY SHELTER

These new emergency shelter systems were designed as uninterruptable power supplies (UPS) to power critical loads in the Enhanced Hurricane Protected Area (EHPA) shelter part of the school. The PV systems for this program were designed with 10 kWp

photovoltaic array and battery in a bi-model inverter configuration as an emergency power systems [4].

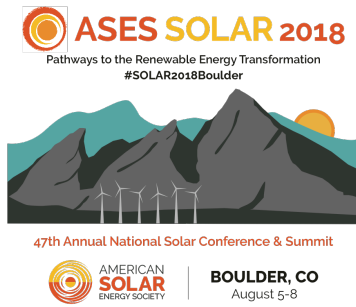
During normal time the new PV system reduces the school's electric utility bill as the initial SunSmart program did. This new program also provides a PV system designed for powering the shelter part of the school as an emergency backup system to energize essential items such as room lights, outlets for medical equipment, communication and operational computers used in a shelter in an emergency, as shown in Fig 5. The load was minimized to be able to be powered by the 10kW PV array/battery system. Each school that is a shelter has a different part of the facility dedicated to the shelter operation, such as a gymnasium, cafeteria, or a set of classrooms. The essential-critical loads of the designated area were wired to a separate critical load panel installed and wired to the general buildings load panel. During normal times the PV and utility power feeds all of the loads of the building as a utility interactive operation with net metering, but during utility outage the PV-battery supplies the power to the essential-critical loads through the added critical load panel.

Figure 5. Essential school loads and supply. (FSEC)

7. DISASTER IMPACTED SCHOOLS

The SunSmart Emergency Shelter program provides a viable, real-life PV emergency power design for any disaster application. As mentioned above, 47 counties participated in the program, covering most of the state of Florida. A hurricane crossing the state could impact any one of these schools.

In 2016, Hurricane Matthew caused no damage to any of the schools. Hurricane Irma in 2017 did present



Conference Proceedings

ASES National Solar Conference 2018

Boulder, Colorado August 5-8, 2018

issues to some schools. Of the 118 shelter schools, 77 closed due to the threat of the hurricane. Of the 41 open, 13 did not lose power. The longest period a shelter was open was 56 hours. Several schools had fossil fuel generators that mechanically failed and others ran out of fuel. Three PV arrays were damaged by debris hitting the array.

None of the damage stopped PV arrays from working, as single modules were damaged. For example, at the Apollo Elementary shelter, damage was to the top glass cover and broken cells as shown in Fig 6. The array was wired in 14 strings of 3 modules, so when a module was broken only one string was out, causing only a loss of less than 10 percent of array production. People entered the shelters the day before the storm arrived and stayed the day after until the 'all clear' to go home. A significant storm's heaviest wind and rain usually lasts 2 days, so designing for 2 to 3 days of autonomy is enough, considering the utility power should be there for half that time before going out. The design goal was to power single phase loads, such as lights, wall outlets and electronic communication equipment. A 3-phase inverter design with loads across each phase limits power losses across the loads.

Figure 6. Damaged module, Apollo Elementary

Several shelters had amateur radio operators providing emergency communication. Knowing the news through AM-FM portable radios and television was a big help to everyone. Charging phones and flashlights was appreciated by all, but not as much as having hot coffee! Special needs people with medical life support equipment were able to use a nebulizer, an oxygen concentrator and a G-tube feeding machine. One shelter was used for special needs people and one for pets. All together there were about 1700 people staying in the shelters and about 500 pets.

PV systems as small as 10 kWp can benefit the utility, the school shelter, home and business customers during a disaster. PV with storage with utility interactive with storage larger than 20 kWp PV would provide more stability and cost benefits to all to school shelters and business.

8. SSES PROGRAM NEXT STEPS

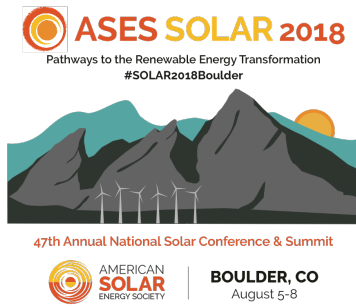
From educational and operational perspectives, the SunSmart Emergency Shelter program needs to address lessons learned more broadly. In hindsight, some new school staff had heard there was a solar installation at their school, but did not know how it worked and what it could do. Maintenance issues with the operation of the PV systems should have been addressed so systems would be fully functional. School staff changes over time should be tracked. Initial training and refresher training for school staff and partner disaster organization personnel could be conducted annually. SunSmart Emergency Shelter Schools with STEM, Technology, Environmental or other such clubs could integrate awareness and understanding of their PV system as part of their club's mission. May is Hurricane Awareness Month and the SSES should be an active part of that.

A program enhancement to check, update and educate people and equipment periodically needs to be implemented to better serve the educational goal of the program and better provide emergency power support.

9. CONCLUSION

Disasters, man-made or natural, can be very destructive, leaving thousands of people without shelter, power, water, sanitation and communications. Advance mitigation is the key to energy resilience. Why deploy thousands of disaster workers and tons of disaster relief supplies when disaster-resistant, renewable energy-powered buildings can mitigate the effects of a disaster, saving energy costs during normal times?

Utilities have made advances in becoming more resilient and sustainable. Distributed generation has played an important part by providing more sources of



Conference Proceedings

ASES National Solar Conference 2018

Boulder, Colorado August 5-8, 2018

energy to the grid. Integrating all available sources together with smart grid technology greatly enhances the resilience of the modern grid. Renewable energy applications, such as roof-top solar, micro-grids and community solar using photovoltaic and wind have done their part to make the grid more resilient and sustainable. New storage technologies being developed will increase the benefit of distributed generation applications. Individual homeowners and business owners using renewables benefit from applying distributed generation concepts to their own buildings' energy supplies. Why not take advantage of the sun's benefit as an endless source of free energy, every day and during disasters, wherever the need?

Modern codes and construction practices have changed evolved to provide for more resilient buildings. Integrating multiple photovoltaic system designs can maximize the resilience of a home or business power system. Dedicating a particular PV design to an energy need functionally will provide greater energy resilience and lower overall operating costs. If utilities' hardware and systems are designed with fault tolerance in mind using palatable energy sources, disaster resistance through renewable resources will be achieved. Proper design withstands disaster forces.[8]

The SunSmart Emergency Shelter program has shown the viability of PV utility-interactive with batteries (solar+storage) effectively integrated into design and operation of a building will lower costs and operate effectively as emergency power in a disaster. Schools and FSEC need to maintain contact; education of school personnel will be critical to maintaining functionality of PV emergency power systems.

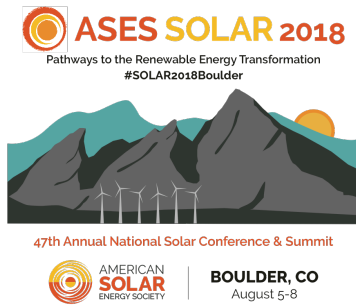
The lower cost of utility-interactive photovoltaics combined with the reliability of the 24-hour operation of photovoltaic battery systems will soon become mainstream. School shelter emergency power should be a fault tolerance PV design. Photovoltaic systems provide a free source of energy from the sun and an economic benefit to everyone during normal times as well as during power outages and following unexpected disasters.

10. ACKNOWLEDGEMENTS

I would like to thank FSEC for many opportunities to gain solar experience, Susan Schleith, FSEC, SunSmart Program Manager, Penny Hall, FSEC, and my wife, Betty Young, for their assistance in completing this paper.

11. REFERENCES

- (1) W. R. Young, "Photovoltaic Applications for Disaster Relief", Florida Solar Energy Center, Cocoa, Florida, FSEC-849-95-C, November 1995, and February 2006.
- (2) Young, William, and Susan Schleith, Florida's Emergency Shelters Go Solar, ASES Solar 2007 Conference, American Solar Energy Society, Cleveland, Ohio, July 2007.
- (3) Young, William, Summary and Performance of Florida's SunSmart Emergency Program, ASES Solar 2013 Conference, American Solar Energy Society, Baltimore, Maryland, July 2013.
- (4) Fact sheets and data, Status Summary, Federal Emergency Management Agency, [online] <http://www.fema.gov/fact-sheets..>
- (5) Hurricane Sandy, Wikipedia, [online], http://en.wikipedia.org/wiki/Hurricane_Sandy
- (6) U.G. Knight, Power Systems in Emergencies: From Contingency Planning to Crisis Management, John Wiley & Son, London, U.K. 2001.



Conference Proceedings

ASES National Solar Conference 2018
Boulder, Colorado August 5-8, 2018

(7) Gilpin, Lyndsey, After the Hurricane, Solar Kept

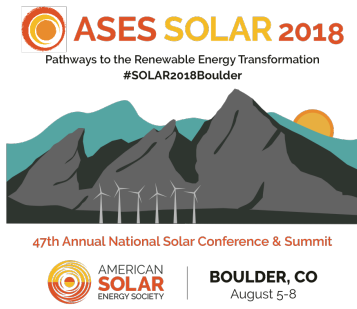
Florida Homes and a City's Traffic Lights Running, September 15, 2017, <http://insideclimatenews.com/article/afterhurricane>

(8) Hotchkiss, Eliza, NREL, October 24, 2017, How is

Solar PV Performing in Hurricane struck Locations?, <http://nrel.com/technical-assistance/bolg/post/pvhurricanestruck>

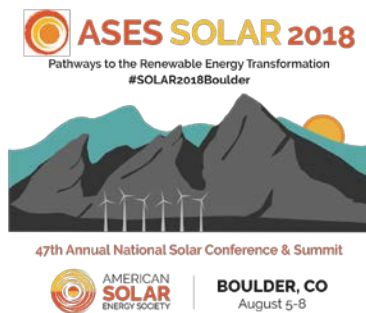
(9) Kryzanowski, Tony, Solar Power Project Weathers

the Storm, enerG, Alternative Sources Magazine, March 2018,



Conference Proceedings

ASES National Solar Conference 2018
Boulder, Colorado August 5-8, 2018



Conference Proceedings

ASES National Solar Conference 2018

Boulder, Colorado August 5-8, 2018

Simulated Performance of a Photovoltaic Thermal Heat Pump System for Single-family Houses

Amirahmad Zare, Weimin Wang, Nenad Sarunac

University of North Carolina at Charlotte, Charlotte, NC

azare@uncc.edu

Abstract

This paper presents the design, operation and performance simulation of a hybrid photovoltaic/thermal (PV/T) heat pump system targeted for single-family houses. The proposed system consists of PV/T collectors, a water-to-water heat pump, an outdoor swimming pool, pumps and a forced air system for space conditioning. Using water as the heat transfer medium, the PV/T collectors are used to collect solar energy in the heating season and to dissipate energy to the sky via radiative cooling in the cooling season. The heated or cooled water from PV/T collectors can be 1) used as the heat source/sink of the water-to-water heat pump, which then provides hot or cold water to the water coils in the air handler for space conditioning; or 2) used to charge the swimming pool, which acts as the thermal storage and connects to the heat pump as needed on the source side. There are a total of six different operational modes, the operation of which depends on the space air temperature, the PV/T collector temperature, and the swimming pool water temperature. The system performance was simulated with TRNSYS software. Preliminary results showed that the proposed system saved 30% annual energy consumption relative to a reference air-source heat pump system.

Keywords: *PV/T, Heat Pump, Radiative Cooling, Energy Saving*

1. Introduction

Buildings consume about 40% of the total primary energy in the U.S., more than a half attribute to the residential sector (EIA 2018). Regarding energy end uses, space heating and cooling accounts for 48% of the energy consumption in residential buildings (EIA 2013). Therefore, it is important to develop innovative space heating and cooling systems that can minimize energy consumption from nonrenewable resources. In this regard, a solar assisted heat pump system that combines photovoltaic/thermal (PV/T) collectors and a water-to-water heat pump (HP) has the advantage of efficiency improvement for both components. Such hybrid systems were explored by different research groups as potential efficient design solutions for energy savings in residential buildings (Nejma et al. 2013). In literature, most PV/T-HP studies focus on using PV/T collectors only as the heat source for heat pump's heating generation (Hailu et al. 2015, Li et al. 2015). As noted by Eicker and Dalibard (2011) and Bourdakos et al. (2016), PV/T collectors can also be used for radiative cooling, a process in which long wave radiation is used to transfer heat from a hotter body to a cooler body, by taking advantage of very cold outer space at night to achieve below-ambient temperatures for the PV/T collectors. However, there is only very limited work on investigation of both the heating and

cooling potential of PV/T collectors (Palla et al. 2014, Fiorentini et al. 2015).

This paper intends to add some knowledge to the PV/T-HP systems by investigating the potential of using PV/T collectors as the heat source and sink of a HP when combined with an air-handling unit for space conditioning. The paper is organized as follows: The proposed PV/T-HP system and its operational modes are presented in Section 2, where the baseline system for performance comparison is also discussed. Then, the hypothetical house is described in Section 3. Section 4 covers TRNSYS simulation with a focus on TRNSYS Types for different components. Section 5 presents preliminary simulation results, which mainly include system operation analysis in selected days of different seasons (i.e., winter, summer, and shoulder seasons) and annual energy savings of the proposed system in comparison with the baseline system. The paper ends up with some conclusions and recommendations for future work.

2. Proposed PV/T-HP system and baseline descriptions

The proposed PV/T-HP system includes PV/T collectors, a water-to-water heat pump, an outdoor swimming pool, water circulation pumps, and an air handler that supplies conditioned air to the space for heating and cooling. The air system includes a cooling coil, a heating coil, and a fan as shown in Figure 1. PV/T collectors can be used to generate electricity and collect thermal energy. Because the paper has a focus on the thermal performance of the system, we do not consider PV/T collector's electricity generation in the current stage. In this system, the swimming pool functions as a massive thermal storage and the water-to-water heat pump provides hot water or cold water to the water coils for air conditioning. Water is used as the heat transfer medium to collect or dissipate thermal energy through the PV/T collectors. The heated (or cooled) water can be circulated to the heat pump or to the swimming pool. The source side of the heat pump can connect to the PV/T collectors or the swimming pool while the load side connects to the water coils in the air handler.

The reference system that is used for energy consumption comparisons and energy savings potential of the proposed system is a split air-source heat pump system.

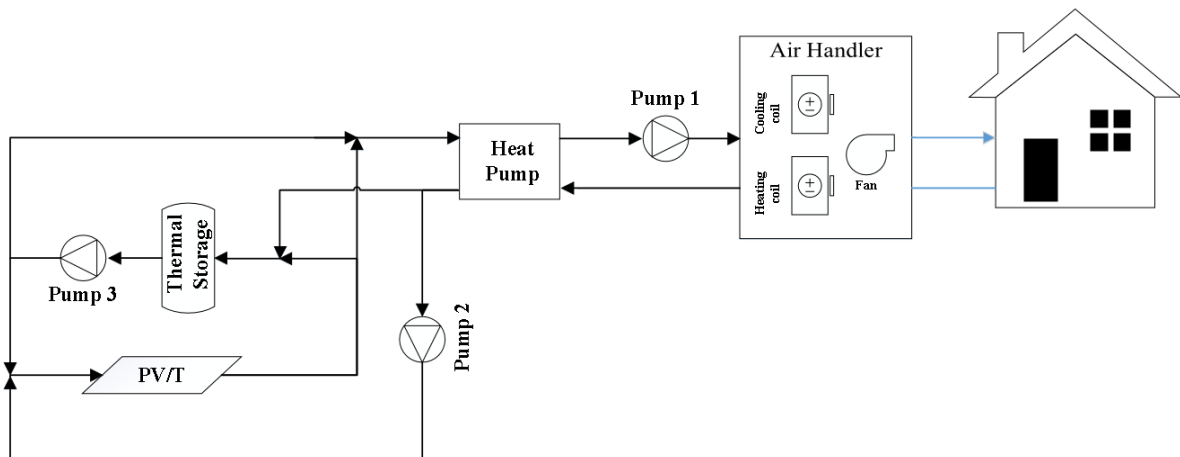


Fig. 1: Schematic diagram of the proposed PV/T-HP system

Six modes are considered for the proposed system operation. Major parameters used to determine the operating mode include space temperature, the PV/T collector temperature, and the pool water temperature. These six modes and their underlying rules are mainly from the 2017 Innovative Energy Project awarded by the Association of Energy Engineers (<https://www.sundrumsolar.com/>). Some simplifications were made to exclude the domestic hot water heating and backup space heating modes. Table 1 summarizes the system operational modes and the associated control strategies.

These six operating modes are divided into heating modes (Mode 1, 2, and 3) and cooling modes (Mode 4, 5, and 6). In Mode 1 (PV/T-HP for heating), water flows from the PV/T collector to the source side of the heat pump; the heat pump runs to provide hot water to the heating coil of the air handler; and the fan in the air handler runs to supply heated air to the house. In Mode 2 (Pool-HP for heating), the source side of the heat

pump is connected to the pool and the rest of connections are similar to Mode 1. In Mode 3 (Pool water heating with PV/T), the water flows through the PV/T collector to heat up the pool water. Mode 4 (PV/T-HP for cooling) operation is analogous to Mode 1 except that the heat pump runs for cooling and provides cold water to the cooling coil of the air handler. This mode operates only at night. In Mode 5 (Pool-HP for cooling), the system operates similarly as Mode 2 except that the heat pump runs for cooling and provides cold water to the cooling coil of the air handler. Mode 6 (pool water cooling with PV/T) operates similarly to Mode 3 except for the pool water is cooled by the water that goes through the PV/T collector at night. Modes 3 and 6 are seasonally active: Mode 3 operates in the winter and shoulder seasons (Oct. 1 to May 31) and Mode 6 operates only in the summer season (Jun. 1 to Sep. 30). In contrast, all other four modes may operate throughout the entire year according to the space thermostat signals. More details about the modes of operation can be found in the authors' previous work (Zare and Wang 2018).

Tab. 1: Operational mode description and control strategy

Operating mode	description	Thermostat signal	Mode activation condition	Yearly time of operation	Daily time of operation
Mode 1	PV/T-HP for heating	Heating on Cooling off	$T_{\text{collector}} > 5.6^{\circ}\text{C}$	All year	6 am to 10 pm
Mode 2	Pool-HP for heating	Heating on Cooling off	$T_{\text{collector}} < 5.6^{\circ}\text{C}$ $T_{\text{pool}} > 1.7^{\circ}\text{C}$	All year	All day
Mode 3	Pool water heating with PV/T	Heating off Cooling off	$T_{\text{collector}} > T_{\text{pool}}$	Oct. 1 to May 31	6 am to 10 pm
Mode 4	PV/T-HP for cooling	Heating off Cooling on	$T_{\text{collector}} < 32.2^{\circ}\text{C}$	All year	10 pm to 6 am
Mode 5	Pool-HP for cooling	Heating off Cooling on	$T_{\text{collector}} > 32.2^{\circ}\text{C}$ at night and no conditions during the day	All year	All day
Mode 6	pool water cooling with PV/T	Heating off Cooling off	$T_{\text{collector}} < T_{\text{pool}}$	Jun 1 to Sep. 30	10 pm to 6 am

In order to avoid mode oscillations, temperature deadbands are introduced to each mode. In this work, the upper and lower deadbands, which are adapted from the 2017 Innovative Energy Project, are set to 5°C and 2°C respectively. Let's use Mode 1 as an example to explain the application of deadbands. Table 1 shows that Mode 1 is activated when the thermostat calls for heating and the PV/T collector temperature is higher than 5.6°C prior to the use of deadbands. After the introduction of deadbands, conditions for activating Mode 1 becomes the thermostat calls for heating and the PV/T collector temperature is higher than 10.6°C (i.e., 5.6°C plus the upper deadband of 5°C). Once initiated, Mode 1 continues as long as the thermostat heating signal is on and the PV/T collector temperature is above 7.6°C (i.e., 5.6°C plus the lower deadband of 2°C). Once the collector temperature falls below 7.6°C , Mode 1 turns off and the PV/T collector temperature needs to reach 10.6°C to reactivate Mode 1. Similarly, temperature deadbands are used in all other modes whenever there is a temperature comparison.

3. House description

The energy performance of the PV/T-HP system was investigated for a hypothetical single-family house in Baltimore, MD. The house has one floor with a total area of 200 m^2 , a rectangular shape with an aspect ratio of 0.86, a flat roof with a floor-to-ceiling height of 2.44 m. Slab-on-grade floor and wood-frame constructions are assumed. The window area on each façade is 2 m^2 . The house has a 100-m^3 swimming pool. Located on the roof, PVT collector is south-oriented and has a slope of 45° and an area of 39 m^2 . Table 2 lists the thermal performance of exterior building envelope that satisfies the residential code requirement (IECC 2006).

Tab. 2: Thermal performance of exterior building envelope

Building Envelope	Thermal Performance
Roof	U factor=0.170 W/m ² K
Ground Floor	R value=1.942 m ² K/W
Exterior Walls	U factor =0.465 W/m ² K
Windows	U factor =1.69 W/m ² K SHGC=0.66

4. TRNSYS simulation

The PVT-HP system, the reference system, and the house were modeled and simulated using TRNSYS software. TRNSYS has available library of validated built-in components for renewable energy systems in buildings and can report and integrate parameters like power, mass flow, and temperature over the desired time frame.

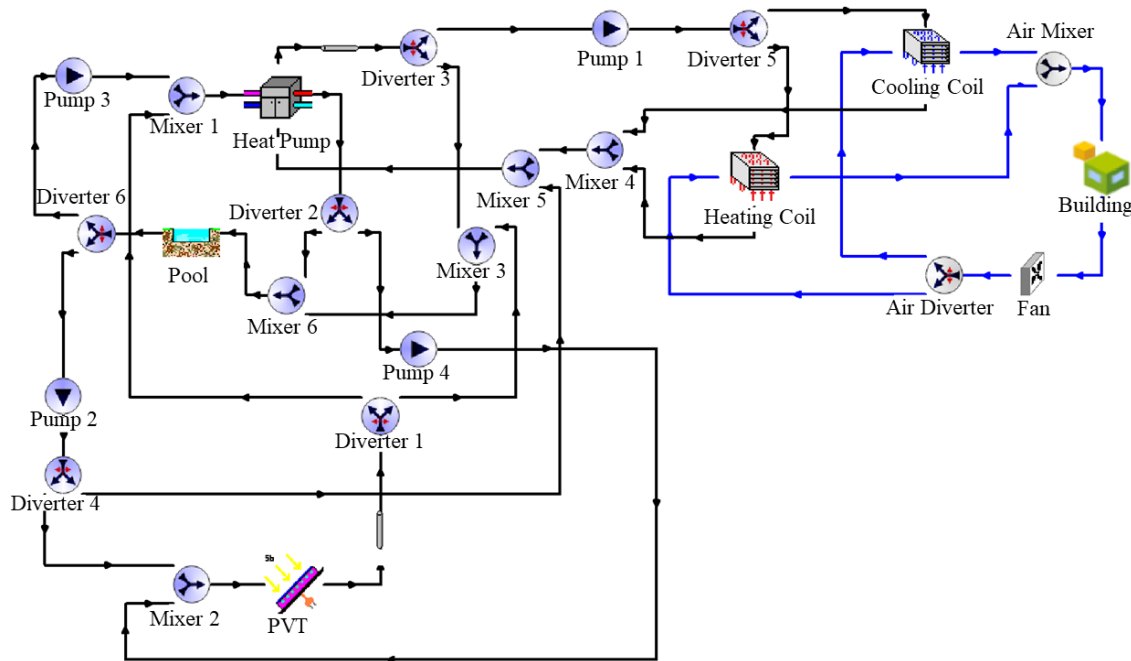


Fig. 2: TRNSYS model

Figure 2 shows the model developed for the proposed PV/T-HP system in TRNSYS. In this figure, water loops are drawn in black while air loops are drawn in blue. Each mode requires different path for the water and air loops. The path of water and air flows are defined by the diverters' control signal and each loops operation is controlled by the pumps' and fan's power control signal. It should be noted that a new TRNSYS type was developed for controlling the system's operation. This type recognizes the operating mode based on the space air temperature, the PV/T collector temperature, and the swimming pool water temperature and then provides the control signal to all of diverters, pumps, fan, and heat pump based on the mode of operation.

The building model was first developed in Google Sketchup and subsequently imported into TRNSYS package tool, TRNBUILD, by using TRNSYS3d plugin. The house was modeled using Type 56 multi zone building. Type 166 thermostat was used to monitor the space air temperature with the heating set point of 21°C and a cooling set point of 26°C, each of which has a deadband of 2°C. An air change rate 10 at 50 Pa was assumed for the air infiltration. Internal heat gain was not modeled in this simulation study. Convective heat transfer coefficients of building envelope were calculated dynamically. Space heating and cooling loads were determined by pre-running the annual simulation of the house while keeping the space air temperature in the desired range. The peak heating and cooling loads were found to be 8700 W and 2500 W respectively, which were then used to size TRNSYS components including water-to-water heat pump, water coils and air-

source heat pump. Table 3 summarizes the major components, their corresponding TRNSYS Types, and their key parameter settings in the simulation. A 3-ton (10,500 W) commercial water-to-water heat pump product from Water Furnace was referred for the rated and part load water-to-water heat pump efficiency. The supply fan, used in both reference and proposed models, was selected to meet 0.5 w/cfm requirement per IECC (2006). The air flowrate was calculated to meet 11°C temperature difference across the coils. Air-source heat pump's cooling and heating efficiency were set to 14 SEER and 8.2 HSPF respectively based on the residential code requirements in 2013 (Amrane et al. 2010). The SEER and HSPF were converted to the simulation inputs using the approach by Wassmer and Brandemuehl (2006).

Tab. 3: TRNSYS components and their main parameters

Component	TRNSYS type	Main Parameters
PVT Collector (parameters from Xia (2017))	563	Area = 39 m ² Absorptivity = 0.9 Emissivity = 0.8 Absorber plate thickness = 0.002 m Thermal conductivity of the absorber = 51 W/m.K Number of water tubes = 150 Outer diameter of water tube = 0.02 m
Pool	344b	Volume = 100 m ³ Height = 1.8 m Area = 55.6 m ² Cover thickness = 0.005 m Cover emissivity = 0.6 Cover absorption coefficient = 0.6 Cover removed from May 1 to September 30
Water-to-water Heat Pump	927	Rated heating capacity = 10027 W Rated COP = 4.8 Rated cooling capacity = 5264 W Rated EER = 15.5 Btu/W.h Rated source and load flow rates = 1363 Kg/hr
Pump	114	Water flow rate = 1363 Kg/hr Rated power = 15 W
Fan	146	Air flow rate = 2570 m ³ /hr Rated power = 756 W total efficiency = 0.38 static pressure = 400 Pa
Heating Coil	140	Rated Total Heating Capacity = 10027 W
Cooling Coil	123	Rated Total Cooling Capacity = 5264 W Rated sensible heat ratio = 0.75
Air-source Heat Pump	119	Rated Heating capacity = 10027 W HSPF= 8.2 Btu/W.h (Rated COP = 3.4) Rated total cooling capacity = 5264 W Rated sensible heat ratio = 0.75 SEER= 14 Btu/W.h (Rated EER = 12 Btu/W.h)

5. Results and discussion

TRNSYS simulations of the baseline and proposed systems were performed using the one-minute time step and the typical meteorological year weather data of Baltimore, MD. In the first subsection, the proposed system operation (mode changes based on the main parameter temperatures) is verified for three representative days in winter, summer and shoulder. For each representative day, ambient temperature, the space air temperature, the PV/T collector temperature, the swimming pool water temperature and the resulting active mode are presented to verify the system operation. In the second subsection, the energy performance of the proposed system is presented in terms of its monthly and annual energy savings in comparison with the baseline air-source heat pump system.

5.1. Representative day analysis

January 19, June 25, and October 10 are selected as the representative days of winter, summer, and shoulder respectively. Figures 3-5 show the system operation in the three selected days. Each of these figures show the space temperature in the house (T_{space}), the outdoor air temperature (T_{OA}), the PV/T collector temperature ($T_{\text{collector}}$), and the pool water temperature (T_{pool}) and the resulting active operational mode.

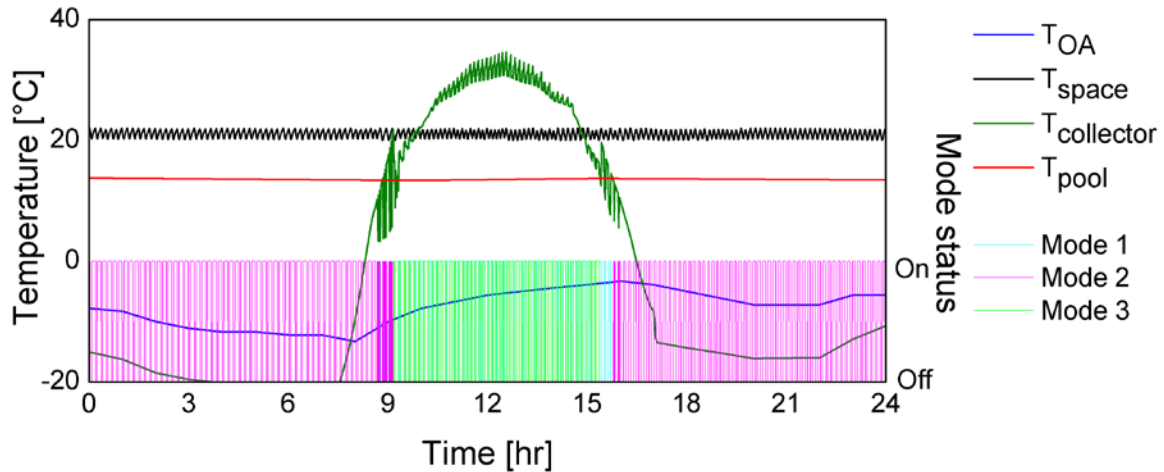


Fig. 3: Operational modes and related temperatures for the system operation on January 19

For the system operation on a winter representative day, Figure 3 leads to the following observations:

- January 19 is a cold winter day for Baltimore with the lowest outdoor air temperature at -14°C . All three possible heating modes (Modes 1, 2, 3) are observed during this day. The thermostat has its heating setpoint at 21°C with a deadband of 2°C (space heating starts when T_{space} reduces to 20°C and it stops when T_{space} reaches 22°C). Mode 2 (i.e., pool-HP for heating, see Section 2) is the active operating mode from 12 am to 9 am, when the thermostat calls for space heating and the PV/T collector and pool temperatures lie in the predefined range (i.e., $T_{\text{collector}} < 10.6^{\circ}\text{C}$ and $T_{\text{pool}} > 6.7^{\circ}\text{C}$). During this time period, Mode 2 cycles on and off, following the same cycle of thermostat heating calls. After 9 am, Mode 1 (PV/T-HP for heating) becomes the active mode when the thermostat calls for space heating because the PV/T collector temperature has increased above 10.6°C . During the period between 9 am and 4 pm, Mode 1 and Mode 3 cycle alternatively: whenever the thermostat calls for heating, Mode 1 is activated; otherwise, whenever the thermostat does not call for heating, Mode 3 (pool water heating) is activated to use PV/T for charging the pool water. The cycle of Modes 1 and 3 continues until around 4 pm when the PVT temperature is lower than 7.6°C . From 4:00 pm to the midnight, Mode 2 cycles on and off with the same behavior and underlying reasons as discussed earlier for the period between 12 am and 9 am.
- Because the outdoor swimming pool is covered and there is a large thermal mass of the pool water, the pool water temperature changes little across the whole day. Starting from 13.8°C at the beginning of the day, the pool water temperature reduces to 13.4°C at 9 am because Mode 2 is activated and the pool water is used as the heat source to provide space heating. From 9 am to 4 pm, the pool water temperature increases to 13.7°C because Mode 3 is activated to charge the pool by PV/T collectors. From 4 pm to the midnight, the pool temperature reduces to 13.5°C because of Mode 2 operation during this period.
- The outdoor air temperature ranges between -14°C and -3°C while the pool water temperature is around 13°C . Such a big difference between the outdoor air temperature and the pool water temperature is the fundamental reason that leads to the higher efficiency of the system than the baseline air-source heat pump system.

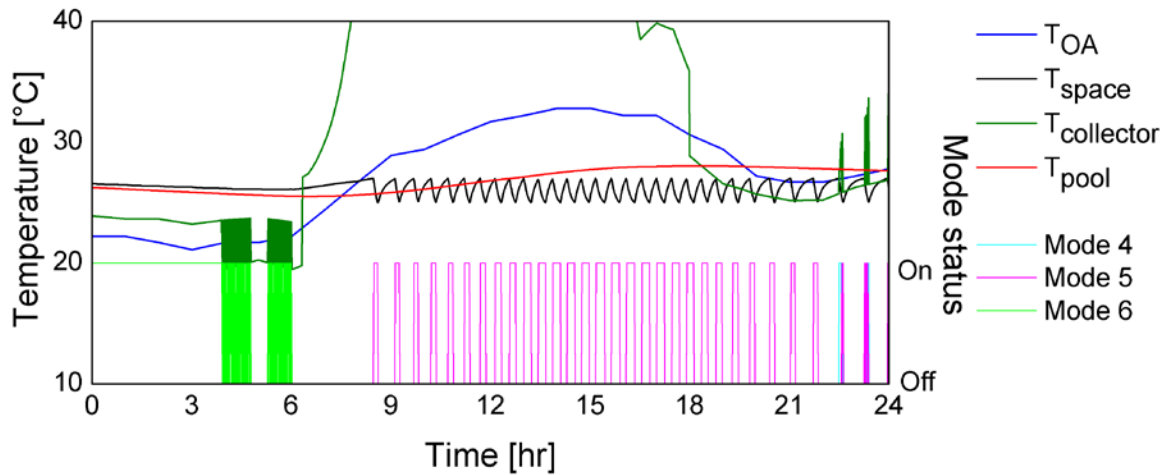


Fig. 4: Operational modes and related temperatures for the system operation on June 25

Figure 4 shows the system operation on June 25, a summer representative day. This figure leads to the following observations:

- June 25 is a hot summer day for Baltimore with peak outdoor air temperature at 35°C. All three possible cooling modes (Modes 4, 5, 6) are observed during this day. The thermostat cooling setpoint is 26°C with the deadband of 2°C. Night time is defined from 10 pm to 6 am and the rest of the day is considered as day time. Mode 6 (i.e., night time pool water cooling, see Section 2) is the active operating mode for the time period of 12 am to 6 am because the PV/T collector temperature is less than pool temperature. Through this mode, night time radiative cooling is used to reduce the pool water temperature. The thermostat first calls for space cooling at 8:30 am and Mode 5 (pool-HP for cooling) becomes the active mode. From 8:30 am to midnight, Mode 5 cycles on and off, following the same cycle of thermostat cooling calls. Mode 5 operation time in each cycle increases until 2 pm, which is the hottest time of the day, and decreases afterwards. The only exception to this cycle happens at 10:30 pm when thermostat calls for space cooling while PV/T collector temperature is less than 27.2°C and therefore Mode 4 (night time PV/T-HP for cooling) is the active operating mode.
- The pool cover is removed from May to September and therefore pool is uncovered in this summer representative day and consequently more pool temperature change compared to the wintertime is noticeable. Starting from 26.3°C at the beginning of the day, the pool water temperature reduces to 25.5°C at 7 am because of two reasons: 1) Mode 6 activation and radiative cooling of the pool; 2) heat transfer to the cooler outdoor air. From 7 am to 6 pm, the pool water temperature increases to 28°C because: 1) Mode 5 is activated and the pool water is used as the heat sink to provide space cooling; 2) heat transfer with warmer outdoor air happens. From 6 pm to 12 am, the pool water temperature is reduced to 27.6°C since the pool's heat loss because of heat transfer with cooler surrounding area overcomes the pool's heat gain from Mode 5 operation.
- The outdoor air temperature ranges between 20°C and 35°C while the pool water temperature range is between 25°C and 28°C. The pool water temperature is mostly lower than the outdoor air temperature when space cooling is needed, which leads to the higher cooling efficiency of the proposed system compared to the baseline air-source heat pump system.

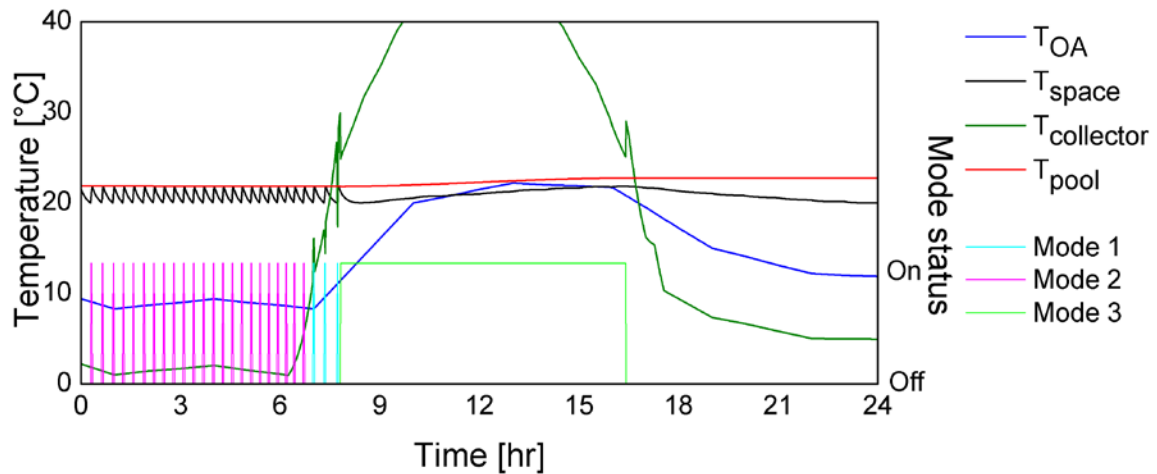


Fig. 5: Operational modes and related temperatures for the system operation on October 10

Figure 5 shows the system operation on October 10, a shoulder representative day. This figure leads to the following observations:

- The outdoor air temperature is around 8°C during early hours of the day and there are several occasions when the thermostat calls for heating during this day. Before 7 am, the temperature of the PV/T collector is low. Thus, Mode 2 (pool water space heating) is activated whenever the thermostat calls for space heating. Between 7 am and 8 am, Mode 1 (PV/T-HP for heating) is activated three times, each of which lasts about one minute. Between 8 am and 4:30 pm, Mode 3 (pool water heating through PV/T collector) runs consistently because no space heating is needed and the PV/T collector temperature is higher than the pool water temperature.
- Starting from 21.8°C, the pool water temperature has negligible changes in the early hours of the day because of the large thermal mass of the pool. However, the continuous operation of Mode 3 for more than 8 hours increases the pool water temperature by 1°C.

5.1. Energy consumption comparison

After verifying the system operation through representative days, the simulation was ran for a whole year to compare the energy consumption between the proposed PV/T-HP system and the baseline split air-source heat pump system. Figure 6 shows the energy consumption of each month and the whole year for both systems. The energy consumption reported here comes from the water-to-water heat pump, pumps, and the supply fan for the proposed system while it is from the air-source heat pump and the supply fan for the baseline system. Figure 6 indicates the following:

- The proposed system is much more efficient than the reference system during the heating season. Specifically, the proposed system consumes 67%, 64%, 58%, 71%, 85%, and 90% of the reference system energy consumption, sequentially from November to April. As mentioned earlier, the heating efficiency mainly comes from the elevated source side temperature (pool water temperature or PV/T collector temperature for the proposed system vs. outdoor-air temperature for the baseline).
- In the cooling season, the proposed system consumes 95%, 87%, 84%, and 108% of energy consumption by the baseline system respectively in June, July, August, and September. These percentages of energy savings are less than those in winter months. The major reason is that the benefits of energy saving from using pool water for cooling at daytime are significantly offset by the pump energy incurred at night time when Mode 6 operation (pool water cooling with PV/T) runs almost continuously. In particular, in September, the magnitude of cooling energy consumption is much lower than other months, which makes the pump energy more significant and thereby leads to more energy consumption than the baseline system.

- In May and October of the shoulder season, the proposed system consumes 83% and 73% of energy consumption by the baseline system. Let's use October as a good example of how the pool heating can make the proposed system more efficient. As the representative day analysis in Figure 5 shows, Mode 3 (pool water heating with PV/T) is the dominant mode during day time because of the high PV/T collector temperature and negligible heating needs. This means that more thermal energy is charged to the pool water than the discharged thermal energy and parasitic heat losses. As a result, favorable pool water temperature exists for the source side of the water-to-water heat pump when heating is needed during this month and even the following months (November and December). This can explain to some extent why the three months (October to December) have the highest percentage of energy savings.
- For the whole year, the proposed PV/T-HP system consumes 70% of annual energy consumption by the baseline system. This value is close to the average percentage of energy savings in the heating season because heating energy dominates the overall HVAC energy use by the modeled house in Baltimore.

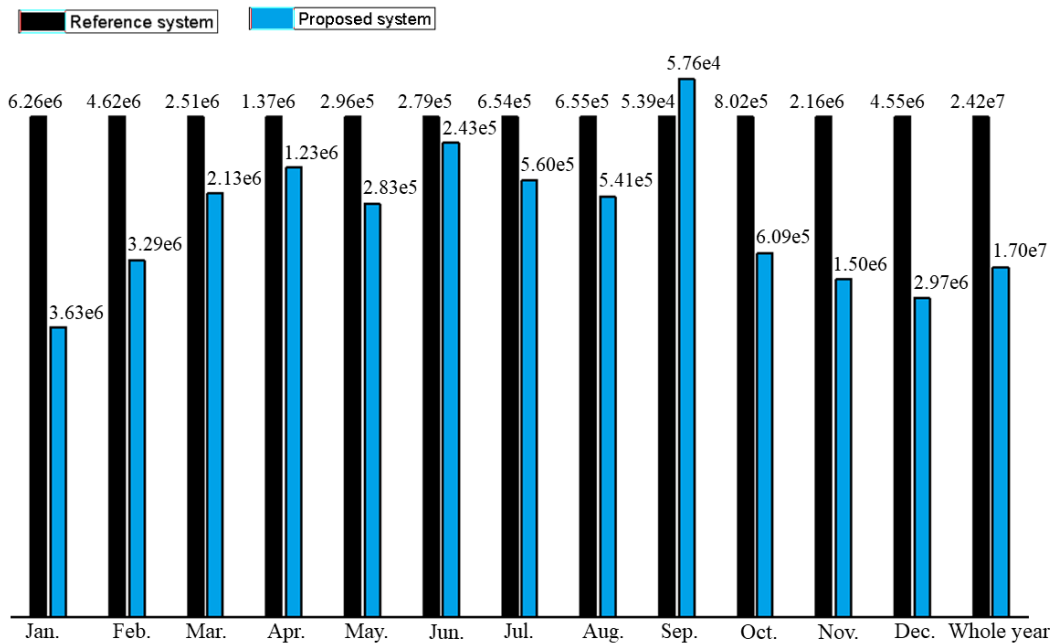


Fig. 6: Onsite energy consumption comparison between the baseline and proposed systems. The energy consumptions are reported in KJ.

6. Conclusions

This paper presents the simulated performance of a proposed hybrid PV/T heat pump system in a 200-m² one-floor house in Baltimore, MD. The proposed system includes a water-to-water heat pump, a PV/T collector, an outdoor swimming pool, pumps, and a forced air system containing water coils and a fan for air conditioning. The proposed system uses a six-mode control strategy that decides the active operating mode based on the space air temperature, the PV/T collector temperature, and the swimming pool water temperature. In the proposed system, the PV/T collectors are used to collect thermal energy and either deliver it to the water-to-water heat pump for space conditioning or store it in the outdoor swimming pool. On the other hand, the charged pool is the source/sink for the water-to-water heat pump when the PV/T collector is not capable of providing enough thermal energy. TRNSYS software was used to study the performance evaluation of the proposed system. The system operation was verified through three representative days in the winter, summer and shoulder months and the system operated as expected in all three representative days. After system operation verification, energy consumption of the proposed system was compared to a split air-source heat pump system. Based on the annual and monthly simulation results, the average monthly energy consumption of the proposed system in the winter, summer, and shoulder months were 72%, 93%, and 78%

of the baseline energy consumption respectively, and the annual energy saving of the proposed system compared to the baseline system was 30%. The experimental or field test verification of the proposed system, addition of the domestic hot water production, and exploring strategies for generated PV electricity self-consumption in the system are the suggested directions for the future of this research.

7. References

- Amrane, K., Nadel, S., Sachs, H. (2010). The regional standards agreement for residential furnaces, air Conditioners, and heat pumps: process, results, and implications. *ACEEE Summer Study on Energy Efficiency in Buildings*, 24-35.
- Bourdakis, E., Péan, T. Q., Gennari, L., & Olesen, B. W. (2016). Daytime space cooling with phase change material ceiling panels discharged using rooftop photovoltaic/thermal panels and night-time ventilation. *Science and Technology for the Built Environment*, 22(7), 902-910.
- EIA. (2013) U.S. Energy Information Administration. 2013. *2009 Residential Energy Consumption Survey – Table CE3.1 Household Site End-Use Consumption in the U.S., Totals and Averages*.
- EIA. (2018) U.S. Energy Information Administration. [Monthly Energy Review – Table 2.1](#) Energy Consumption by Sector-2015 data.
- Eicker, U., & Dalibard, A. (2011). Photovoltaic–thermal collectors for night radiative cooling of buildings. *Solar Energy*, 85(7), 1322-1335.
- Fiorntini, M., Cooper, P., & Ma, Z. (2015). Development and optimization of an innovative HVAC system with integrated PVT and PCM thermal storage for a net-zero energy retrofitted house. *Energy and Buildings*, 94, 21-32.
- Hailu, G., Dash, P., & Fung, A. S. (2015). Performance evaluation of an air source heat pump coupled with a building-integrated photovoltaic/thermal (BIPV/T) system under cold climatic conditions. *Energy Procedia*, 78, 1913-1918.
- IECC (2006). *International Energy Conservation Code (IECC)*. International Code Council, Inc.
- Li, S., Joe, J., Hu, J., & Karava, P. (2015). System identification and model-predictive control of office buildings with integrated photovoltaic-thermal collectors, radiant floor heating and active thermal storage. *Solar energy*, 113, 139-157.
- Nejma, H. B., Guiavarch, A., Lokhat, I., Auzenet, E., Claudon, F., & Peuportier, B. (2013, August). In-situ performance evaluation by simulation of a coupled air source heat pump/PV-T collector system. In *Proceedings of BS2013: 13th conference of international building performance simulation association, Chambéry, France* (pp. 1927-1935).
- Palla, N., Braun, R., Jobard, X., Mitina, I., Cremers, J., & Eicker, U. (2014). Development of Multivalent PV-Thermal Collectors for Cooling, Heating and Generation of Electricity. In *International Plea Conference* (Vol. 30, No. 2014, pp. 16-18).
- Wassmer, M., Brandemuehl, M. J., 2006, Effect of Data Availability on Modeling of Residential Air Conditioners and Heat Pumps for Energy Calculations. *ASHRAE Transactions*, vol. 111, part 1, p. 214-225.
- Xia, L., Ma, Z., & Kokogiannakis, G. (2017). Performance Simulation of a Ground Source Heat Pump System Integrated with Solar Photovoltaic Thermal Collectors for Residential Application.
- Zare, A., & Wang, W. (2018). An innovative hybrid photovoltaic thermal heat pump system for houses. 5th International High Performance Buildings Conference at Purdue, July 9-12, 2018.

Author Index

A

Amaral, D.

"Homebrew" Wind Turbines for Integration into Small-Scale Renewable Energy Systems 62

Anderson, K.R.

Powering Third World Countries for the Same Cost as Building the Border Wall 4

Simulation and Lessons Learned from the Ivanpah Solar Plant Project 13

B

Benfield, J.

Renewable Resources of the Northern Half of the United States; A Pathway to Total... 39

C

Calderon, A.

Forecasting Carbon Emissions in States of Hawaii, California, Colorado, and Florida;... 32

Cliburn, J.

SOLAR 2018: Pathways to a Renewable Energy Transformation 1

G

Gaither, J.

Powering Third World Countries for the Same Cost as Building the Border Wall 4

H

Hoskins, M.

A Data-Driven Framework for Deploying Solar PV At Penn State University 23

J

Jansson, P.M.

Comparative Analysis of Energy Storage for Photovoltaics: Electrical vs Virtual 105

K

Khoie, R.

Forecasting Carbon Emissions in States of Hawaii, California, Colorado, and Florida;... 32

Renewable Resources of the Northern Half of the United States; A Pathway to Total... 39

M

Mansy, K.

Challenging Conventional Wisdom in the Age of Computing 51

Martin, J.

"Homebrew" Wind Turbines for Integration into Small-Scale Renewable Energy Systems 62

Miller, S.W.

A Data-Driven Framework for Deploying Solar PV At Penn State University 23

O

Okafor, G.

Multi-Generation Modeling and Building Energy use optimization based on a Natural... 72

P

Prinkey, M.

A Data-Driven Framework for Deploying Solar PV At Penn State University 23

S

Sankriti, M.

Preliminary Design and Analysis of Low-Cost Concentrating Offshore Solar Energy Innovations 85

Sarunac, N.

Simulated Performance of a Photovoltaic Thermal Heat Pump System for Single-family... 133

Schirtzinger, W.

Research Reveals the Hidden Methods to Democratize Solar 98

Schleith, S.

Providing Emergency Power and Surviving on Solar, Boulder, Colorado, Usa 119

Sikder, O.

Comparative Analysis of Energy Storage for Photovoltaics: Electrical vs Virtual 105

Smithpeter, I.

A Low-Cost IoT Approach to Real-Time Cloud Motion Detection 110

T

Taherian, H.

Multi-Generation Modeling and Building Energy use optimization based on a Natural... 72

Tharp, J.

Simulation and Lessons Learned from the Ivanpah Solar Plant Project 13

Torres, C.

Comparative Analysis of Energy Storage for Photovoltaics: Electrical vs Virtual 105

U

Ugale, K.

Renewable Resources of the Northern Half of the United States; A Pathway to Total... 39

W

Wang, W.

Simulated Performance of a Photovoltaic Thermal Heat Pump System for Single-family... 133

Y

Young, W.R.

Providing Emergency Power and Surviving on Solar, Boulder, Colorado, Usa 119

Z

Zare, A.

Simulated Performance of a Photovoltaic Thermal Heat Pump System for Single-family... 133

